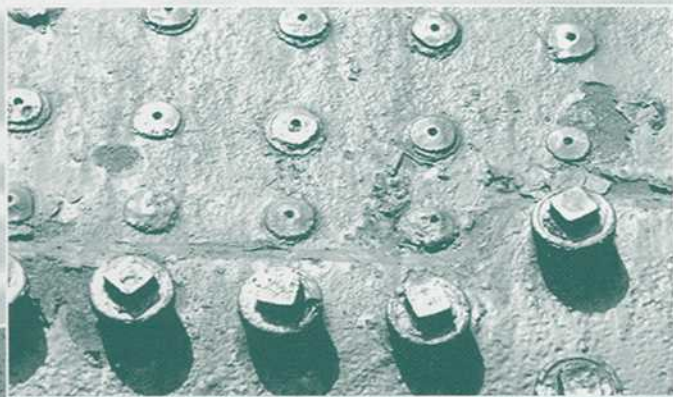


MARINE CORROSION in TROPICAL ENVIRONMENTS

Sheldon W. Dean
Guillermo Hernandez-Duque Delgadillo
James B. Bushman

EDITORS



STP
1399

STP 1399

Marine Corrosion in Tropical Environments

*Sheldon W. Dean, Guillermo Hernandez-Duque
Delgadillo, and James B. Bushman, editors*

ASTM Stock Number: STP1399



ASTM
100 Barr Harbor Drive
PO Box C700
West Conshohocken, PA 19428-2959

Printed in the U.S.A.

Library of Congress Cataloging-in-Publication Data

Marine corrosion in tropical environments/Sheldon W. Dean, Guillermo Hernandez-Duque Delgadillo, and James B. Bushman, editors.

p. cm.—(STP; 1399)

“ASTM Stock Number: STP1399”

Includes bibliographical references and index.

ISBN 0-8031-2873-8

1. Corrosion and anti-corrosives. 2. Seawater corrosion. 3. Concrete—Corrosion. I. Dean, S. W., 1935– II. Hernandez-Duque Delgadillo, Guillermo, 1961– III. Bushman, James B., 1939–

TA462.M364 2000

620.1'1223—dc21

00-060556

Copyright © 2000 AMERICAN SOCIETY FOR TESTING AND MATERIALS, West Conshohocken, PA. All rights reserved. This material may not be reproduced or copied, in whole or in part, in any printed, mechanical, electronic, film, or other distribution and storage media, without the written consent of the publisher.

Photocopy Rights

Authorization to photocopy items for internal, personal, or educational classroom use, or the internal, personal, or educational classroom use of specific clients, is granted by the American Society for Testing and Materials (ASTM) provided that the appropriate fee is paid to the Copyright Clearance Center, 222 Rosewood Drive, Danvers, MA 01923; Tel: 978-750-8400; online: <http://www.copyright.com/>.

Peer Review Policy

Each paper published in this volume was evaluated by two peer reviewers and at least one editor. The authors addressed all of the reviewers' comments to the satisfaction of both the technical editor(s) and the ASTM Committee on Publications.

To make technical information available as quickly as possible, the peer-reviewed papers in this publication were prepared “camera-ready” as submitted by the authors.

The quality of the papers in this publication reflects not only the obvious efforts of the authors and the technical editor(s), but also the work of the peer reviewers. In keeping with long-standing publication practices, ASTM maintains the anonymity of the peer reviewers. The ASTM Committee on Publications acknowledges with appreciation their dedication and contribution of time and effort on behalf of ASTM.

Foreword

This publication, *Marine Corrosion in Tropical Environments*, contains papers presented at the symposium of the same name held in Orlando, Florida, on 13 November 2000. The symposium was sponsored by ASTM Committee G01 on Corrosion of Metals, in cooperation with NACE International and the University of Mayab, Merida, Yucatan, Mexico. Sheldon W. Dean, Air Products and Chemicals, Inc., Guillermo Hernandez-Duque Delgadillo, Universidad del Mayab, and James B. Bushman, Bushman & Associates, presided as symposium chairmen and are editors of this publication.

Ann Chidester Van Orden 1954 to 1998

Dedication



This volume is dedicated as a memorial to our friend and colleague—Ann Chidester Van Orden, Professor, Old Dominion University, Norfolk, Virginia, who passed away on 14 October 1998.

Ann was a talented teacher, enthusiastic leader, and thorough researcher who gave tirelessly to those with whom she worked. She was a member of ASTM Committee G01 for years, and chaired the G01.99 standing subcommittee on Liaison with other Corrosion-related Organizations. She also was the vice chair for G01.11, subcommittee on Electrochemical Methods of Corrosion Testing and the task group on Electrochemical Corrosion Testing of Aluminum Alloys. She also was vice chair of the ASTM symposium on Electrochemical Modeling of Corrosion. Ann served on the ASTM Sam Tour Award Selection Committee. She was awarded the ASTM Committee G01 Certificate of Appreciation in 1993 for her many contributions to the committee and to electrochemical corrosion technology. Ann is a co-author of a paper in this STP.

Ann was also very active in NACE International, serving as vice chair for two symposia and chairing five others on a range of topics from the use of computers in corrosion control,

electrochemical methods of corrosion testing, and atmospheric corrosion. Ann authored more than thirty technical papers and twelve technical reports. She supported two graduate student research projects and advised twenty undergraduate student research projects. She received the NBS Outstanding Performance Award in 1980, 1984, and 1986 and the NASA Special Accomplishment Award in 1992.

Beyond these and many other accomplishments, Ann was a very special person who brightened the lives of all whom she encountered. Her enthusiasm made difficult tasks easy and her joy in living shone through the most troubling times. Though she will be sorely missed as we move forward, the energy and creativity of her life will stand as a beacon illuminating our progress.

Contents

Overview

ix

ATMOSPHERIC CORROSION

Marine Atmospheric Corrosion of Reference Metals in Tropical Climates of Latin-America —L. MARIACA-RODRIGUEZ, E. ALMEIDA, A. DE BÓSQUEZ, A. CABEZAS, J. FERNANDO-ALVAREZ, G. JOSEPH, M. MARROCOS, M. MORCILLO, J. PEÑA, M. R. PRATO, S. RIVERO, B. ROSALES, G. SALAS, J. URUCHURTU-CHAVARÍN, AND A. VALENCIA	3
Application of a Model for Prediction of Atmospheric Corrosion in Tropical Environments —J. TIDBLAD, A. A. MIKHAILOV, AND V. KUCERA	18
Mechanisms of Atmospheric Corrosion in Tropical Environments —I. S. COLE	33
Aerosol Model Aids Interpretation of Corrosivity Measurements in a Tropical Region of Australia —R. KLASSEN, B. HINTON, AND P. ROBERGE	48
Thirty-Eight Years of Atmospheric Corrosivity Monitoring —B. S. PHULL, S. J. PIKUL, AND R. M. KAIN	60
Atmospheric Corrosion in Marine Environments along the Gulf of México —D. C. COOK, A. C. VAN ORDEN, J. REYES, S. J. OH, R. BALASUBRAMANIAN, J. J. CARPIO, AND H. E. TOWNSEND	75
Electrochemical Evaluation of the Protective Properties of Steel Corrosion Products Formed in Ibero-American Tropical Atmospheres —J. URUCHURTU-CHAVARÍN, L. MARIACA-RODRIGUEZ, AND G. MICAT	98
A Methodology for Quantifying the Atmospheric Corrosion Performance of Fabricated Metal Products in Marine Environments —G. A. KING AND P. NORBERG	114

CONCRETE DETERIORATION

The Moisture Effect on the Diffusion of Chloride Ion in Hydrated Cement Paste—A. T. C. GUIMARÃES AND P. R. L. HELENE	135
Electrical Conductivity of Concrete and Mortar Prepared with Calcareous Aggregates for Construction in the Gulf of Mexico—L. MALDONADO	150
Time of Wetness and Temperature as Tools to Evaluate Corrosion Risk in Concrete Blocks Exposed to a Humid Tropical Environment—P. CASTRO AND L. P. VÉLEVA	159
Model Solutions of Concrete Environment and Effect of Chloride Ions on the Electrochemical Corrosion Behavior of Reinforcing Mild Steel—L. P. VÉLEVA AND M. C. CEBADA	170
Permeability Properties of Cement Mortars Blended with Silica Fume, Fly Ash, and Blast Furnace Slag—R. DE GUTIÉRREZ, S. DELVASTO, AND R. TALERO	190
Degradation of Fiber Reinforced Mortar in a Marine Environment—R. DE GUTIÉRREZ, L. A. CALDERÓN, AND S. DELVASTO	197
Corrosion Control on Concrete Structures: Zinc-Hydrogel Technology—J. L. PIAZZA	207
Design and Protection Criteria for Cathodic Protection of Seawater Intake Structures in Petrochemical Plants—Z. CHAUDHARY	218
Methodology for Service Life Prediction of Stainless Steel Reinforced Structures Based on the Correlation between Electrochemical and Mechanical Manifestations of Corrosion—L. TULA AND P. R. L. HELENE	231
CATHODIC PROTECTION, MICROBIOLOGICAL INFLUENCED CORROSION, AND SEAWATER	
Cathodic Protection of Structures in Coral Sands in the Presence of Salt Water—E. W. DREYMAN	247
An Evaluation of Fungal-Influenced Corrosion of Aircraft Operating in Marine Tropical Environments—B. J. LITTLE, R. K. POPE, AND R. I. RAY	257
Features of SRB-Induced Corrosion of Carbon Steel in Marine Environments—H. A. VIDELA, C. SWORDS, AND R. G. J. EDYVEAN	270
Use of Coatings to Assess the Crevice Corrosion Resistance of Stainless Steels in Warm Seawater—R. M. KAIN	284
Indexes	301

Overview

Economic pressures on companies in the concluding decades of the 20th century have inspired a drive towards globalization. The need for continuing growth has pushed manufacturing, sales, and marketing beyond national boundaries to encompass all regions of the globe where populations present opportunities for these activities. One result of this initiative has been the economic development of tropical areas. Previously these areas were considered "third world" regions with little potential for growth. However, a number of factors have now combined to make these areas attractive for development. These include a more open political climate, discovery of oil and other natural resources, and improved transportation and communication means.

Tropical areas offer desirable climate, willing workers, and a large population with many needs and desires. The growth in industrialization has also promoted the development of infrastructures necessary to support this growth. Airports, marine terminals, power plants (hydroelectric, thermal, and nuclear), power distribution systems, water treatment plants and supply systems, highways, bridges, railroads, oil refineries, and chemical manufacturing facilities are some of the infrastructures which are required in most marine locations. As a result, atmospheric corrosion, concrete deterioration, and seawater corrosion are major concerns for infrastructures in tropical areas.

Papers were invited for this STP on atmospheric corrosion, corrosion of rebar in concrete, marine corrosion, and other related corrosion phenomena. It was intended that these papers would cover laboratory evaluation methods, test methods, and model prediction.

Atmospheric Corrosion

In the area of atmospheric corrosion, eight papers are included in this STP, covering a wide range of topics. M. Morcillo et al. have included summary results from sixteen tropical test sites participating in the "Ibero-American Map of Atmospheric Corrosiveness" (MICAT) project. This paper presents results from rural and marine locations without sulfur dioxide pollution and in marine sites with sulfur dioxide present. The four reference metals used were steel, zinc, copper, and aluminum exposed for one-year periods. Information is presented on the corrosion rate, corrosion products, and morphology of attack.

J. Tidblad et al. have analyzed data from the UN ECE and the ISO CORRAG programs and found that corrosion rates increased with ambient temperature up to 10°C and then decreased. They have created models for predicting the corrosion of steel, zinc, and copper as a function of time, temperature, relative humidity, sulfur dioxide, ozone, rainfall amount, and acidity. Different models are derived when chloride deposition occurs. These relationships are shown to give better predictions of corrosion than simple three variable expression.

I. S. Cole has analyzed data from five Pacific countries for steel and zinc. He has used regression analyses to develop model expressions for the corrosion rates of these metals as a function of time of wetness, acidity of precipitation, sulfur dioxide, and deposition of chlorides. In analyzing the atmospheric corrosion processes, he has examined both the absorption of acid gases in the moisture films and the deposition of aerosols from the atmosphere, including the effects of ammonia and the oxidation of sulfite to sulfate in corrosion product layers.

R. Klassen et al. have examined the corrosivity pattern near Townsville, Australia over a four-year period using the aluminum wire on copper bolt CLIMAT specimens and wet candle

chloride collection units. The results showed that the corrosion rate of the specimen correlated with the chloride deposition measured by the wet candles. The authors used a computer fluid flow simulator to predict the effects of surface contours on the rate of salt deposition from marine surf generated aerosols. The predictions provided a framework for understanding the unusual pattern of salt deposition and resulting corrosivity.

B. S. Phull et al. have presented a summary of their 38 years of atmospheric corrosivity monitoring at the Kure Beach sites. They have used two reference materials, steel and zinc, in this work while also monitoring chloride deposition, relative humidity, time of wetness, temperature, prevailing wind direction, and rainfall. One important conclusion from their work is that violent hurricanes do not have a significant effect on the one-year corrosion losses but can cause mechanical damage and loss of specimens. They have concluded that actual exposure data is the best indication of a material's performance in the atmosphere.

D. C. Cook et al. have examined results for twelve sites located around the Gulf of Mexico. One-year exposures of steel, aluminum, copper, and zinc were used along with measurements of time of wetness, chloride deposition, and sulfur dioxide concentrations. They have evaluated the estimated corrosivity classes based on the ISO 9223 method and compared it with the class obtained by mass loss measurements. They found substantial disagreements between corrosion classification based on environmental parameters and specimen losses. They have also provided some detailed analyses of the rust layer found on the carbon steel panels.

J. Uruchurtu-Chavarín et al. have looked at a variety of electrochemical techniques including linear polarization resistance and electrochemical potential noise to evaluate the protectiveness of rust layers on carbon steel specimens exposed as part of the MICAT program. These measurements were able to provide a measure of protectiveness of the rust layers, including the observation that low levels of sulfur dioxide improved the protectiveness of the rust. Low levels of chloride deposition reduced the protectiveness of the rust but sulfur dioxide was still beneficial. Extreme levels of chloride and sulfur dioxide were very detrimental.

G. A. King and P. Norberg have developed an approach for evaluating fabricated metal products in marine atmospheres. They have specifically addressed the issue of sheltering which greatly aggravates the damage in marine sites because rain is not able to wash chloride from the surfaces. They considered a variety of coatings on sheet steels including zinc, 5% Al zinc, 55% Al zinc, sheet aluminum, and sheet stainless steel. Specimens with organic coatings were included as well. These specimens included a variety of defects such as cut edges, bends, domes, scribes, and holes. A system of evaluating and rating damage was developed. Exposures were made at three marine sites. Comparisons were presented for open versus sheltered locations.

Concrete Deterioration

Nine papers on various aspects of concrete deterioration are included. A. T. C. Gumarães and P. R. L. Helene have examined the issue of chloride diffusion in hydrated and cured portland cement paste. They applied a chloride-containing mixture to the surface of their specimens and observed the degree of penetration of chloride into the specimens as a function of degree of saturation of the specimens with water. They concluded the diffusion of chloride into the concrete was strongly influenced by degree of saturation, and this effect should be taken into consideration in evaluations.

L. Maldonado has studied the electrical conductivity of concrete and mortars as a function of water to cement ratio and curing times of 7 and 28 days. Specimens were immersed in a solution of 1, 2, 3, and 4M sodium chloride, and the conductivity of the specimens was measured. It was found that the conductivity increased with salt concentration and water

content of the mixture. The mortars cured for 28 days had higher conductivities than those cured for 7 days, while the concrete specimen showed lower conductivity with longer cure times. This behavior was explained by the difficulty of water transport in the gel pore structure.

P. Castro and L. P. Véleva have examined the issue of internal relative humidity in concrete during settling, curing, and service. They have conducted experiments using the ASTM G 84 Cu/Au wetness sensor at various depths in concrete specimens to trace moisture levels high enough to produce wetness response on the sensor. They have examined diurnal temperature variations and found corresponding time of wetness variations corresponding to the temperature changes. They have proposed this approach for understanding why concrete structures show variations in deterioration from rebar corrosion.

L. P. Véleva and M. C. Cebada have examined the use of saturated calcium hydroxide solutions as compared with pore solutions from concrete to model the corrosion of rebar from chloride intrusion. They noted significant differences in the electrochemical responses of steel in those solutions using both potentiodynamic polarization and electrochemical impedance spectroscopy. They concluded that the concrete pore solution was somewhat more protective than the saturated calcium hydroxide.

R. de Gutiérrez et al. have examined the properties of cement mortar blended with silica fume, fly ash, and blast furnace slag. They have run tests on compressive strength, water absorption, chloride diffusion and permeability, mercury intrusion, and x-ray diffraction. The densifying effects of these materials improved the resistance of concrete to chloride intrusion although the fly ash and slag additions lowered early strengths more than silica fume.

R. de Gutiérrez et al. have investigated the use of a variety of fiber materials to improve the ductility and tensile strength of concrete mortar. They included both natural and synthetic fibers in this study. Silica fume and superplasticizer were added to some of the mixtures. The durability of the various mixtures was evaluated by measuring chloride penetration and water absorption. The compressive strength was also measured. It was found that all the fibers reduced the compressive strength of the mortars with steel showing the smallest reduction and sisal the greatest. The addition of silica fume improved the compressive strength after 90 days curing so that mortars with steel, glass, and coconut fibers had greater strength than mortar without fibers. Likewise, water absorption was greatest for sisal and fique and smallest for steel and polypropylene. Addition of silica fume and superplasticizer reduced the water absorption in all cases. Chloride penetration was also reduced when silica fume was used.

Another approach to dealing with the problem of rebar corrosion in concrete was presented by J. L. Piazza II. He has reviewed a number of approaches for dealing with both preventing corrosion of rebar from chloride intrusion and remediation of damage. He has focused his discussion on the use of zinc hydrogel anodes as a low maintenance cathodic protection system for concrete buildings in tropical marine environments. This approach is particularly desirable for existing structures that are showing the effects of chloride intrusion and rebar corrosion.

Z. Chaudhary presented his experience with cathodic protection systems for seawater intake structures in petrochemical plants in Saudi Arabia. Seawater is used here for cooling and, as a result, there are extensive canals and distributions systems. Both impressed current and sacrificial anode galvanic systems were used to provide protection for the rebar in these concrete structures. The design philosophy is covered together with monitoring, repair, and performance evaluations over a seven-year period. Recommendations are provided for the applied current density and protection potential criterion for these structures. He also recommends that impressed current systems should be included in the design of new units.

L. Tula and P. R. L. Helene have examined the possibility of using Type 316L stainless steel rebar rather than carbon steel to avoid concrete failures from rebar corrosion. They examined polarization curves of these metals in concrete with various chloride contents and determined that carbon steel would have about 10 times greater corrosion rate at a chloride content greater than 0.4%. They also examined the extent of corrosion required to achieve loss of bond strength and cracking of the concrete. The stainless required a somewhat greater extent of corrosion to lose bond strength in the concrete but somewhat smaller extent of corrosion to cause cracking of the concrete. The stainless steel showed substantially greater strength at equivalent weight loss values. Calculations were made on the expected service lives for a marine pier and an industrial chloride solution reservoir for stainless steel as compared to carbon steel rebar. The results varied from two to eight times for stainless steel greater than carbon steel.

Cathodic Protection Microbiological Influenced Corrosion and Seawater

Four papers are included in this section. E. W. Dreyman has considered the unique challenge presented by the need to place metal items in coral sands with seawater present. This includes items such as water and gas lines and tanks to hold water, fuel, and other fluids. The challenge here is to establish protection criteria for steel and aluminum construction in this service. He covers rectifiers, cables, and galvanic and impressed current anodes. He also provides information on monitoring and design parameters for this type of condition.

B. J. Little et al. have examined fungi growing inside aircraft operating in tropical marine environments. These organisms grow on painted and bare surfaces particularly in occluded areas where cleaning is difficult. The high humidity of tropical environments encourages fungal growth. Fungal growth can cause paint deterioration and corrosion attack on aluminum surfaces. Cultures taken from aircraft were grown on a variety of surfaces including bare aluminum, glossy polyurethane coated surfaces, and flat finish polyurethane coated surfaces both with and without fungicide and fungistat additives. The flat finish was somewhat better than glossy finishes. Aged paint fouled more rapidly than new coatings and the additives produced mixed results.

H. A. Videla et al. have analyzed the action of sulfate-reducing bacteria (SRB) on the corrosion of carbon steel in seawater and marine mud. They have noted that SRB cause a variety of changes to pH, ion concentrations, and corrosion product films with results of acceleration of corrosion and related problems such as corrosion fatigue, crack growth, and hydrogen embrittlement. The presence of SRB can also decrease the performance of cathodic protection and protective coatings used in seawater. A review of electrochemical techniques for corrosion assessment, surface analyses, and microscopy methods is also provided.

R. M. Kain has evaluated epoxy coatings for protecting Type 316L stainless steel, 6Mo stainless steel (N08367), and a CrNiMnMo stainless steel. A variety of different specimens was exposed to warm filtered seawater in a large tank for 6 months. The results showed that all the specimens suffered crevice corrosion and paint delamination. Grit-blasted surfaces had much better paint adhesion. The 6Mo stainless steel gave the best performance but was not immune to crevice attack. This work demonstrated the effectiveness of epoxy coatings as crevice formers in seawater.

This book should be of particular interest to engineers responsible for designing and maintaining protection programs for physical plants in tropical marine locations. In addition, many of the papers present models and data that are of specific interest to scientists studying degradation mechanisms that occur in natural environments. Some of the papers are of specific interest to researchers developing new products for use in these environments. Also, these papers have many important insights for standards' developers, especially those inter-

ested in standards with global reach. In particular, these papers will be of interest to standards' developers concerned with corrosion resistant alloys, coatings and linings, cathodic protection, concrete, seawater, and atmospheric corrosion.

The editors of this book are especially grateful to Victor Chaker for his efforts in organizing this activity. Victor's visions and enthusiasm were responsible for the concept and initial plans. Unfortunately Victor had to withdraw from this project due to his personal situation, but his contributions are recognized and much appreciated.

Sheldon W. Dean

Air Products and Chemicals, Inc.

Allentown, PA

Symposium co-chair and co-editor

Guillermo Hernandez-Duque Delgadillo

Universidad del Mayab

Merida, Mexico

Symposium co-chair and co-editor

James B. Bushman

Bushman & Associates

Medina, OH

Symposium co-chair and co-editor

Atmospheric Corrosion

Liboria Mariaca-Rodriguez, Elisabete Almeida, Agnes de Bósquez, Ada Cabezas, Juan Fernando-Alvarez, Gunter Joseph, Marcelo Marrocos, Manuel Morcillo,¹ Julian Peña, Maria Rosario Prato, Susana Rivero, Blanco Rosales, Guillermo Salas, Jorge Uruchurtu-Chavarín, and Asdrubal Valencia

Marine Atmospheric Corrosion of Reference Metals in Tropical Climates of Latin-America

Reference: Mariaca-Rodriguez, L., Almeida, E., de Bósquez, A., Cabezas, A., Fernando-Alvarez, J., Joseph, G., Marrocos, M., Morcillo, M., Peña, J., Prato, M. R., Rivero, S., Rosales, B., Salas, G., Uruchurtu-Chavarín, J., and Valencia, A., “**Marine Atmospheric Corrosion of Reference Metals in Tropical Climates of Latin-America,**” *Marine Corrosion in Tropical Environments, ASTM STP 1399*, S. W. Dean, G. Hernandez-Duque Delgadillo, and J. B. Bushman, Eds., American Society for Testing and Materials, West Conshohocken, PA, 2000.

Abstract: This article presents the results obtained at 16 tropical test sites participating in the “Ibero-American Map of Atmospheric Corrosiveness” (MICAT), a project on atmospheric corrosion carried out during the period 1988-1994 at some 70 test sites distributed across 12 countries of the Latin-American region, Spain and Portugal.

The tropical climate and its different climatic variants are characterized by high average air temperatures, with considerable daily thermal fluctuations, high average relative humidity, and generally high precipitation volumes.

The work is structured in three main blocks: apparently unpolluted atmospheres (i), and marine atmospheres, differentiating between pure marine atmospheres (ii) and those in which both chloride (Cl⁻) and sulfur dioxide (SO₂) pollutants coexist (iii).

In each block an attempt was made to determine the role of the tropical climate in the magnitude of corrosion attack shown by four typical reference metals (mild steel, zinc, copper and aluminum) exposed for one-year periods in tropical atmospheric exposure conditions.

Keywords: atmospheric corrosion, tropical climates, mild steel, zinc, copper, aluminum.

Introduction

At room temperature in a perfectly dry atmosphere, metallic corrosion progresses at a very slow rate and for practical purposes can be ignored. However, when the metallic surface is wetted the corrosion process becomes more significant. The corrosion mechanism is electrochemical, the electrolyte being constituted either by an extremely

¹Head of the MICAT project, Centro Nacional de Investigaciones Metalúrgicas, Gregorio del Amo 8, 28040 Madrid (Spain). The affiliations of the authors, members of the MICAT Working Group, are indicated under “Acknowledgments.”

thin film of condensed moisture (just a few monolayers) or by an aqueous film up to hundreds of micrometers in thickness when the metal is perceptibly wetted, e.g., by dew, rain, mist, etc. With regard to the former it should be noted that a considerable part of the damage caused to structures and equipment by atmospheric corrosion can be attributed to the condensation of moisture (dew) during the periodic cooling of the air.

The atmospheric corrosion process is the sum of the individual corrosion processes that take place whenever an electrolyte layer forms on metals, i.e., the time of wetness (TOW) during which metallic corrosion is possible. ISO Classification of Corrosivity of Atmospheres (ISO 9223) estimates TOW as the number of hours/year during which RH \geq 80% and the air temperature (T) is simultaneously above 0°C.

It is universally accepted that the intensity of the atmospheric corrosion process is mainly determined by (i) the lifetime of the electrolyte film on the metal surface, (ii) the chemical composition of the atmosphere (air pollution by gases, acid vapours and seawater aerosols), and (iii) the air temperature. The participation of a large number of other factors is generally considered to be secondary.

With regard to precipitation, which contributes to the magnitude of TOW, it should not be forgotten that this can also play a beneficial role by washing off (removal) the atmospheric pollutants retained on the metallic surface, especially in strongly polluted atmospheres. Thus it is common to find situations where rain is rather less corrosive than dew or mist, which do not usually clean pollutants from the metallic surface.

The Tropical Climate in Ibero-America. General Considerations

The climate is a synthesis of the fluctuating combination of atmospheric conditions in a certain area, over a sufficiently long period of time to be geographically representative.

According to Köppen's classification [1], which distinguishes between 12 main climatological types, the tropical climate (type A) is represented by three variants: *Af* = tropical rain forest, *Aw* = tropical savannah, and *Am* = tropical monsoon.

Rychtera and Němcova [2], in the five climatic regions that they consider for the use of materials in the machinery and electricity industries, differentiate between humid and arid tropical climates. The humid tropical climate, which corresponds for instance to the tropical Latin-American region, is characterized by: (i) frequently high RH, (ii) high number of hours/year (6000 or more) during which RH \geq 70% and T \geq 0°C, and (iii) at least 7 months a year during which the maximum monthly average RH \geq 85% and the annual average temperature is \geq 10°C.

Of all the different climatic factors, consideration will be made of three in particular – thermometric regime, pluviometric regime and atmospheric humidity – due to their great influence on the atmospheric corrosion process.

The tropical climate in Latin-America [3] extends almost exactly from tropic to tropic, covering all of Central America, including the Antilles, and most of South America.

The tropical rain forest (*Af*) is characterized by the extraordinary uniformity (regularity) of temperatures throughout the year, something that does not occur in other climatic types; the formation of dew, common in this type of climates, occurs throughout most of the year. However, maximum temperatures are not excessive, and are often exceeded by summer maximums in temperate latitudes.

With regard to the pluviometric regime, this climate is characterized by an enormous variability, with great variations in total annual rainfall in different zones and even within one same zone. Almost all precipitation occurs in the form of prolonged showers (between two and four hours duration), usually coinciding with the hours of highest temperatures. During the rainy season it rains almost every day.

The tropical savannah (*Aw*) does not differ from the tropical rain forest (*Af*) in terms of its thermometric regime. The differences between these climates are of pluviometric type, by the existence in the former of a more or less prolonged dry season. In general, total annual rainfall values recorded in *Aw* zones are lower than in *Af* zones.

The tropical monsoon climate (*Am*) is an exaggeration of subtype *Aw*, from which it is barely distinguishable. The pluviometric regime is characterized by two conditions: (i) the total annual rainfall is the highest in the world, and (ii) there is a perfectly well-defined dry season.

On the basis of the preceding considerations, climatic subtypes can be classified by order of atmospheric corrosivity, the most corrosive being subtype *Af* (tropical rain forest), due to the non-existence of a dry season, and the least corrosive being subtype *Am* (tropical monsoon), which presents a long dry season (almost totally arid). Between these two is subtype *Aw* (tropical savannah).

The MICAT Project - Results Obtained at Tropical Test Sites

Prior to the MICAT project, data on atmospheric corrosion at tropical sites in Ibero-America was very scarce in the literature. Specific studies had been carried out only in Brazil [4], Cuba [5] and Panama [6], though considering a limited number of test sites. Thus there was a clear need for field studies in a sufficiently broad network of tropical test sites in order to consider the role of the tropical climate in the atmospheric corrosion of metals, both in rural atmospheres (unpolluted) and in atmospheres with chloride (Cl^-) and sulfur dioxide (SO_2) pollution.

The MICAT project was launched in 1988, sponsored by the Ibero-American Programme "Science and Technology for Development" (CYTED). Fourteen countries were involved in the project: Argentina, Brazil, Chile, Colombia, Costa Rica, Cuba, Ecuador, Mexico, Panama, Peru, Portugal, Spain, Uruguay and Venezuela. Research was conducted both at laboratories and in a network of 75 atmospheric exposure test sites throughout the Latin-American region, considering a broad spectrum of climatological and pollution conditions.

Experimental

The organizational structure, methodology and some results have been given elsewhere [7]. Though with its own peculiarities, the MICAT project has basically followed the experimental methodology of the ISOCORRAG collaborative programme [8].

A final report on the MICAT project has been published [9], considering the large number of atmospheric test sites from the point of view of atmospheric aggressivity (according to ISO 9223), without entering into an analysis of the different climatic types.

6 MARINE CORROSION IN TROPICAL ENVIRONMENTS

The materials investigated were reference metals, in the form of flat plate specimens, with the following characteristics: mild steel (unalloyed, low carbon), zinc (98.5% min.), copper (99.5% min.), and aluminum (99.5% min.).

Specimens were withdrawn from the test sites after one year (for three consecutive years), two, three and four years of atmospheric exposure. On each occasion, four specimens of each material were withdrawn, three of which were used to determine weight losses, according to ISO Determination of Corrosion Rate of Standard Specimens for the Evaluation of Corrosivity (ISO 9226). The fourth specimen was used for laboratory studies: analysis of corrosion products, microscopic examination of the morphology of the corrosion products layer and attack of the base metal, etc.

This work focuses on the main results obtained at 16 tropical MICAT test sites. Figure 1 indicates the location of the tropical network of atmospheric test sites. The names, codes and some environmental features of the test sites are listed in Table 1.

Table 1 - Environmental characteristics of tropical MICAT test sites. The data in columns 5-10 are average values for the first three years of atmospheric exposure.

Code	Name	Country	Climate ¹	T, °C	RH, %	TOW ²	An. Precip.,	Dep. rate, mg/m ² .d		ISO
							mm	Cl ⁻	SO ₂	
B8	Belem	Brazil	Af	26.4	86	τ_5	2466	(*)	(*)	S ₀ P ₀
PE6	Pucallpa	Peru	Af	26.1	81	τ_5	1369	(*)	(*)	S ₀ P ₀
C03	Cotove	Colombia	Aw	27.0	76	τ_4	900	(*)	0.3	S ₀ P ₀
EC1	Guayaquil	Ecuador	Aw	25.9	76	τ_4	599	1.5	3.0	S ₀ P ₀
PA4	Chiriqui	Panama	Am	27.1	68	τ_4	2225	8.7	8.2	S ₁ P ₀
CR4	Sabanilla	Costa Rica	Aw	19.9	83	τ_5	1780	11.3	4.9	S ₁ P ₀
V4	Matanzas	Venezuela	Aw	27.7	75	τ_4	990	15.9	9.3	S ₁ P ₀
M4	Acapulco	Mexico	Aw	27.6	76	τ_4	870	23.8	9.6	S ₁ P ₀
CR1	Puntarenas	Costa Rica	Aw	28.0	80	τ_4	1598	33.4	7.1	S ₁ P ₀
CR2	Limon	Costa Rica	Af	25.4	88	τ_5	3531	220.0	3.5	S ₂ P ₀
CU3	Bauta	Cuba	Aw	24.0	81	τ_4	1488	6.4	16.4	S ₁ P ₁
PA3	Veraguas	Panama	Am	27.2	70	τ_4	2278	14.8	16.5	S ₁ P ₁
PA1	Panama	Panama	Aw	26.9	71	τ_4	1557	9.8	21.7	S ₁ P ₁
CU1	Ciq	Cuba	Aw	25.2	79	τ_4	1347	12.0	31.6	S ₁ P ₁
PA2	Colon	Panama	Am	27.1	77	τ_5	3950	16.8	47.4	S ₁ P ₂
CU2	Cojimar	Cuba	Aw	25.1	79	τ_4	1311	104.0	22.5	S ₂ P ₁

¹ Climatic classification according to Köppen [1]

² Time of wetness classification according to ISO 9223

³ Pollution classification by chloride (S) and SO₂ (P) according to ISO 9223

*Apparently uncontaminated

Figure 2 shows the tropical test sites considered in this research according to their Cl⁻ and SO₂ pollution categories, established by ISO 9223, ordered into three groups:

- (i) Rural, very low Cl⁻ (≤ 3 mg/m²/d) and SO₂ (≤ 10 mg/m²/d) pollution,
- (ii) Pure Marine, very low SO₂ pollution (≤ 10 mg/m²/d), and
- (iii) Mixed Marine, polluted by SO₂ (> 10 mg/m²/d).

The results considered in this work correspond to the 3 one-year periods of atmospheric exposure in tropical MICAT tests sites. The average corrosion rates for these 3 one-year exposure periods and the nature of the corrosion products found on the reference metals are indicated in Tables 2-4.

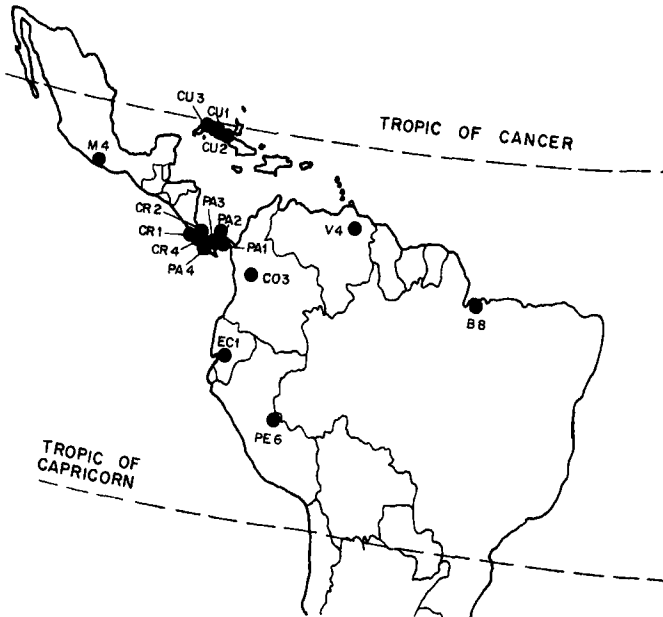


Figure 1 - Network of tropical MICAT test sites

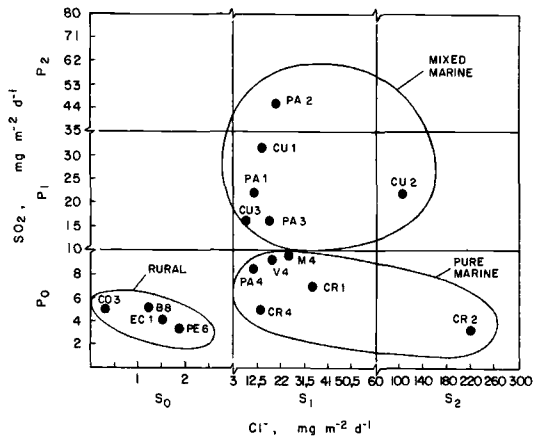


Figure 2 - Classification, according to ISO 9223, of tropical MICAT test sites on the basis of measured levels of SO₂ and Cl⁻ atmospheric pollution during the first three years of exposure

Table 2 - Average first year corrosion rates (and the corresponding corrosivity categories of the atmosphere) and nature of corrosion products in reference metals exposed during one year at rural tropical test sites participating in the MICAT project. Data are average values of 3 one-year exposures.

Test site (Table 1)	Mild steel			Zinc			Copper			Aluminum		
	Corr. rate $\mu\text{m}/\text{y}$	Corr. Category ¹	Corr. products	Corr. rate $\mu\text{m}/\text{y}$	Corr. Category ¹	Corr. products	Corr. rate $\mu\text{m}/\text{y}$	Corr. Category ¹	Corr. products	Corr. rate $\text{g}/\text{m}^2\cdot\text{y}$	Corr. Category ¹	Corr. products
Belem	19.4	C2	L,G	1.10	C3	...	0.64	C3	Cu,At	0.22	Negligible	N
Pucallpa	14.3	C2	L,G	1.01	C3	Z,H	0.56	C2	Cu	0.03	Negligible	N
Cotovo	19.6	C2	L,G	3.30	C4	Z	0.73	C3	Cu	0.11	Negligible	-
Guayaquil	22.6	C2	L	0.21	C2	Z	0.71	C3	Cu	0.03	Negligible	N

Table 3 - Average first year corrosion rates (and the corresponding corrosivity categories of the atmosphere) and nature of corrosion products in reference metals exposed during one year at pure marine tropical test sites participating in the MICAT project. Data are average values of 3 one-year exposures.

Test site (Table 1)	Mild steel			Zinc			Copper			Aluminum		
	Corr. rate $\mu\text{m}/\text{y}$	Corr. Category ¹	Corr. products	Corr. rate $\mu\text{m}/\text{y}$	Corr. Category ¹	Corr. products	Corr. rate $\mu\text{m}/\text{y}$	Corr. Category ¹	Corr. products	Corr. rate $\text{g}/\text{m}^2\cdot\text{y}$	Corr. Category ¹	Corr. products
Chiriqui	23.0	C2	G,L,Mg	0.64	C2	...	2.71	C4
Sabanilla	16.6	C2	L,G	0.72	C3	H,CZ	1.23	C3	Cu	0.14	Negligible	N
Matanzas	23.0	C2	L,G	2.73	C4	...	0.95	C3	...	0.28	Negligible	...
Acapulco	22.1	C2	L,G,M	1.79	C3	S,Z,H	1.23	C3	Cu,At	1.63	C3	...
Puntarenas	61.6	C4	L,G,Mg	20.5	C3	H,CB	2.98	C5	Cu,At	1.93	C3	A
Limón	371.5	>C5	L,G,M	2.66	C4	H,CB	3.68	C5	Cu,At	0.86	C3	A

Table 4 - Average first year corrosion rates (and the corresponding corrosivity categories of the atmosphere) and nature of corrosion products in reference metals exposed during one year at mixed marine tropical test sites participating in the MICAT project. Data are average values of 3 one-year exposures.

Test site (Table 1)	Mild steel			Zinc			Copper			Aluminum		
	Corr. rate $\mu\text{m}/\text{y}$	Corr. Category ¹	Corr. products	Corr. rate $\mu\text{m}/\text{y}$	Corr. Category ¹	Corr. products	Corr. rate $\mu\text{m}/\text{y}$	Corr. Category ¹	Corr. products	Corr. rate $\text{g}/\text{m}^2\cdot\text{y}$	Corr. Category ¹	Corr. products
Bautá	33.8	C3	L,G	1.22	C3	H,S	1.80	C4	Cu,At,An Br,Co	0.99	C3	N
Veraguas	20.2	C2	L,G,Mg	1.49	C3	...	1.89	C4
Panama	27.6	C3	L,G,Mg	1.06	C3	...	1.24	C3	...	0.43	C2	...
Ciudad	30.4	C3	G,L	1.20	C3	S,CZ	1.45	C4	Cu	1.11	C3	N
Colón	108.0	C5	G,L	3.60	C4	...	5.25	C5
Cajamar	268.3	<C5	M,L,G	7.09	C5	S,CZ,H	4.89	C5	Cu,At	3.01	C4	N

¹ According to ISO 9223, based on 1st year corrosion rate: ... Not available; L: Lepidocrocite ($\delta\text{-FeOOH}$); Mg: Magnetite ($\delta\text{-Fe}_2\text{O}_3$); M: Magnetite (Fe_3O_4); Z: Zincite (ZnO); H: Hydrozincite ($\text{Zn}_2(\text{CO}_3)(\text{OH})_2$); CZ: Zinc carbonate (ZnCO_3); S: Simonkolleite ($\text{Zn}_2\text{Cl}_2(\text{OH})_2\cdot\text{H}_2\text{O}$); CB: Basic zinc carbonate ($\text{Zn}_2\text{CO}_3(\text{OH})_2$); Cu: Cuprite (Cu_2O); At: Atacamite ($\text{Cu}_2\text{Cl}(\text{OH})_2$); An: Antlerite ($\text{Cu}_3\text{SO}_4(\text{OH})_4$); Br: Brochantite ($\text{Cu}_2\text{SO}_4(\text{OH})_2$); Co: Covellite (CuS); A: Alumina ($\delta\text{-Al}_2\text{O}_3$); N: No corrosion product detected

Discussion

The discussion is structured in three main blocks: (i) apparently unpolluted atmospheres ($Cl^- \leq 3 \text{ mg/m}^2/\text{d}$ and $SO_2 \leq 10 \text{ mg/m}^2/\text{d}$), and marine atmospheres, in turn differentiating between (ii) pure marine atmospheres ($SO_2 \leq 10 \text{ mg/m}^2/\text{d}$), and (iii) those in which both chloride and SO_2 pollutants coexist ($SO_2 > 10 \text{ mg/m}^2/\text{d}$).

In each block an attempt is made to determine the role of the tropical climate in the magnitude of corrosion attack shown by four typical reference metals (mild steel, zinc, copper and aluminum) exposed for one-year periods in tropical atmospheric exposure conditions.

Rural Atmospheres (Apparently Unpolluted by Cl^- and SO_2)

Table 2 displays the corrosion data recorded at tropical MICAT test sites of this atmospheric type.

In the absence of atmospheric pollution, metallic corrosion should depend mainly on meteorological factors, and thus analysis of the corrosion observed in this type of atmospheres can shed light on the effect of climate on atmospheric corrosion.

It is common to read in the literature [6,10] that a material subjected to the action of tropical climates corrodes more than when it is exposed to temperate climates. But is this completely true? Can this behaviour be generalized to all metals? In principle, it may be thought that the singularities of the tropical climate (high average T, RH and pluviocity), promoting a high TOW of metallic surfaces, would lead to high atmospheric corrosion rates. However, this is not necessarily always so, as corrosion rates ultimately also depend on the deposition and retention of atmospheric pollutants in the aqueous films that form on metallic surfaces.

The MICAT project, which included a relatively high number of rural atmospheres (19) in different climatic regions [9] can provide some information in this respect. Table 5 displays average corrosion rate values recorded for mild steel, zinc, copper and aluminum during one-year atmospheric exposure in different climates.

Table 5 - Average first year corrosion rates in rural atmospheres [9] versus prevailing climate in the atmosphere surrounding the test site

Climate		Number of MICAT test sites [9]	Ave. Corrosion rates			
Type	Köppen Clas. [1]		Mild steel $\mu\text{m}/\text{y}$	Zinc $\mu\text{m}/\text{y}$	Copper $\mu\text{m}/\text{y}$	Aluminum $\text{g}/\text{m}^2\cdot\text{y}$
Tropical	A	5	17.9	1.40	0.59	0.13
Arid	B	2	10.2	0.22	0.19	0.05
Temperate	C	12	11.7	0.87	0.88	0.12

As could be expected, the lowest corrosion rates are presented for type B climates (arid) according to Köppen's climatic classification [1]. Tropical climates (type A) promote the highest corrosion rates for mild steel and zinc, but not for copper, whose highest corrosion rates correspond to temperate climates (type C). Possible causes of this differential behaviour of copper will be considered below. As to the behaviour of aluminum, no differentiation can be made on the grounds of climatic type as attack of this metal is not significant in unpolluted atmospheres (annual corrosion $< 0.3 \text{ g}/\text{m}^2$). The

weight losses obtained when calculating corrosion rates in the laboratory may be attributed to attack by the chemical cleaning agent used rather than to an atmospheric corrosion process [9].

It is not possible to make an analysis of the influence of the different climatic subtypes in tropical atmospheres (rain forest or savannah) on atmospheric corrosion due to the small number of test sites corresponding to each subtype.

The following are some comments on the characteristics of the atmospheric corrosion process of the different metals in unpolluted (rural) tropical atmospheres (Table 2).

Mild Steel - Despite the aforementioned effect of climate on promoting the corrosion rate, the aggressivities of these unpolluted atmospheres for mild steel are low (category C2 of ISO 9223).

Corrosion products are usually mainly composed of lepidocrocite (γ -FeOOH). As exposure time increases there is a partial transformation from lepidocrocite to goethite (α -FeOOH), in a similar way to what occurs in temperate climates. Figures 3 A-B display the typical small lamellar and acicular open structures characteristic of lepidocrocite and quasi-amorphous goethite aggregates (like small cotton balls).

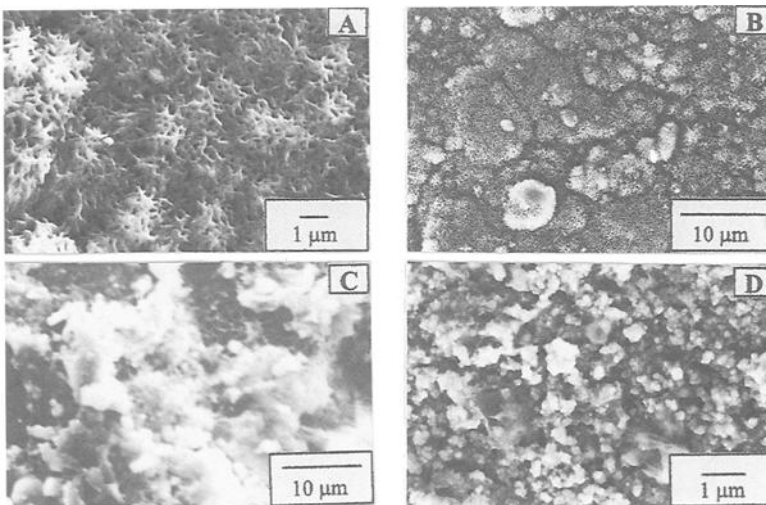


Figure 3 - Scanning Electron micrographs (SEM) showing microstructures of lepidocrocite (A) and goethite (B), zincite (C), and cuprite (D) formed on mild steel, zinc and copper respectively during exposure in tropical rural atmospheres

Zinc - The aggressivity of these types of atmospheres for zinc is variable, from low (Guayaquil, category C2) to high (Cotove, category C4). High TOW values favour the corrosion process, and attack rates of more than $1 \mu\text{m}/\text{y}$ are generally found.

Corrosion products tend to be comprised by zincite (ZnO) and hydrozincite ($\text{Zn}_5(\text{CO}_3)_2(\text{OH})_6$), Fig. 3C, though the small thickness of the latter phase often causes it to disappear in X-Ray Diffraction analysis (XRD).

Copper - Contrary to the cases of mild steel and zinc, copper in rural tropical atmospheres does not tend to show high attack rates; annual copper corrosion ($0.6\text{-}0.7$

μm) being lower than that exhibited in temperate type climates where it can reach $2 \mu\text{m}$ [9]. There is no clear explanation for the differential behaviour of copper from the other reference metals, though it could be that the high volumes of precipitation generally recorded in tropical atmospheres have the effect of washing off background atmospheric pollution, with which the copper has a great affinity, as is noted by Graedel [11], thus reducing the probability of its retention in corrosion product films.

Due to this affinity of copper for background pollution of the atmosphere, which is confirmed by the presence of basic sulphates and chlorides among the corrosion products [9], the corrosion rates presented by this metal in rural atmospheres of temperate climates are greater than those expected for unpolluted atmospheres.

Corrosion products tend to be composed practically exclusively of cuprite (Cu_2O), which appears in a granular and discontinuous form on the copper surface, configuring open structures of poor compactness (Fig. 3D).

Aluminum - As has been mentioned above, in these types of atmosphere aluminum does not undergo significant attack. Deterioration, if any, consists of soiling by dust particles, loss of shine and tarnishing of the surface. The data displayed in Table 2 can be attributed to attack by the chemical cleaning reagent used for the determination of weight losses, rather than to an atmospheric corrosion process [9].

Marine Atmospheres

Similarly to the case of rural atmospheres, a first criterion could be to question whether the characteristics of the humid type tropical climate being considered has a significant influence on the atmospheric corrosion rate of metals exposed there.

In an attempt to answer this question, one possible approach would be to consider damage functions (regression equations) that relate corrosion rates and environmental parameters and observe the influence of the different climatic parameters: T, RH, TOW, precipitation, etc. A very significant effect of one or more of these parameters on the metallic corrosion rate would permit conjectures on the role played by the tropical climate on the magnitude of the corrosion process.

Table 6 presents damage functions obtained in the MICAT project [9] for one-year corrosion of the different metals as a function of statistically significant environmental variables. For their obtainment, using a statistical computer program (BMDP), consideration was made of all the individual annual data (N) corresponding to corrosion in one-year exposure obtained during the MICAT project at some 70 test sites, irrespective of the type of atmosphere or climate. Table 6 also shows the multiple correlation coefficient (R) and the correlation coefficient R_{Cl} , with only Cl intervening as a variable. It is clear to see the enormous weight of Cl in the multiple correlation coefficient, indicating the importance of this variable in the overall atmospheric corrosion at MICAT test sites. Due to its significance, SO_2 pollution becomes a secondary environmental variable in the cases of mild steel, copper and aluminium.

With regard to climatic variables (T, RH, TOW, P), these intervene in the regression equation with such a low weight as to preclude the possibility of obtaining indications about the effect of the tropical climate on the atmospheric corrosion of the different metals.

Another approach to the question of the effect of climate on corrosion in marine atmospheres would be to make comparisons, not in general terms as above, but in an

individualized way for each type of atmosphere. This can be done by comparing pairs of test sites, one in a tropical climate and another in a temperate climate, whose characteristics from the point of view of atmospheric pollution are very similar.

In the following discussion, this second approach will be used occasionally to try to analyse in greater detail the effect of climate in these types of atmosphere.

Table 6 - Relationships between the annual corrosion of mild steel, zinc, copper and aluminum and the environmental parameters [9]

Equations	Remarks
$C_{Fe} = 2.49 + 1.59 S + 0.96 Cl$ N = 172 R = 0.75 $R_{Cl} = 0.70$	C_{Fe} = mild steel annual corrosion (μm)
$C_{Zn} = 2.0493 + 0.0351 RH + 0.0006 P + 0.0234 Cl$ N = 141 R = 0.72 $R_{Cl} = 0.66$	C_{Zn} = zinc annual corrosion (μm) C_{Cu} = copper annual corrosion (μm) C_{Al} = aluminum annual corrosion (μm) T = temperature annual average ($^{\circ}\text{C}$) RH = relative humidity annual average (%) TOW = time of wetness (annual fraction)
$C_{Cu} = -0.9789 + 1.6275 TOW - 0.0002 P + 0.0166 S + 0.0118 Cl$ N = 155 R = 0.77 $R_{Cl} = 0.64$	P = annual precipitation (mm) S = SO_2 pollution annual average ($\text{mgSO}_2/\text{m}^2.\text{d}$) Cl = chloride pollution annual average ($\text{mgCl}/\text{m}^2.\text{d}$)
$C_{Al} = -0.5767 + 0.0356 T + 1.0654 TOW - 0.0004 P + 0.0222 S + 0.0071 Cl$ N = 146 R = 0.67 $R_{Cl} = 0.50$	R = multiple correlation coefficient R_{Cl} = chloride correlation coefficient

Pure Marine Atmospheres (very low SO_2 pollution: $< 10 \text{ mg}/\text{m}^2/\text{d}$)

Table 3 indicates the annual corrosion rate and corrosion products found for the different metals in atmospheres of this type. The test sites have been ordered in the table according to increasing atmospheric salinity.

Mild Steel - The corrosion rate increases with the chloride content of the atmosphere [12]. The aggressivity of atmospheres in zones very close to the coast (e.g., Limon) can exceed category C5 indicated by ISO 9223.

The different phases found in the corrosion products (Fig. 4A), in addition to lepidocrocite and goethite, also include maghemite ($\gamma\text{-Fe}_2\text{O}_3$) and magnetite (Fe_3O_4). The appearance of akagenite ($\beta\text{-FeOOH}$) is not observed after one-year atmospheric exposure. Maghemite is originated by the transformation of goethite [13] and possesses a defective spinel structure. Its presence seems to be associated with high air temperatures; in the MICAT project this phase was only clearly detected in tropical atmospheres [9]. Magnetite is usually found in the lower strata of corrosion product layers, close to the base steel, which in these atmospheres tends to present a saw-tooth attack profile due to the existence of pitting phenomena resulting from the action of the chloride ion. The corrosion product layers exhibit two differentiated zones: one very compact inner zone, comprised almost exclusively by magnetite, and another outer zone which is furrowed by parallel fissures along which exfoliation is oriented (Fig. 4B), this being a typical phenomenon in atmospheres of high salinity.

Zinc - The corrosion rate increases slightly with the chloride content in the atmosphere, though to a lesser extent than in the case of mild steel, something which does not occur in atmospheres of this type in other climatic regions. In other such regions

annual corrosion is rather high (up to 7 μm) and it is common to encounter simonkoellite ($\text{Zn}_5\text{Cl}_2(\text{OH})_8 \cdot \text{H}_2\text{O}$) among the corrosion products.

All the signs seem to be that the frequent washing of the zinc surface by precipitation in these tropical atmospheres presents an obstacle to the interaction of the chloride ion and the zinc surface. The low thickness of the corrosion product layers facilitate this washing action. In fact, simonkoellite was only found among the corrosion products formed in the tropical atmosphere of Acapulco, which has a relatively low precipitation rate (Table 1). The chloride ion also favours the formation of pitting on the base metal (Fig. 4C).

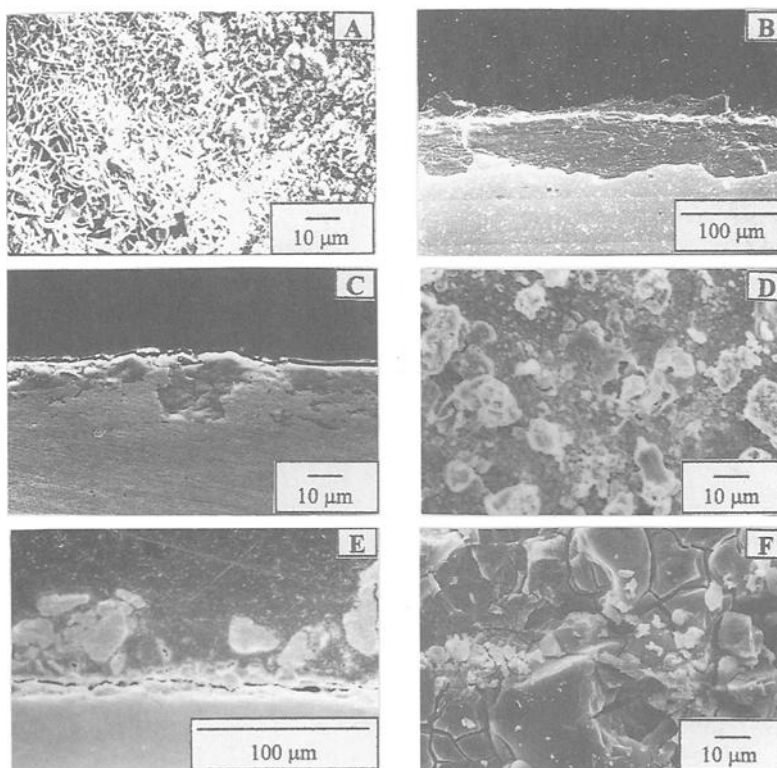


Figure 4 - SEM micrographs of mild steel (A, B), zinc (C), copper (D, E) and aluminum (F) surfaces after exposure in the tropical pure marine atmosphere of Acapulco

Copper - The corrosion rate increases with the chloride content in the atmosphere. The aggressivity of these atmospheres to copper is high, reaching up to ISO 9223 category C5 (Limon), and once again the aforementioned affinity of copper for background atmospheric pollution is seen (presence of basic sulphates among corrosion products). There seems to be a critical salinity level around 20 $\text{mg Cl}^-/\text{m}^2/\text{d}$ after which the action of the chloride ion is clearly noted [9], with the formation of atacamite ($\text{Cu}_2\text{Cl}(\text{OH})_3$) among the corrosion products. This grows in a disorderly and irregular way on the cuprite film initially formed on the copper surface (Fig. 4D). The corrosion

product layers present a rough, imperfect structure of low compactness, with great internal porosity (Fig. 4E).

The tonality of the patinas that form on copper in this type of atmospheres is lighter than the typical brown-red shades of copper in rural atmospheres, and with exposure time they acquire greenish spots due to the formation of basic chlorides on the surface.

Aluminum - In a similar way to copper, there seems to be a critical salinity level, around 25 mg Cl⁻/m²/d, above which the chloride ion interacts more effectively with the aluminum surface [9], giving rise to the formation of pits which is the typical attack of aluminum in the atmosphere. Aluminum in the marine atmospheres with salinities of less than 25 mg Cl⁻/m²/d (Chiriqui, Sabanilla and Matanzas) behaves in a similar way to in unpolluted rural atmospheres, i.e., is without significant attack.

Bearing in mind the high salinity of Limon atmosphere (220 mg Cl⁻/m²/d), higher attack rates of the aluminum would be expected than at Acapulco or Puntarenas, which have much lower salinities (24 and 33 mg Cl⁻/m²/d), but in fact the reverse is true. The reason for this apparently anomalous behaviour may lie in the high rainfall of Limon atmosphere (3531 mm), in contrast with the relatively low pluviosity of Acapulco and Puntarenas (particularly the former with 870 mm). The frequent washing of the aluminum surface in Limon atmosphere must in some way impede interaction between the chloride anion and the aluminium surface, and thus slow down the appearance of pits, which otherwise would be more numerous due to the high atmospheric salinity of Limon atmosphere.

Only on specimens with abundant pitting was it possible to detect alumina (δ -Al₂O₃) among the corrosion products (Fig. 4F).

Mixed Marine Atmospheres (polluted by SO₂: > 10 mg SO₂/m²/d)

Table 4 indicates the annual corrosion rates and corrosion products found for the different metals in atmospheres of this type.

Mild Steel - The corrosion products found on mild steel in this type of atmospheres are the same as in pure marine atmospheres: lepidocrocite (γ -FeOOH), goethite (α -FeOOH), maghemite (γ -Fe₂O₃) and magnetite (Fe₃O₄). From detailed observation of Table 4 it can be inferred that as the chloride content in the atmosphere increases, so the predominant phase ceases to be lepidocrocite and becomes goethite, or even magnetite when atmospheric salinity is higher. Considering all MICAT test sites of this type (tropical or otherwise), only the tropical atmospheres (Ciq, Colon and Cojimar) favour a rapid transformation (already observed in the first year of exposure) from lepidocrocite to goethite or even magnetite, depending on atmospheric salinity. The high average air temperature and RH of tropical atmospheres may favour these phase transformations in the corrosion products. According to Misawa et al. [14], the dissolution of SO₂ in the moisture layer also favours the lepidocrocite to goethite transformation.

The corrosion rate increases with the atmospheric Cl⁻ and SO₂ content, a synergetic effect being observed between these two pollutants. This is the case in Colon atmosphere, where despite a not particularly high salinity (16.8 mg Cl⁻/m²/d), similar to that of Veraguas (14.8 mg Cl⁻/m²/d), the simultaneous presence of relatively high SO₂ levels (47.4 mg SO₂/m²/d) promotes high attack rates of the steel (corrosivity category C5 of ISO 9223). In Veraguas atmosphere, on the other hand, annual steel corrosion is

only 20 μm . The corrosion product films formed in these atmospheres (Fig. 5A) are compact, though with abundant fissures parallel to the surface along which exfoliation is oriented, as occurs in the pure marine atmosphere of Acapulco.

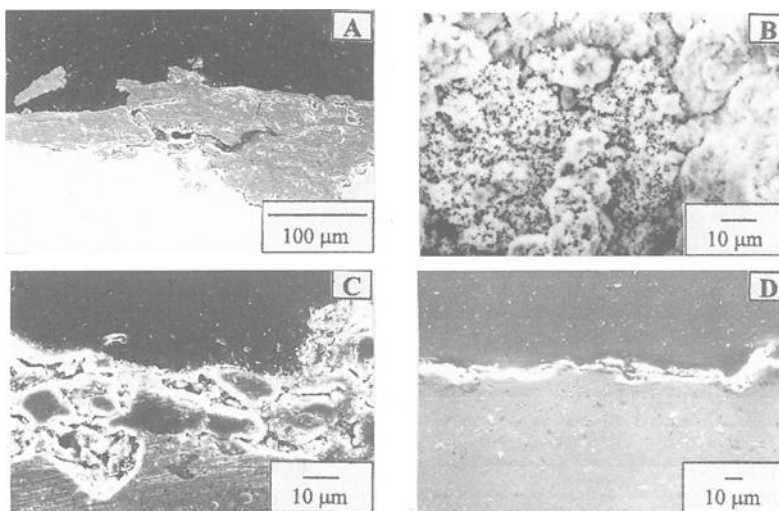


Figure 5 - SEM micrographs of mild steel (A), zinc (B, C) and aluminum (D) surfaces after exposure in tropical mixed marine atmospheres

Zinc - As in the case of mild steel, zinc corrosion increases with the chloride content of the atmosphere, reaching up to ISO 9223 atmospheric aggressivity category C5. It is also possible to observe the aforementioned synergetic effect of the combined action of Cl^- and SO_2 pollutants (e.g., the high zinc corrosion rate presented in Colon atmosphere, see Table 4).

Among the corrosion products (Fig. 5 B and C) it is common to find simonkoellite ($\text{Zn}_5\text{Cl}_2(\text{OH})_8\cdot\text{H}_2\text{O}$), together with zinc carbonates (ZnCO_3) and/or hydrozincite ($\text{Zn}_5(\text{Cu}_3)_2(\text{OH})_6$), which does not occur in atmospheres of this type in other climatic regions [9].

Copper - Similarly to mild steel and zinc, the copper corrosion rate in this type of atmospheres increases with the chloride content of the atmosphere, it again being possible to observe the aforementioned synergetic effect of the combined action of both pollutants (see the high copper corrosion rate for Colon atmosphere in Table 4).

With regard to the nature of the corrosion products formed in these atmospheres, not much information is available. In addition to cuprite, basic copper chlorides are also detected, very probably coexisting with basic sulphates that give the patinas their characteristic greenish colours.

Aluminum - This material presented pitting in all the tropical atmospheres of this type considered in the MICAT project (Fig. 5D). However, the pluviosity of the region can decay the apparition of the pitting phenomenon. This is the case of Panama test site (1557 mm) where to the naked eye the upward facing side of the specimens appeared free

of pitting (due to the washing action of the rain), while the material on the downward facing side (protected from the rain) already exhibited abundant pitting.

In other atmospheres of this type [9], though not tropical and with low pluviosity (e.g., Valparaiso with 463 mm) and similar salinity to Panama atmosphere, the upward facing side exhibited abundant pitting and total aluminum corrosion was 3.56 g/m^2 compared with 0.43 g/m^2 at Panama.

Aluminum corrosion in this type of atmospheres increases with the chloride content of the atmosphere, and the aforementioned synergetic effect promoted by the combined action of both pollutants is considerably exacerbated in this metal.

Conclusions

The tropical climates in Latin-America are characterized by high average air temperatures (with great daily thermometric fluctuations), high relative humidity and generally high precipitation volumes.

As a result of the research carried out at 16 tropical test sites in this region the following conclusions, that are not intended to be universally valid but to reflect certain tendencies, are drawn:

- In rural tropical atmospheres, with very low pollution by Cl^- ($\leq 3 \text{ mg/m}^2/\text{d}$) and SO_2 ($\leq 10 \text{ mg/m}^2/\text{d}$), the annual corrosion of mild steel and zinc is greater than that found in temperate climates. In the case of copper the reverse is true, possibly because the frequent rainfall in this type of atmosphere washes out the background pollution with which copper has a great affinity, reducing the annual corrosion of this metal. Insignificant attack was observed on the aluminum specimens.
- In pure marine tropical atmospheres ($\text{SO}_2 \leq 10 \text{ mg/m}^2/\text{d}$) atmospheric salinity is the main factor affecting corrosion. The annual corrosion rate increases with the chloride content of the atmosphere. In the case of zinc and aluminium, annual corrosion rates are somewhat lower than envisaged, a fact which could be attributed to the washing of the metallic surface by the abundant precipitation. The high average air temperatures favour the transformation from lepidocrocite ($\gamma\text{-FeOOH}$) to goethite ($\alpha\text{-FeOOH}$) in the atmospheric corrosion products on mild steel.
- In mixed marine atmospheres (polluted by SO_2) the corrosion of all four reference metals increases with the Cl^- and SO_2 content in the atmosphere. Here again, the high average air temperatures favour $\gamma\text{-FeOOH}$ to $\alpha\text{-FeOOH}$ transformations and the high pluviosity delays the appearance of pitting on rain-exposed aluminium surfaces.

Acknowledgments

This paper is a small homage of the Ibero-American MICAT group to Liboria Mariaca, who generously dedicated the final years of her life to the MICAT project. L. Mariaca died in a car crash in Mexico on 12 th November 1999.

The MICAT Working Group: L. Mariaca (Instituto de Investigaciones Eléctricas, Cuernavaca, México), E. Almeida (Instituto Nacional de Engenharia e Tecnologia Industrial, Lisbon, Portugal), A. F. de Bósquez (Universidad de Panamá, Panamá, Panamá), A. Cabezas (Centro de Investigaciones Químicas, Habana, Cuba), J. Fernando-Alvarez (Instituto Tecnológico de Costa Rica, Cartago, Costa Rica), G. Joseph

(Universidad de Chile, Santiago, Chile), M. Marrocos (Centro de Pesquisas de Energia Elétrica, Rio de Janeiro, Brazil), M. Morcillo (Centro Nacional de Investigaciones Metalúrgicas, Madrid, Spain), J. Peña (Escuela Superior Politécnica del Litoral, Guayaquil, Ecuador), M. R. Prato (Centro de Investigaciones Tecnológicas, Coro, Venezuela), S. Rivero (Universidad de la República Oriental del Uruguay, Montevideo, Uruguay), B. Rosales (Instituto de Investigaciones Científicas y Técnicas de las Fuerzas Armadas, Buenos Aires, Argentina), G. Salas (SENATI, Lima, Perú), J. Uruchurtu (Instituto de Investigaciones Eléctricas, Cuernavaca, México) and A. Valencia (Universidad de Antioquia, Medellín, Colombia).

References

- [1] Köppen, W., "Das Geographische System der Klimate" in *Handbuch der Klimatologie*, 3, Gebruder, Berlin, 1936.
- [2] Rychtera, M. and Nemcova, B., *The Climatic Map for Electrical and Machine Industry*. Kartografické nakladatelství, Prague, 1969.
- [3] Jansá, J. M., *Curso de Climatología*. Instituto Nacional de Meteorología, Madrid, 1969.
- [4] Dutra, A. C. and Vianna, R. O., "Atmospheric Corrosion Testing in Brazil," *Atmospheric Corrosion*, W. H. Ailor, Ed., John Wiley, New York, 1982, pp. 755-774.
- [5] Corvo, F., "Atmospheric Corrosion of Steel in Humid Tropical Climate. Influence of Pollution, Humidity, Temperature, Rainfall and Sun Radiation," *Corrosion*, 40(4), 1984, p. 170.
- [6] Southwell, C. R. and Bultman, J. D., "Atmospheric Corrosion Testing in the Tropics," *Atmospheric Corrosion*, W. H. Ailor, Ed., John Wiley, New York, 1982, pp. 943-967.
- [7] Morcillo, M., "Atmospheric Corrosion in Ibero-America: The Micat Project," *Atmospheric Corrosion, ASTM STP 1239*, W. W. Kirk and H. H. Lawson, Eds., American Society for Testing and Materials, Philadelphia, 1995, pp.257-275.
- [8] Knotkova, D. and Vrobel, L., "ISOCORRAG: The International Testing Program with ISO/TC156/WG 4." Proc. 11th International Corrosion Congress, Vol. 5, AIM, Milano, 1990, p. 5.581.
- [9] Several authors, *Corrosión y Protección de Metales en las Atmósferas de Iberoamérica. Parte I – Mapas de Iberoamérica de Corrosividad Atmosférica*, M. Morcillo, E. Almeida, B. Rosales, J. Uruchurtu and M. Marrocos, Eds., CYTED, Madrid, 1999.
- [10] Delrieu, A., *La Tropicalisation*, Desforges, Paris, 1974.
- [11] Graedel, T. E., Nassau, K. and Franey, J. P., "Copper Patinas Formed in the Atmosphere - I. Introduction," *Corrosion Science*, 27, 1987, p. 639.
- [12] Morcillo, M., Chico, B., Otero, E. and Mariaca, L., "Effect of Marine Aerosol on Atmospheric Corrosion," *Materials Performance*, 38(4), 1999, p. 72.
- [13] Leidheiser, Jr. H. and Music, S. "The Atmospheric Corrosion of Iron as Studied by Mössbauer Spectroscopy." *Corrosion Science* , 22 (1982) 1089.
- [14] Misawa, T., Asami, K., Hashimoto, K. and Shimodaira, S., "The Mechanism of Atmospheric Rusting and the Protective Amorphous Rust on Low Alloy Steel," *Corrosion Science*, 14, 1974, p. 279.

Johan Tidblad,¹ Alexander A. Mikhailov,² and Vladimir Kucera¹

Application of a Model for Prediction of Atmospheric Corrosion in Tropical Environments

Reference: Tidblad, J., Mikhailov A. A., and Kucera V., “**Application of a Model for Prediction of Atmospheric Corrosion in Tropical Environments,**” *Marine Corrosion in Tropical Environments, ASTM STP 1399*, S. W. Dean, G. Hernandez-Duque Delgadillo, and J. B. Bushman, Eds., American Society for Testing and Materials, West Conshohocken, PA, 2000.

Abstract: Based on analysis of data from field exposure programs within, e.g., UN ECE and ISO CORRAG a model describing atmospheric corrosion of common technical metals has been developed. The model uses environmental parameters that are easily available on different geographical scales. The combination of temperature and relative humidity can be used to express the time of wetness based on a probability model for the prediction of time of wetness from annual temperature and relative humidity data. The sulfur dioxide air concentration and the chloride deposition are included in different parts of the model and these two parts contain separate expressions for the combination of temperature and relative humidity (or temperature and time of wetness). This makes it possible to apply the model in marine areas with different deposition of chlorides and different pollution levels. The development of the model has contributed to a better understanding of the conditions for atmospheric corrosion, including tropical regions. The individual terms of the model have been adapted using physical and chemical principles. This makes the model useful for predictions also in regions outside those defining the original data set. Examples of independent data from field exposures not included in the model development are shown and discussed.

Keywords: atmospheric corrosion, tropical environment, marine atmosphere, modelling, dry and wet deposition, temperature effect, time of wetness

Introduction

The frequent use of metals in outdoor constructions and the huge cost caused by corrosion damage are the reason for the extensive research of the process of atmospheric corrosion. Numerous investigations have been performed both in the laboratory and as field exposures. They have greatly enhanced the understanding of mechanisms and of quantitative effects of dominating parameters. Based on mainly field exposure

¹Doctors of Sciences, Swedish Corrosion Institute, Roslagsvägen 101, Bldg. 25, SE-104 05 Stockholm, Sweden.

²Doctor of Sciences, Institute of Physical Chemistry, Russian Academy of Sciences, Leninskij Prospekt 31, 117915 Moscow, Russian Federation.

programs, dose-response relations have been derived expressing corrosion attack as a function of environmental parameters.

The knowledge has finally been adapted for the development of an international classification system of atmospheric corrosivity within the International Standardisation Organisation, "Corrosion of metals and alloys – Corrosivity of atmosphere – Classification" (ISO 9223). ISO 9223 is based on three parameters: time of wetness, SO₂ concentration and deposition of sea salt aerosols.

In 1987 an extensive international exposure program (ICP Materials) was started within the long-range transboundary (LRTAP) Convention of the United Nations Economic Commission for Europe (UN ECE), which aimed at assessment of the effects of acid deposition on materials including historic and cultural monuments. The programme [1], performed on non-marine sites in Europe and North America, has resulted in dose-response functions containing dry deposition effects of gaseous SO₂ and wet deposition effects of H⁺ ions in precipitation.

Both ISO 9223 and ICP Materials are to a great extent based on data from field exposures performed in the temperate climatic zone. This exerts a limitation for their use in more extreme climates. New data from different field exposure programs like the ISO CORRAG [2] and other programs [3] in subtropical and tropical regions gives the possibility for a better understanding of the complex problem of atmospheric corrosion. This will lead to a development of improved dose-response relations and will be helpful for the anticipated revision of ISO 9223.

This paper gives the present status of development of a model for prediction of atmospheric corrosion, which is based on the results obtained in the UN ECE ICP Materials and ISO CORRAG programs with special attention to the specific problems on subtropical and tropical regions.

Model Description for SO₂ Polluted Atmospheres

Atmospheric corrosion is a complex process. It can therefore be modelled in several ways and the selections of environmental parameters are practically unlimited. The present model is based on a characterisation of the environment by using only environmental parameters that are easily available on different geographical scales. The advantage of this is obvious, the model can be used by almost anyone without collection of sophisticated data. On the other hand this requirement may for some locations enforce the model to be too simplified, thereby missing the incorporation of important phenomena.

For unsheltered exposure conditions the materials damage is usually expressed in terms of dry and wet deposition of pollutants. Wet deposition includes transport of pollutants by means of precipitation and dry deposition transport by any other process. Therefore, and also because it makes sense from a mechanistic point of view, the model describes the total corrosion attack, K, in terms of dry, f_{dry} , and wet, f_{wet} , deposition separated as additive terms, [4-6]

$$K = f_{dry} + f_{wet} \quad (1)$$

The most important gaseous pollutant is sulfur dioxide while for coastal regions the particulate deposition of chlorides is dominating. The effect of wet deposition is often quantified as the total deposition of H^+ ions in rain. It is thus, as a first approximation, possible to divide the total corrosion effect into three dominating parts

$$K = f(SO_2) + f(Cl^-) + f(H^+) \quad (2)$$

The original version of the model is described in this section after a presentation of the climatic parameters used in the model: temperature, relative humidity and time of wetness. This version of the model, which includes a description of the dry deposition of SO_2 in combination with the wet deposition of H^+ , has been thoroughly verified using data from the ICP Materials exposure program. In the next section the model is developed for marine atmospheres and includes a description of the dry deposition of SO_2 in combination with chlorides. At present stage it has not been possible to develop a model that includes all three contributions described in equation 2 due to lack of sufficient amount of data from field exposure programs.

Time of Wetness, Temperature and Relative Humidity

Atmospheric corrosion is an electrochemical process and proceeds only when the surface is sufficiently wet. The corrosion rate increases with air humidity, starting from the "critical" humidity value, where the adsorbed water layer begins to act as an electrolyte. The effect of temperature is more complicated as will be discussed in the following.

Time of wetness (T_{ow}) is a concept commonly used in atmospheric corrosion of metallic materials and refers to the time when the metal is sufficiently wet for corrosion to occur. It depends to a large extent on the temperature (T) and relative humidity (Rh). According to the ISO 9223 classification, T_{ow} is defined as the time when $T > 0^\circ C$ and $Rh > 80\%$. Time of wetness as defined by ISO 9223 has traditionally been used as the main *climatic* parameter for explaining atmospheric corrosion effects.

Being directly calculated from continuous temperature and relative humidity data, there is also a strong relationship between long-term averages of T_{ow} , T and Rh [7]. This is illustrated in Fig. 1 for monthly averages but the same qualitative relationships are also valid for yearly averages. The increase in time of wetness with monthly average temperature in the low temperature range is due to the increase of the time when temperature is above $0^\circ C$. At higher temperatures the time of wetness decrease since the relative humidity decreases with increasing temperature.

Compared to the temperature dependence the effect of relative humidity is simple, an increase of monthly average relative humidity results in an increase in time of wetness when temperature is above $0^\circ C$. Relative humidity has no effect on time of wetness at negative temperatures as indicated by the points in the right lower corner of the T_{ow} - Rh plot in Fig. 1. Using the data presented in Fig. 1 a statistical relationship between T_{ow} , Rh and T has been derived, which is based on a probability model. It can be used for calculations of T_{ow} based on yearly averages of temperature and relative humidity. The equation simplifies the use of the present model and of the ISO classification system as it includes only the easily available parameters of temperature and relative humidity.

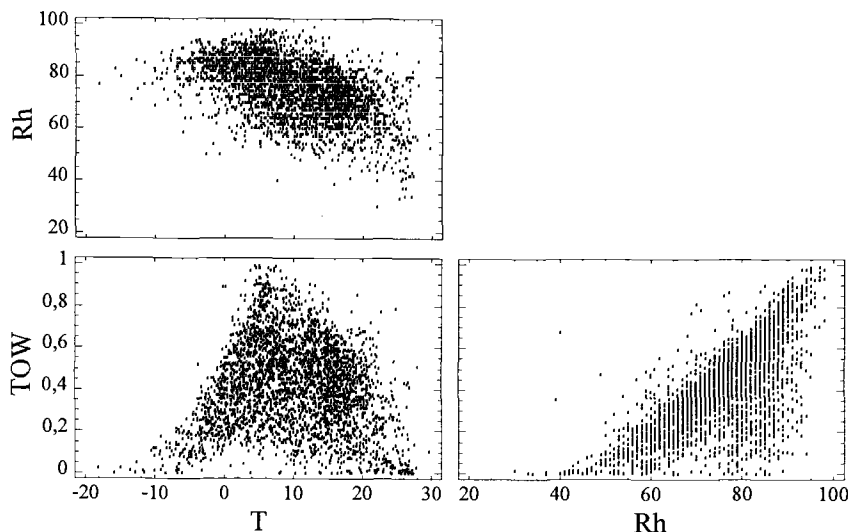


Figure 1 – Relationship between relative humidity (Rh) and temperature (T), top, time of wetness (Tow) and temperature (T), left / relative humidity (Rh), right, illustrated by plots of monthly data from the ICP Materials exposure program.

The Combined Effect of Dry Deposition of SO₂ and Wet Deposition of H⁺

SO₂ is the main anthropogenic contributor to atmospheric corrosion. Chamber experiments and dry deposition tests have shown that the uptake of SO₂ by a given surface is significantly accelerated when the surface is wet. Therefore it is natural to express the SO₂ term in equation 2 as follows [4-6]

$$f(\text{SO}_2) = A \cdot \text{SO}_2^B \cdot \text{Tow}^C \quad (3)$$

This form was used in the unified analysis of data from the International Co-operative Program on Effects on Materials, Including Historic and Cultural Monuments (ICP Materials), except that the expression for Tow was replaced with a combined multiplicative Rh and T function. ICP Materials was started in September 1987 and involves 39 exposure sites in 12 European countries and in the United States and Canada. The aim of the program is to perform a quantitative evaluation of the effect of sulphur pollutants in combination with NO_x and other pollutants as well as climatic parameters on the atmospheric corrosion of important materials. This is achieved by measuring gaseous pollutants, precipitation and climate parameters at or nearby each test site and by evaluating the corrosion effects on the materials [1]. The analysis of data after 8 years of exposure is the basis for the present description.

The wet deposition term in equation 2 that has been used within ICP Materials is given as [8]

$$f(H^+) = k \cdot \text{Rain}[H^+] \tag{4}$$

where

Rain = amount of precipitation in mm/year

[H⁺] = hydrogen ion concentration in precipitation in mg/l.

The SO₂ and wet deposition terms can be exemplified with ICP Materials dose-response functions for zinc and copper

$$ML_{Zn} = 1.4[SO_2]^{0.22} \exp\{0.018Rh + f_3(T)\} t^{0.85} + 0.029\text{Rain}[H^+] \cdot t \tag{5}$$

$$ML_{Cu} = 0.0027[SO_2]^{0.32}[O_3]^{0.79} Rh \cdot \exp\{f_6(T)\} t^{0.78} + 0.050\text{Rain}[H^+] \cdot t^{0.89} \tag{6}$$

where

ML = mass loss in g/m²

f₃(T) = 0.062(T-10) when T ≤ 10°C and -0.021(T-10) when T > 10°C

f₆(T) = 0.083(T-10) when T ≤ 10°C and -0.032(T-10) when T > 10°C

A description of all other parameters including ranges is given in Table 1 [4-6].

The general temperature dependence for the corrosion attack given for zinc and copper in equations 5 and 6, respectively, is schematically illustrated in Fig. 2. According to the ICP Materials results, the effect of temperature has a maximum at about 9-11°C annual mean temperature.

The similarity between the temperature dependence for time of wetness (Fig. 1, left) and corrosion attack (Fig. 2) is striking. The increasing part in Fig. 1, left-bottom and Fig. 2 (a) can both be related to the increase of the time when temperature is above 0°C since this quantity is correlated with the annual average temperature. The decreasing part in Fig. 2 (b), is due to a negative correlation of ambient relative humidity and temperature values, Fig. 1, left, and also due to periods with a surface temperature

Table 1– Parameters used in final ICP Materials dose-response functions including symbol, description, interval measured in the program and unit.
All parameters are expressed as annual averages

Symbol	Description	Interval	Unit
t	Time	1-8	year
T	Temperature	2-19	°C
Rh	Relative humidity	56-86	%
[SO ₂]	SO ₂ concentration	1-83	µg/m ³
[O ₃]	O ₃ concentration	14-82	µg/m ³
Rain	Rainfall	327-2144	mm
[H ⁺]	H ⁺ concentration	0.0006-0.13	mg/l

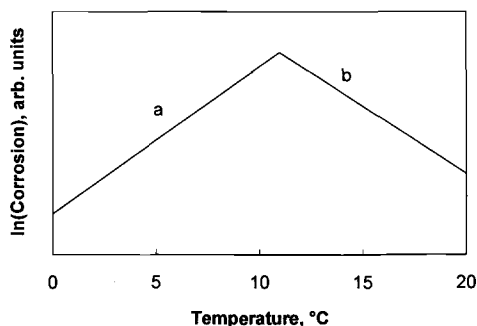


Figure 2 – Schematic representation of the observed temperature dependence for many materials: a) increase of corrosion with temperature in the low temperature range and b) decrease of corrosion with temperature in the high temperature range

above the ambient temperature, partly related to sun radiation. An elevated surface temperature leads to a faster evaporation of moisture after rain or condensation periods and to a decrease of the thickness of the adsorbed water layer and, consequently, to a decrease of the time when the metal surface is wet. Thus, the intense solar radiation in inland tropics causes the time when surfaces are wet during unsheltered exposure to become relatively short. It can therefore be expected that the corrosion rates on unsheltered exposed metals in tropical unpolluted atmospheres are lower than in temperate climate as will be verified below.

The equations given for wet deposition do not involve temperature as an explanatory variable. However, in preliminary analyses the ICP Materials data set was subdivided into low and high temperature sites and separate equations were obtained. The results indicated that the effect of wet deposition could be higher at higher temperatures. One should thus be careful using these functions in warm regions outside the specified temperature range.

Development of the Model for Cl⁻ Containing Marine Atmospheres

Chlorides may deposit on a metal surface by dry or wet deposition. Dry chloride deposition dominates in coastal areas while wet deposition can be a significant source of chlorides in inland areas. The discussion will be limited to dry deposition of chloride aerosols.

The atmospheric corrosion rate of metals depends on the amount of chlorides deposited on the surface. The dry deposition is determined by the local geographical and topographical situation in combination with the distance from the shore, wind speed and directions. In most cases the maximum corrosion rates are observed in tropical marine atmospheres where the corrosion is much higher than in marine locations of the temperate zone and frequently higher than in tropical urban and industrial regions.

As the aim of ICP Materials, which was the program used as a basis for the development of the model for SO₂ polluted areas, is to perform a quantitative evaluation of the effect of acidifying pollutants, no typical marine sites are included in the

program. In order to extend the model to chloride containing atmospheres a different data set needs to be used.

The ISO CORRAG program was initiated in 1987-1989 in order to provide world wide corrosion data from a wide variety of test sites complying with ISO/TC 156 testing methods and procedures. It includes 53 test sites in 14 countries on four continents with a high variation in climate types and pollution levels [2]. The present development of the model is based on ISO CORRAG data and includes a wide temperature range, including subtropical and tropical regions for different SO₂ and Cl⁻ levels. It gives the possibility for a better understanding of atmospheric corrosion processes for common technical metals and can be applied in marine areas with different deposition of chlorides and SO₂ pollution levels.

Dry Deposition Effect of Chlorides

It is known that chlorides are a main accelerating factor of atmospheric corrosion in coastal regions. The corrosion rate of most metals is strongly affected by the concentration of chlorides on the surface. One reason is that the chlorides have hygroscopic properties and thus contribute to the creation of an electrolyte layer. This leads to a prolongation of the periods when the surface is wet even at higher temperatures. Moreover, which is important to stress, atmospheric corrosion in a chloride-containing atmosphere increases with temperature. At least two attempts have been made to take into account the effect of temperature on atmospheric corrosion in the presence of chlorides [3,9], but using very limited experimental data or by a limited statistical analysis. Most present models are based on time of wetness data and dry deposition of Cl⁻.

Instead of the most commonly used relation for the description of corrosion due to dry deposition of chlorides,

$$f(\text{Cl}^-) = A \cdot [\text{Cl}^-]^B \cdot T^{\text{ow}^C} \quad (7)$$

the effect of temperature is also included in the present model. The following equation has been used to describe ISO CORRAG data for carbon steel

$$f(\text{Cl}^-) = A1 \cdot [\text{Cl}^-]^{B1} \cdot T^{\text{ow}^{C1}} \cdot \exp(k \cdot T) \quad (8)$$

Equation 8 indicates that the corrosion in marine atmospheres increases with temperature exponentially even above 10°C annual temperature. This is illustrated in Fig. 3, which is valid for carbon steel, but needs to be verified for other metals.

Modification of Dry Deposition Effect of SO₂ in Chloride Containing Atmospheres

The temperature dependence for the dry deposition effect of SO₂ was illustrated in Fig. 2 and in equations 5-6. As mentioned in the previous section chlorides have hygroscopic properties and can thus contribute to the creation of an electrolyte layer and to a prolongation of the periods when the surface is wet. In a chloride-containing

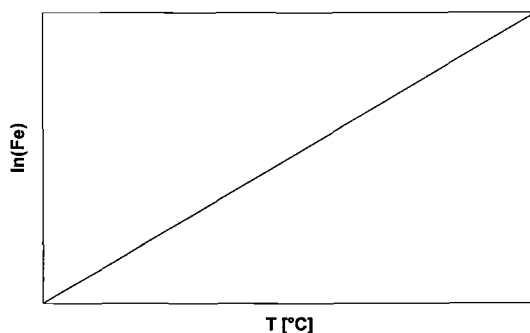


Figure 3 – Schematic representation of the observed temperature dependence of corrosion of carbon steel in marine atmosphere

atmosphere the expression therefore needs to be modified so that the decrease of the SO_2 term with temperature is less extreme than indicated in Fig. 2.

The present data does not permit a full determination of the preferred form among the possibilities that exist to adjust the temperature dependence. Instead an assumption has been made that the temperature effect changes from a negative slope, as in Fig. 2, to a constant value when the chloride deposition exceeds a limiting value. This does not mean that the data shows that there exists a critical chloride concentration but is rather an attempt to separate the influence in the SO_2 term of prolonged time of wetness caused by chloride deposition from other effects of chlorides.

Derivation of Dose-Response Functions

As shown in equation 2 the corrosion in marine SO_2 polluted atmosphere due to dry deposition is simply the sum of the individual contributions for dry deposition of SO_2 and chloride. The described model has been used to analyse the 1 year ISO CORRAG data for flat carbon steel samples. A description of all parameters including ranges is given in Table 2.

Table 2 – Parameters used in the dose-response functions for carbon steel based on ISO CORRAG data including symbol, description, interval measured in the programme and unit. All parameters are expressed as annual averages

Symbol	Description	Interval	Unit
T	Temperature	-17 - +28	°C
Tow	Time of wetness	206-8097	h/year
SO_2	SO_2 concentration	0.9-215	$\mu\text{g}/\text{m}^3$
Cl	Cl^- dry deposition	0.3-1093	$\text{mg}/\text{m}^2\text{day}$

The following five equations (9-13) with increasing complexity and for the same number of observations ($N = 261$) have been estimated:

$$ML = 0.014 \exp\{0.0105SO_2\} Tow^{0.86} Cl^{0.16} \quad R^2 \quad 0.66 \quad (9)$$

$$ML = 0.021 SO_2^{0.35} Tow^{0.73} Cl^{0.16} \quad 0.69 \quad (10)$$

$$ML = 0.30 SO_2^{0.30} Tow^{0.44} Cl^{0.17} \exp\{f_{11}(T)\} \quad 0.73 \quad (11)$$

$$ML = 0.24 SO_2^{0.43} Tow^{0.46} \exp\{f_{12}(T)\} + 0.158 Cl^{0.51} Tow^{0.18} \exp\{0.094T\} \quad 0.81 \quad (12)$$

$$ML = 0.34 SO_2^{0.34} Tow^{0.45} \exp\{f_{13}(T)\} + 0.086 Cl^{0.62} Tow^{0.13} \exp\{0.087T\} \quad 0.82 \quad (13)$$

where

$$\begin{aligned} f_{11}(t) &= 0.060(T-9) \text{ when } T \leq 9^\circ\text{C} \text{ and } -0.033(T-9) \text{ when } T > 9^\circ\text{C} \\ f_{12}(t) &= 0.062(T-9) \text{ when } T \leq 9^\circ\text{C} \text{ and } -0.12(T-9) \text{ when } T > 9^\circ\text{C} \\ f_{13}(t) &= 0.065(T-9) \text{ when } T \leq 9^\circ\text{C} \text{ and } -0.13(T-9) \text{ when } T > 9^\circ\text{C} \text{ and } Cl \leq 3 \text{ mg/m}^2\text{-day} \\ & \quad 0 \text{ otherwise.} \end{aligned}$$

The difference between the equations is not only in the explained variability (R^2). The exponents for Cl^- in equations 12-13 are significantly higher (0.51-0.62) compared to equations 9-11 (0.16-0.17). A further drawback of equations 9-11 is that they imply that the presence of both SO_2 and Cl^- is needed to obtain high corrosion rates. This is in contrast with experience since it is possible to obtain significant corrosion rates both in the absence of SO_2 (marine sites) and Cl^- (highly polluted sites). This was one of the reasons for choosing the general form of the present model (equation 2). Different values of the limiting chloride concentration have been examined and the final value of $3 \text{ mg/m}^2\text{-day}$ in equation 13 was chosen using the equation with highest R^2 value. For other metals the limiting chloride concentration may be different. For example, in a similar analysis for zinc the value $30 \text{ mg/m}^2\text{-day}$ provides a better fit.

Figure 4 shows observed vs. predicted logarithmic values and Fig. 5 shows fitted models, $\ln(ML)$ vs T , for different Cl^- concentrations, both figures based on equation 13. When Cl^- is below $3 \text{ mg/m}^2\text{-day}$ the temperature dependence has a maximum (Fig. 5, top, left), similar to what was obtained using data from ICP Materials. The decreasing part is attributed to a surface temperature above the ambient temperature and an elevated surface temperature leads to a faster evaporation of moisture after rain or condensation periods and to a decrease of the thickness of the adsorbed water layer. When Cl^- is high the increase of T leads to the increase of corrosion (Fig. 5, bottom, right). Corrosion between these two limiting cases are observed at the intermediate Cl^- concentrations (Fig. 5, top, right and bottom, left).

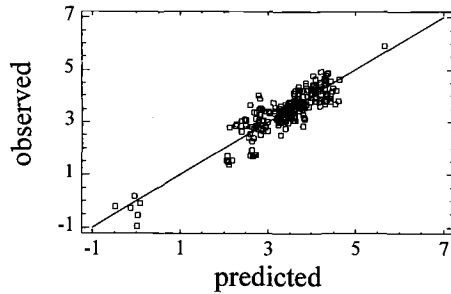


Figure 4 – Observed vs. predicted logarithmic mass loss values of carbon steel based on equation 13

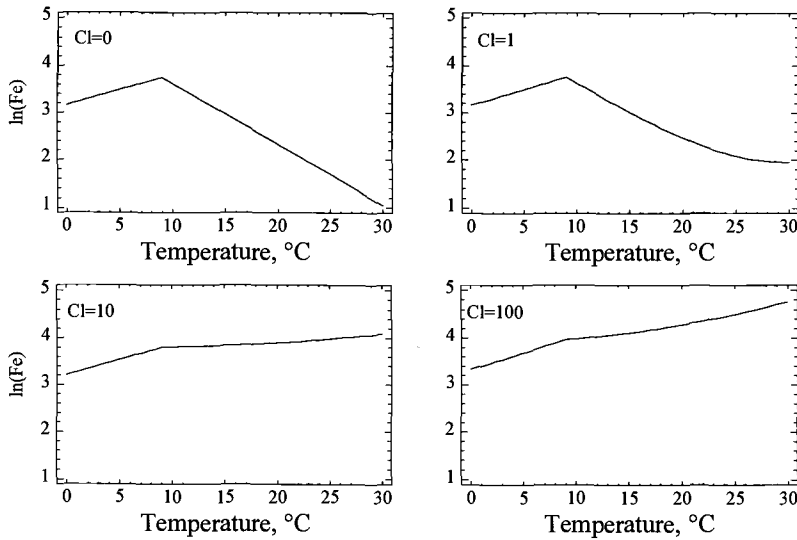


Figure 5 – Plot of fitted models for corrosion of carbon steel vs. annual average temperature for different Cl^- concentrations in $mg/m^2/day$ using equation 13 and values of $SO_2=20 \mu g/m^3$ and $T_{ow}=5000$ hours/year

Comparison of Model Results with Field Exposure Data

Taking into account the topic of the present conference it is interesting to compare the data calculated from the model with results from field exposures with special attention to tropical and subtropical regions. This comparison is based on both data used for the development of the model and on independent data. A special attention is devoted to the effect of temperature in rural and in marine atmospheres.

In rural areas of the subtropical and tropical zones the corrosion rates are usually lower than in temperate climates (Table 3). This is in accordance with Fig. 2 (b), Fig. 5

($Cl^- = 0$) and equations 5, 6 and 13. It may be mentioned that typical values of corrosion rates of carbon steel, 140 g/m²year, zinc, 6 g/m²year and copper, 14 g/m²year in the temperate climatic region are higher than corresponding values in the warm regions, where ISO 9223 Tow values based on temperature/humidity data and rain amounts are higher. In cold areas the yearly corrosion rate of metals in a rural atmosphere is very low, especially for carbon steel, and increases with the increase of temperature in accordance with Fig. 2 (a).

In marine atmospheres the temperature increases the corrosion rate in the whole temperature range as shown in Fig. 6 and in Table 4, which gives corrosion rates of carbon steel in different climatic regions. This is accordance with Fig. 3 and Fig. 5 ($Cl^- = 100$ mg/m²day). The table gives corrosion values for individual marine sites and the figure approximate ranges from Table 4 of corrosion values for marine sites situated in different climates and with high but similar chloride deposition values. The site Sines, which is classified as a subtropical site in Table 4, is a borderline case between subtropical/tropical climate. Both experimental and calculated data show that the corrosion rate of carbon steel in severe marine atmosphere increases with up to one order of magnitude in tropical climate compared to the temperate zone. The data also illustrates the extremely high corrosion rates in severe marine atmospheres in tropical regions.

Table 3 - Yearly mass losses of common technical metals in rural areas of the world

Country/ Continent	Site	Climate	T °C	Rh %	Rain mm	Tow hr/yr	Steel g/m ²	Zn g/m ²	Cu g/m ²	Ref.
Russia	Oimyakon	Extr. cold	-16	60		348	5.8	1.9	0.68	[2, 10]
Russia	Atka	Extr. cold	-12	72	489	987	15	1.7	0.98	[9, 11]
Russia	Bilibino	Extr. cold	-11	73	455	692	5.4	1.6	0.84	[9, 11]
Canada	Norman Wells	Cold					12			[12]
Russia	Kluitchi	Cold	-1	76	884	1916	23	2.0	2.8	[9, 11]
Sweden	Abisco	Cold	-1	84			40	3.4		[12, 13]
Norway	Noatun	Cold	0	77	216	1752	78	5.4		[14]
Sweden	Gällivare	Cold	1				47	5.7		[15]
Russia	Zvenigorod	Temperate	5	82	600	3800	140	6.6	6.5	[16]
Sweden	Aspvreten	Temperate	6	83	543	4534	81-147	6-8	10.7	[17, 18]
Czech Rep.	Kasperske Hory	Temperate	7	74	941	3063	148-153	4-9	15.0	[17, 18]
Germany	Garmish-Part.	Temperate	8	82	1492	4989	86-133	4-8	11.4	[17, 18]
Spain	Leon	Temperate	11	65	494	2604	162	2.6	7.2	[3]
Uruguay	Trinidad	Subtrop.	17	74	1210	5084	59	3.6	7.3	[3]
Nigeria	Nkpoku, jungle	Wet Trop.					40	3.6		[14]
Vietnam	Dalat, mountain	Wet Trop.	18	84	1820		112	5		[19]
Argentina	Iguazu	Wet Trop.	21	75	2172	5637	45	8.4	7.6	[3]
Brazil	Caratinga	Wet Trop.	21	74	1003	5225	87	4.8	8.8	[3]
Peru	Pucallpa	Wet Trop.	26	82	1269	5382	110	5.4	6.7	[3]
Argentina	San Juan	Dry	18	50	80	903	38	1.4	1.5	[3]

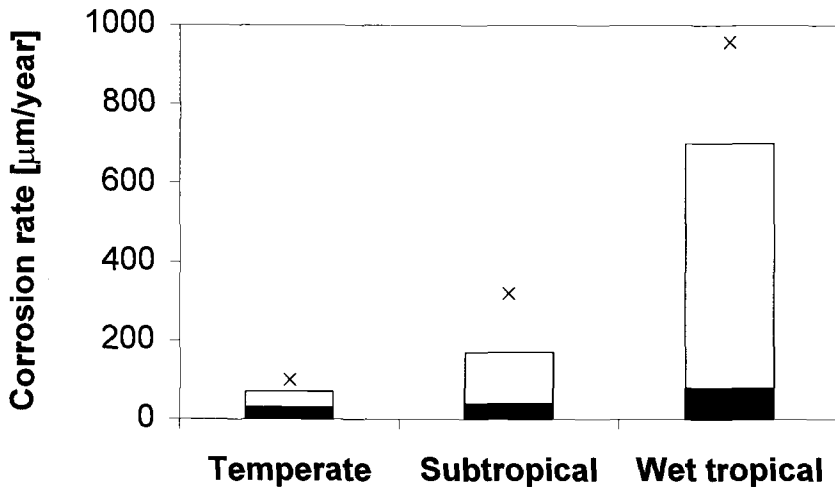


Figure 6 – Minimum, maximum and extreme (x) corrosion rates of carbon steel from table 4 after one year of exposure in different marine atmospheres

Table 4 – Corrosion rates of carbon steel for one year exposure on test sites situated in temperate, subtropical and wet tropical marine sites. Sites have been chosen with generally high chloride deposition values (approximately $>100 \text{ mg/m}^2 \text{ day}$). Extreme values (x) are not included in the given ranges.

Climate	Corrosion rate	Ref.
Temperate ¹	30-70 $\mu\text{m/year}$	[2, 20-22]
Subtropical ²	40-170 $\mu\text{m/year}$	[2, 20-25]
Wet tropical ³	80-700 $\mu\text{m/year}$	[20-26]

¹Kvarnvik (42-62), Tananger (60), Ostende (99, x), Rue (59), South Africa (30-50).

²Saint Remy (43), Qingdao (131), Salin de Giraud (73), Ponteau Martiques (72), Kure Beach (38), Walvis Bay (165), South Africa (50-80), Sines (320, x), Leixoes (65-79), Punta del Este (43-57).

³Viriato (411), Cojimar A (172-391), Galeta Point (618), Canal Zone (375), Colon (108), Christobal (83), Lagos Lighthouse Beach 70 m (378), Lagos Lighthouse Beach 15 m (958, x), Arrial do Cabo (142-195), Aracaju 100 m (586), Alexandria (135), Port Said (117), Durban-Bluff (231), Durban-Congella (108-122), Digha 300 m (311), Ubatuba (219-382).

Conclusions

- A step-wise development of a model of atmospheric corrosion of common structural metals is described using temperature, relative humidity, time of wetness, SO₂, chloride deposition and H⁺ load of precipitation as explanatory variables.
- For rural and urban atmospheres the model is based on UN ECE ICP Materials data and separates the effect of dry and wet deposition of pollutants.
- A further development of the model for SO₂ and chloride-containing atmospheres has been performed based on the ISO CORRAG results, which does not contain data on wet deposition.
- For both data sets nonlinear dose-response function have been obtained with a high-explained variability.
- Both models show the complicated effect of temperature on atmospheric corrosion. In the low temperature region the corrosion rate increases with increasing mean temperature. In warm/hot regions a negative temperature effect is observed in absence of chlorides, which is due to a reduced time of wetness.
- In marine atmospheres a positive temperature effect is observed also in warm/hot regions due to the presence of hygroscopic salts at the metal surface that prolong the time of wetness. As the temperature also increases the corrosive effect of chloride, the corrosivity in tropical marine atmospheres with high deposition of chlorides can be extremely high.
- For verification of the model, calculated data have been compared with independent values from field exposures and show in general good correlation for both cold, temperate and warm/hot regions.

References

- [1] "Technical Manual, UN/ECE International Co-operative Programme on Effects -on Materials, including Historic and Cultural Monuments," Report No 1, Swedish Corrosion Institute, Stockholm, 1988.
- [2] Knotkova, D., "Atmospheric Corrosivity Classification. Results of the International Testing Program ISOCORRAG," *Corrosion Control for Low-Cost Reliability, 12th International Corrosion Congress, Vol. 2, Progress Industries Plant Operations*, NACE International, Houston, Texas, 1993, pp. 561-568.
- [3] "Funciones de Dano (Dosis/Respuesta)de la Corrosion Atmosferica en Iberoamerica," *Corrosion y Proteccion de Metales en las Atmosferas de Iberoamerica*, M. Morcillo, M. Elisabete M. Almeida, Blanca M. Rosales *et al.* EDS., Programma CYTED, Madrid, Spain, 1998, pp. 629-660.
- [4] Tidblad J., Kucera V., and Mikhailov A. A., "Statistical Analysis of 8 Year Materials Exposure and Acceptable Deterioration and Pollution Levels," UN/ECE International Co-operative Programme on Effects on Materials, including Historic and Cultural Monuments," Report No 30, Swedish Corrosion Institute, Stockholm, 1998. 49 pp.

- [5] Tidblad J., Mikhailov A. A., and Kucera V., "Unified Dose-Response Functions after 8 Years of Exposure," *Proceedings of the UN/ECE Workshop on Quantification of Effects of Air Pollutants on Materials*, Berlin 1998, Germany, UMWELTBUNDESAMT, 1999, pp.77-86.
- [6] Tidblad J., Kucera V., Mikhailov A. A., Henriksen J., Kreislova K., Yates T., Stöckle B., and Schreiner M., "Final Dose-Response Function and Trend Analysis from the UN ECE Project on the Effects of Acid Deposition," *Co-operation in Corrosion Control, 14th International Corrosion Congress*, Document Transformation Technologies, Cape Town, South Africa, 1999, Paper 337,1, 12 pp.
- [7] Tidblad J., Mikhailov A. A., and Kucera V., "A Model for Calculation of Time of Wetness using Relative Humidity and Temperature Data," *Co-operation in Corrosion Control, 14th International Corrosion Congress*, Document Transformation Technologies, Cape Town, South Africa, 1999, Paper 337,2, 11 pp.
- [8] Kucera, V., Tidblad J., Henriksen, J., Bartonova, A., and Mikhailov, A. A., "Statistical Analysis of 4 year Materials Exposure and Acceptable Deterioration and Pollution Levels", UN/ECE International Co-operative Programme on Effects on Materials, including Historic and Cultural Monuments, Report No 18, Swedish Corrosion Institute, Stockholm, 1995.
- [9] Panchenko Yu.M., Shuvakhina L-A., Mikhailovskij Yu.N., "Dependence of the Rate of Atmospheric Corrosion on climatic conditions of the Far East", *Zashchita Metallov*, 1984, Vol. 20. N 6. pp. 851-863.
- [10] Strelalov P.V., "Monitoring of Atmospheric Corrosivity on Standard Flat and Wire Metal Samples: The Russian Part of the ISOCORRAG International Test Program," *Protection of Metals*, 1996, Vol. 32, No 6. pp. 572-586.
- [11] Panchenko Yu.M., Shuvakhina L.A., Mikhailovskij Yu.N., "Atmospheric Corrosion of Metals in the regions of the Far East," *Zashchita Metallov*, 1982, Vol. 18. No 4. pp. 575-581.
- [12] Hudson J.C., Stanners J.F., "The Effect of Climate and Atmospheric Pollution on Corrosion," *Journal of Applied Chemistry*, 1953, Vol. 3. pp. 86-95.
- [13] Trägårdh K.F., "Försök med omålat stål," *Nordisk Korrosionsmode*, 1954, No 8, pp. 13-16.
- [14] Henriksen J.F., Mikhailov A.A., Mikhailovskij Yu.N., "Atmospheric Corrosion Tests Along the Norwegian-Russian Border," Report NILU OR/54/92, Norwegian Institute for Air Research, Lillestrom, Norway, 1992, 54 P.
- [15] Kucera V., Haagenrud S., Atteraa L., Gullman J., "Corrosion of Steel and Zinc in Scandinavia with Respect to the Classification of the Corrosivity of Atmospheres," *Degradation of Metals in Atmosphere, ASTM STR 965*. S. W. Dean and T. S. Lee, Eds., American Society of Testing and Materials, Philadelphia, 1988, pp. 264-281.

- [16] Barton K., Cerny M., "Connection between the Properties of the Media and the Kinematics of Atmospheric Corrosion of Steel, Zinc, Copper and Aluminium," *Zashchita Metallov*, 1980, Vol. 14. No 4. pp. 387-395.
- [17] Kreislova K., Knotkova D. and Boschek Petr, "Trends of Corrosivity Based on Corrosion Rates and Pollution Data," UN/ECE International Co-operative Programme on Effects on Materials, including Historic and Cultural Monuments, Report No 29, Part 2, SVÚOM Praha a. s., Prague, Czech Republic, 1997.
- [18] Stöckle B., Pöhlmann G., Mach M. and Snethlage R., "Corrosion attack on copper and cast bronze. Evaluation after 1 and 2 years of exposure," Report No 5, Bavarian State Conservation Office, München, Germany, 1991.
- [19] Vuy V.D., Strekalov P.V., Kozhevnikov A.I. and Ruzinov V.L., *Zashchita Metallov*, 1983, Vol. 19, No 1, pp. 40-46.
- [20] Knotkova D., 1993. Classification of corrosivity of atmosphere. Document ISO/TC 156/WG 4 - N 243.
- [21] Callaghan B.G., "Atmospheric Corrosion Testing in Southern Africa," *Atmospheric Corrosion*, John Wiley and Sons Interscience. New York, 1982, pp. 893-911.
- [22] Callaghan B.G., "Atmospheric Corrosion Testing in Southern Africa, -Results of a twenty year national exposure programme," Scientia Publishers, CSIR, Republic of South Africa, 1991, 75 pp.
- [23] Feng Zhu, Hedlund S., Kucera V., Jianzhong Huang., Atmospheric corrosion at different test sites in Sweden and China – results after 8 years exposure, Swedish Corrosion Institute, Stockholm, 1996.
- [24] Kucera V., "Corrosion of Structures and Cultural Properties," *Acidification in Tropical Countries*, H. Rodhe and R. Herrera, EDS, John Wiley and Sons Interscience, Chichester-New York-Brisbane-Toronto-Singapore, SCOPE, ICSU and UNEP, Scope 36, 1988, pp. 167-194.
- [25] Morcillo M., "Atmospheric Corrosion in Iberoamerica," *Atmospheric Corrosion, ASTM STR 1239*, W.W.Kirk and Herbert H. Lawson, Eds., American Society for Testing and Materials, Philadelphia, 1995, pp. 257-275.
- [26] Rao K.N., Lahiri A.K., "Corrosion map of India", Corrosion Advisory Bureau. Council of Scientific and Industrial Research, Jamshedpur, India, 1972.

Ivan S. Cole¹

Mechanisms of Atmospheric Corrosion in Tropical Environments

Reference: Cole, I. S., “Mechanisms of Atmospheric Corrosion in Tropical Environments,” *Marine Corrosion in Tropical Environments, ASTM STP 1399*, S. W. Dean, G. Hernandez-Duque Delgadillo, and J. B. Bushman, Eds., American Society for Testing and Materials, West Conshohocken, PA, 2000.

Abstract: The paper presents results from a five-nation (Australia, Indonesia, the Philippines, Thailand, and Indonesia) study into the relationship between climatic/pollutant factors and corrosion of zinc and mild steel. While a good correlation was found between the corrosion rate of mild steel and gaseous SO₂ and rainwater pH, no such relationship was found between these parameters and the corrosion rate of zinc. This observation has prompted an investigation into the forms of pollutant deposition. Particulate deposition, gaseous absorption into moisture layers on metal surfaces, and deposition in fine and coarse raindrops are discussed. The discussion focuses on the rate of each process and the chemistry of the moisture formed on metal surfaces as a result of the processes. A chemical reaction simulator is used to model the changing chemistry of moisture layers under a number of environmental scenarios. These scenarios highlight the importance of the ratio of the gaseous NH₃/SO₂ and of oxidation of S(IV) in controlling both the acidity and composition of moisture films. The relevance of these processes to the rates of corrosion is discussed, and some hypothesis for the low corrosion rate of zinc in the five-nation study is presented.

Keywords: atmospheric corrosion, mechanism, tropical, sulfur dioxide, ammonia, gaseous absorption, particulate, moisture films

Introduction

It has long been established that industrial atmospheres can cause enhanced corrosion [1–4]. This has been associated with acidification of moisture films by the absorption of sulfur dioxide. More recent work has highlighted the importance of nitric oxide and ozone in the corrosion process, and it has been postulated that these gases have a synergistic effect with sulfur dioxide [5–6]. Work by Graedel [7] and Farrow et al. [6] has highlighted the role of the various chemical reactions that occur in the aqueous phase between sulfur products and water.

A recent five-nation study was undertaken by Australia, Indonesia, Thailand, the Philippines and Vietnam to gain an understanding of the relationship between pollutants and corrosion of steel and zinc in tropical countries [8]. Eighteen sites were established in industrial, marine, urban and rural locations [9]. Specimens were exposed on a three-month and yearly basis. Analysis indicated that although there was a strong correlation between steel corrosion and airborne SO_x level and rainwater pH, only a weak correlation was established for zinc [9]. This low correlation was not consistent with previous

¹Principal Research Scientist, CSIRO BCE, PO Box 56, Highett, Victoria 3190, Australia.

work in North America and Europe [1-4]. In order to understand this difference, a detailed analysis has been undertaken to determine the factors controlling the chemistry of wet and dry deposition of sulfates and of moisture films on plates. In the analysis, the implication to corrosion has been studied with an emphasis on understanding why the corrosion rate of zinc specimens should show a different dependence on pollutant parameters in tropical compared to temperate parameters. Thus, in this paper the data on the five-nation study is presented in a summary form with full details having been previously presented [8,9].

Procedures and Results of the Five-Nation Study

The position and the characteristics of each site are given in Table 1, while in Table 2, pollutant parameters, time of wetness (TOW) and mass loss data are also given. Airborne salinity is measured using a standard wet candle technique according to ISO 9223, where NO_x , SO_x and HNO_3 are measured using a passive sampling technique. The monsoonal periods fall between May and September/October in Thailand, June and August in the Philippines, and December and February in Australia. The mass loss data is for a three-month exposure of specimens of mild steel and zinc with compositions given in Table 3 (dimensions 100×150 mm) exposed as per ASTM G1. Fuller details are available in reference [9].

In assessing the correct exposure period for metal samples, an appreciation of the purpose of the model is required. The aim of the modeling work was to build an appreciation of the role of various climatic factors in influencing corrosion mechanisms and rates. As such, it was important to choose a period in which the climatic and pollutant patterns were relatively uniform, but was long enough to generate significant and representative surface changes and mass loss. Seasonal exposures provided a useful compromise between these two requirements. If the aim of modeling is to understand regional variations in corrosion by developing average climatic parameters which are representative of long-term variations, then clearly longer exposures would have been appropriate. However, this latter type of modeling would not (by itself) provide sufficient detail to assist building of detailed process models.

Table 1 – Australian and South-East Asian Sites

Country	Location	Type	Latitude/Longitude	Salient Features
Australia	Cowley Beach	Severe marine	17°41'S; 146°06'E	On beach facing SE
	Walkamin	Highland	17°08'S; 145°25'E	On tableland NE of Cowley Beach
Philippines	Cabuyao	Industrial	14°10'N; 121°07'E	Large industrial centre
	Bicutan	Urban	14°30'N; 121°02'E	Metro Manila
	Baguio	Highland	16°30'N; 120°33'E	1500 m above sea level
Thailand	Bangkok	Urban/industrial	13°40'N; 100°30'E	On building near major road
	Rayong	Industrial	12°41'N; 101°19'E	500 m from sea
	Phrapradaeng	Industrial	13°39'N; 100°34'E	Adjacent to river 10 km from sea
	Phuket	Marine	7°50'N; 98°20'E	On seashore
Vietnam	Hanoi	Urban	21°01'N; 105°52'E	
	Hue	Urban	16°28'N; 107°36'E	
	Nha Trang	Marine	12°20'N; 109°00'E	
	Ho Chi Minh City	Urban/industrial	10°46'N; 106°43'E	

Table 2 – Measured Pollutant, TOW and Corrosivity Criteria

Location	Season	Corrosion Rate ($\mu\text{m}/\text{year}$)		Measured TOW (%)	Rainwater pH	Rainwater Conductivity ($\mu\text{S}/\text{cm}$)	Airborne Salinity ($\text{mg}/\text{m}^2\cdot\text{day}$)	SO_2 ($\mu\text{g}/\text{m}^3$)	NO_2 ($\mu\text{g}/\text{m}^3$)	HNO_3 ($\mu\text{g}/\text{m}^3$)
		Mild Steel	Zinc							
Baguio	Jan.-March (99)	13	1.4	80	5.0	10	4*	2.2	10.4	3.7
	March-May	11.8	2.6	92	5.4	25	4*	2.9	10.2	4.9
	July-Sept.	8.5	5.2	100	5.0	21	4*	1.4	7.3	2.9
	Oct.-Dec.	11	2.5	100	4.9	55	4*	1.8	4.0	3.8
Bicutan	Jan.-March (99)	41.5	2.1	34	4.1	48	10*	10.3	26.4	5.1
	March-May	26.4	0.7	40	4.4	32	10*	14	6.5	4.2
	July-Sept.	92.1	1.7	41	4.4	35	10*	34	21	8.9
	Oct.-Dec.	67.8	2.3	41	4.1	35	10*	16.7	19.8	8.3
Cabuyao	Jan.-Mar (99)	35.7	1.7	83	4.6	26	10*	8.9	20.1	3.4
	March-May	33.6	1.2	24	4.0	38	10*	5.8	11.5	3.5
	July-Sept.	62.4	2.9	63	5.1	38	10*	20.9	16.3	7.0
	Oct.-Dec.	62.6	2.0	91	4.9	34	10*	15.4	13.9	6.9
Pinaprapdaeng	March-June	87	1.8	62	5.7	63	16.1	105	0.04	3.9
	July-Sept.	90	3.0	57	5.6-6.9	25-39	7.4	61	0.02	5.5
	Oct.-Dec.	50	5.9	34	5.9	30	4	33.9	21.9	14.4
	Jan.-March	76	1.7	59	5.5-6.3	29-98	6.7	72	23	11
Rayong	April-June (99)	99	1.8	89	5.6-6.2	31-32	6.1	67	22	7
	March-May	38	5.2	51	6.4	196	36.6	2.4	2.9	0.9
	July-Sept.	42	4.0	74	5.6-6.9	21-45	33.2	8.9	5.4	2.5
	Oct.-Dec.	41	1.7	55	5.9	41-62	3.9	30.7	20.9	8.1
Phuket	Jan.-March	47	1.0	72	5.5-6.3	64	12.7	18.1	10.4	5.0
	April-June (99)	46	8.4	82	5.6-6.2	25-59	42	3	4	1.6
	March-May	30	1.7	43	5.7	44	34.1	3.2	2.4	1.4
	July-Sept.	66	3.2	70	5.8-5.9	23-30	184.1	2.7	1.9	1.2
Bangkok	Oct.-Dec.	41	2.9	64	5.8	12	43.7	8.0	2.4	3.6
	Jan.-March	27	0.9	56	6.5	14	—	3	2	1
	April-June (99)	71	7.3	86	6.4	25	—	32	1.7	1.7
	March-May	39	0.9	22	6.3	25	12.3	31	30	10
Bangkok	July-Sept.	39	2.8	32	5.1-6.9	8.7-46.6	4.0	18	24	9.5
	Oct.-Dec.	24	1.6	16	5.5-5.7	18.9-23.7	6.0	13.2	34.8	11.9
	Jan.-March	35	0.6	35	5.2	68	4.4	21.2	56.7	8.8
	April-June (99)	46	1.7	28	5.3-5.8	9.3-27.0	8	17.8	24.6	9.5

* Estimated using models in Reference [14].

cont...

Table 2 – continued

Location	Season	Corrosion Rate ($\mu\text{m}/\text{year}$)		Measured TOW (%)	Rainwater pH	Rainwater Conductivity ($\mu\text{S}/\text{cm}$)	Airborne Salinity ($\text{mg}/\text{m}^2 \cdot \text{day}$)	SO_2 ($\mu\text{g}/\text{m}^3$)	NO_2 ($\mu\text{g}/\text{m}^3$)	HNO_3 ($\mu\text{g}/\text{m}^3$)
		Mild Steel	Zinc							
Ho Chi Minh	March-May	35	0.8	39	6.7	—	7	14	15	5
	June-Sept.	40	1.8	39	6.6	18	4	15	15	8
	Oct.-Jan.		1.2	44	6.0	20	4	20	18.3	6.7
	Feb.-April		0.8		6.9	69	7	25.5	21.1	8.9
Hue	March-May	10	1.7				8	0.8	0.04	0.08
	Oct.-Dec.	57	5.5					0.7	1.2	0.1
Nha Trang	March-May	16	0.7				21	0.6	1.7	0.1
Hanoi	March-May	42	1.9		5.7	66	8	4.7	6.4	3.3
	June-Sept.	25	2.4	95			9	3.9	4.9	3.2
	Oct.-Jan.	36	1.1	85			8	10.1	9.8	6.0
Cowley Beach	Nov.-Feb.	348	8.5	91	6.5	60	317	33	0.9	0.02
	March-May	392	10.6	92	5.0	172	326			
	June-Aug.	421	35.6	94	5.5	220	516	0.7	1.3	0.4
	June-Aug.	71	6.3				48	1.1	1.9	0.7
Walkamin	Nov.-Feb.	6.2	0.7	66	4.9	16	4	1.0	1.3	1.0
	March-May	11	1.7	77	3.9	94	11	1.0	1.3	1.0
	June-Aug.		2.5	67	4.9	22	9	0.6	1.5	0.7
Lembang	March-June	6.2	2.4	39	5.1	17	7	3.9	4.2	1.7
Cikampek	March-June	43.4	2.0	70	5.1	53	25	17.2	28.0	8.4
Gresik	March-June	78.4	4.6	30	4.8	177	10	28.8	0.08	5.0
Jebus	March-June	39.5	1.9	24	7.1	44	47	1.8	2.6	1.1
Mentok	March-June	61.6	1.9	15	5.4	27	20	67.9	10.5	6.1

Table 3 – *Composition of Test Materials*

Material	Chemical Composition									
	Fe	C	Si	Mn	S	P	Ni	Cr	Cu	Zn
Mild steel	Bal.	0.15	0.015	0.73	0.011	0.021	0.022	0.016	0.007	
Zinc	0.003								0.064	Bal.

Regression Analysis of the Five-Nation Study

For all of the seasonal data, regression analysis was carried out to determine the model with the highest R-Sq value for mass loss of steel and zinc (in $\mu\text{m}/\text{year}$). Composite variables were also included in the analysis in line with past work. For example, the variable $\text{TOW}^{F*(A-pH)}$ was introduced in line with the work of Benarie and Lipfert [2]. The models with the best fit are given below along with their R-Sq, mean average error (MAE) and values of the coefficients in Table 4.

Table 4 – *Coefficients of Regression Analysis for Steel and Zinc Mass Loss Equations*

	A	B	C	D	E	F	R-Sq	MAE
Steel	1.3	0.9	0.3	0.81	—	0.27	0.86	1.3
Zinc	0.065	0.5	3.3	0.014	0.9	1.4	0.78	1.6

For steel:

$$\text{Corrosion rate} = A \times \text{TOW}^{F*(A-pH)} \times (B \times \text{SO}_x + C \times \text{salinity})^D \quad (1)$$

For zinc:

$$\text{Corrosion rate} = E + A \times \text{TOW}^{F*(5.5-pH)} + D \times (B \times \text{SO}_x + C \times \text{salinity}) \quad (2)$$

Although the fit for the zinc data appears reasonable with an mean average error of 1.6, much of this fit is associated with the variations caused by the effect of salinity. If the marine sites (Cawley Beach and Phuket) are removed from the data, it is not possible to generate meaningful fits with R-Sq values greater than 0.4. As stated previously, this is inconsistent with models developed in Europe and North America. For example, Tidblad et al. [4] found the following relationships from the UN/ECE relationships for sites with temperatures greater than 10°C:

$$\text{Mass loss} = 1.35[\text{SO}_2]^{0.22} \exp [0.018 \text{RH} - 0.021 (T - 10)]t^{0.85} + \text{Rain}[\text{H}+]t \quad (3)$$

with R-sq = 0.84.

And for weathering steel:

$$\text{Mass loss} = 3.54 + 0.33\text{Ln}(t) + 0.13\text{Ln}[\text{SO}_2] + 0.020 \text{RH} - 0.036 (T - 10) \quad (4)$$

with R-sq = 0.68. Here mass loss is in g/m^2 , T is temperature (°C) and t is time in years.

Thus, in the five-nation study, the lack of dependence of zinc mass loss on gaseous SO_x level (or rainwater pH) is in contrast to the dependence exhibited by mild steel in that study, and by both zinc and mild steel in the UN/ECE study. The levels of SO_2 and

[H+] in rain observed in the UN/ECE study were from 1 to 83 μm^3 and 6×10^{-7} mg/L to 1.3×10^{-4} mg/L (pH from 3.9 to 6.2). Thus, the range of airborne SO_2 and rainwater acidity are similar in both the UN/ECE and the five-nation study.

Modeling of Deposition of Pollutants onto Metal Surfaces

The lack of agreement between the UN/ECE study and the five-nation study is not an isolated occurrence, as there have been a large number of dose functions [1-4] developed for zinc and steel mass loss which show different dependencies on pollutant parameters. A fundamental understanding of chemical processes in pollution deposition may not only provide an understanding of the factors promoting the variations in dose functions, but it may also provide a base to construct more universal models of atmospheric corrosion in polluted environments.

Forms of Deposition

Traditionally in corrosion studies, pollutant deposition has been labeled as "dry" or "wet" deposition – wet deposition being deposition in rain or fog and dry deposition being almost everything else. These groupings tend to obscure significant differences that can occur between different mechanisms in the one group. The forms of deposition could be sub-divided into the following mechanisms.

For dry deposition some of the mechanisms are:

1. aerosol deposition;
2. gaseous deposition into a moisture film; and
3. gaseous deposition onto a truly "dry" surface.

For wet deposition it is useful to include:

4. deposition by fogs;
5. deposition by fine raindrops; and
6. deposition by coarse raindrops.

All of these mechanisms except No. 3 depend on the chemistry of gaseous/aqueous phase interactions and on aqueous phase reactions. It is thus useful to quickly review the principal reactions that control gaseous absorption into moisture layers. The principal approximation [10] for gaseous absorption is Henry's law, which states:

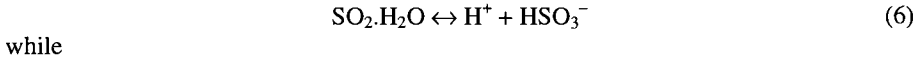
$$[A(\text{aq})] = H_a p_a \quad (5)$$

where $[A(\text{aq})]$ is the aqueous phase concentration in mol L^{-1} , and p_a is the partial pressure in the gas phase in atm. Henry's law coefficients are taken from Seinfeld and Pandis [10] and are given in Table 5.

Table 5 – *Henry's Law Coefficients for Common Gases*

Species	H (M atm^{-1}) at 298°K
O_2	1.3×10^{-3}
NO_2	1.0×10^{-2}
CO_2	3.4×10^{-2}
SO_2	1.23
NH_3	62
NO_3	2.1×10^5
OH	25
O_3	1.1×10^{-2}

Once the gases are dissolved the hydrolyzed products may dissociate. The reactions are presented below:



The balance of HSO_3^- versus SO_3^{2-} depends on pH, with the former dominating at pH values of 2.5–7, and the latter above this.

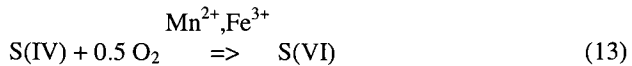


The Henry's law coefficient for NH_3 is 62 M atm^{-1} , while the equilibrium constant (K_{eq}) value for the dissociation of $\text{NH}_3 \cdot \text{H}_2\text{O}$ is 1.7×10^{-5} . Calculation readily indicates that in solutions with $\text{pH} < 8$ the dissolved ammonia is predominately in the form of ammonia ion.



The Henry's law coefficient for CO_2 absorption is 3.4×10^{-2} , while the K_{eq} constant for equations (11) and (12) are respectively 4.3×10^{-7} and 4.7×10^{-11} . Thus, the absorption of CO_2 is quite low at acidic pH values but rises rapidly as the pH increases into the basic range.

A major aqueous reaction of importance is the oxidation of SO_3^{2-} or other forms of S(IV) to SO_4^{2-} or other forms of S(VI). This may occur via a variety of mechanisms, including reactions with O_3 , H_2O_2 and O_2 (catalyzed by Mn (II), Fe (III) and NO_2).



for example, where S(IV) may be HSO_3^- or SO_3^{2-} and S(VI) is HSO_4^{2-} or SO_4^{2-} .

According to Hoffman and Calvert [11], the reaction rate is given by:

$$1.2 \times 106 [\text{Fe(III)}][\text{S(IV)}] \quad (14)$$

The sulfate that forms from oxidation of S(IV) may exist as SO_4^{2-} or HSO_4^- (H_2SO_4 dissociates to HSO_4^- under pH ranges likely for droplets in the atmosphere or on surfaces). The balance is governed by:



The K value for equation (15) is 1×10^{-2} and thus the concentration of HSO_4^- will increase with acidity. Having outlined the equations that control the moisture film reactions (in wet particulates, raindrops and moisture films on surfaces), it is appropriate to return to the discussion of the forms of deposition.

Aerosol Deposition

Atmospheric aerosols consist of particles that span size ranges from 0.01 to 100 μm [10]. This range is usually divided into three, viz.: the nuclei range ($<0.1 \mu\text{m}$), the accumulation range (0.1–2.5 μm) and the coarse range ($>2.5 \mu\text{m}$). Gaseous absorption into wet aerosol through the processes outlined above controls the chemistry and (along with physical cycles of evaporation, wetting and impact) the growth of particles in the accumulation mode [10]. For atmospheric corrosion, aerosol in the accumulation and coarse range is most important. Figure 1 (from Wall *et al.* [11]) shows the measured size distribution of aerosol sulfate, nitrate, ammonium, chloride, sodium and hydrogen ion. The units used in this figure are standard in atmospheric chemistry. The value on the y-axis is the concentration of particles per m^3 of air in a diameter size band proportional to $\log D_{ae}$. For this discussion consider the ammonium and sulfates. Both have two peaks in the accumulation (around 0.7 μm) and in the coarse range (around 3 μm). Approximately three-quarters of the particles are in the accumulation range, with the remaining one-quarter in the coarse range.

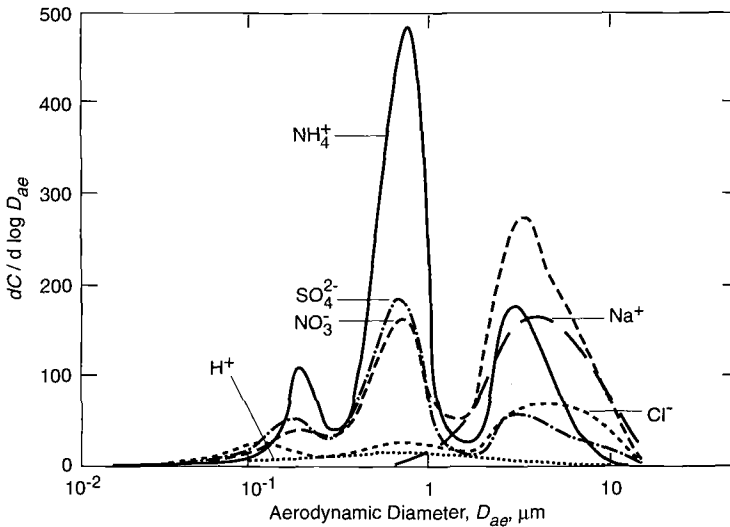


Figure 1 – Measured Size Distribution of Aerosols in an Urban Location (from Reference [12])

The deposition of particles on horizontal surfaces is given by the following relation:

$$F = -v_d \times C \quad (16)$$

where F is the dry deposition flux, v_d is the proportionality constant known as the deposition velocity, and C is the local concentration of the depositing species. The equivalent formula for vertical surfaces is:

$$F = -\eta v_w C \quad (17)$$

where v_w is the local wind speed perpendicular to the surface and η is a collection efficiency in the range 0–1. The efficiency approaches 1 for large aerosol particles and 0 for small aerosol particles.

The exact definitions of v_d and η are complicated and outside the scope of this paper. Work by Sehmel [13] provides a useful estimation of the deposition velocity. The deposition velocity for 0.7 and 3 μm particles would be approximately 10^{-4} and 10^{-3} m s^{-1} . By way of contrast, a typical wind speed is 3 m s^{-1} and collection efficiencies for these particles are roughly 0.0027 and 0.18, giving product velocities ηv_w of 8.1×10^{-3} and 0.54 m s^{-1} . From this it is clear that the deposition on vertical surfaces is larger.

The concentration of particulates varies significantly with location and climate. A high concentration of ammonia and sulfate particulates would be 20 $\mu\text{g m}^{-3}$ (dry weight). Let us assume that 15 $\mu\text{g m}^{-3}$ are fine and 5 $\mu\text{g m}^{-3}$ are coarse. The flux on vertical surfaces would then be 0.12 $\mu\text{g m}^{-2} \text{s}^{-1}$ and 2.7 $\mu\text{g m}^{-2} \text{s}^{-1}$ for the fine and coarse particles respectively, while the flux on horizontal surfaces would be 1.5×10^{-3} $\mu\text{m}^2/\text{m}^2 \text{s}$ and 5×10^{-3} $\mu\text{m}^2/\text{m}^2 \text{s}$ for fine and coarse particles respectively. A plate exposed at an angle of 45° , will have deposition with both vertical and horizontal components, but will be dominated by the horizontal component which, for standard size exposure plates (100 \times 150 mm), would be approximately 2600 μg per day (an analysis based on equation (16) alone yields only 10 μg per day).

It is a simple exercise to calculate the volume of these particles and the number and coverage. Assuming that the wet weight is twice the dry and that the density of the wet aerosol is 1.5 g cm^{-3} (values applicable to H_2SO_4 aerosol at a humidity of around 55%), then the wet volume is 3.5 mm^3 . If this were to form a 2 μm film on the plate, it would have an area of approximately 1.8×10^3 mm^2 which is one-nineth of the surface area of the plate.

If we assume that the surface was wet, the contribution of aerosol deposition to the chemistry of the moisture layer depends primarily on the thickness of that moisture layer. The molecular weights of the ammonia/sulfate aerosol range from 98 g/M for sulfuric acid, 115 g/M for ammonia bisulfate and 113 g/M for ammonia sulfate. Assuming the moisture film was 1, 10 and 100 μm thick and covered the whole surface of the plate, particulate deposition then raises the concentration of solution per hour by 8×10^{-2} , 8×10^{-3} and 8×10^{-4} M/L.

These cases of aerosol deposition onto a dry surface and onto a wet surface result in surface moisture films with very different concentrations. In the case of deposition

onto a dry surface, a large number of very small but concentrated droplets will reside on the surface. These droplets will either continue to wet or will evaporate, depending on the deliquescence relative humidity (DRH). The values of DRH range from 80% for ammonia sulfate to 52% for ammonia bisulfate, while H_2SO_4 does not have a deliquescence point and absorbs significant moisture to below 20% RH. Thus, such deposition could lead to a significant number of active corrosion sites. However, these sites will be small and may not persist for any significant length of time (due to evaporation). In contrast, deposition into a moisture film will result in a moisture film which is much less concentrated than the aerosol and thus is likely to be less aggressive to the metal.

Simulation of Gaseous Absorption and Aqueous Processes

In order to understand the effect of gaseous absorption and the subsequent aqueous reactions, a chemical simulator has been used to determine the development of the chemistry of the moisture films. The simulator – the Chemical Kinetics Simulator (CKS) – is produced by IBM–Almaden Research Centre. It uses a stochastic method, based on reaction probabilities, to calculate the time history of a chemical system using the specified reaction's mechanism and the initial conditions. It treats the reacting system as a volume filled with a limited number of particles which represent reactants and products. The model specified was relatively simple. It is assumed that moisture layer/gaseous layer is an open system in that the composition of the gas phases remains constant. Further, it is assumed that the moisture layer has a fixed volume and is at a constant temperature of 298°K, and that the substrate is effectively inert. Clearly this last assumption is not valid and in further work it will be relaxed. However, the complexity of the system increases dramatically if an active surface is permitted, and with this level of complexity it would be difficult to determine clearly the role of absorption of the different gases on moisture layer chemistry.

To highlight in a systematic way the effect of absorption of a different range of gases, the following systems are studied:

1. CO_2 only at 400 ppm;
2. CO_2 at 400 ppm and SO_2 from 5, 10, 20, 40, 75, 150 and 300 ppb;
3. CO_2 at 400 ppm, SO_2 from 20, 40, 75, 150 and 300 ppb and NH_3 at 20ppb; and
- 4a. CO_2 at 400 ppm, SO_2 at 75 ppb, O_3 at 200 ppb and H_2O_2 at 10 ppb.
- 4b. CO_2 at 400 ppm, SO_2 at 75 ppb, NH_3 at 20 ppb, O_3 at 200 ppb and H_2O_2 at 10 ppb.
- 4c. CO_2 at 400 ppm, SO_2 at 75 ppb and NH_3 at 20 ppb and Fe^{3+} (aqueous) at 6×10^{-6} M/L.

System 1 – The system behaved as expected from equilibrium considerations. Limited dissociation of absorbed $\text{CO}_2 \cdot \text{H}_2\text{O}$ (concentration 1.2×10^{-5} M/L) resulted in a pH of 5.6 and a low concentration of HCO_3^- at 2.5×10^{-6} M/L after 0.02 s when stable conditions were reached.

System 2 – The system reaches a stable condition relatively quickly (by 2×10^{-2} s in all cases). Not surprisingly, the pH is lowest with the highest SO_2 gas concentration and then increases progressively towards (but never reaching) the CO_2 -only value of 5.6. HCO_3^- concentrations are low and increase as SO_2 gas concentrations decrease (and pH increase), while all aqueous forms of S(IV) decreases as gaseous SO_2 is decreased. The results are given in Figure 2.

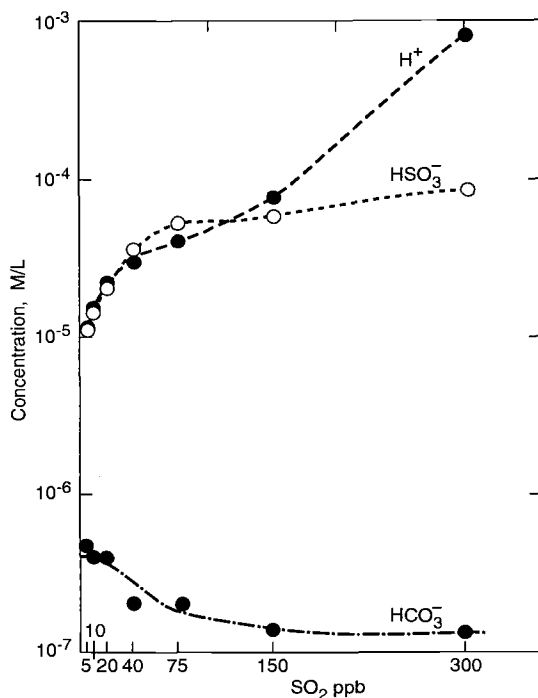


Figure 2 – Ion Concentration in System 2 as a Function of Gaseous SO₂ Concentration

System 3 – Compared to system 2, the effect of adding NH₃ is not only a dramatic increase in pH (for the same gaseous SO₂ level), but also a dramatic increase in HSO₃⁻ (five times greater in System 3 after 2 × 10⁻² s compared with equilibrium conditions of System 2) and SO₃²⁻ content. A pH is established where the rate of HSO₃⁻ formation and NH₄⁺ formation match, and thus pH remains constant while HSO₃⁻ concentration increases. This could have a curious effect on corrosion rate. If the rate is primarily pH-dependent, then the corrosion rate should decrease with decreasing gaseous SO₂. However, if the rate is ligand-dependent, then the corrosion rate could actually increase with decreasing gaseous SO₂. At moderate and low gaseous SO₂ concentrations a significant concentration of HCO₃⁻ develops. The effect of HCO₃⁻ on corrosion is unclear as, while HCO₃⁻ may promote ligand-assisted dissolution which promotes corrosion, the metal carbonates that form are likely to be more stable than metal sulfates or sulfites.

System 4 – A review by Seinfeld and Pandis [10] indicated that the three most efficient oxidants (or catalysts) for S(IV) at pH values expected for moisture films on metal surfaces (pH 3–7) were H₂O₂ and O₃ and Fe(III), and thus Systems 4a–4c investigate each in turn. System 4a considers the effect of H₂O₂ and O₃ when there are no basic gases, and System 4b when NH₃ is present. In both cases the gaseous concentration of H₂O₂ and O₃ are at the upper end of the normal range. In System 4c, Fe(III) is the catalyst for the oxidation reaction [13]. The value chosen for Fe(III) was 6 × 10⁻⁶ M/L. If

the corrosion rate of steel is 100 $\mu\text{m}/\text{year}$, a 33 μm moisture film would be enriched by exactly this amount of Fe^{3+} each second. The chemistry of the moisture films resulting from the different oxidants is given in Table 5 after 1.0 s of simulation. After this period of time, the pH of the solution was stable although the concentration of S(VI) ions was still increasing.

The effect of the oxidants on System 4a was to moderately increase the acidity compared to the same SO_2 concentration without oxidants (System 2 as illustrated in Figure 2) and to decrease significantly the HSO_3^- and SO_3^- level. It is notable that HSO_4^{2-} dissociates much more readily than HSO_3^- so that the addition of the oxidant actually decreases ligand concentration. The addition of the oxidants to a system containing both SO_2 and NH_3 gas increases the acidity significantly and decreases the HSO_3^- and SO_3^- level compared to the same gaseous concentrations (System 3 in Table 6 and Figure 3). This is much more marked in System 4c when the catalyst was Fe(III) compared to System 4b where the oxidants were H_2O_2 and O_3 . In the case of System 4c, the acidity is increased back to the same level as System 2 where there is no NH_3 to counteract the acidification of SO_2 absorption. In all cases the transformation of S(IV) to S(VI) reduces the concentration of sulfur-containing ligands.

Comparison of Effect of Particulate Deposition and Gaseous Absorption

The concentration of possible ligands varies depending on which system (studied above) is taken as representing the physical environment. With only SO_2 and CO_2 gas (system 2), HSO_3^- concentrations vary from 1 to 9×10^{-5} M/L. If NH_3 is added, HSO_3^- concentrations increase from 1 to 8×10^{-4} M/L. These concentrations are established within 0.2 s of exposure. The relative magnitude of particulate deposition and gaseous absorption depends on the thickness and residence time of moisture on surfaces. However, fine films are likely to have a short residency time. The effect of particulate deposition into a 1 μm film that exists for 6 minutes would be the same as 100 μm that exists for 10 hours. In both cases, particulate deposition raises the concentration by around 8×10^{-3} M/L, which is of the same order as gaseous absorption with NH_3 , and an order of magnitude high than gaseous absorption without NH_3 .

Discussion

The study of the gaseous absorption and aqueous phase reactions has indicated that the chemistry of moisture layers or droplets in populated environments is highly influenced by:

1. the ratio of ammonia to sulfur dioxide; and
2. the presence of species promoting oxidation of S(IV) to S(VI).

Table 6 – Concentration of Key Ions After 1.0 s

System	Oxidant	[H]	$[\text{HCO}_3^-]$	$[\text{HSO}_3^-]$	$[\text{HSO}_4^-]$	$[\text{SO}_3^{2-}]$	$[\text{SO}_4^{2-}]$
3	None	2.8×10^{-7}	2.0×10^{-5}	4.2×10^{-3}	—	1.0×10^{-3}	—
4a	$\text{O}_3, \text{H}_2\text{O}_2$	3.2×10^{-4}	—	7.7×10^{-6}	—	—	1.5×10^{-4}
4b	$\text{O}_3, \text{H}_2\text{O}_2$	1.8×10^{-6}	2.7×10^{-6}	9.3×10^{-4}	—	2.9×10^{-5}	2.2×10^{-4}
4c	Fe(III)	1.5×10^{-6}	6×10^{-8}	10×10^{-5}	1.6×10^{-6}	—	1.0×10^{-4}

Acidity of moisture films is promoted by low ammonia to sulfate ratios and high levels of oxidizers. Dissolution of oxide films (particularly metal hydroxides that will form under moisture layers) will be facilitated by both proton-promoted and ligand-promoted dissolution. According to Farrow et al. [6], bisulfite (HSO_3^-) is particularly effective in promoting dissolution, as bonding of a metal hydroxide to the HSO_3^- weakens the bonding of the same metal surface atom with its neighbors. It would be reasonable to suppose that HSO_4^- would have similar properties. Thus, the rate of dissolution of metal hydroxide is likely to be highly influenced by proton, bisulfate and bisulfite concentrations. Higher proton concentrations will of course be promoted by lower ammonia to sulfur dioxide ratios, but higher bisulfite will be promoted by higher ammonia to sulfur dioxide ratios, and higher bisulfate by greater oxidant concentrations. Higher oxidant concentrations will also of course increase the proton concentrations.

The above discussion is valid for wet aerosol, rain droplets and moisture films on surfaces. The major difference would be residency time.

There are however some specific factors relevant to only specific deposition modes. Firstly consider aerosols – in the absorption and aqueous phase reactions occurring in fine aerosols, a range of ammonia sulfates form in the aqueous reactions depending on the ratio of availability of NH_3 and SO_2 . These range from H_2SO_4 to NH_4HSO_4 to $(\text{NH}_4)_3\text{H}(\text{SO}_4)_2$ to $(\text{NH}_4)_2\text{SO}_4$, with the last three compounds having DRHs of 40, 69 and 80% respectively. Thus, the wettability of aerosol deposited on a metal surface will also depend on the NH_3/SO_2 ratio, with those compounds forming at low ratios being the most wettable.

Thus, the exact chemistry of atmospheric gases will significantly influence the corrosion rate. The worst scenario is a high SO_2 level and high oxidant level. The most benign environment is a low SO_2 and high NH_3/SO_2 ratio. The relative aggressivity of moderate SO_2 and NH_3/SO_2 ratios depends on the relative effect of proton exchange dissolution and ligand exchange dissolution.

This analysis may indicate why the five-nation study into mass loss of zinc demonstrated such a weak dependence on SO_2 levels. A full elemental analysis has not yet been carried out on rainwaters from the industrial/tropical locations in the five-nation study. However, the analysis of the aqueous reactions indicates that to have a near-neutral pH in an area with high SO_x , such as the industrial Thai sites, there must be a relatively high level of NH_3 . Further, the surface wetting was consistent with contamination by an ammonia sulfate [8]. If there is a significant NH_3 concentration it would also imply that significant acidification of moisture films on zinc surfaces by SO_2 absorption would be negated by the generation of hydroxide during absorption of NH_3 . However, it is possible that on steel surfaces, significant Fe(III) may promote greater SO_2 absorption, increasing the acidity of the moisture films and promoting greater corrosion.

It has already been highlighted that fine raindrops and fogs are likely to be more acidic than heavy droplets. Moonsoonal rains consist predominately of coarse droplets, thus it is probable that they will have lower acidity than the fine rains and fogs of Europe and North America.

The work outlined in this paper has looked at reactions that occur in moisture films assuming that the geometry of the moisture film does not vary with time. Clearly this is, in general, invalid as moisture will evaporate and condense on the surface in line with the diurnal climate cycle. However, the simulations in this paper were run for short

intervals over which the assumption of a static moisture layer is correct. Future work will assess the significance of longer temporal cycles in moisture layers. The occurrence of such cycles is unlikely to alter the importance of the role of the absorption and aqueous processes outlined in this paper, although it may alter the details of the processes.

Conclusion

Results from a five-nation study indicate a poor relationship between zinc corrosion rates and gaseous SO_2 levels. This was in contrast to results from the same study for steel and from previous studies in Europe and North America.

An analysis was undertaken of the gaseous absorption and aqueous phase reactions that control the chemistry of wet aerosol, rain droplets and moisture films on surfaces. The analysis indicates that the acidity and $\text{HSO}_3^-/\text{HSO}_4^-$ content is highly influenced by the ratio of gaseous NH_3/SO_2 and by the concentration of oxidizing agents for S(IV). Further, low NH_3/SO_2 ratios also promote aerosol which wets at a low RH. Thus, it is probable that corrosion rates will be higher in locations where the NH_3/SO_2 ratio is low and oxidant level is high.

Indications from the five-nation study are that, at least for the Thai sites, the NH_3/SO_2 ratio is quite high and thus aerosol rainwater and surface moisture films will have limited acidity and be less corrosive than if the NH_3/SO_2 ratio is high. The higher corrosion rate for steel could arise if the presence of Fe(III) promotes oxidation of S(IV) to S(VI), and greater SO_2 absorption and acidification of surface moisture layers.

References

- [1] Atteraa, L., and Haagenrud, S., "Atmospheric Corrosion in Norway," *Atmospheric Corrosion*, W. H. Ailor, Ed., John Wiley & Sons, New York, 1982, pp. 873–891.
- [2] Benarie, M., and Lipfert, F. L., "A General Corrosion Function in Terms of Atmospheric Pollutant Concentration and Rain pH," *Atmospheric Environment*, 1986, Vol. 20, No. 10, pp. 1947–1958.
- [3] Spence, J. W., and Haynie, F. H., "Derivation of a Damage Function for Galvanised Steel Structures: Corrosion Kinetics and Thermodynamic Considerations," in *Corrosion Testing and Evaluation: Silver Anniversary Volume, ASTM STP 1000*, American Society for Testing and Materials, West Conshohocken, PA, 1990, pp. 208–224.
- [4] Tidblad, J., Mikaliyov, A. A., and Kucera, V., "Unified Dose-Response Functions After 8 Years of Exposure," Proc. UN/ECE Workshop on Quantification of Effects of Air Pollutants on Materials, Berlin, Germany, 24–27 May 1998, p. 77.
- [5] Svensson, J. E., and Johansson, L. G., "A Laboratory Study of the Effect of Ozone, Nitrogen Dioxide and Sulphur Dioxide on the Atmospheric Corrosion of Zinc", *Journal of the Electrochemical Society*, 1993, Vol. 140, pp. 2210–2216.
- [6] Farrow, L. A., Graedel, T. E., and Leygraf, C., "Gildes Model Studies of Aqueous Chemistry: II – The Corrosion of Zinc in Gaseous Exposure Chambers," *Corrosion Science*, 1998, Vol. 38, No. 12, pp. 2181–2199.
- [7] Graedel, T. E., "Gildes Model Studies of Aqueous Chemistry: I – Formulation and Potential Applications of the Multi-Regime Model, *Corrosion Science*, 1998, Vol. 38, No. 12, pp. 2153–2180

- [8] Cole, I. S., Neufeld, A. K., Kao, P., Ganther, W. D., Chotimongkol, L., Bharmornsut, C., Hue, N. V., and Bernardo, S., "Corrosion Mechanisms and Performance Tests for Tropical Environments," Proc. 14th International Corrosion Conference, Cape Town, South Africa, 27 September to 1 October 1999, Paper 265.2 (CD-ROM).
- [9] Cole, I. S., Neufeld, A. K., Kao, P., Ganther, W. D., Chotimongkol, L., Bharmornsut, C., Hue, N. V., Bernardo, S., and Purwadaria, S., "Development of Performance Verification Methods for the Durability of Metallic Components in Tropical Countries," Proc. 11th Asia-Pacific Corrosion Control Conference, Ho Chi Minh City, Vietnam, 1-5 November 1999, Vol. 2, pp. 555-570.
- [10] Seinfeld, J., and Pandis, S., *Atmospheric Chemistry and Physics: From Air Pollution to Climate Change*, Wiley Interscience, 1997.
- [11] Hoffman, M. R., and Calvert, J. G., *Chemical Transformation Modules for Eulerian Acid Deposition Models: Vol. 2 - The Aqueous-Phase Chemistry*, EPA/600/3-85/017, US Environmental Protection Agency, Research Triangle Park, NC, 1985.
- [12] Wall, S. M., John, W., and Ondo, J. L., "Measurement of Aerosol Size Distribution for Nitrate and Major Ionic Species," *Atmospheric Environment*, 1988, Vol. 22, pp. 1649-1656.
- [13] Sehmel, G. A., "Particle and Gas Deposition: A Review," *Atmospheric Environment*, 1980, Vol. 14, pp. 983-1011.
- [14] Cole, I. S., Furman, S. A., Neufeld, A. K., Ganther, W. D., and King, G. A., "A Holistic Approach to Modelling Atmospheric Corrosion," Proc. 14th International Corrosion Conference, Cape Town, South Africa, 27 September to 1 October 1999, Paper 265.4 (CD-ROM).

Robert Klassen,¹ Bruce Hinton,² and Pierre Roberge³

Aerosol Model Aids Interpretation of Corrosivity Measurements in a Tropical Region of Australia

Reference: Klassen, R., Hinton, B., and Roberge, P., **Aerosol Model Aids Interpretation of Corrosivity Measurements in a Tropical Region of Australia,”** *Marine Corrosion in Tropical Environments, ASTM STP 1399*, S. W. Dean, G. Hernandez-Duque Delgadillo, and J. B. Bushman, Eds., American Society for Testing and Materials, West Conshohocken, PA, 2000.

Abstract: The corrosivity pattern near the tropical coastal city of Townsville, Australia is of interest because of concerns related to the corrosion of RAAF aircraft. The corrosivity at seven sites near Townsville was characterized over a four-year period with bimetallic specimens (CLIMAT units) and salt candles. The CLIMAT results highlight the effects of elevation above the ground and topography on local corrosivity. The increase in corrosivity due to elevation at the same site is readily explained by the increase in aerosol deposition. The flow pattern around objects that significantly obstruct wind is very complicated but one clear conclusion is that the wind flow speed and turbulence are highest near the top. Thus aerosol deposition, and therefore corrosion, rates are higher near the top of obstructions to wind such as hills and buildings. The main conclusion is that the principles of salt aerosol transport and deposition offer a physical framework for understanding and predicting patterns of aerosol deposition and consequently the patterns of corrosivity.

Keywords: aerosol transport, aerosol deposition, modeling, corrosivity patterns, tropical marine environment

Introduction

A good deal of effort has been expended in characterizing the atmospheric corrosivity near Townsville, Australia because of the presence of an RAAF Base (Townsville) located about 4 km from the coast. These efforts are part of a larger

¹Research Associate, Dept. Chem./Chem. Eng., Royal Military College of Canada, Kingston, Ontario, Canada K7K 7B4.

²Head, Aircraft Corrosion Control, Maritime Platforms Division, Aeronautical and Maritime Research Laboratory, Melbourne, Victoria, Australia 3207.

³Professor, Dept. Chem./Chem. Eng., Royal Military College of Canada, Kingston, Ontario, Canada K7K 7B4.

endeavor to allow aircraft maintenance to be responsive to the corrosivity of the environments to which they are exposed. An outline of Australia is illustrated in Fig. 1, showing the location of Townsville (latitude $19^{\circ} 16'$) along the Coral Sea coast.

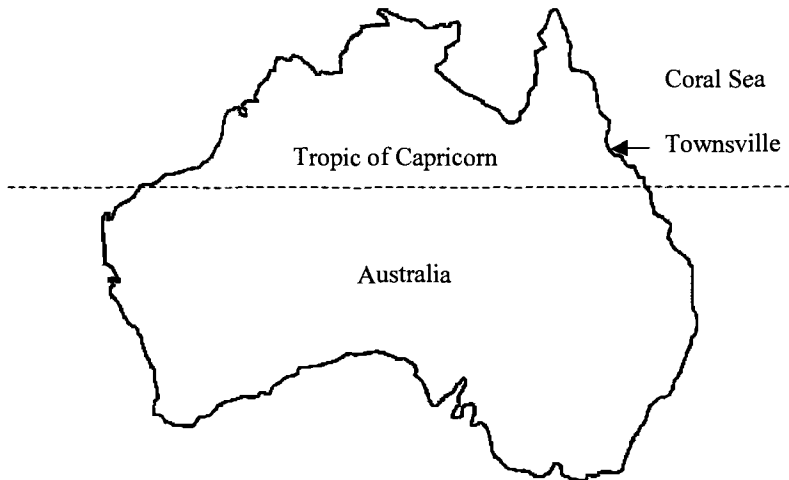


Figure 1- *Outline of Australia identifying the location of the city of Townsville, Queensland.*

Townsville qualifies as a tropical marine site because it is situated between the Tropic of Capricorn and the equator and because it has a coastal location. The city enjoys an average of 320 days of sunshine per year, winter (June to August) temperatures that range from $13\text{-}26^{\circ}\text{C}$ and summer (Jan. to Mar.) temperatures that range from $23\text{-}31^{\circ}\text{C}$. The average wind direction changes from being predominately from the east during the summer to being from the southeast during the winter. The average rainfall, between 1884 and 1985, for the city of Cairns, which is approximately 400 km north of Townsville along the coast, was 2075 mm. The pattern of rainfall has a clear seasonal trend as shown in Fig. 2 with most of the rain falling during the summer months.

According to the Pacer-Lime algorithm [1], the city of Townsville should be classified as a marine site because it is within the cut-off distance of 11 km from a salt-water body. Therefore corrosivity measurements, including CLIMAT units [2, 3] at seven sites and salt candles at two sites, are being conducted on an ongoing basis.

The dry deposition rate of chloride aerosol particles is one of the factors that influence the corrosion rate of objects along with relative humidity and exposure to pollutants such as SO_2 [4]. The principles of aerosol transport and surface deposition can provide a theoretical framework for interpreting salt aerosol deposition patterns and therefore for predicting atmospheric corrosion patterns [5, 6].

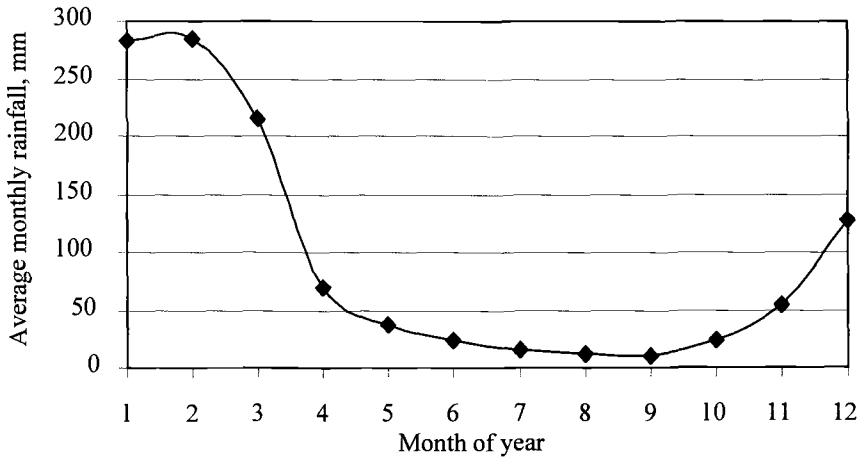


Figure 2- Average monthly rainfall in Townsville, Queensland

Aerosol Transport and Deposition

Aerosol chloride particles are transported from sources such as salt-water bodies or salted roads via the wind. Although the largest particles in a marine aerosol settle to the ground by sedimentation, most particles are freely transported by convection and turbulent diffusion [5]. Within the planetary boundary layer (PBL) of the earth the horizontal wind velocity profile, $U(y)$, is characterized by the following equation [7]:

$$U(y) = \frac{u^*}{k} \log\left(\frac{y}{y_0}\right) \tag{1}$$

where u^* is the friction velocity at the surface, y is the height above ground, y_0 is the surface roughness and k is the von Karman constant (~ 0.4).

There are two modes of aerosol deposition that are relevant for particles in the size range of marine-type aerosols: (i) inertial impaction and (ii) turbulent diffusion. Inertial impaction is significant for objects that are small enough not to cause gross changes in the surrounding air flow pattern as illustrated in Fig. 3. Essentially, some of the upstream aerosol particles are not able to follow the flow lines around the object due to inertia. Examples include devices used for measuring atmospheric corrosivity such as CLIMAT units and salt candles. The deposition rate due to inertial impaction is

$$R_d = C_\infty U_\infty A_t \eta \tag{2}$$

where R_d is the aerosol deposition rate, C_∞ is the upstream aerosol concentration, U_∞ is the upstream wind velocity, A_t is the projected target area and η is the capture efficiency of the target.

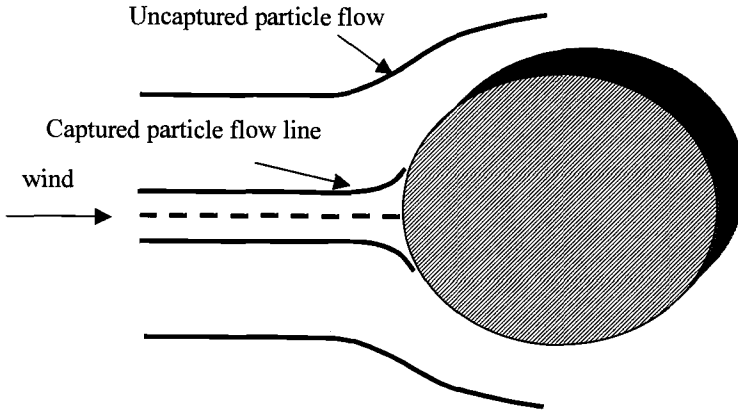


Figure 3- *Aerosol capture onto a cylinder due to inertial impaction*

The capture efficiency for several shapes such as cylinders, spheres and airfoils has been estimated based on solving the appropriate equation of motion for particles and an assumed fluid velocity profile around the target [8]. The capture efficiency depends on characteristics of the aerosol such as particle density and size as well as the target diameter and the upstream wind velocity. An overall capture efficiency, E , may be defined as the volume fraction of aerosol particles that are captured at a given wind speed, target size, particle density and aerosol size distribution,

$$E = \int_{D_{p,min}}^{D_{p,max}} \frac{g(D_p)\eta(D_p, U_\infty, D_t, \rho_a)dD_p}{D_p} \tag{3}$$

where $g(D_p)$ is the log-normal volume distribution function of particles. Therefore, $g(D_p)dD_p/D_p$ is the volume fraction of particles in the size range D_p and D_p+dD_p . The minimum and maximum particle size, $D_{p,min}$ and $D_{p,max}$, for a marine aerosol may be taken as 1 and 70 μm . A plot of E versus wind speed for three target diameters is shown in Fig. 4.

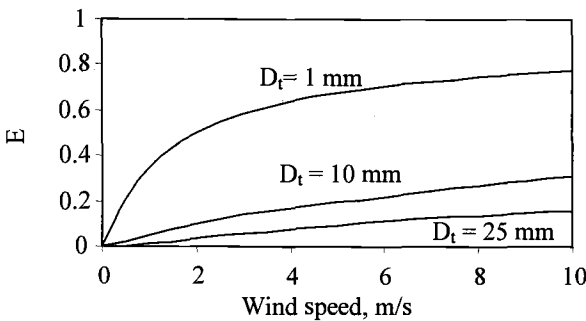


Figure 4- *Capture efficiency, E , for a marine aerosol as a function of wind speed with cylinder, D_t*

The target diameter of 25 μm simulates an ISO salt candle and the target size of 10 μm simulates a CLIMAT bolt. Based on the capture curve in Fig. 4, only the largest particles in a marine aerosol are captured at low wind speeds. However, since these particles constitute a very small volume fraction of the aerosol, the volume fraction of particles that are captured is low. As the wind speed increases, increasingly smaller particles are captured. As is evident from Fig. 4, at a wind speed of 10 m/s, which is a fairly strong wind, most of the particles are not captured onto an ISO salt candle. Thus the ISO salt candle is a rather inefficient collector of marine aerosols.

The mode of aerosol deposition onto surfaces that is relevant for aerosol particles in the outside environment is turbulent diffusion. Particles are transported by turbulent diffusion to a diffusion sub-layer along the surface and then follow a free path to the wall due to inertia. The details of these calculations for the illustrative example are presented in Ref. [6].

Simulated Salt Candle Deposition Field Around an Obstacle

The airflow and salt candle deposition fields were calculated for the geometry shown in Fig. 5. The obstacle is 3 m high by 2 m wide and was intended to simulate a small shed.

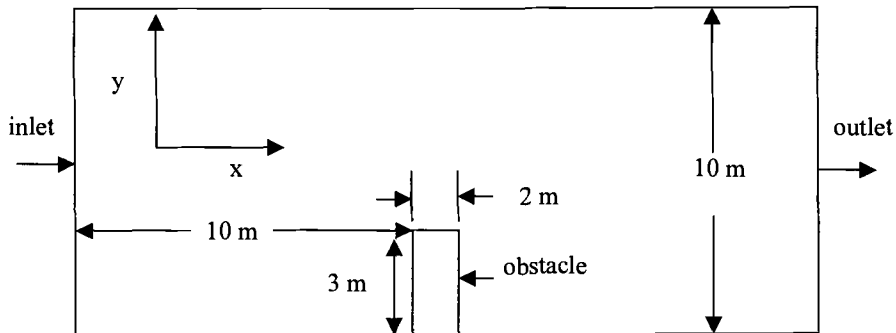


Figure 5- Geometry of the calculation domain

Wind was considered to enter the domain at the left edge at a constant velocity of 10 m/s. The inlet aerosol concentration was set to unity from $y = 0$ to $y = 3$ m and zero above 3 m in order to simulate a surface salt source such as an ocean. The flow field was obtained using commercial software [9]. The horizontal and vertical turbulent diffusivities were obtained from the turbulence intensity and velocity gradient fields. The aerosol concentration field was obtained by assuming the aerosol is transported by convection and turbulent diffusion [10]. Equation (2) was then employed to calculate the salt candle deposition rate at each control volume

A contour plot of the horizontal velocity (U) field is shown in Fig. 6. The obstacle has an obvious and strong influence on the wind flow field in its vicinity. The flow slows

considerably in front of the obstacle but speeds up near the top of the obstacle and then recirculates behind the obstacle.

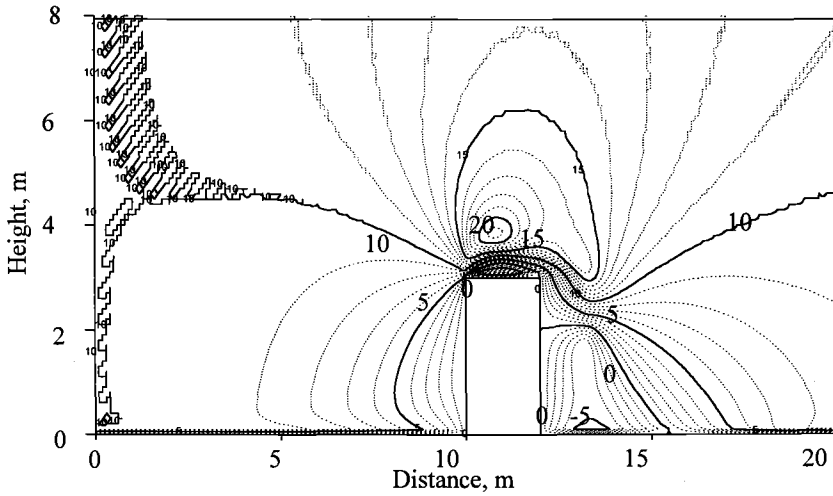


Figure 6- Contour plot of the horizontal velocity, u , around the obstacle

The relative aerosol concentration field is shown in Fig. 7. The concentration on the front side of the obstacle is nearly the same as the source. A smooth concentration

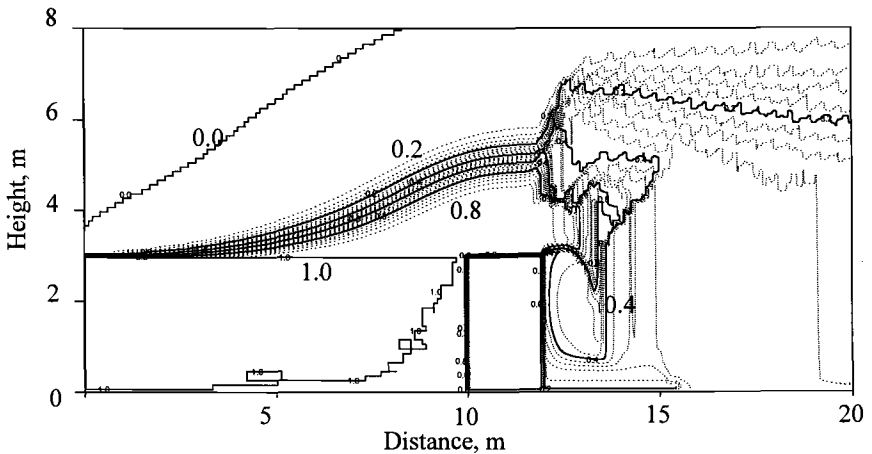


Figure 7- Contour plot of the relative aerosol concentration field around the obstacle

gradient between unity and zero develops in front of and above the obstacle until near the back edge. Downstream and above the obstacle the concentration profiles are ragged due to the influence of turbulent diffusion. One effect of the obstacle is to vertically disperse the aerosol and subsequently the concentration immediately downstream of the obstacle is between 20% and 40% of that upstream of the obstacle.

The contour map for the salt candle deposition field is shown in Fig. 8. The maximum rate is just above the obstacle and slightly on the upstream side. This is due to two factors. One, the relative aerosol concentration at this point is high, namely 96-100% of the source level. Two, the peak horizontal velocity, U , is also located just above the obstacle (Fig. 6). The salt candle deposition rate near the base of the obstacle on both the upstream and downstream sides is nearly zero due to the relatively low wind velocities in these areas. The pattern of ragged contour lines above and downstream of the obstacle is identical to the ragged contour lines of the aerosol concentration in this area (Fig. 7).

The salt candle deposition field near the obstacle has a highly localized structure. Near the top of the obstacle, a small change in location results in nearly an order of magnitude change in response. This is in contrast to another corrosivity factor, relative humidity, whose scale extends typically from hundreds to thousands of meters. Thus more measurements are required to characterize aerosol deposition than relative humidity for a given geographic area.

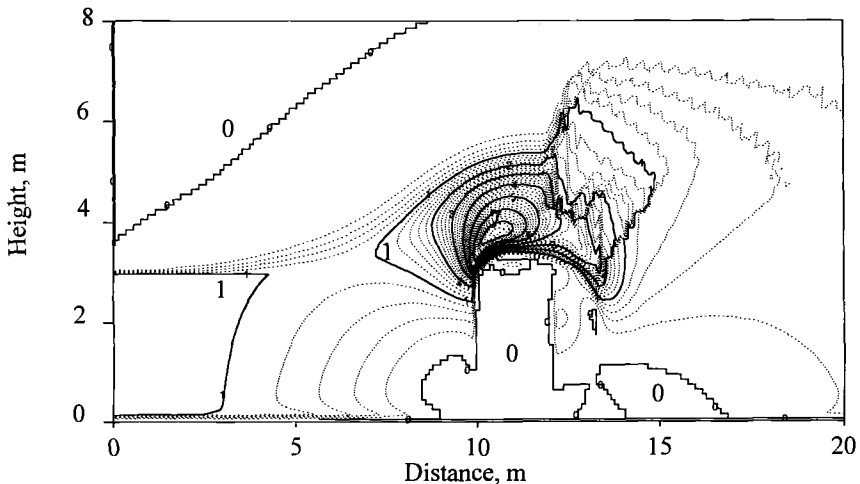


Figure 8- Contour plot of the salt candle deposition rate near the obstacle

Experimental

CLIMAT units were exposed between 1995 and 1998 at the seven sites near Townsville shown in Fig. 9. Only copper bolt/aluminum wire combinations were

exposed and not steel or plastic bolts. Salt candles were also exposed at the RAAF maintenance site between 1995 and 1998.

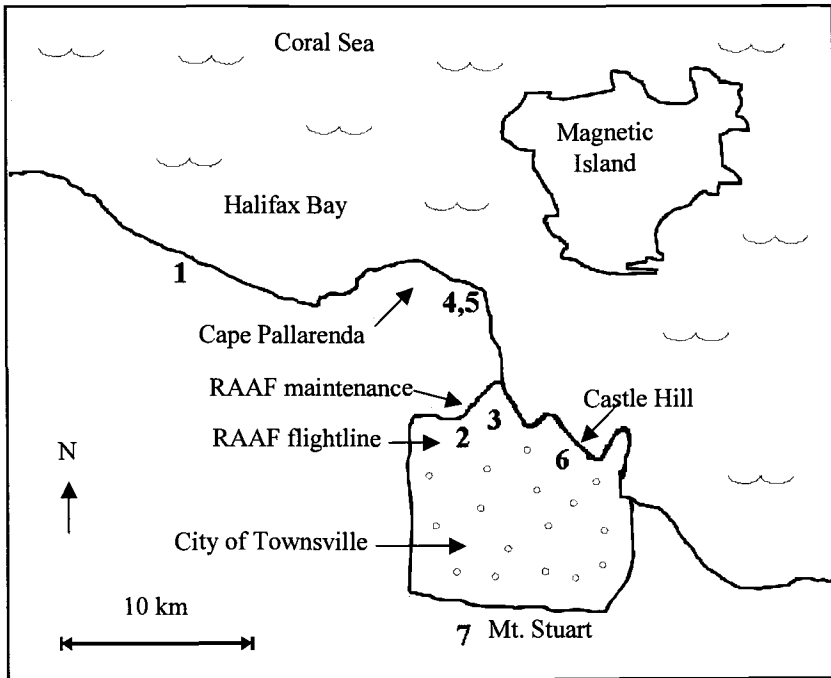


Figure 9- Townsville illustrating the location of the CLIMAT sites (see Table 1 for the description of each site)

The main factors distinguishing each site are the distance from the coast and elevation and these factors are listed in Table 1.

Table 1- Distance from the coast and elevation for each measurement site

Site number on Fig. 9	Site	Distance to coast, km	Approximate elevation above sea level, m
1	Halifax Bay	0.2	100
2	RAAF-flight line	3.5	100
3	RAAF maintenance	1.5	100
4	Cape Pallarenda-fence	0.5	100
5	Cape Pallarenda-radar	0.5	120 ^a
6	Castle Hill	1.4	300
7	Mount Stuart	11.7	700

^aAbout 18.5 m above ground.

Results and Discussion

The monthly composite salt candle deposition rates at RAAF Townsville (maintenance) are shown in Fig. 10. There is an increase in the salt candle deposition rate during the summer months (Dec. to Mar.). Winds from the east, which predominate during the summer, have a high salt aerosol concentration due to passage over the Coral Sea. Whereas winds from the southeast, which predominate during the winter, have lower chloride aerosol concentrations because they partially pass over land.

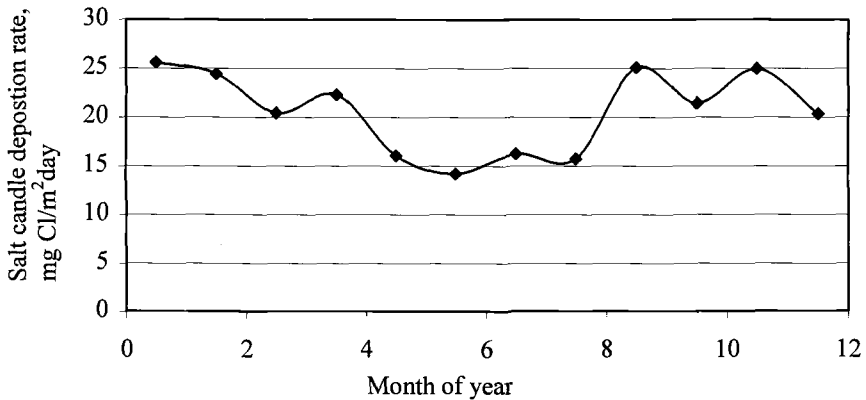


Figure 10- Composite monthly average of salt candle deposition rates at RAAF Townsville (maintenance) and RAAF Townsville (flightline)

Composite monthly CLIMAT responses were averaged for each site and are shown in Fig. 11. Trends related to the month of year and to elevation are evident. For each site there was a decrease in corrosivity during the winter months that was similar in magnitude to the decrease in salt candle deposition rate at the RAAF maintenance site. However, the decrease in corrosivity was not nearly as sharp as the decrease in relative humidity that is suggested by the rainfall pattern in Fig. 2. Thus the seasonal pattern of corrosivity are more related to the seasonal changes in salt aerosol deposition, rather than the seasonal changes in relative humidity.

The corrosivities of these sites correlate closer with elevation than with distance from the coast. The four sites with measurements taken near to the ground, i.e., Cape Pallarenda fence, Halifax Bay, RAAF maintenance and RAAF flightline, were very similar even though the distance from the coast ranged from 0.2 to 3.5 km. There was a very marked contrast between the corrosivity at Cape Pallarenda at the fence level (1.5 m above the ground) and at the radar level (20 m above the ground). The ratio of corrosivity at the radar to that at the fence level ranged from 2 to 3. This is readily explained by the difference in horizontal wind velocity in a boundary layer (Eq. 1). The ratio of wind velocity at 20 m to that at 1.5 m is 3.3 given a surface roughness of 0.5 m.

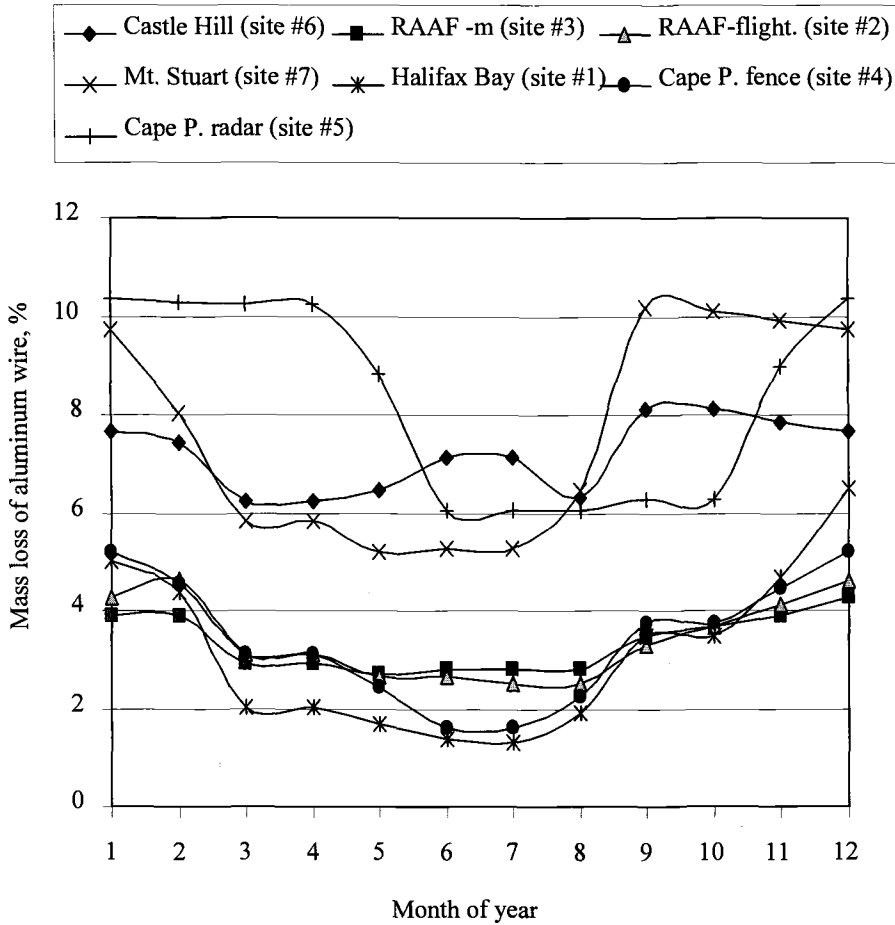


Figure 11- Composite monthly average of the CLIMAT response at the sites near Townsville

There is a nearly linear increase in capture efficiency with wind velocity for a CLIMAT bolt (Fig. 4) in the range of typical wind velocities. Thus objects placed at higher elevations are subject to greater chloride deposition rates and therefore to greater corrosion rates.

The corrosivities on Mt. Stuart and Castle Hill are consistently higher than the ground level sites even though they are nearer to the coast. This effect can be qualitatively explained by examining the effects around an obstacle according to the illustrated example. The obstacle in the example was not intended to model the effects of wind flow over a hill in detail but to obtain qualitative patterns of corrosivity. The shape of the obstacle is therefore much simpler and more regular than the shape of either hill.

There are also differences in the velocity and aerosol concentration profiles between the model and the actual site. However, significant aerosol concentrations have been measured up to 1000 m above the surface of a salt-water body [8] and therefore simulating the height of aerosol source to be the same as the obstacle should not be too far out of line. According to the illustrated example, the aerosol concentration near the top of the obstacle was the same as that at the source. A combination of a maximum horizontal wind velocity and undiluted aerosol concentrations at the top of the obstacle yielded a maximum deposition rate to salt candles and therefore suggested a maximum corrosivity.

Conclusions

The corrosivity pattern, as measured by CLIMAT units near Townsville, are readily explained within the framework of the physical processes of aerosol transport and deposition. Increasing elevation above the earth is associated with increased wind speed which increases the aerosol capture efficiency of objects and therefore the rate of aerosol deposition and the corrosion rate. The flow pattern around objects that significantly obstruct wind is very complicated but one clear conclusion is that the wind flow speed and turbulence are highest near the top. Thus aerosol deposition and therefore corrosion rates are higher near the top of wind obstructions such as hills and buildings. The seasonal corrosivity trends are consistent with the seasonal trend in the salt aerosol deposition rate rather than the seasonal trend in relative humidity.

The low aerosol capture efficiency of the ISO salt candles and the dependence of their capture efficiency on wind velocity suggest that improvements are possible. One possibility is to measure the aerosol chloride concentration in air, which would allow the aerosol deposition rate on various surfaces to be estimated based on the structure of the wind flows. Another approach is to measure surface deposition directly with surface patches that absorb aerosol particles and that allow for chloride measurement after exposure. The advantage of the second approach is that the salt deposition rate to the surface of interest would be directly measured rather than the salt deposition rate to a nearby salt candle. The distinction is important because the mechanism of aerosol deposition is different for each, i.e. inertial impaction for a salt candle and turbulent diffusion for a surface.

References

- [1] Summitt, R. and Fink, F. T., "The USAF Corrosion Testing Program and a Corrosivity Severity Index Algorithm," Chap. 17, Atmospheric Corrosion, Edited by W. H. Ailor, 1982, pp. 245-263.
- [2] Doyle, D. P and Wright, T. E., "Rapid Methods for Determining Atmospheric Corrosivity and Corrosivity Resistance," Chapter 16 in Atmospheric Corrosion, Edited by W.H. Ailor, 1982, pp. 227-243.

- [3] ASTM G 116—93, “Standard Practice for Conducting Wire-on-Bolt Test for Atmospheric Galvanic Corrosion.”
- [4] ISO 9223, “Corrosion of metals and alloys--Classification of Corrosivity of Atmospheres.” International Organization for Standardization, 1992.
- [5] Klassen, R. D. and Roberge, P. R., “Aerosol transport modeling as an aid to understanding atmospheric corrosivity patterns”, *Materials and Design*, Vol. 20, 1999, p. 159-168.
- [6] Klassen, R. D. and Roberge, P. R., “Modeling the Effects of Local Topography on Atmospheric Corrosivity”, NACE 2000, Paper No. 272, Orlando, Florida.
- [7] Bird, R. B., Stewart, W. E. and Lightfoot, E. N., “Transport Phenomenon,” John Wiley & Sons, Inc., 1960.
- [8] Hidy, G. M., “Aerosols--An Industrial and Environmental Science,” Academic Press, Inc., 1984.
- [9] FLUENT Version 5.0.2, FLUENT Inc., 1998.
- [10] Patankar, S. V., “Numerical Heat Transfer and Fluid Flow,” Hemisphere Publishing Corporation, New York, 1980.

Bopinder S. Phull,¹ Stanley J. Pikul,¹ and Robert M. Kain¹

Thirty-Eight Years of Atmospheric Corrosivity Monitoring

Reference: Phull, B. S., Pikul, S. J., and Kain, R. M., “**Thirty-Eight Years of Atmospheric Corrosivity Monitoring**,” *Marine Corrosion in Tropical Environments, ASTM STP 1399*, S. W. Dean, G. Hernandez-Duque Delgadillo, and J. B. Bushman, Eds., American Society for Testing and Materials, West Conshohocken, PA, 2000.

Abstract: The marine atmospheric test site at Kure Beach, North Carolina, has long been recognized for its corrosion severity. It represents a benchmark for testing materials’ resistance to marine atmospheric corrosion. The two test areas at the site have often been referred to as the 80-foot and 800-foot test lots (or the 25-meter and 250-meter lots), respectively. For over 38 years the amount of airborne chlorides from the sea spray have been monitored monthly. Chloride deposition is only one of several environmental factors which can contribute to atmospheric corrosion. Some of the other important factors include relative humidity, time of wetness, temperature, prevailing wind direction, and rainfall — which are all also monitored routinely. Corrosivity is monitored more directly by determination of mass loss for two reference materials, carbon steel and zinc.

Because of a number of recent changes, the 25- and 250-meter test locations have now been designated as the “oceanfront” and the “near-ocean” lots. Continued monitoring of these sites will benefit existing and future marine atmospheric test programs, including those of various ASTM subcommittees. Examples of materials on continuous exposure in the “museum areas” of the oceanfront and the near-ocean lots are reviewed for the purpose of educating new corrosion engineers on the importance of long-term testing in natural environments.

Keywords: atmospheric corrosion, marine environment, corrosivity, monitoring

Introduction

While the primary objective of accelerated corrosion testing is to reduce the testing time, this goal is not always attainable because the results are flawed. One of the best examples of this problem is the indiscriminate use of salt-spray testing to predict the performance of materials, coatings, and other protective schemes in service applications. Indeed, subjecting test specimens or components to a fog of atomized NaCl solution

¹ Principal Corrosion Scientist, Senior Research Technologist, and Senior Corrosion Scientist, respectively, LaQue Center for Corrosion Technology, Inc., P. O. Box 656, Wrightsville Beach, NC 28480.

continuously in a cabinet test, [e.g., per ASTM Standard Practice for Operating Salt Spray (Fog) Apparatus (B117)] is a commonly used approach to create a very harsh environment; however, the correlation of results with performance in actual application environments is often dismal. This is partly due to the fact that many real-world effects such as concentration of salts by evaporation, salt washing off by rain, solar and ultraviolet radiation, temperature, and dew-point are not simulated in a continuous salt-fog test. In recent years, attempts have been made to at least partly palliate such concerns by the development of so-called cyclic corrosion tests, [e.g., per ASTM Standard Practice for Modified Salt Spray (Fog) Testing (G85)]. However, while they represent an advancement, even these tests fail to completely replicate service conditions. Moreover, performance in actual environments remains the ultimate benchmark to assess the validity of the accelerated procedures.

Historically, outdoor atmospheric corrosion testing has been performed at various test sites in many countries [1]. In the US, a large number of test sites, designated as rural, urban, industrial, and marine have been used to develop corrosion test data. There are no universally accepted quantitative demarcations between the constituents that typify atmospheric environments. Therefore, distinctions are often based on qualitative and semi-quantitative factors. For instance, marine environments are characterized by the presence of airborne salt as the major corrosive constituent transported from the ocean. In comparison, typically, SO₂ is the primary component in industrial and urban atmospheres, although other species such NO_x, NH₃, Cl₂, O₃, and H₂S may also be present at lower concentrations. Environments containing relatively low levels of pollutants are considered rural or arid. The development and implementation of pollution abatement technology over the past three decades has significantly reduced emissions in industrialized nations; this, together with population increase and attendant urbanization of hitherto rural areas has made distinctions between many atmospheres more tenuous. In contrast, marine environments continue to be characterized essentially on the basis of salt deposition.

The Kure Beach Marine Atmospheric Corrosion Test Site

The LaQue Center's test site in Kure Beach, NC, was established circa 1941 for corrosion testing in marine atmospheres and sea water. In 1950, a new test site devoted to corrosion testing in sea water was inaugurated in nearby Wrightsville Beach, NC; since then the Kure Beach site has been used exclusively for marine atmospheric corrosion testing. Both sites are very well known in the marine corrosion field in the US as well as internationally. The Kure Beach site is one of a number of ASTM designated test locations in the US; over the years it has been used by several ASTM committees for generating corrosion data for developing testing standards. In 1988 the Kure Beach site was designated as an historic landmark by ASM International.

The atmospheric site is located on the Atlantic Ocean coast at latitude 34° N and longitude 77.5° W. The site comprises two test lots with prevailing winds from the ocean. Historically, the test area very close to the ocean was known as the 80-foot (25-meter) lot and the area further back as the 800-foot (250-meter) lot. In 1999, due to hurricane-related beach renourishment and for business reasons, the test lot boundaries

were moved. The new test areas have been designated as the “Oceanfront” and “Near-ocean” lots; their mean distances from mid-tide are ~70 and ~190-meters, respectively. The test site is used by hundreds of clients, typically for generating long-term corrosion data on alloys, coatings, and components. Fairly comprehensive monitoring of environmental parameters is performed routinely to characterize the local conditions, as discussed later.

Factors Affecting Marine Atmospheric Corrosion

The pioneering work of Ambler and Bain [2] nearly 50 years ago demonstrated a strong correlation between salinity of marine atmospheres and corrosivity toward carbon steel. The mass loss corrosion rate of steel versus salinity exhibited a log-log relationship in tests performed in Nigeria and the UK. The effect of inland distance from the ocean on salt deposition and consequently corrosion has been addressed by a number of researchers [2-5]. While deposition is typically considered to decrease significantly within the first kilometer or so, local conditions such as shoreline geography, the way the surf breaks, and air currents can sometimes reportedly result in appreciable airborne salt transportation over 30 kilometers [6].

Despite the prominence commonly given to amount of airborne salt and its deposition, there are a number of other important factors that govern corrosivity. Since electrochemical reactions on metals and alloys (and some non-metals like graphite) are feasible only when, among other factors, electrolyte is present on the surface, the time of wetness (TOW) exerts a very strong influence on corrosion. However, TOW itself is dependent on provisos like relative humidity, hygroscopic nature of salt deposits and/or corrosion products, surface temperature, dew point, etc. Thus, there is often a complex interrelation between multiple factors on the overall corrosion damage incurred by a given material. In other words, even the local climate is not constant; it is subject to diurnal, seasonal, annual, and anthropogenic changes. Since multiple and often interrelated effects are involved concurrently, delineating the contributions of individual variables toward corrosion becomes a daunting exercise. Nevertheless, it is important to monitor as many factors as possible, and as frequently as economy allows, so that data are gathered in anticipation of future developments leading to more reliable and meaningful data analysis and possible correlations. Table 1 shows a typical summary of environmental parameters monitored at Kure Beach; some of the more significant ones are addressed later.

Overview of Corrosivity Monitoring Tools

Although these terms are often used interchangeably, there is an important semantic distinction between corrosivity and corrosion rate. In atmospheric environments, corrosivity connotes relative severity or harshness with respect to some location or benchmark. Corrosivity is typically determined in two ways. The most common approach involves determination of corrosion rate, usually by mass loss, for some “standard” or reference material(s). Often, a relatively corrodible material such as carbon steel is chosen so that a reasonable specimen size can be exposed for a relatively

Table 1 - Kure Beach Atmospheric Test Site Daily Weather Summary for January 1998

Day	Temperature °C			Relative Humidity			Dew Point °C	Rainfall		Time of Wet- ness	Wind (km/h)			Solar Radiation 30° South	
	max	min	avg	max	min	avg	avg	mm	hrs	hrs	avg	max	dir	Total	TUVR
1	4.4	-2.2	1.1	84	33	54	-7.6	0.0	0.0	0.4	7.7	30.0	NNW	21.69	0.70
2	14.2	-2.2	5.7	96	40	74	0.9	0.0	0.0	7.1	6.1	25.4	WSW	21.57	0.70
3	16.8	3.9	11.6	97	70	86	9.2	0.0	0.0	8.9	4.3	15.9	E	17.89	0.62
4	17.4	10.6	14.1	96	74	88	12.0	0.0	0.0	12.6	7.8	19.8	NE	17.23	0.65
5	16.6	12.2	14.8	98	83	92	13.4	1.5	3.0	12.2	9.1	24.3	NNE	14.37	0.59
6	18.5	13.9	15.9	100	91	98	15.5	54.1	11.0	13.4	7.1	32.5	ESE	8.84	0.38
7	21.1	14.6	16.9	100	87	98	16.5	2.5	5.0	8.1	9.4	36.3	SSE	10.58	0.49
8	18.6	14.6	16.4	100	99	100	16.3	17.0	9.0	18.8	12.2	49.7	S	1.52	0.09
9	18.2	9.9	14.7	100	60	84	11.8	0.3	1.0	8.2	13.4	50.1	WSW	19.66	0.70
10	12.4	6.2	9.1	96	69	84	6.4	0.0	0.0	0.0	6.2	19.1	WNW	20.83	0.71
11	15.7	2.5	9.3	98	47	83	6.2	0.0	0.0	6.4	5.8	18.0	WNW	20.85	0.69
12	14.8	4.2	10.9	98	74	89	9.1	0.0	0.0	5.8	7.7	21.9	NNE	14.00	0.52
13	20.0	11.2	15.2	98	74	90	13.5	2.3	2.0	2.6	7.0	30.0	SW	4.85	0.27
14	12.7	8.0	9.6	99	61	80	6.2	0.0	0.0	2.1	23.9	51.1	NE	3.40	0.21
15	14.7	8.1	11.3	99	90	97	10.8	4.8	9.0	12.7	11.2	41.3	NNE	2.32	0.16
16	17.0	9.0	12.0	100	83	95	11.1	16.5	7.0	5.3	10.8	50.5	WSW	2.64	0.16
17	11.0	5.3	8.8	98	86	92	7.6	0.0	0.0	2.1	6.5	29.6	W	2.34	0.14
18	12.2	3.9	7.7	96	45	73	2.8	0.0	0.0	8.9	7.6	31.8	NNW	20.52	0.75
19	11.0	3.4	7.3	93	59	83	4.5	13.0	6.0	4.6	18.5	71.6	NNE	1.53	0.10
20	9.4	2.6	4.7	96	59	81	1.6	0.0	0.0	3.0	6.7	27.9	NNW	10.35	0.42
21	9.1	1.8	6.2	79	49	64	-0.2	0.0	0.0	0.0	12.6	30.3	NE	20.97	0.76
22	15.0	9.1	11.6	94	72	85	9.2	0.0	0.0	2.8	18.4	33.9	ENE	10.82	0.48
23	17.3	13.3	14.7	100	83	97	14.2	64.0	16.0	21.4	9.5	53.6	SSE	0.70	0.06
24	16.0	6.5	12.8	100	81	96	12.2	1.0	2.0	11.7	7.6	42.3	W	6.33	0.34
25	10.7	1.7	5.8	93	40	68	0.0	0.0	0.0	0.0	7.5	38.1	WNW	21.07	0.75
26	11.5	0.7	7.7	97	62	80	4.2	0.0	0.0	5.0	15.2	42.0	NNE	19.28	0.72
27	16.3	9.2	12.7	99	82	93	11.6	22.1	8.0	8.2	23.9	67.0	E	1.30	0.09
28	9.2	6.5	7.4	97	83	92	6.1	0.3	1.0	7.1	14.0	46.6	WNW	2.59	0.17
29	13.2	5.3	9.1	94	59	81	5.8	0.0	0.0	4.2	9.0	26.1	WSW	21.24	0.79
30	14.1	4.9	10.2	95	56	80	6.7	0.0	0.0	12.6	7.1	22.9	W	21.08	0.75
31	10.3	1.6	6.1	79	39	60	-1.4	0.0	0.0	0.1	9.3	37.0	N	19.53	0.76
(1)	21.1	-2.2	10.4	100	33	84	7.6	199.4	80.0	216.3	10.4	71.6		381.69	14.7
MONTHLY ACCUMULATION															
											CHLORIDE (mg/m ² /day) Oceanfront (25-meter) lot		451.9		
											CHLORIDE (mg/m ² /day) Near-ocean (250-meter) lot		133.3		

* Not recorded

(1) Monthly maximum, average, minimum, or total

short period to attain an easily measurable mass loss. Corrosivity of exposure sites determined in this manner provides a relative ranking of harshness (in this case, based on using carbon steel as a reference standard) but no direct indication of how other materials will perform; that is based on empiricism or service experience in nominally similar conditions.

The second approach involves determination of environmental factors, for example, salt deposition in marine atmospheres and SO₂ in industrial ones. Using this approach, it is assumed that some previously established relationship between pollutant concentration and corrosivity, usually based on laboratory results, will apply. Other factors such as time of wetness, relative humidity, temperature, and dew point may also be monitored and taken into account. This is a more indirect method compared to determination of actual corrosion rate, albeit it on some standard reference material such as carbon steel. It relies even more heavily on empirical data and service experience when actual materials performance is to be predicted.

As stated earlier, the outdoor atmospheric conditions at any location are potentially subject to wide variations. Therefore, interpretation of data from long-term corrosion studies will be most meaningful if corrosivity monitoring is performed over corresponding periods rather than relying on short-term values.

Corrosivity Monitoring Using Iron, Carbon Steel, and Zinc Panel Specimens

Routine corrosivity assessment was initiated at Kure Beach in 1949, using nominally 4-inch x 6-inch x 1/8-inch (~100 mm x 150 mm x 3 mm) ingot iron "calibration" specimens. In order to permit corrosivity monitoring for many years in the future, a large amount of sheet stock material was reportedly purchased so that heat to heat differences would not be a variable. Replicate specimens were exposed in the two test lots vertically for one-year periods to attain an annual corrosivity indication based on corrosion rate determination from mass loss. Figure 1 provides a comparison of the corrosivities of the 25- and 250-meter lots over a 30-year period [7]. The long-term trend indicates the 25-meter lot to be about four to five times more corrosive than the 250-meter lot. Concurrent tests performed for four years, using specimens exposed vertically and at 30° to the horizontal, revealed that the corrosion rate of ingot iron in the 25-meter lot was nearly double for the vertical specimens; this was ascribed to formation of less protective and nonuniform corrosion products [8]. Since 1976, calibration test specimens have been exposed at 30° to the horizontal per ASTM Standard Practice for Conducting Atmospheric Corrosion Tests on Metals (G50); the specimens in the 25-meter lot face east while those in the 250-meter lot face south. The southerly choice for the 250-meter lot is based on testing of coated panels to allow maximum exposure to solar and UV effects at this latitude.

As the original ingot iron stock was nearing depletion in the 1980s, replacement steel samples were evaluated since ingot iron was no longer available commercially. Collateral trials with A-36 steel panels gave considerably lower corrosion rates in the 25-meter lot relative to ingot iron exposed for the same time, probably due to the "weathering steel" effect of the copper content in the former. (ASTM Standard Practice

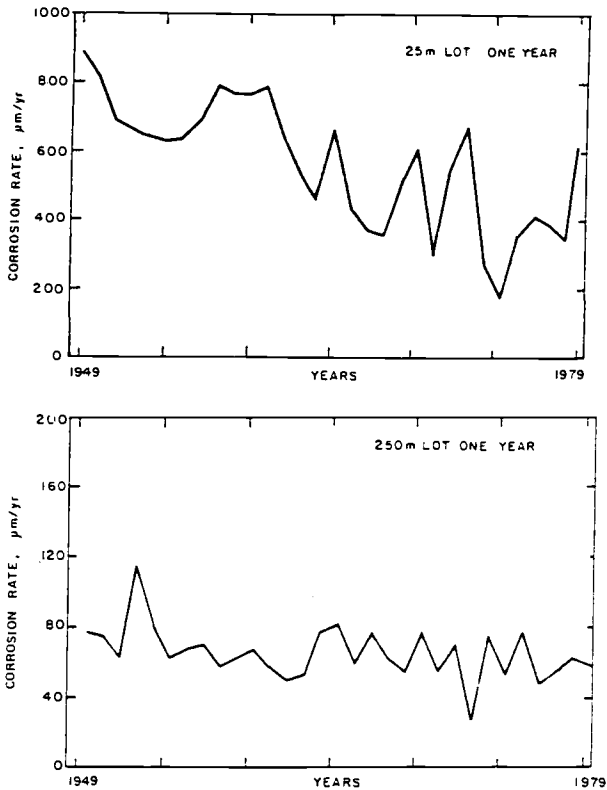


Figure 1 - Corrosion Rates of Iron Calibration Specimens Exposed Vertically for 1-year Periods in the 25- and 250-meter Marine Atmospheric Test Lots at Kure Beach, NC, 1949-1979 (Ref. 7).

for Characterization of Atmospheric Test Sites (G92) recommends A-36 steel with minimum 0.2% copper and high purity grade B6 zinc specimens.) The mass loss corrosion rate results representing corrosivity from 1989 through 1997, using A-36 steel (1989-1995) and 1008 steel (1996-1997) specimens facing east are summarized in Table 2. The steel compositions are shown in Table 2a. A number of features are apparent. As expected, in any given year, corrosivity in the 250-meter lot is considerably less than in the 25-meter lot. The low corrosion rates in 1990 and 1994 are attributed to material heat variations in A-36 steel. After 1995, 1008 steel was selected as the reference calibration material. Despite two major hurricanes (*Bertha* and *Fran*) in 1996, no major accelerating affect on the yearly mass loss corrosion rates was apparent. Scrutiny of historical data, for example, for hurricane years 1984 (*Diana*) and 1989 (*Hugo*) also does not support any such correlation with corrosivity. This is not surprising since hurricanes are very short-term events, with each one lasting only about 24 hours in the local area. The adverse effects of hurricanes seem to be more in the way of possible

“sandblasting” of specimens (with resultant removal of corrosion products) or, as worst-case, outright loss of specimens due to very strong winds. Even the much-reported “Storm of the Century” in March 1993 did not produce any extraordinary effects on annual corrosion rates of steel or zinc (use of Zn calibration specimens is discussed below). The chloride content in the 250-meter lot appeared to peak toward a maximum value while that in the 25-meter lot was relatively unaffected.

Table 2 - Corrosion Rates of A-36 and 1008 Carbon Steel at Kure Beach, NC ($\mu\text{m}/\text{yr}$).

Year	Steel	25-meter Lot	250-meter Lot
1989	A-36	256	31
1990	A-36	64	17
1991	A-36	576	41
1992	A-36	390	31
1993	A-36	248	31
1994	A-36	62	17
1995	A-36	361	26
1996	1008	93	26
1997	1008	80	34

Table 2a* - Compositions of A-36 and AISI-1008 Steel Corrosivity Calibration Panels Exposed at Kure Beach, NC.

A-36 Steel										
Year	C	Mn	P	S	Si	Cr	Ni	Mo	V	Cu
1990	0.15	0.68	0.016	0.009	0.2	<0.1	<0.1	<0.05	<0.01	<0.05
1991	0.033	0.25	0.010	0.022	<0.1	<0.1	<0.1	<0.05	<0.01	<0.05
1992	0.039	0.26	0.017	0.028	<0.1	<0.1	<0.1	<0.05	<0.01	<0.05
1993	0.038	0.27	0.013	0.028	<0.1	<0.1	<0.1	<0.05	<0.01	<0.05
1994	0.11	0.41	0.009	0.010	<0.1	<0.1	<0.1	<0.05	<0.01	<0.05

* Balance is Fe

AISI-1008 Steel					
Year	C	Mn	P	S	Fe
1996-1997	0.04	0.36	0.008	0.01	Bal.

Table 3 - Corrosion Rates of Zinc at Kure Beach, NC ($\mu\text{m}/\text{yr}$)

Year	25-meter Lot	250-meter Lot
1989	3	1.5
1990	2.4	2.4
1991	2.3	1.3
1992	1.2	1
1993	2	1.5
1994	2.6	1.5
1995	1.8	1.3
1996	2.2	2.7
1997	3	1.6

Table 3a - Composition of Zinc Corrosivity Calibration Panels Exposed at Kure Beach, NC

Cu	Fe	Zn
< 0.005	0.0019	Bal.

Corrosivity monitoring using zinc (Zn) specimens was commenced routinely at Kure Beach in 1989. Comparing the results for Zn in Table 3 with those for steel in Table 2 shows that the corrosion rate for Zn is significantly lower, as anticipated. The Zn panel composition is shown in Table 3a. Again any detrimental effects of hurricanes, for example, *Bertha* and *Fran* in 1996 are not apparent. Overall, it can be inferred that, unlike steel, the Zn specimens are much less sensitive in indicating corrosivity differences between the two lots; this, despite the fact that experience in testing a wide range of materials, coatings and components over nearly six decades has clearly and consistently shown the 25-meter lot to be much more corrosive than the 250-meter location. This exemplifies the importance of selecting "sensitive" corrosivity calibration standard materials.

Mass loss corrosion rates for steel and zinc are based on the composite attack incurred by skyward and groundward facing sides of the respective test panels. For steel, groundward sides sometimes exhibit higher rates of attack; this is attributed to less effective rain washing of accumulated salts, and due to greater time of wetness associated with formation of dew and poorer solar drying effects. Therefore, corrosion rates based on total mass loss belie the fact that actual penetration rates on the groundward sides can be higher. However, it has been reported that groundward facing surfaces on zinc coated steel exhibited lower corrosion rates [9].

Corrosivity Monitoring Using Wire-on-Bolt

Doyle and Wright [10] adapted a classical atmospheric galvanic corrosion evaluation set-up for monitoring relative corrosivities of outdoor environments. Their wire-on-bolt (WOB) device consists of a preweighed aluminum wire tightly wrapped into the threads of a carbon steel bolt for determining the corrosivity of marine atmospheres. (Al wire wrapped around a copper bolt is used for corrosivity monitoring of industrial atmospheric environments.) The percent mass loss incurred by the Al wire (which is typically due to general corrosion in mild environments and general plus pitting attack in severe environments) normalized to 90 days' exposure is used to provide a qualitative ranking of environment severity. Doyle and Wright's Marine Corrosivity Index (MCI) is shown in Table 4. Results of the WOB technique used to monitor corrosivity quarterly at Kure Beach since 1992 are summarized in Table 5. It is apparent that the 25-meter lot consistently ranks as "severe" or "very severe"; while the 250-meter lot corresponds to a "moderate" to "moderately severe" environment. Again, any histrionic effects of hurricanes *Bertha* and *Fran* in the third quarter in 1996 on corrosivity are not evident.

Presently, ASTM Practice for Conducting the Wire-on-Bolt Test for Atmospheric Galvanic Corrosion (G116) covers the WOB method for atmospheric galvanic corrosion evaluation but not for marine corrosivity monitoring as developed by Doyle and Wright. The procedure described in the standard can be used to prepare Al wire on steel bolts for the latter; however, interpretation in terms of corrosivity will require a key of the type shown in Table 4.

Table 4 - *Marine Corrosivity Classifications Using the Wire-on-Bolt Technique (Ref. 12)*

MCI Range*	Classification	Significance
0-2	Negligible	Average habitable area
>2-5	Moderate	Seaside
>5-10	Moderately Severe	Seaside and exposed
>10-20	Severe	Very exposed
>20	Very Severe	Very exposed, wind swept, and sand swept

* MCI - Marine Corrosivity Index; figures represent % mass loss of nominally 1-m long Al wire, wrapped around steel bolt, normalized to 90 days' exposure.

Chloride Monitoring at Kure Beach

Airborne salt levels have been monitored routinely at Kure Beach since 1962, using the wet candle method which was officially adopted as G140 in 1998. A moist surgical gauze "captures" airborne salt transported by wind blowing against it. At the end of the exposure period, typically one month, the salt is dissolved in a known volume of distilled water; the associated chloride is determined analytically and reported as average chloride deposition in mg/m²/day. The chloride deposition results for the two lots in Kure Beach

Table 5 - Corrosivity Classifications of Marine Atmosphere at Kure Beach, NC

Year	Period	25-meter lot		250-meter lot	
		% Mass loss	MCI Classification	% Mass loss	MCI Classification
1992	Jan-Mar	14	S*	9	MS
	Apr-Jun	13	S	10	MS
	Jul-Sept	24	VS	7	MS
	Oct-Dec	16	S	9	MS
1993	Jan-Mar	14	S	8	MS
	Apr-Jun	13	S	4	M
	Jul-Sept	10	S	5	M
	Oct-Dec	13	S	7	MS
1994	Jan-Mar	11	S	5	M
	Apr-Jun	15	S	5	M
	Jul-Sept	15	S	5	M
	Oct-Dec	15	S	5	M
1995	Jan-Mar	11	S	4	M
	Apr-Jun	13	S	7	MS
	Jul-Sept	16	S	6	MS
	Oct-Dec	13	S	6	MS
1996	Jan-Mar	9	MS	6	MS
	Apr-Jun	16	S	5	M
	Jul-Sept	10	MS	5	M
	Oct-Dec	11	S	5	M
1997	Jan-Mar	16	S	5	M
	Apr-Jun	13	VS	7	M
	Jul-Sept	22	VS	4	M
	Oct-Dec	15	S	6	MS

VS = Very Severe, S = Severe, MS = Moderately Severe, M = Moderate

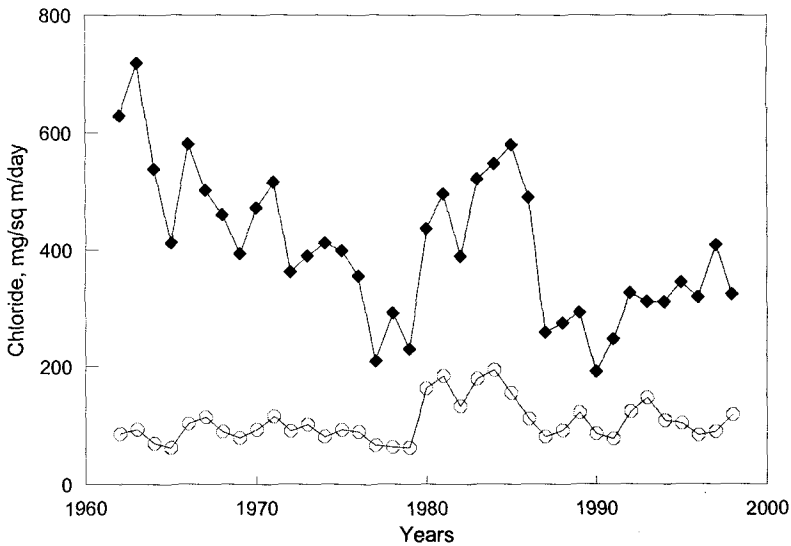
(1962-1998) are shown graphically in Figure 2. The mean chloride levels for this entire period were ~400 and ~100 mg/m²/day for the 25- and 250-meter test lots, respectively. Interestingly, the corrosion rate of carbon steel also differs by about the same factor if considered over this entire period. A direct correlation between short-term chloride deposition and short-term corrosion rate is less obvious. For example, even though the chloride deposition for 1996 was dramatically increased by the hurricanes mentioned earlier, the corrosion rate of steel or WOB calibration specimens was not. As stated earlier, corrosion damage isn't a simple function of salt deposition in marine atmospheres because other independent, climatic variables also play important roles.

Hurricane-associated beach renourishment, and some business-related changes in 1999 resulted in some changes in the boundaries of the two test lots at Kure Beach. As noted earlier, the previous 25-meter location is now known as the "Oceanfront" lot whose nominal distance from mean tide is ~52 meter and the 250-meter location which is

now called the “Near-ocean” lot is nominally ~192 m from mean tide. The chloride contents monitored for the newer locations, shown in Table 6, generally are comparable to the previous 25- and 250-meter locations. The intent is to continue routine monitoring of corrosivity using carbon steel, zinc and WOB specimens; and via chloride deposition, time of wetness, relative humidity, and temperature.

Table 6 - Average Monthly Airborne Chloride Levels for the “New” Locations at Kure Beach, NC (mg Cl/m²/day)

Month	52-m	137-m	192-m	203-m
11/99	179	118	70	48
12/99	198	166	89	61
01/00	109	83	52	43
02/00	219	176	105	64



◆ Oceanfront (25-meter)
 ○ Near-ocean (250-meter)

Figure 2 - Average monthly airborne chloride at Kure Beach, NC 1962-1998.

Time of Wetness Monitoring

As mentioned earlier, the time of wetness (TOW) is an important factor because aqueous electrochemical corrosion requires the presence of an electrolyte. Of course, even in the presence of an electrolyte, electrochemical corrosion can only proceed if cathodic and anodic reactions are viable. For example, one of most important cathodic reactions is reduction of dissolved oxygen. In atmospheric environments, the kinetics of this reaction are heavily favored by the plentiful supply of oxygen from air and easy diffusion through thin film electrolytes such as those formed by condensates, hygroscopic salts, rain, dew, etc. The TOW at Kure Beach is monitored in accordance with ASTM Standard Practice for Measurement of Time-of-Wetness on Surfaces Exposed to Wetting Conditions as in Atmospheric Corrosion Testing (G84).

Monitoring of Pollutants

Pollutants such as SO₂ and NO_x are common in industrial and automotive emissions. Since deposition of pollutants can accelerate corrosion, it is prudent to monitor them in the atmosphere as possible contributors to corrosivity. At Kure Beach, airborne SO₂ was routinely monitored for a number of years using commercial sulfation plates per ASTM Standard Practice for Characterization of Atmospheric Test Sites (G91). The NO_x was monitored concurrently using a vendor's proprietary plates. An example of the SO₂ and NO_x results is included in summary Table 1. Unfortunately, this routine monitoring practice was discontinued in 1997 when the vendor stopped producing the monitoring hardware; to date an alternate vendor has not been identified.

Examples of Long-Term Materials Testing and Performance at Kure Beach

Stainless Steel

Many grades of stainless steel have been tested in a number of programs. For example, the results of performance of Types 201, 202, 16-16-1, 301, 302, 304, 304L, 316, 316L, 321, 347, 410, and 430 after 26 years' exposure at Kure Beach were reported in ASTM STP 965 [11]. Surface finish, metallurgical condition, welds, skyward versus groundward facing sides, and crevices at lap joints were among the variables investigated. A subsequent paper in ASTM STP 1000 [12] reported on the effects on mechanical properties and surface reflectivity of selected alloys from the aforementioned 26-year study. Basically, all of the grades exhibited rust staining, more in the 25-meter and less in the 250-meter lot; there was minimal crevice corrosion at the faying surfaces; and mechanical properties were not adversely affected.

A number of stainless steel museum specimens exposed in 1941 remain on exposure at the time of this writing. Some panels from another program commenced in 1967 also remain on exposure. Electropolished surfaces exhibit the best performance relative to as-produced mill and other finishes.

Thermal-Spray Coatings

The results of 34-years' exposure of thermal spray coatings (Zn + Al, Al + Zn, Zn + Mg, Al + Mg, Zn + Al + Mg, and Sn + Zn) on steel in the 250-meter lot at Kure Beach were reported in ASTM STP 947 [13]. In general, the Zn-rich and Al-rich coatings, with a minimum thickness of 0.15 mm (~6 mils) and seal top coat exhibited the best long-term performance. At this writing, the "surviving" thermal spray coatings have been on exposure for almost 48 years. These data have proved extremely pertinent because of renewed interest and application, for example, for corrosion protection on offshore platforms in recent years.

Alloy C and Cr-Plated Type 301 Stainless Steel

A Ni-Cr-Mo-Fe alloy (Hastelloy® C) was exposed in the 250-meter lot at Kure Beach in 1941 and a Cr-plated Type 301 stainless steel hubcap exposed in 1950. At this writing, both continue to be tarnish free. Again, these types of data are very helpful for designers selecting materials for critical and/or remote applications in severe marine atmospheres where very long-term maintenance-free service is required.

Statue of Liberty Demonstration Tests

In the early 1980s, the principal corrosion problem afflicting the Statue of Liberty was identified as severe packout rusting of the original iron support members in the interior of the structure, under copper saddle brackets riveted to the exterior copper skin [14]. Because of the severity of the 25-meter lot at Kure Beach, corrosion tests were initiated to evaluate and demonstrate the performance of candidate replacement materials for the corroding iron members in the statue. Using iron as a control, the extent of corrosion incurred in the statue in 100 years was reproduced at Kure Beach in about five years. Simultaneous testing revealed that all of the candidate replacement materials, viz., Type 316 stainless steel, alloy 400, and bronze would perform satisfactorily. For a variety of reasons, Type 316 stainless steel was selected ultimately as the replacement material in the rehabilitation of the statue. The demonstration pieces are still on exposure (~15 years) and continue to provide a worst-case scenario indication of how the replacement material in the statue is likely to perform — another example of practical, real-world testing for materials selection and continued monitoring of performance.

Summary and Conclusions

The Kure Beach marine atmospheric corrosion test site has served as a benchmark for testing of materials under harsh but real-world conditions for 50+ years. To date, accelerated testing, such as in salt spray cabinets, has not successfully replaced outdoor exposures because of the failure to consistently reproduce corrosion damage incurred in actual service environments. Despite the fact that environmental conditions in natural atmospheres are themselves variable, long-term exposures still produce the most

authentic corrosion data. Such testing also offers an independent monitoring tool because routine access to service applications is often precluded by various factors. The interrelation between corrosion and environmental factors is complex because of the influence of many independent and dependent variables. Nevertheless, as much monitoring as can be performed economically is highly desirable to fully characterize the local conditions so as to permit data analysis for any possible correlations, even if these are not found until sometime in the future. Typical routine monitoring at Kure Beach has comprised corrosivity assessment via iron, carbon steel, zinc and wire-on-bolt specimens. Airborne chloride is determined by the wet candle method and time of wetness with the aid of electronic sensors. Other parameters such as relative humidity, temperature, wind speed and direction are also monitored routinely. There is no indication of any adverse effects due to recent changes in the setback distances of the test lots from the ocean.

Long-term exposures in very aggressive oceanfront and somewhat less severe conditions further back have provided very useful and often sought data on materials such as stainless steel, thermal sprayed Zn and Al coatings on steel, high alloys, plated components, and so forth, for practical marine applications.

References

- [1] *Atmospheric Corrosion*, W. H. Ailor, Ed., J. Wiley & Sons, New York, NY, 1982.
- [2] Ambler, H. R. and Bain, A. A. J., "Corrosion of Metals in the Tropics," *Journal of Applied Chemistry*, Vol. 5, September, 1955, pp. 437-467.
- [3] King, G. A. and O'Brien, D. J., "The Influence of Marine Environments on Metals and Fabricated Coated Metal Products, Freely Exposed and Partially Sheltered," *Atmospheric Corrosion, ASTM STP 1239*, W. W. Kirk and H. H. Lawson, Eds., American Society for Testing and Materials, West Conshohocken, PA, 1995, pp. 167-192.
- [4] Duncan, J. R. and Ballance, J. A., "Marine Salts Contribution to Atmospheric Corrosion," *Degradation of Metals in the Atmosphere, ASTM STP 965*, S. W. Dean and T. S. Lee, Eds., American Society for Testing and Materials, West Conshohocken, PA, 1988, pp. 317-326.
- [5] Morcillo, M. Chico, B. Otero, E., and Mariaca, L., "Effect of Marine Aerosol on Atmospheric Corrosion," *Materials Performance*, Vol. 38, No. 4 (April), NACE International, Houston, TX, 1999, pp. 72-77.
- [6] Callaghan, B. P., in *Atmospheric Corrosion*, W. H. Ailor, Ed., J. Wiley & Sons, New York, NY, 1982, pp. 242-243.
- [7] Baker, E. A. and Lee, T. S., "Calibration of Atmospheric Corrosion Test Sites," *Atmospheric Corrosion of Metals, ASTM STP 767*, S. W. Dean, Jr. and E. C.

- Rhea, Eds., American Society for Testing and Materials, West Conshohocken, PA, 1982, pp. 250-256.
- [8] LaQue, F. L. in *Proceedings*, American Society for Testing and Materials, Vol. 51, 1951, p. 495.
- [9] Townsend, H. E., "Atmospheric Corrosion Resistance of Skyward and Groundward Exposed Surfaces of Zinc and 55% Al-Zn Alloy Coated Steel Sheet", *Corrosion*, Vol. 54, No. 7, pp. 561-565.
- [10] Doyle, D. P. and Wright, T. E., "Rapid Methods for Determining Atmospheric Corrosivity and Corrosion Resistance," *Atmospheric Corrosion*, W. H. Ailor, Ed., J. Wiley & Sons, New York, NY, 1982, pp. 227-243.
- [11] Baker, E. A. and Lee, T. S., "Long-Term Atmospheric Corrosion Behavior of Various Grades of Stainless Steel," *Degradation of Metals in the Atmosphere*, ASTM STP 965, S. W. Dean and T. S. Lee, Eds., American Society for Testing and Materials, West Conshohocken, PA, 1988, pp. 52-67.
- [12] Baker, E. A. and Kirk, W. W., "Long-Term Atmospheric Corrosion Behavior of Various Grades of Stainless Steel in Rural, Industrial, and Marine Environments," *Corrosion Testing and Evaluation: Silver Anniversary Volume*, ASTM STP 1000, R. Baboian and S. W. Dean, Eds., American Society for Testing and Materials, West Conshohocken, PA, 1990, pp. 177-190.
- [13] Kain, R. M. and Baker, E. A., "Marine Atmospheric Corrosion Museum Report on the Performance of Thermal Spray Coatings on Steel," *Testing of Metallic and Inorganic Coatings*, ASTM STP 947, W. B. Harding and G. A. DiBari, Eds., American Society for Testing and Materials, West Conshohocken, PA, 1987, pp. 211-234.
- [14] Baboian, R., Ballante, E.L. and Cliver, E.B., Eds., *The Statue of Liberty Restoration*, NACE International, Houston, TX, 1990.

Desmond C. Cook,¹ Ann C. Van Orden (dec.),¹ Javier Reyes,² Sei J. Oh,³ Rama Balasubramanian,¹ Juan J. Carpio,² and Herbert E. Townsend⁴

Atmospheric Corrosion in Marine Environments along the Gulf of México

Reference: Cook, D. C., Van Orden, A. C., Reyes, J., Oh, S. J., Balasubramanian, R., Carpio, J. J., and Townsend, H. E., “**Atmospheric Corrosion in Marine Environments along the Gulf of México,**” *Marine Corrosion in Tropical Environments, ASTM STP 1399*, S. W. Dean, G. Hernandez-Duque Delgadillo, and J. B. Bushman, Eds., American Society for Testing and Materials, West Conshohocken, PA, 2000.

Abstract: Atmospheric corrosion in México is creating significant structural problems in the tropical marine regions of the Gulf of México. This is especially true along the southern Gulf coast where increasing petrochemical pollution is present with the extremely high chloride concentrations resulting from strong onshore winds, and the ever-present high time-of-wetness. The climatic and environmental parameters have been measured, between 1993 and 1998, at 12 coupon exposure sites at marine locations around the Gulf of México. Corrosion classifications for iron, aluminum, copper and zinc have been calculated for each site using mean values of the time-of-wetness, chloride and sulfur dioxide concentrations. The theoretically predicted corrosion rates have been determined from the site classification data, and compared to the 12-month corrosion rates measured by coupon mass loss for the four metals exposed at the same sites. The data show that all sites have at least a C4 classification with most having C5 even though many are located over 1 km from the shoreline. The measured corrosion rates of different metals are often not in good agreement with those predicted using the environmental parameters, providing evidence that other climatic factors such as frequency of precipitation can modify the corrosion rates and distort the correlation with theoretical corrosion predictions and models. Spectroscopic analysis of corrosion products from exposed carbon steel coupons shows that large fractions of akaganeite form in high chloride environments, along with lepidocrocite and goethite. The oxides form in distinct layers on the steel surface. The amount of akaganeite formed is related to some extent by the precipitation frequency which controls if pollutants are regularly flushed from the steel surfaces.

Keywords: marine corrosion, corrosivity, México, Mössbauer spectroscopy

¹Professors and Graduate Research Assistant, Physics Department, Old Dominion University, Norfolk, VA 23529.

²Graduate Research Assistant and Professor, Programa de Corrosion del Golfo de México, Autonomous University of Campeche, Campeche 24030 México.

³Postdoctoral Fellow, Materials Science and Engineering Department, Pohang University of Science and Technology, Pohang, Kyungbuk 790-784 Korea.

⁴Senior Research Consultant, Bethlehem Steel Corporation, Bethlehem, PA 18016.

Introduction

Corrosion research in Latin America is an expanding field of scientific and engineering study due mainly to the increasing demand to understand the performance of structural materials in some of the world's most adversely corrosive regions. The quest for corrosion data, models and prediction of materials performance is being driven by significant rural and industrial development in this the world's largest accessible tropical location. It is well known that structural materials presently used in many of the locations, have severely reduced serviceable lifetimes, particularly in the marine environment. This is especially true in developing regions in México, along the Caribbean coastline and around the Gulf of México where industry and urban expansion are exposing building materials to prolonged humid, marine environments, as well as to high concentrations of industrial pollutants. In order to evaluate some of the corrosion problems, Mexican research groups in Mérida, Campeche and México City, have made important contributions to the understanding of the corrosion sources by measurement of environmental conditions and determination of the corrosivity index and the corrosion rates of different metals in many of the commercially important areas along the Gulf of México and Caribbean coastline. Researchers from Old Dominion University, in collaboration with the Mexican corrosion groups, have subsequently exposed structural steels produced in the United States, México and Japan at several locations, and are undertaking a spectroscopic investigation of the corrosion products to identify the iron oxides which form and transform as a function of exposure time and environmental conditions. The locations of the oxides within the corrosion product layers are also being mapped in order to understand the mechanism by which some rust layers are adherent and protective against further corrosion, particularly for the High-Strength Low-Alloy, HSLA, structural steels. One basic scientific advantage of performing such research in the tropical regions of the Gulf of México, is the availability of exposure sites with a large range of environmental pollutants and annually high mean temperatures and humidity, which produces high time-of-wetness for the exposed metals.

México is located between the latitudes 15° and 30° N and the longitudes 86° and 116°. Two thirds of the country is located in the tropics, including 90% of the coastal regions on the Gulf of México. The geographical characteristics of México are varied, from the large southwest coastline bordering the Pacific Ocean, the dry, hot regions in the north, the high central mountainous region, including México City, to the flat, heavily vegetated regions of the southern and eastern coast of the Gulf of México. The most easterly section of México includes the Yucatan Peninsula, a flat limestone tableland which is rich in Mayan culture and tradition. Its west coast, bordering the Gulf of México, is a region of agriculture and fishing, where the inhabitants have maintained their traditional living style, in contrast to the more popularly known tourist resorts on the east coast along the Caribbean Sea from Cancun and Cozumel in the north to Chetumal 400 km to the south. The four main climatic zones in México are shown in Figure 1 along with the location of cities in which atmospheric exposure sites are located. The region along the Gulf of México is classified as Humid Tropical, [I], having a mean annual relative humidity greater than 75% and mean precipitation greater than about 1500 mm/yr. The mean annual temperature is greater than 26 °C which is about the same temperature as the Gulf waters in this region. One interesting exception to this classification is the north-west corner of the Yucatan Peninsula which is

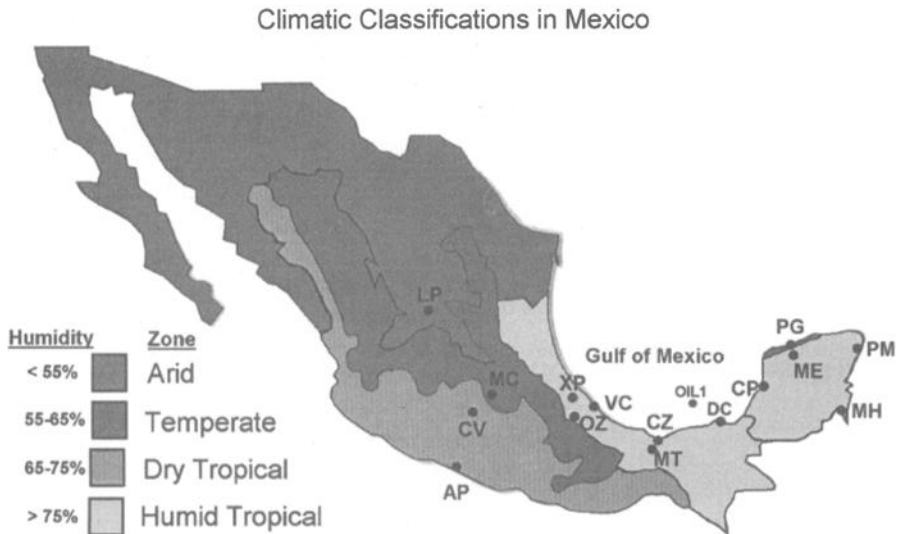


Figure 1 - Map of México showing the four main climatic zones and the mean annual relative humidity for each zone.

classified as Arid. This region contains the important shipping port of Progreso which has a mean rainfall less than 400 mm/yr, but with the high relative humidity and temperature of a sub-tropical location.

Throughout México there are over 380 National Meteorological Stations, (SMN), most of which have been recording daily weather conditions for over 50 years [2]. This data is included in a comprehensive set of maps available from the National University of México, (UNAM) in México City. Table 1 lists a summary of the main weather conditions at the cities shown on Figure 1 where atmospheric exposure sites are located. Important features in the Gulf region include the coastal cities of Veracruz and Coatzacoalcos which have very high rainfall and very strong year-round winds which blow predominantly from the north and northeast off the Gulf of México. This makes both regions severe marine environments with high chloride concentrations. Some data for the marine exposure site at Kure Beach, NC are also included for comparison. Detailed descriptions of the regional weather conditions and their daily changes for each season are beyond the scope of this article. They are contained in the recent work by Reyes [3, 4]. In general however, the data of Table 1 would allow the prediction of high rates of atmospheric corrosion in the region of the Gulf of México.

The region surrounding the Gulf of México has been the location of significant economic development with the building of structures, ranging from industrial sites such as refineries and petrochemical processing plants, to homes and schools, and infrastructures including roads and bridges. This is particularly true in the cities of Coatzacoalcos, Minatitlan and Cd. Del Carmen, and is primarily due to the oil discoveries in the Gulf of

Table 1 - *Weather conditions at the Mexican exposure sites.*

City Code	City	Annual Precip., mm/yr	Mean Annual Temp. °C	Annual Relative Humidity %	Annual Solar Radiation hr	Wind Energy, W/m ²	Average Wind Speed, m/s	Prev. Wind Direction
CP	Campeche	800-1200	>26	>75	2600	40-80	6.0	SE
DC	Cd. Del Carmen	1500-2000	>26	>75	2400	40-60		
CZ MT	Coatzacoalcos Minatitlan	2000-2500	22-26	>75	2200	80-160	9.0	N
VC	Veracruz	1500-2000	>26	>75	2400	>160	11.0	NE
XP	Xalapa	1200-1500	12-18	>75	<1800	10-20	3.0	SE
OZ	Orizaba	800-1200	12-18	65-75	<1800	0-10	3.0	E
ME	Merida	800-1200	>26	>75	3000	0-10	5.0	SE
PG	Progreso	125-400	22-26	65-75	2600	20-40		NE
PM	Puerto Morelos	1500-2000	>26	>75	3000	10-20	5.0	SE
MH	Majahual	1200-1500	>26	>75	3000	0-10	5.0	SE
MC	México City	400-600	12-18	55-60	2400	0-10	4.0	All
LP	San Luis Potosi	125-400	12-18	65-70	2200	10-20	5.5	E
AP	Acapulco	1200-1500	>26	65-75	2800	10-20	5.5	SW
KB	Kure Beach NC	1200-1500	18	79			3.4	NE

México off the coast of Cd. Del Carmen in the 1970s, see OIL1 on Figure 1. Three oil refineries have since been built by PEMEX-petrochemical at Pajaritos, Cangrejera and Morelos near Coatzacoalcos. Accompanying the refineries has been the emergence of a large number of support and petrochemical related facilities producing plastics, detergents, fertilizers and rubber. All have led to the growing urban development in Coatzacoalcos and Minatitlan. They have also led to the increase in atmospheric contamination in this region as well as in the regions to the south and west including Veracruz which are severely affected by the wind-carried pollutants from the oil rigs to the northeast. In the period 1984 to 1991, the pH of the rain in Veracruz has decreased from 5.75 to 4.32, and the ozone level is up to 8.58 ppm [5, 6]. It has been reported that a typical PEMEX petrochemical plant has annual emissions of 52.2 tons of oxides of sulfur, 23.4 tons of particulates, 14 tons of carbon monoxide and 7 tons of hydrocarbons [6].

The increasing occurrence of acid rain in the tropical environments whose relative humidity regularly exceeds 80%, accompanied with the high marine chloride concentrations, has resulted in extremely high corrosion rates of structural materials along the southern coast of the Gulf of México [4]. In reported cases, structural failures due to atmospheric corrosion in the area of Coatzacoalcos-Minatitlan, have resulted in very serious accidents with loss of

life and economic loss [3, 7]. There is also serious concern about possible damage to the limestone structures at the Mayan cultural areas as a result of increased acid rain in regions to the northeast along the Yucatan Peninsula. Recently, rainwater pH levels in Campeche have been measured between 4.2 and 8.2, throughout the year [3, 8].

Marine Corrosion México

Two well-established corrosion research groups exist in México in the area of the Yucatan Peninsula. In Mérida, the Corrosion Research Group is located in the Department of Applied Physics at Centro de Investigación y de Estudios Avanzados del Instituto Politécnico Nacional, Unidad Mérida (CINVESTAV-IPN, Mérida). This group has an outstanding reputation and is involved in research on a wide range of corrosion problems in México including the performance of structural and stainless steels in developing regions along the Caribbean Sea. It maintains at least 5 atmospheric exposure sites from the northwest corner of the Yucatan Peninsula between Mérida and Progreso, to the east towards Cancun and Puerto Morelos and south along the Caribbean coastline to Majahual. In Campeche, Programa de Corrosión del Golfo de México (PCGM), is located at the Universidad Autónoma de Campeche. PCGM works specifically with corrosion-related problems in concrete and structural steels in regions of the Gulf of México from Campeche south to Veracruz, (600 km). The program set up more than 13 atmospheric exposure sites in 1993 between Campeche and Veracruz as well as on oil rigs off Cd. Del Carmen.

The sites used by both programs are all located in large cities in the Humid Tropic region shown in Figure 1. Several sites are often located in the same city whose local environmental conditions are known to vary geographically. All sites are located at sea level except for Xalapa and Orizaba which are 1100 and 1900 m in altitude respectively. Table 2 lists coupon exposure sites along the Gulf of México and Caribbean Sea and the distance of each from the shoreline. Also listed are five sites located in the other three climatic zones and for which corrosivity data have been published. Four US exposure sites are included as reference. The groups at Mérida and Campeche collaborate with researchers at Old Dominion University for the spectroscopic analysis of exposed coupons. A detailed description of most sites, including photographs, can be found at www.physics.odu.edu/~cmmf/mx [4].

Until recently, very little research had been performed to determine the corrosivity of various regions in México. In 1988 work began to characterize the atmospheric aggressiveness in 14 Latin American countries through the project known as Ibero-American Map of Atmospheric Corrosividad (MICAT). In México, four stations at Acapulco, Cuernavaca, México City and San Luis Potosí were used to produce the first map of atmospheric corrosivity in México [9-11]. Following that, the Mérida group began to add data for its Caribbean sites [12].

In 1993, PCGM began a five-year study of the atmospheric corrosion at 12 sites along the Gulf of México between Campeche and Xalapa. The research monitored the climatic and environmental parameters to determine site corrosivity classification and to permit theoretical corrosion rates to be calculated. Coupons of Mexican produced carbon steel, aluminum, copper and zinc were also exposed at many sites to determine the measured

Table 2 - Location of exposure sites for corrosion research in México.

Site Code	City	Location Code	Location	Dist. from coast, m
CP1	Campeche	PCGM	Programa de Corrosion del Golfo de Mexico	300
CP2	Campeche	SMNC	National Meteorological Station	4000
CP3	Campeche	CRIP	Centro Regional de Investigacion Pesquera	4
DC1	Cd. Del Carmen	SMND	National Meteorological Station	700
CZ1	Coatzacoalcos	CETIS	Centro de Estudios Tecnologicos, Industriales y de	1000
CZ2	Coatzacoalcos	PAJARITOS	PEMEX Refinery	1000
CZ3	Coatzacoalcos	CANGREJERA	PEMEX Refinery	3000
CZ4	Coatzacoalcos	MORELOS	PEMEX Refinery	3000
MT1	Minatitlan	ITM	Instituto Tecnologico de Minatitlan	20 km
VC1	Veracruz	ITV	Instituto Tecnologico de Veracruz	1000
VC2	Veracruz	IUV	Instituto de Ingenieria de la Universidad Veracruzana	800
XP1	Xalapa	FIEUV	Universidad Veracruzana, Xalapa (el. 1100 m)	70 km
OZ1	Orizaba	ITO	Instituto Tecnologico de Orizaba (el. 1900 m)	100 km
OIL1	Gulf of Mexico	GOM1	PEMEX2 Oil Rig 300 km offshore Cd. Del Carmen	300 km
ME1	Merida	IPNMERIDA	CINVESTAV-IPN, Merida	50 km
PG1	Progreso	ROTM	Residencia de Operaciones de Transportacion Maritima	50
PM1	Puerto Morelos	PM1	Puerto Morelos	500
PM2	Puerto Morelos	PM2	Puerto Morelos	1000
MH1	Majahual	MH1	Majahual	500
MC1	México City	UNAM	Universidad Nacional Autonoma de México	300 km
MC2	México City	UAM	Universidad Autonoma Metropolitana (Atzacapotzalco)	300 km
CV1	Cuernavaca	IIEUNAM		300 km
LP1	San Luis Potosí	UASLP	Universidad Autonoma San Luis Potosi (Mexinox)	300 km
AP1	Acapulco			1000
KB25	Kure Beach, NC	LCCT	LaQue Center for Corrosion Technology, NC	25
KB250	Kure Beach, NC	LCCT	LaQue Center for Corrosion Technology, NC	250
BSC1	Bethlehem, PA	BSC1	Bethlehem Steel Corporation, PA	300 km
SB1	Saylorsburg, PA	BSC2	Bethlehem Steel Corporation, PA	300 km

corrosion rates by mass loss. At several sites, coupons were first placed on the racks at 4 different times during the year in order to measure the corrosion rates as a function of the initial exposure season. Coupons were normally exposed for 1, 2, 3, 6, 9 and 12 months. Researchers at PCGM undertook the corrosion related calculations in order to determine the main factors controlling the atmospheric corrosion at each site. Researchers at Old Dominion University performed the spectroscopic analysis and microscopic mapping of the corrosion products on the carbon steel coupons, in order to correlate the type and amount of each iron oxide formed with the exposure conditions. The exposure program is continuing using new US produced high strength structural steels and coated steels.

Corrosivity Classifications and Corrosion Rates in México

Most of the exposure sites in México are located within 1 km of the Gulf or Caribbean shorelines and it could be anticipated that the atmospheric marine corrosion in this tropical region will be high and due mainly to large amounts of chlorides and high time-of-wetness. However, it could also be anticipated that the chloride concentrations at different regions along the Gulf shoreline will vary as a result of different predominant wind directions, and therefore different site corrosivity classifications will result from geographical influences even though proximities to the shoreline are similar. In order to correlate the Mexican corrosivity data with other international studies, the standard exposure and environmental monitoring techniques and parameters measured, were as recommended by the MICAT project. A full list of all environmental parameters measured has been reported by Reyes [3, 4]. The continuous measurements included air temperature, relative humidity, wind speed and direction, precipitation, evaporation, time and energy of solar radiation. This data was statistically processed to determine for each parameter, its monthly and annual mean values over 5 years. The airborne chloride and SO₂ concentrations were measured monthly. Exposed materials were in the form of 0.10 m x 0.15 m rectangular coupons of thickness 0.003 m for carbon steel, (type A36), and 0.001 m for aluminum, copper and zinc. Helical test coils, 0.10 m long and 0.024 m diameter, of carbon steel, aluminum and copper were wound from 1 m long and 0.003 m diameter wires. All materials were cleaned and weighed prior to exposure using #400 and #600 abrasive paper to remove oxide scale, and chemically cleaned with either dilute hydrochloric and/or sulfuric acids and acetone. Samples were exposed between 1 and 1.5 m above the ground on insulated racks angled at 45°. The coupons faced the water in marine environments and north in non-coastal locations in accordance with ISO 8565 - General Requirements for Field Tests. Each exposure rack contained protected chloride candles and sulfation plates for monthly pollution measurement in accordance with ISO 9225 - Measurement of Pollution. Following exposure the corrosion products were chemically removed from the coupons according to ISO DIS 8467 - Determination of Weight Loss. Average mass loss was determined from triplicate coupons exposed for twelve months.

The corrosion classifications for iron, aluminum, copper and zinc at each site were determined according to ISO 9223 - Corrosivity of Atmospheres - Classification, following measurement of the time-of-wetness, and airborne chloride and SO₂ concentrations. Table 3 shows the data and classifications from the 12 sites used in the PCGM project. Also included are data from 4 sites characterized by the Mérida group and the 4 sites used for the MICAT project. Again the data from 4 US sites are included as reference. It can be seen that

the time-of-wetness at all marine sites around the Gulf of México is significantly higher than at Kure Beach, due mainly to the higher mean annual temperature in the tropics. Chloride concentrations are significantly varied along the coastline due mainly to the predominant wind direction, average wind speed and also distance from the shoreline. For example, the predominant wind direction in Mérida and Campeche is SE, (offshore), thereby keeping the chloride concentrations relatively low. This is also true at site CP3 which is located just 4 m from the shoreline at Campeche [4]. However, along the southern Gulf and the Caribbean coasts, as well as at Progreso, the predominant winds are onshore, which result in high chloride concentrations up to 1 km inland. Industrial pollutants from the petrochemical refineries in the Coatzacoalcos-Minatitlan area are seen to be high especially within the Pemex-Pajaritos grounds, site CZ2. Also in Veracruz which contains very little heavy industry, the SO₂ concentrations are high due to windblown pollutants originating from the oil-rigs off the coast of Cd. Del Carmen.

The corrosion classifications show that every marine site has at least a C4 rating for one of the metals, with most sites having a C5 classification, even though they are located generally 1 km or more inland. In general the high time-of-wetness in the tropical regions sets the stage for high corrosivity in the presence of even small amounts of pollutants.

The 12-month corrosion rate of each metal, as predicted theoretically from the site corrosivity, is shown in Table 4 along with the measured corrosion rate using the 12 month mass loss of exposed coupons. In general there is fair correlation between prediction and measured corrosion rates for sites having corrosivity classification of C4 or less. Even then there are anomalies, for examples site CP1 which measures low for steel and high for copper and zinc, and site VC1 which measures very high for steel, copper and zinc. Very high corrosion rates were measured in the marine locations having predominantly onshore winds increasing the chloride concentrations. The extremely high corrosion rates at the petrochemical site CZ2 is in part due to other locally emitted gases such as ammonia which add to the continuous acid rain/humid environment inside the plant. Just outside the plant at site CZ1, the corrosion rates are lowered towards those observed at the Kure Beach 25 m lot. The high corrosion rates at Veracruz are also effected by the high mean wind velocity and the weekly sandstorms that the city experiences. The measured corrosion rates at the C5 sites shows a very broad range of values, and it is misleading to evaluate many of the locations by corrosion classifications and predicted corrosion rates alone. In the case of the tropical marine environments, observing corrosion rates 2-4 times greater than the lower limit for the classification, can result in severely reduced serviceable lifetimes and increased maintenance costs if the structure is designed according to predicted data. For example, at the University of Veracruzana, site VC2, each of the four metals has a corrosion rate at least twice the lower predicted value. Clearly the model for predicting site corrosivities needs to be improved by perhaps including additional parameters, or more likely by initially improving measurement of the pollutants and time-of-wetness at the surface of the exposed metal.

In order to make a general prediction of the corrosion rates of steel, aluminum, copper and zinc in tropical marine environments, which may contain some industrial influence, the experimental data of Table 4 were statistically analyzed to correlate the corrosion with time-of-wetness, chloride and sulfur dioxide concentrations in the air. Table 5 shows the results with an estimated error of about 5%. It should be noted that aluminum, copper and zinc were not exposed at all sites particularly at several of those with higher SO₂ concentrations at

Table 3 - Corrosion classifications for the Mexican exposure sites determined from the measured time-of-wetness and atmospheric pollutants.

Site Code	Time of Wetness, hr/yr	Pollutants, mg/m ² day				Corrosion classification			
		Cl ⁻	SO ₂	Iron	Aluminum	Copper	Zinc		
CP1	4894 τ ₄	70.5 S ₂	2.61 P ₀	C4	C3-C4	C4	C4		
CP2	4576 τ ₄	17.0 S ₁	2.64 P ₀	C3	C3-C4	C3	C3		
CP3	4572 τ ₄	76.2 S ₂	5.35 P ₀	C4	C3-C4	C4	C4		
DC1	4950 τ ₄	17.6 S ₁	3.33 P ₀	C3	C3-C4	C3	C4		
CZ1	6617 τ ₅	174.8 S ₂	13.00 P ₁	C5	C5	C5	C5		
CZ2	6250 τ ₅	180.9 S ₂	24.67 P ₁	C5	C5	C5	C5		
CZ3	6250 τ ₅	46.2 S ₁	9.84 P ₀	C4	C5	C4	C4		
CZ4	6250 τ ₅	90.2 S ₂	9.10 P ₀	C5	C5	C5	C5		
MT1	6617 τ ₅	19.6 S ₁	10.72 P ₁	C4	C5	C4	C4		
VC1	5439 τ ₄	242.2 S ₂	6.67 P ₀	C4	C3-C4	C4	C4		
VC2	4922 τ ₄	384.3 S ₃	15.83 P ₁	C5	C5	C5	C5		
XP1	3828 τ ₄	6.4 S ₁	1.13 P ₀	C3	C3-C4	C3	C3		
ME1	τ ₄	11 S ₁	3.8 P ₀	C3	C3-C4	C3	C3		
PG1	τ ₄	430 S ₃	12.2 P ₁	C5	C5	C5	C5		
PM1	τ ₄	360 S ₃	3.1 P ₀	C5	C5	C5	C5		
MH1	τ ₄	405 S ₃	3.7 P ₀	C5	C5	C5	C5		
MC1	τ ₃	S ₀	P ₁	C3	C3	C3	C3		
CV1	τ ₃	S ₀	P ₀	C2	C3	C3	C3		
LP1	τ ₃	S ₀	P ₁	C3	C3	C3	C3		
AP1	τ ₄	S ₁	P ₀	C3	C3-C4	C3	C3		
KB25	4290 τ ₄	311 S ₃	0 P ₀	C5	C5	C5	C5		
KB250	4290 τ ₄	110 S ₂	0 P ₀	C4	C3-C4	C4	C4		
BSC1	τ ₄	5 S ₀	26 P ₁	C3	C3	C3	C3		
SB1	τ ₄	5 S ₀	17 P ₁	C3	C3	C3	C3		

Table 4 - Predicted and measured corrosion rates in México, determined from site corrosivity and 12-month coupon exposure, respectively. Data from four US sites are included. Some sites did not include all four metals.

Site	Corrosion Rate, mg/m ² yr							
	carbon steel		aluminum		copper		zinc	
	Predicted	Measured	Predicted	Measured	Predicted	Measured	Predicted	Measured
CP1	400-650	183.5	0.6-5		12-25	58.3	15-30	44.5
	50-80	23.3	0.25-2		1.3-2.8	0.66	2.1-4.2	6.24
CP2	200-400	100.7	0.6-5	1.89	5-12	11.9	5-15	23.7
	25-50	12.8	0.25-2	0.70	0.6-1.3	1.33	0.7-2.1	3.32
CP3	400-650	585.5	0.6-5	5.19	12-25	46.6	15-30	32.6
	50-80	74.4	0.25-2	1.92	1.3-2.8	5.23	2.1-4.2	4.57
DC1	200-400	167.1	0.6-5	2.59	5-12	35.8	15-30	10.8
	25-50	21.2	0.25-2	0.96	0.6-1.3	4.02	2.1-4.2	1.51
CZ1	>650	1497.3	>5	1.29	>25	49.2	>30	
	>80	190.3	>2	0.48	>2.8	5.53	>4.2	
CZ2	>650	2347.1	>5		>25		>30	
	>80	298.2	>2		>2.8		>4.2	
CZ3	400-650	576.8	>5		12-25		15-30	
	50-80	73.3	>2		1.3-2.8		2.1-4.2	
CZ4	>650	363.5	>5		>25		>30	
	>80	46.2	>2		>2.8		>4.2	
MT1	400-650	683.8	>5	0.70	12-25	26.9	15-30	
	50-80	86.9	>2	0.26	1.3-2.8	3.02	2.1-4.2	
VC1	400-650	1621.8	0.6-5	4.09	12-25	45.1	15-30	72.9
	50-80	173.0	0.25-2	1.51	1.3-2.8	5.07	2.1-4.2	10.2
VC2	>650	1654.9	>5	9.02	>25	52.9	>30	105.6
	>80	210.3	>2	3.33	>2.8	5.94	>4.2	14.8
XP1	200-400	145.0	0.6-5	0.71	5-12	6.78	5-15	6.36
	25-50	18.4	0.25-2	0.26	0.6-1.3	0.76	0.7-2.1	0.89
KB25	>650	1291	>5		>25		>30	36
	>80	164	>2		>2.8		>4.2	5
KB250	400-650	362	0.6-5		12-25		15-30	14
	50-80	46	0.25-2		1.3-2.8		2.1-4.2	2
BSC1	200-400	598	0.6-2		5-12		5-15	14
	25-50	76	0.25-0.8		0.6-1.3		0.7-2.1	1.9
SB1	200-400	260	0.6-2		5-12		5-15	11
	25-50	33	0.25-0.8		0.6-1.3		0.7-2.1	1.6

Coatzacoalcos. The corrosion rate, $\text{mg/m}^2 \text{ yr}$, has been constrained to linear correlations with the chloride and sulfur dioxide concentrations, $\text{mg/m}^2 \text{ day}$ and the time-of-wetness, TOW, hr/yr . It can be seen that the TOW is the dominant parameter controlling the corrosion rates for each metal except for the case of copper and aluminum in very high chloride environments.

Table 5 - Corrosion rates predicted by linearly correlating the mass loss data with the measured environmental parameters. The corrosion rate, $\text{mg/m}^2 \text{ yr}$ is generally dominated by the time-of-wetness, TOW, hr/yr , except in high chloride concentrations, $\text{mg/m}^2 \text{ day}$, for the case of aluminum and copper.

Material	Corrosion rate, $\text{mg/m}^2 \text{ yr}$
Carbon steel	$C_{\text{CS}} = 0.228\text{TOW} + 0.290[\text{Cl}^-] + 0.410[\text{SO}_2]$
Aluminum	$C_{\text{AL}} = 0.042\text{TOW} + 0.497[\text{Cl}^-] + 0.490[\text{SO}_2]$
Copper	$C_{\text{CU}} = 0.078\text{TOW} + 0.318[\text{Cl}^-] + 0.616[\text{SO}_2]$
Zinc	$C_{\text{ZN}} = 0.327\text{TOW} + 0.756[\text{Cl}^-] - 0.04[\text{SO}_2]$

Corrosion Product Analysis

To understand how the various atmospheric conditions control the formation of corrosion products and the role some of these oxides in protecting the steel through increased corrosion resistance, a full analysis of the chemical and phase composition of the coatings is required. The analytical capabilities of Mössbauer spectroscopy, Micro-Raman spectrometry, X-ray diffraction and Infrared spectrometry are important for complete oxide identification including measurement of the fraction of each phase present. Corrosion coating impurity content and morphology require the use of Electron Probe Micro-analysis (EPMA), Energy Dispersive X-ray analysis (EDS) and Scanning Electron Microscopy (SEM).

Mössbauer spectroscopy alone is able to identify each oxide phase, but spectra need to be recorded at 300K, 77K and often down to 4K. Liquid nitrogen temperatures are required to separately identify akaganeite, $\beta\text{-FeOOH}$, and lepidocrocite, $\gamma\text{-FeOOH}$. Even then, the identification of superparamagnetic maghemite, $\gamma\text{-Fe}_2\text{O}_3$, and goethite, $\alpha\text{-FeOOH}$, is difficult due to magnetic relaxation effects [13]. Analysis down to 4K, and perhaps in applied magnetic fields, is often required for accurate identification, depending on the fraction of nanophase oxides present in the corrosion coating. The oxide identification should therefore be supported by other techniques. X-ray diffraction is able to identify akaganeite, but cannot easily distinguish between maghemite and magnetite, Fe_3O_4 . Infrared spectrometry easily identifies goethite and lepidocrocite but gives broad patterns for akaganeite and magnetite.

Raman spectrometry is able to identify most of the oxide phases but until recently was susceptible to transforming the oxyhydroxide phases through laser heating, resulting in incorrect phase determination, especially hematite, $\alpha\text{-Fe}_2\text{O}_3$. However, high quality micro-Raman spectrometers have now become an important, and perhaps necessary, analytical technique for detailed analysis and mapping of the oxide layers that exist in the corrosion coatings. The newer spectrometers have significantly reduced the data acquisition times to only several seconds per sampling point. This allows the oxides to be mapped to spatial resolution less than $1\ \mu\text{m}$, in less than one hour. Additionally the location of each oxide, whether it formed as single or mixed phase layers or in clusters, can be mapped in three-dimensions, across the surface of the corrosion coating and in depth profile through the thickness of the coating.

The Micro-Raman and Mössbauer techniques together provide complete, in-situ, non-destructive, three-dimensional identification of corrosion products. Mössbauer spectroscopy is the only technique able to accurately measure the fraction of each oxide in a corrosion coating. In corrosion research, this data is essential for monitoring oxide growth and phase transformations under different exposure conditions.

Experimental Procedure

Coupons of type A36 low carbon mild steel were exposed at the three Campeche sites for times up to 12 months. Several sets of coupons exposed between April 1993-March 1994 and May 1997-April 1998 were analyzed for consistency of corrosion product composition for each exposure year. The data was compared with carbon steel coupons previously exposed for 16 years at the US sites of Kure Beach (250 m lot), Bethlehem and Saylorburg [14]. Table 6 summarizes the coupon coding and exposure conditions.

The corrosion products were initially studied in-situ, still attached to their steel substrates, using scattering Mössbauer spectroscopy, by detecting the re-emitted Gamma radiation, (GMS) and the Conversion Electrons, (CEMS). The corrosion products were also removed from the steel by scraping, and analyzed by transmission Mössbauer spectroscopy, (TMS) at 4K, 77K and 300K. CEMS spectra were also recorded of the material that remained on the steel substrates following coating removal. Infrared spectra of the corrosion products were recorded with an FTIR spectrometer, using the diffused reflectance technique, in the range of $400 - 4000\ \text{cm}^{-1}$. Raman spectrometry was used to study metallographic cross-sections of the corroded steel coupons over the range $200 - 800\ \text{cm}^{-1}$ using a 25 mW He-Ne laser which was de-powered to 6 mW and focused to $2\ \mu\text{m}$ spot diameter. The cross-sections were polished with silicon carbide papers and finally $0.25\ \mu\text{m}$ diamond paste. X-ray powder diffraction analysis was performed on the intact corrosion coatings using Cu K_α radiation of wavelength $1.54056\ \text{Å}$. X-ray diffraction has only limited application in corrosion product identification. It cannot easily distinguish between maghemite, $\gamma\text{-Fe}_2\text{O}_3$ and magnetite, Fe_3O_4 because of their similar crystal structure and lattice parameters. X-ray diffraction cannot identify the nano-phase oxides of particle size less than about 20 nm. This is predominantly because the diffraction peaks are broad, overlapping, and masked behind the multiple high intensity peaks of the large particle oxides. However, X-ray diffraction can easily identify the presence of akaganeite, $\beta\text{-FeOOH}$, through the presence of the (521) peak, ($d=1.6361\ \text{Å}$, $\text{Cu-K}_\alpha\ 2\theta=56.3625^\circ$), which is well resolved from the diffraction peaks of all other iron oxides.

Table 6 - Coupon exposure conditions at the Campeche sites. The coupon code lists the exposure site.

Coupon Code	Exp. Time, mths	Exposure Period	Average Humidity, %	Time-of-wetness, hrs	Chloride mg/m ² day	Total Precipitation, mm
CP2-01	1	Apr.93-May 93	60	144	18.6	18
CP2-02	2	Apr.93-Jun.93	63	512	12.6	58
CP2-03	3	Apr.93-Jul.93	67	828	13.1	324
CP2-06	6	Apr.93-Sep.93	70	2047	19.0	950
CP2-12	12	Apr.93-Mar.94	72	4576	17.0	1405
CP3-07	7	Sep.93-Mar.94	71	2991	81.0	729
CP1-04	2	May.97-Jun.97	67	1007	5.0	113
CP1-08	3	May 97-Jul.97	70	1627	13.6	408
CP1-14	6	May 97-Oct.97	75	3496	12.5	826
CP1-18	9	May 97-Jan.98	76	5232	12.7	948
CP2-32	6	May 97-Oct.97	75	3496	13.2	826
CP2-36	9	May 97-Jan.98	76	5232	17.2	948

Spectroscopic Data

At the end of 1, 2 and 3 months exposure, the corrosion coatings all contained a predominance of a mixture of amorphous and crystalline lepidocrocite as indicated by both broad and narrow IR peaks at 1020 cm⁻¹. Very small peaks possibly corresponding to akaganeite and goethite were also present. Between 4 and 6 months exposure, the lepidocrocite transformed from the amorphous to the crystalline phase as shown by the sharpening of the IR peak at 1020 cm⁻¹ and the formation of a sharp peak at 750 cm⁻¹. IR spectrometry showed that for exposure times up to 12 months, crystalline goethite formed as the second dominant phase in amounts which increased with exposure time. Figure 2 shows the IR pattern of carbon steel coupon CP2-12 exposed at Campeche for 12 months in 1993. Well crystallized phases of lepidocrocite, (750 and 1020 cm⁻¹) and goethite, (790 and 890 cm⁻¹) are clearly present.

X-ray diffraction analysis identified the presence of lepidocrocite, goethite and maghemite/magnetite in all samples in amounts that varied with exposure time and location. Coupons exposed in 1993 at sites CP2 and CP3 clearly showed the presence of akaganeite in the coatings as can be seen in Figure 3 for coupon CP3-07. This was not unexpected for exposure at site CP3 having high chloride concentration of 76 mg/m² day, but it was interesting to identify it also at site CP2 having only 17 mg/m² day of chloride. The half-widths for all oxide diffraction peaks were very broad for exposure times of 2 months and narrowed as exposure time increased. This showed the initial formation of a large amount

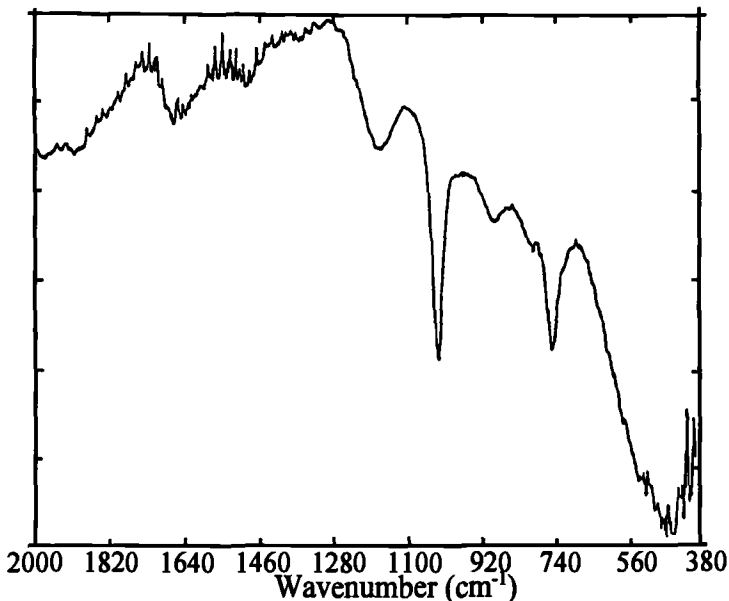


Figure 2 - Infrared spectrum of the corrosion products on carbon steel coupon CP2-12 exposed in Campeche, México for 12 months. Lepidocrocite and goethite are the two main iron oxides identified.

of nano-phase material of low crystallinity, and the development towards larger more crystalline particles as exposure time increased. Analysis of the particle size of each oxide phase by X-ray diffraction and Mössbauer spectroscopy is presently being performed to determine the fractions of each nanophase oxide in the corrosion coatings [15]. After 12 months exposure, the peaks were still broader than those obtained for crystalline high purity iron oxide standards [16], and were superimposed on much narrower peaks at the same diffraction angle, showing a mixture of large, > 50 nm, and small particle sizes of the same oxide phase. The coupons exposed in 1997 again contained lepidocrocite, goethite and maghemite/magnetite but no akaganeite was identified from either the CP1 or CP2 exposure sites.

Mössbauer analysis was performed to complete the identification of the oxides and to measure the fraction of each in the corrosion coating of each carbon steel coupon. The spectra of coupons CP2-12, CP3-07 exposed in 1993 and coupon CP2-36 exposed for 9 months in 1997 are shown in Figures 4-6 respectively. The scattering Mössbauer spectra show a large magnetic sextet due to the steel substrate which was being probed through the corrosion coating. However magnetic and non-magnetic oxides are present in the coatings. From the transmission spectra recorded at room temperature, significant differences can be seen between the coupons exposed in 1993 and 1997. The earlier exposed coupons contain

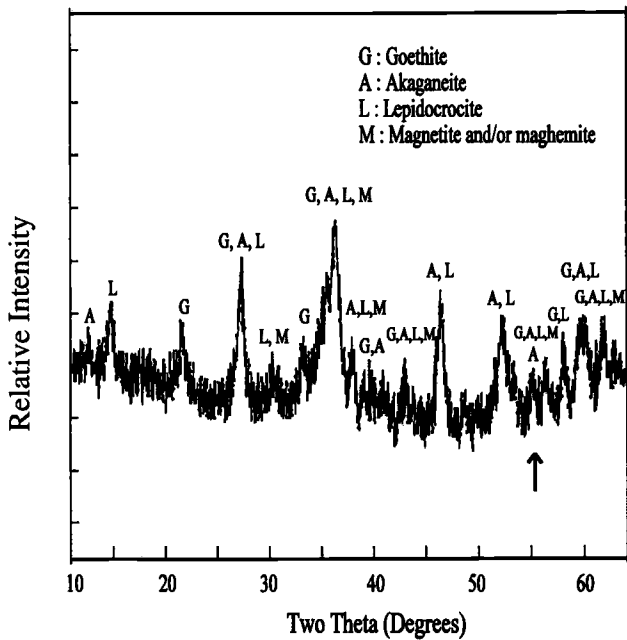


Figure 3 - X-ray diffraction pattern of the corrosion products on carbon steel coupon CP3-07 exposed at Campeche in 1993.

the magnetic sextet of goethite at 300K, Figures 4(b) and 5(b), indicating the particle size at least 40 nm. The coupons exposed in 1997 showed only a non-magnetic doublet, Figure 6(a), indicating that if goethite was present, it was exhibiting superparamagnetism and had particle size < 40 nm.

For spectra recorded at 77K, a full computer analysis showed that all samples contained lepidocrocite, goethite and maghemite. However the coupons exposed in 1993 also contained akaganeite, confirming the X-ray diffraction identification. No akaganeite was identified in any coupons exposed in 1997. Table 7 summarizes the fraction of each oxide identified by Mössbauer spectroscopy. Lepidocrocite was the most abundant oxide, 43%, to form after 12 months at site CP2 in 1993. Nearly equal fractions of goethite and akaganeite was also present. However in the same year and in the presence of higher chloride concentrations at site CP3, the coupon exposed for just 7 months contained 43% akaganeite and nearly equal fractions of lepidocrocite and goethite. The magnetic field for the goethite in these coupons was measured to be about 50 T confirming that the goethite particle size was > 40 nm. The low temperature spectrum for the coupon exposed at CP2 in 1997 confirmed the presence of goethite, but with a reduced magnetic field of 43 T. This indicated that goethite was present with reduced particle size, in the order of 20 nm. It should be noted that this particle size is still larger than that of the goethite formed in the inner protective layer of HSLA

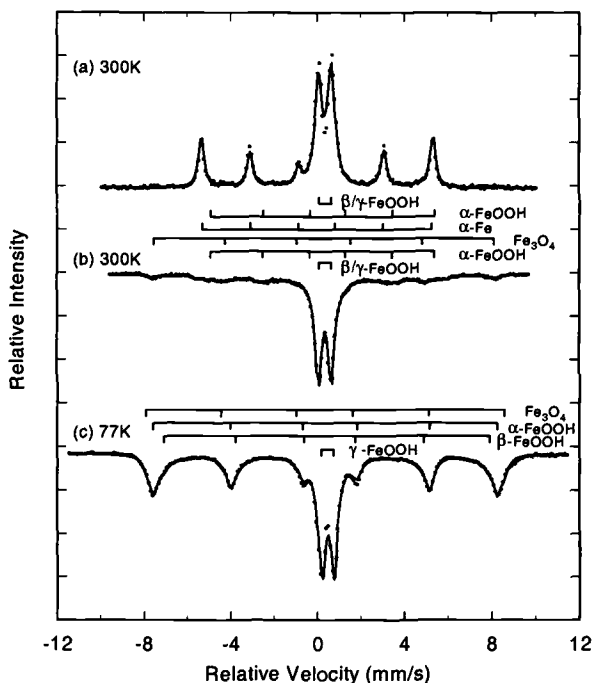


Figure 4 - Mössbauer spectra of the corrosion products on coupon CP02-12 exposed at Campeche site CP2 for 12 months in 1993. Spectra were recorded in (a) scattering geometry at 300K, and in transmission geometry at (b) 300K and (c) 77K.

steels, that being 5-15 nm in diameter [17, 18]. As also has been reported recently by Balasubramanian et al. [19], the coupons exposed for shorter times in Campeche in 1997 did show the presence of smaller mean particle size through the collapsed magnetic field. It was evident however that the growth of the crystals rather than re-nucleation of new nano-phase goethite particles, was favored in the carbon steel exposures in Campeche.

Micro-Raman spectrometry was used to map the location of the oxides in the corrosion coatings to spatial accuracy of a few micrometers. Surprisingly, the analysis proved to show very similar trends to those observed in coupons exposed in the US for 16 years [17, 18]. Figures 7 and 8 show the data from the Raman patterns recorded for the metallographic cross-section and surface scan of the corrosion coating on coupon CP2-12. The corrosion coating is distinctly bi-layered, Figure 7 (a), with the inner layer next to the steel substrate comprised of mainly goethite, and the upper layer being mainly lepidocrocite. No akaganeite or maghemite was identified from the coating cross-section. The composition of the bi-layered coating was similar to that observed in weathering and carbon steels exposed in the US for 16 years with the exception of the lack of nano-phase goethite and the absence of

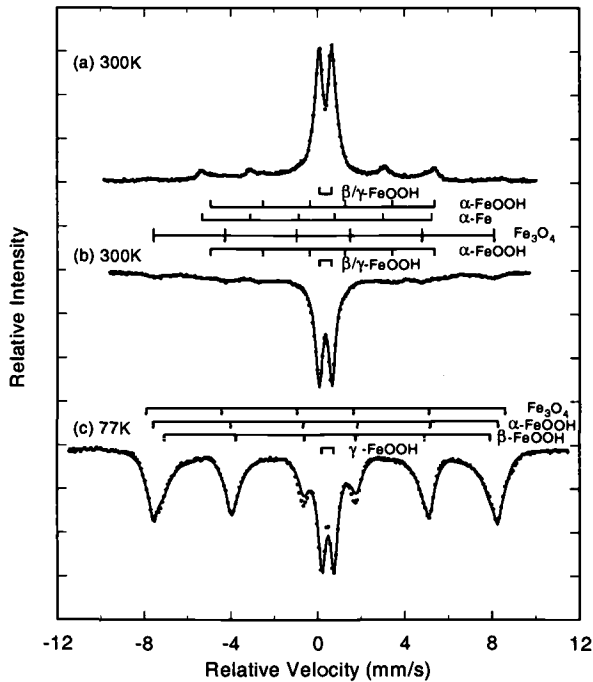


Figure 5 - Mössbauer spectra of the corrosion products on coupon CP03-07 exposed at Campeche site CP3 for 7 months in 1993. Spectra were recorded in (a) scattering geometry at 300K, and in transmission geometry at (b) 300K and (c) 77K.

Table 7 - Percentage of each iron oxide phase in the corrosion coatings of some of the carbon steel coupons exposed at the three sites in Campeche, México in 1993 and 1997.

Oxide Phase	Site CP1	Site CP2		Site CP3
	CP1-18	CP2-12	CP2-36	CP3-07
α -FeOOH	54	28	43	23
β -FeOOH	0	24	0	42
γ -FeOOH	38	43	49	27
$\text{Fe}_3\text{O}_4/\gamma\text{-Fe}_2\text{O}_3$	8	5	8	8

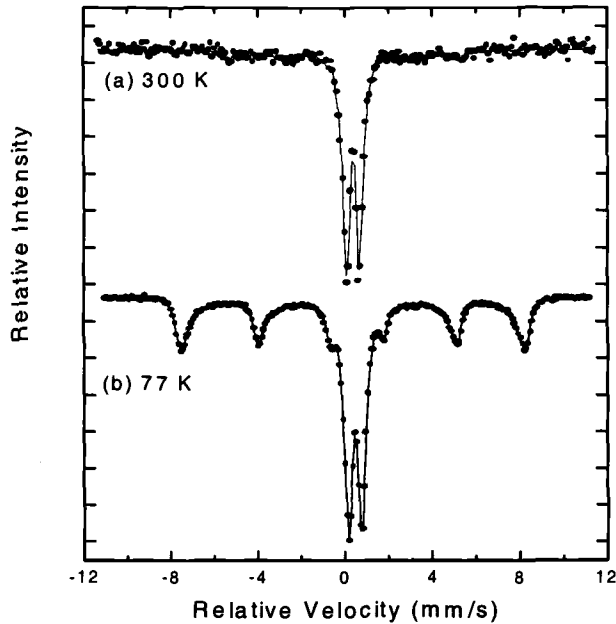


Figure 6 - Mössbauer spectra of the corrosion products on coupon CP02-36 exposed at Campeche site CP2 for 9 months in 1997.

the maghemite identified in carbon steel exposed at Kure Beach [17]. The surface scan, shown in Figure 8, identified islands of akaganeite, lepidocrocite and goethite across the top of the corrosion coating. At the present time it is not possible to measure the fraction of each oxide by Raman spectrometry. However it was apparent that the amount of akaganeite measured by Mössbauer spectroscopy was not detected by Raman spectrometry. Raman analysis of the coupons exposed in 1997 showed a similar bi-layered structure having the same basic composition to that described above. For these coupons however, maghemite was detected in the inner layer close to the steel substrate. In a recent publication by Balasubramanian et al. [19], it was shown that the broadened spectral lines indicated the possibility that the maghemite and goethite in the inner layer were nanophase, 5-15 nm, similar to that identified in the 16 year exposures in the US.

Discussion

Detailed spectroscopic analysis of the corrosion products on all coupons exposed in Campeche has shown that the oxides, predominantly lepidocrocite and goethite, formed at

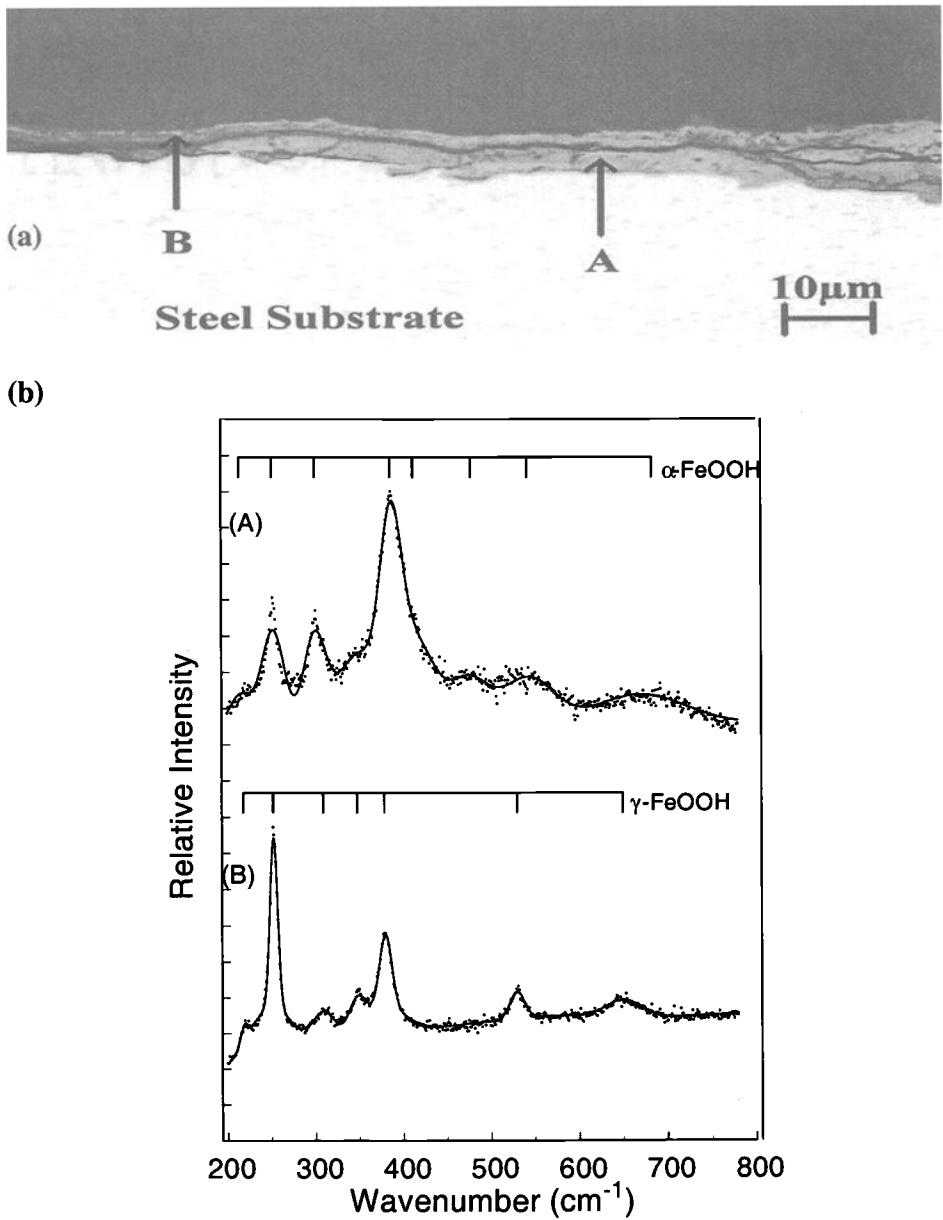
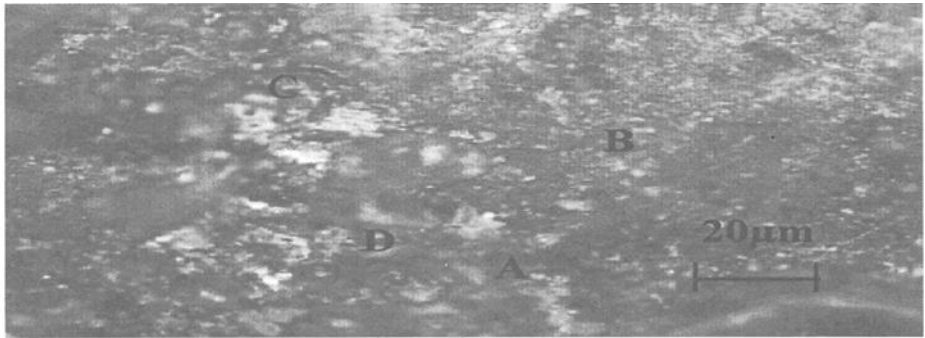


Figure 7 - (a) Metallographic cross-section, and (b) Raman spectra of the layered corrosion products formed on the coupon CP2-12. The (A) inner layer is mainly goethite and the (B) outer layer consists of lepidocrocite.



(a)

(b)

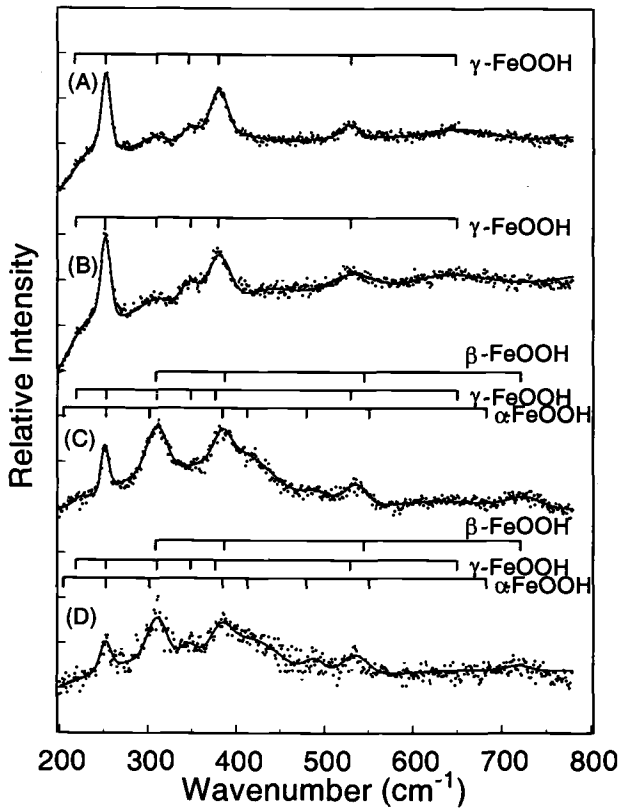


Figure 8 - (a) Surface Image and (b) Raman spectra of the corrosion products formed on the coupon CP2-12. Across the surface, lepidocrocite, akaganeite and goethite are identified.

low exposure times are the same as identified in long-term exposures. The exception was the presence of akaganeite in the 1993 exposures in contrast to the lack of this phase in the 1997 exposures, and also in any of the coupons exposed in the US for 16 years. The distinct oxide layering seen in long term exposures was already present after a just a few months and it would be of interest to monitor the development of these layers during longer exposures up to say five years. Such a project is being designed for México and the United States using carbon and weathering steels. Information is being sought on the development of the nanophase oxides which appear to be more abundant in the HSLA steels and are believed to be important in the formation of the adhesive protective layer on these steels.

The presence of large amounts of akaganeite on the coupons exposed at CP2 and CP3 in 1993 is not surprising since akaganeite is known to form in chloride containing environments. It is believed however that a critical concentration of chloride is required to form the akaganeite, although this has not been confirmed numerically. Certainly twice as much akaganeite formed at CP3 due to the high mean chloride concentration of $81 \text{ mg/m}^2\text{day}$ during the 7 months exposure, and most likely helped by occasional Gulf storms which saturated the coupons with seawater.

It is difficult to predict if akaganeite should form at site CP2 having a low mean chloride concentration of $17 \text{ mg/m}^2\text{day}$. It was observed on the coupons in 1993 but not in 1997. This shows the need to study monthly climatic conditions during the actual exposure periods rather than working with mean values. For example, the coupons exposed in 1993 and 1997 at site CP2 were in fact subjected to different monthly chloride concentrations even though the mean values of all exposure conditions, shown in Table 6, are very similar. In 1993, the CP2 coupons were exposed to higher chloride concentrations in the first few months when the rainfall was very low. In 1997, the coupons were exposed to the opposite criteria, low chlorides and high rainfall in the first few months of exposure. This was also true for the coupons exposed at site CP1 in 1997 and in which akaganeite was not detected.

These data show the possible intervention of another important climatic parameter, rainfall and its frequency of occurrence relative to months of high pollutant deposition. Precipitation is commonly associated with increased time-of-wetness, but in the very humid tropical environments, this is not significant. Alternatively, rainfall is able to wash pollutants off the surfaces of exposed materials, thereby decreasing the corrosion rates. It should also be noted that the chloride candles are to some extent protected from the rain by a metallic cover as specified by ISO 9225. Therefore the measured chloride concentrations, and other pollutants, are probably higher that at the coupon surface during months of higher precipitation. Again this is justification for a much improved surface pollution monitor.

Conclusions

The establishment of many coupon exposure sites in México, and the detailed measurement of the climatic and environmental parameters around the Gulf of México, has provided valuable information concerning the varied corrosion rates in developing regions. The research has also shown that the effects of industrial pollutants, especially in adverse marine environments can double the local exposure rates, and that measured rather than theoretically predicted corrosion rates are required for regions of highest corrosion classification. The measured corrosion rates of different metals are often not in good

agreement with those predicted using the environmental parameters, leading to a conclusion that pollutant measurements at the actual material's surface should be a future goal to achieve. There is strong evidence that other climatic factors such as frequency of precipitation can modify the corrosion rates and distort the correlation with theoretical corrosion predictions and models.

From the viewpoint of correlating corrosion product formation with exposure parameters, it is clear that chlorides control the formation of akaganeite and that predicting its formation from measurement of airborne chloride concentration is difficult. Indeed the present data indicates that locally high chloride concentrations must be present on the steel surface for some period of time for appreciable quantities of akaganeite to form. Spectroscopic analysis of the coupons exposed in Campeche continues to build the data-base of information concerning the formation of nanophase oxides, particularly goethite, on different steels. The present data support the findings of exposure programs in the United States that only small fractions of nanophase goethite form on atmospherically exposed carbon steels, possibly resulting in the exfoliation of the corrosion coating and subsequent exposure of the bare metal to the environment.

Acknowledgment and Disclaimer

Some of the material is based upon work supported by the National Research Foundation under Grant No. 9602990. Any opinions, findings, and conclusions expressed in this material are those of the authors and do not necessarily reflect the views of the National Science Foundation.

References

- [1] Climates, National Maps of México, Map IV.4.7, (1992), Institute of Geography, University of México, México City, Mx.
- [2] National Meteorological Stations, National Maps of México, Map IV.4.2, (1992), Institute of Geography, University of México, México City, Mx.
- [3] Reyes, J., "Influences of the main climatic factors and the quality of the air on the atmospheric corrosion of metals in the southeast coast of the Gulf of México." MS Thesis, University of Veracruzana, July 1999.
- [4] Condensed Matter and Materials Physics Web Site, Old Dominion University, www.physics.odu.edu/~cmmp/mx.
- [5] Kanuga, K. K., "Atmospheric Pollution Potential in the Republic of México," Department of Physics, University of Veracruzana, Xalapa, Ver, Mx. 1984.
- [6] Bravo, A. H. and Torres, J. P., "Gulf of México: Contamination and Environmental Impact," University of Campeche, EPOMEX Scientific Series Vol. 5, 1996.
- [7] PEMEX-Petrochemical, "Preliminary Design for the Study of the Effects of the Contamination in the Deterioration of the Metals in the Petrochemical Complexes of the Industrial area of Coatzacoalcos," 1994.
- [8] Reyes, J. and Perez, T., "Study of the Influence of the Seasonal Variations in the Rate of Atmospheric Corrosion of the Steel in the City of Campeche," Corrosion Program

- of the Gulf of México, Autonomous University of Campeche. Campeche, Camp. México, 1998.
- [9] Genescá, J. and Rodriguez, C., "Calibration of the Atmospheric Aggressiveness," First International Workshop of Metallic Corrosion. CONACYT-CINVESTAV (Mérida), Mérida, Yuc. México, 1990.
- [10] Felliú, S., Morcillo, M., and Felliú, S. Jr., "The Prediction of Atmospheric Corrosion from Meteorological and Pollution Parameters-I. Annual Corrosión." *Corrosion Science*. Vol. 34, No. 3, pp. 403-414, 1993.
- [11] Felliú, S. and Morcillo, M., "Corrosion and Protection of Metals in the Atmosphere." Ed. Bellaterra S.A., Barcelona, Spain, 1982.
- [12] Pereyra, D., Natividad, M. A., Sosa, I., and Reyes, J., "Statistical Model to Estimate the Concentration of NaCl and SO₂, of Atmospheric Corrosion in Xalapa Veracruz," Mexican Geophysical Union, D.F., 1996.
- [13] Morup, S., Dumesic, J. A., and Topsoe, H., *Applications of Mössbauer Spectroscopy*, Vol II, R. L. Cohen, Ed., Academic Press, New York, 1980.
- [14] Oh, S. J., Cook, D. C., and Townsend, H. E., "Atmospheric Corrosion of Different Steels in Marine, Rural and Industrial Environments." *Corrosion Science*, Vol. 41, No. 9, 1999, pp. 1687-1702.
- [15] Balasubramanian, R., Old Dominion University, personal communication, 1999.
- [16] Oh, S. J., Cook, D. C., and Townsend, H. E., "Characterization of Iron Oxides Commonly Formed as Corrosion Products on Steel." *Hyperfine Interactions*, Vol. 112, 1998, pp. 59-65.
- [17] Cook, D. C., Oh, S. J., and Townsend, H. E., "The Protective Layer Formed on Steels after 16 Years of Atmospheric Exposure," Corrosion/98, paper 343, 1998, NACE International, Houston, TX.
- [18] Cook, D. C., Oh, S. J., Balasubramanian, R., and Yamashita, M., "The Role of Goethite in the Formation of the Protective Corrosion Layers on Steels," *Hyperfine Interactions*, Vol. 122, 1999, pp.59-70.
- [19] Balasubramanian, R., Cook, D. C., Perez, T., and Reyes, J., "Development of Nano-phase Iron Oxides from Short-term Atmospheric Corrosion of Carbon Steel," Corrosion/2000, paper 453, 2000, NACE International, Houston, TX.

Jorge Uruchurtu-Chavarrín,¹ †Liboria Mariaca-Rodríguez,¹ and Grupo Micat²

Electrochemical Evaluation of the Protective Properties of Steel Corrosion Products Formed in Ibero-American Tropical Atmospheres

Reference: Uruchurtu-Chavarrín, J., Mariaca-Rodríguez, L., and Micat, G., “**Electrochemical Evaluation of the Protective Properties of Steel Corrosion Products Formed in Ibero-American Tropical Atmospheres,**” *Marine Corrosion in Tropical Environments*, ASTM STP 1399, S. W. Dean, G. Hernandez-Duque Delgadillo, and J. B. Bushman, Eds., American Society for Testing and Materials, West Conshohocken, PA, 2000.

Abstract: The purpose of the MICAT project (Ibero-American Map of Atmospheric Corrosiveness) was to foster collaborative ventures between groups conducting research on atmospheric corrosion. Overall 14 Ibero-American countries, including Spain and Portugal were involved with a network of 75 test stations distributed throughout the region and on 3 continents, and many of them were set within tropical regions representing a broad spectrum of climatological and atmospheric pollution conditions. The general objective of the MICAT electrochemical studies was to characterize the electrochemical and protective properties of the corrosion products formed during different periods of atmospheric exposure (1 to 4 years). The particular objective of the present work is to present electrochemical results associated to the protective properties of steel corrosion products formed in test sites with tropical atmospheres. After atmospheric exposure, pre-rusted mild steel specimens were immersed in a sodium sulfate solution and electrochemically evaluated. Linear polarization resistance (LPR) and electrochemical potential noise (EPN) measurements were performed after one hour of immersion. Electrochemical measurements were related to the presence of the atmospheric oxides formed and associated to climatological and atmospheric pollution data; its protective properties reflected in the weight loss data obtained during exposure. For specimens rusted in marine atmospheres, the presence of chlorides promotes localized corrosion. The electrochemical measurements were able to characterize and evaluate the protective properties of oxides according to the nature and environmental conditions to which specimens were exposed.

Keywords: MICAT, atmospheric corrosion, electrochemical measurements evaluation, mild steel, oxide protective properties.

¹ Researchers IIE, Reforma 113, Palmira, Temixco 62490, Morelos, México.

² Researchers CYTED, Gregorio del Amo 8, 28040, Madrid, España.

Background.

Before the MICAT project, little was known about atmospheric corrosion in tropical atmospheres. Systematic studies, were carried by just a few countries and data was seldom published [1-4]. The MICAT international project (Ibero-American Map of Atmospheric Aggressiveness) was set up in 1988, within the CYTED Programme of Science and Technology for Development. The aim of the project was to foster collaborative ventures between groups that have been conducting research on atmospheric corrosion in their respective countries and to train others on this topic [5]. Overall, 14 Ibero-American countries including Portugal and Spain were involved. Research was encompassed both at laboratories and in a network of 75 atmospheric exposure test sites distributed throughout the region and on 3 continents, most of them located in tropical regions. These considered a broad spectrum of climatological and atmospheric pollution data. The MICAT project aimed to attain the following objectives:

- To gain greater knowledge about atmospheric corrosion mechanisms in the different Ibero-American atmospheres.
- To establish, through the adequate statistical treatment of results, mathematical expressions which allow prediction of atmospheric corrosion as a function of climatic and pollution parameters and
- To draw up the Ibero-American Map of Atmospheric Corrosiveness (MICAT).

Meeting the above objectives will allow optimal selection of materials and coatings under specific conditions of atmospheric aggressiveness. The project followed some aspects outlined by ISOCORRAG and ICP/UNECE [6, 7] projects, and whenever possible, ISO standards have been followed for field studies. Four groups were established to study different aspects of the exposed specimens. These include: corrosion product morphology, chemical analysis of corrosion products and water soluble contaminants, statistical analysis of environmental and corrosion data and electrochemical evaluation.

Introduction

Atmospheric corrosion accounts for more than 50% of the economic losses caused by corrosion according to Tomashov [8]. The atmospheric corrosion of metals is directly related to the environmental and pollution conditions to which they are exposed and can be hundreds of times higher in some places than in others. This accounts for the increasing interest in determining which variables are involved in the process [5]. The characteristic properties of oxides depend on the pollutants present, the environmental and climatic conditions, and the time of exposure of the metals to the atmosphere. In Ibero-American countries, atmospheric corrosion data are scarce and little is known about the protective properties of oxides developed during variable corrosion conditions.

The objective of the MICAT electrochemical studies was to characterize the protective properties and electrochemical behavior of the corrosion products formed on the metal as a consequence of its atmospheric exposure. This work presents results obtained using linear polarization resistance (LPR) and electrochemical potential noise (EPN) on low carbon steels pre-rusted in different Ibero-American atmospheres to characterize the protective properties of the oxides developed during different times of exposure.

Experimental Procedure

The MICAT project basically follows the outlines of the ISOCORRAG collaborative program, although with its own peculiarities [6]. The location of the Ibero-American network of atmospheric corrosion testing stations (Fig. 1), covered a wide range of



Figure 1- Ibero-American atmospheric corrosion testing stations

environmental and pollution conditions. Details of the stations are given in Table 1. The stations were set up in accordance with ISO "Metals and Alloys-Atmospheric Corrosion Testing-General Requirements for Field Tests" standard (ISO 8565). The atmosphere at each test site has been characterized from meteorological and atmospheric pollution data according to ISO "Corrosion of Metals and Alloys-Corrosivity of Atmospheres-Classification of Corrosivity of Atmospheres" standard (ISO 9223) and ISO "Corrosion of Metals and Alloys-Corrosivity of Atmospheres-Methods of Measurement of Pollution" standard (ISO 9225). At the same time a categorization of the corrosiveness of the atmospheres was made on the basis of the corrosion rates during the first year of exposure in accordance with ISO 9223 (see Table 1).

Table 1- *Field Results*³

No.	Code	Name	Climatic Classif*[9]	T °C	TOW	Dep. rate	Estimated corrosivity	Mild Steel		
								Corrosion rate, $\mu\text{m}\cdot\text{y}^{-1}$		
MICAT								1	3-4	ISO
								year	years	Classifi- cation
								ISO Classification**		
3	A3	Iguazú	Cf	21.2	τ_5	S ₀ P ₀	C3-C4	5.7	2.8	C2
4	A4	San Juan	Bw	18.8	τ_3	S ₀ P ₀	C3-C4	4.9	1.9	C2
21	CO3	Cotové	Aw	27.0+	τ_4	S ₀ P ₀	C3	19.6	6.1	C2
35	EC1	Guayaquil	Aw	25.9	τ_4	S ₀ P ₀	C3	22.6	---	C2
6	A6	La Plata	Cf	16.8	τ_4	S ₀ P ₀	C3	28.1	15.3	C3
49	M2	Cuernavaca	Aw	21.0	τ_3	S ₀ P ₀	C2-C3	13.4	7.3	C2
2	A2	V. Martelli	Cf	16.9	τ_4	S ₀ P ₀	C3	14.7	7.7	C2
48	M1	México	Cw	15.3+	τ_3	S ₀ P ₁	C3	9.7	6.6*	C2
38	EC4	Esmeraldas	Am	26.8+	τ_5	S ₀ P ₁	C3-C4	69.2	---	C4
50	M3	S.L.Potosí	Bs	18.0	τ_3	S ₀ P ₁	C3	31.1	20.3	C3
12	B6	Sao Paulo	Cf	19.6	τ_5	S ₀ P ₂	C4-C5	20.6	8.3	C2
7	B1	Caratinga	Cw	21.2	τ_4	S ₁ P ₀	C3	11.1	6.6	C2
55	PA4	Chiriqui	Am	27.1	τ_4	S ₁ P ₀	C3	23.0	8.9	C2
51	M4	Acapulco	Aw	27.6	τ_4	S ₁ P ₀	C3	22.1	10.0	C2
39	EC5	San Cristóbal	Bs	24.6+	—	S ₁ P ₀	---	34.5	---	C3
37	EC3	Salinas	Bw	23.3+	τ_4	S ₁ P ₀	C3	55.9	44.9	C4
1	A1	Camet	Cf	14.1	τ_5	S ₁ P ₀	C3-C4	49.5	27.2	C3-C4
28	CU3	Bauta	Aw	24.0+	τ_4	S ₁ P ₁	C3	33.8	18.8	C3
8	B2	Ipatinga	Cw	23.2	τ_4	S ₁ P ₁	C3	49.4	24.7	C3
24	CR3	Arenal	Af	22.9+	τ_5	S ₁ P ₁	C3-C4	69.3	61.6*	C4
52	PA1	Panamá	Aw	26.9	τ_4	S ₁ P ₁	C3	27.6	16.4	C3
26	CU1	Ciq	Aw	25.2	τ_4	S ₁ P ₁	C3	30.4	16.1	C3
54	PA3	Veraguas	Am	27.2	τ_4	S ₁ P ₁	C3	20.0	9.6	C2
13	B7	Rio de Janeiro	Cf	21.4	τ_4	S ₁ P ₂	C4	110.5	58.5	C5
53	PA2	Colón	Am	27.1+	τ_5	S ₁ P ₂	C4-C5	108.1	60.4	C5
10	B4	Cubatao	Cf	22.7	τ_4	S ₁ P ₂	C4	158.9	85.2	C5
19	CO1	Isla Naval	Aw	27.8+	τ_5	S ₂ P ₁	C5	33.5	25.0	C3
27	CU2	Cojimar	Aw	25.1	τ_4	S ₂ P ₁	C4	280.0	228.0	C5

³ *Koppen climatic nomenclature. That is, capital letter indicates climatic group and lower case letter indicates climatic type. **ISO 9223 nomenclature based on deposition rate: P for SO₂, S for chlorides, and number for degree of pollution level. + data estimated. • data obtained after 3 years.

Materials

The materials, used in the form of flat plate specimens 150 x 100 mm were mild steel (unalloyed, low carbon), and were exposed to the atmosphere in conventional racks at the test sites according to ISO "Corrosion of Metals and Alloys - Corrosivity of Atmospheres - Determination of Corrosion Rate of Standard Specimens for the Evaluation of Corrosivity" standards (ISO 9226 and ISO 8565). The exposure sequence includes: three 1 year, one 2 year, one 3 year and one 4 year. Four specimens were exposed in each sequence, of which three were used for mass loss calculations and the fourth for special studies, including electrochemical testing. After the exposure period, the pre-rusted steel specimens were kept in a sealed plastic bag and removed from the test stations ready for mass loss calculation and special studies. The fourth specimen was cut in four pieces to perform the electrochemical measurements, as well as chemical analysis of soluble salts and corrosion products characterization, described elsewhere [5, 10]. No further treatment of the surface was carried out

Working Conditions

The electrochemical cell was built by attaching a 3.1-cm diameter and 1-cm high glass tube to the specimen with a clip holder. A neoprene ring was placed between the glass tube and the metal sample to prevent the electrolyte from leaking. The cell system includes a graphite counter electrode, a saturated calomel reference electrode (SCE) and the working electrode which corresponds to the metal under study, in a three electrode setup. As support electrolyte, a solution containing 0.1M sodium sulfate (Na_2SO_4) was used, providing a non-aggressive conductive media.

Instrumentation

An ACM electrochemical instrument or other suitable potentiostat coupled to a personal computer, which acted as data logger/analyzer was used for all electrochemical measurements. After about an hour, the corrosion potential reached a steady state and it was recorded. Afterwards, electrochemical potential noise (EPN) and linear polarization resistance (LPR) measurements were obtained on each sample.

Electrochemical Tests

The electrochemical measurements were basically those of corrosion potential and linear polarization resistance for all the groups involved. Also if desired, other electrochemical methods could be used. The measurement of corrosion potential makes it possible to obtain information about the corrosion tendency of the base metal and LPR measurements allow evaluation of corrosion kinetics or overall corrosion rate and the protective properties of the oxides or corrosion products formed.

LPR - A 10-mV anodic pulse was applied around the corrosion potential, and the current decay response was registered until it became asymptotically stable. At this point, the current response was obtained, and the polarization resistance was calculated.

EPN - The procedure adopted for this work consisted of measuring the corrosion potential oscillations as a function of time between the working electrode and the SCE. This was achieved at a sampling rate of one reading every 0.7 seconds. After gathering the data as a potential time record of 2048 samples, the DC drift was removed, fitting a straight line to the original data. The deviations of individual points with respect to that line produce a new set of data that comprises negative and positive values around the base line. The power spectral density plots were obtained using an algorithm based on the fast Fourier transform (FFT) of spectral analysis. The resolved frequency bandwidth of interest lies between 0.7 and 700-mHz. An EPN time record and corresponding power spectral density (PSD) plots were obtained. Also, the standard deviation of the EPN as an indication of increasing localized corrosion activity was calculated. High standard deviations are indicative of passive conditions or localized attack while lower values, of generalized attack and less protective oxide conditions [11-13].

The detailed procedure adopted for the present work is described elsewhere [5, 12-14].

Results and Discussion

Linear Polarization Resistance

To evaluate the protective properties of corrosion products formed over steel, a simple approach was established due to the nature and characteristics of this project. For oxide covered steels it was proposed that the determinant factor in the reaction kinetics and protective efficiency is the resistance of the rust layer [15]. Assuming an important contribution of this resistance to the overall LPR obtained, a measure of the linear polarization resistance (LPR) was performed.

Table 2 presents the electrochemical parameters obtained for the steel specimens exposed to different periods, atmospheric and climatic conditions. In order to support and correlate the electrochemical results obtained, phase analysis of corrosion products and water soluble contaminants are also presented (Table 3) [16].

Great variability was obtained in the corrosion potentials and LPR registered, for the steel samples exposed to different periods of atmospheric exposure, and even for the same time of exposure within the same group of ISO (S_xP_y) classified atmospheres. These could be explained in terms of the nature and great heterogeneity of the corrosion products formed and morphology observed even within the same sample. Film thickness reported, between 2 to 100- μm forming crests and valleys, and variable concentrations of Cl and S within the same sample appear to be enough conditions to explain the low reproducibility of the electrochemical results presented [16].

Rural- For rural atmospheres (S_0P_0) after 1 year of exposure samples, active corrosion potentials were registered, except Cuernavaca (-130 mV). The LPR values obtained varied from 0.10 $\text{k}\Omega\cdot\text{cm}^2$ for San Juan up to 3.50 $\text{k}\Omega\cdot\text{cm}^2$ for Cuernavaca. At the end of the exposure period, more noble potentials were obtained except San Juan which continued presenting an active potential. The LPR values increased in the range of 3.25 $\text{k}\Omega\cdot\text{cm}^2$ for Iguazu, up to 19.34 $\text{k}\Omega\cdot\text{cm}^2$ for La Plata. The higher LPR values for Cuernavaca and Cotove after one year of exposure, are associated to the presence of lepidocrocite and goethite as corrosion products compared to the other samples that present only lepidocro-

cite. After two years Cotove presents a LPR value of $9.52 \text{ k}\Omega\cdot\text{cm}^2$ and at the end of the exposure period, Cuernavaca and La Plata present the highest values while the other values are similar to the *blank* ($4.3 \text{ k}\Omega\cdot\text{cm}^2$) condition. Guayaquil presents active potentials and low LPR values for the different test samples, probably associated to the highest soluble salts content in the corrosion products formed.

Table 2- *Electrochemical Results*⁴

No.	Code Name MICAT		Potential, mV			Polarization resistance $\text{k}\Omega\cdot\text{cm}^2$			Standard deviation Potential Noise, mV		
			1	2	3-4	1	2	3-4	1	2	3-4
			year	years	years	year	years	years	year	years	years
3	A3	Iguazú	-488	-220	-73	0.29	1.11	3.25	---	---	---
4	A4	San Juan	-560	-535	-458	0.10	1.46	3.38	0.56	---	---
21	CO3	Cotové	-573	-490	---	2.29	9.52	---	0.25	---	---
35	EC1	Guayaquil	-535	-529	---	0.80	0.23	---	9.82	---	---
6	A6	La Plata	---	-559	-251	1.04	3.88	19.34	---	---	---
49	M2	Cuernavaca	-130	---	-282	3.50	---	13.00	1.89	---	1.98•
2	A2	V. Martelli	-507	-421	-291	0.16	3.03	4.92	1.20	---	---
48	M1	México	-140	-176	-163•	0.54	13.33	60.01	2.87	0.71	4.52
38	EC4	Esmeraldas	-565	-504	---	0.35	0.38	---	---	---	---
50	M3	S.L.Potosí	-487	-407	-577•	1.04	3.14	23.98	1.99	0.54	0.52
12	B6	Sao Paulo	-49	-230	-171•	13.30	22.05	67.41	---	---	---
7	B1	Caratinga	-479	---	---	3.95	---	---	2.84	---	---
55	PA4	Chiriqui	-242	-88	-204•	10.00	10.00	3.70	---	0.05	---
51	M4	Acapulco	-492	-112	-189	0.09	9.70	22.00	8.26	0.58	1.01•
39	EC5	San Cristóbal	-541	-525	---	0.24	0.35	---	---	---	---
37	EC3	Salinas	-582	-574	---	0.15	0.28	---	---	---	---
1	A1	Camet	-483	---	-384	0.13	3.25	6.25	---	---	---
28	CU3	Bauta	-154	---	-337	21.45	25.50	5.88	---	---	---
8	B2	Ipatinga	-342	-402	---	8.62	1.15	---	2.33	---	---
24	CR3	Arenal	-220	-480	---	7.10	---	---	0.12	---	---
52	PA1	Panamá	-181	-458	-366•	1.58	1.21	1.75	---	---	---
26	CU1	Ciq	-322	---	-243•	3.10	14.16	3.91	---	---	---
54	PA3	Veraguas	-68	-52	-89•	12.50	5.10	3.33	---	---	---
13	B7	Rio de Janeiro	-100	+20	-196•	3.60	4.63	1.95	---	---	---
53	PA2	Colón	-241	-62	-386•	2.1	25.18	8.33	---	---	---
10	B4	Cubatao	-556	+216	-428•	3.59	13.96	9.08	---	---	---
19	CO1	Isla Naval	-51	---	-330	2.42	---	2.11	0.50	---	---
27	CU2	Cojimar	-330	-116	-288•	3.22	1.08	1.63	---	---	---

Urban-Industrial- For urban and industrial atmospheres, samples from Mexico and Sao Paulo present noble potentials while active potentials for Esmeraldas and S. L. Potosí were registered under the electrochemical test conditions. These correspond to the steel samples exposed in the atmosphere during one, two and three year periods. LPR values as low as $0.35 \text{ k}\Omega\cdot\text{cm}^2$ (Esmeraldas) and as high as $13.30 \text{ k}\Omega\cdot\text{cm}^2$ (Sao Paulo) were ob-

⁴ *Blank* (one hour of immersion): - 452 mV; $4.3 \text{ k}\Omega\cdot\text{cm}^2$; standard deviation 1.82 mV.

• data obtained after 3 years.

tained for the first year of exposure samples, increasing up to $60.01 \text{ k}\Omega\cdot\text{cm}^2$ and $67.41 \text{ k}\Omega\cdot\text{cm}^2$ for Mexico and Sao Paulo respectively. The exception being Esmeraldas located near a petrochemical plant, presenting active potentials and low LPR values, associated to porous corrosion products being formed due to the presence of H_2S in the atmosphere. For S. L. Potosí and Sao Paulo with the highest soluble sulfate salt content in the corrosion products formed, lepidocrocite and goethite are already present as corrosion products after one year, and in

Table 3- Chemical Analysis and Corrosion Products Results⁵

No Code	Name	Soluble salts, mg/m ²						Corrosion products			
		MICAT			Soluble salts, mg/m ²			Time of exposure			
					Sulfate						
		Chloride			Sulfate			Time of exposure			
		1 year	2 years	3 years	1 year	2 years	3 years	1 year	2 years	3 years	4 years
3 A3	Iguazú	38	33	28	104	91	120	L	L	---	---
4 A4	San Juan	96	---	---	341	---	---	L	L	---	---
21 CO3	Cotové	61	---	---	128	---	---	L,G	L,G	---	---
35 EC1	Guayaquil	249	---	---	487	---	---	L	---	---	---
6 A6	La Plata	34	---	---	294	---	---	---	---	---	---
49 M2	Cuernavaca	65	---	---	522	---	---	L,G	---	---	---
2 A2	V. Martelli	52	50	25	245	301	344	L	L	---	---
48 M1	México	84	262	151	518	599	412	L	L,G	---	---
38 EC4	Esmeraldas	---	---	---	---	---	---	L	---	---	---
50 M3	S.L.Potosí	49	35	181	1282	1519	1534	L,G	---	---	---
12 B6	Sao Paulo	270	---	---	1020	714	---	L,G	L,G	L,G	L,G
7 B1	Caratinga	106	73	43	339	216	249	L,G,Mg	L,G,Mg	L,G	L,G
55 PA4	Chiriqui	80	187	201	115	258	291	G,L,Mg	G,L,Mg	G,L,M	G,L,M
51 M4	Acapulco	215	409	473	714	706	900	L,G,M	---	---	---
1 A1	Camet	257	1099	587	117	123	140	L,G	L,G	---	---
28 CU3	Bauta	108	---	---	96	---	---	L,G	L,G	L,G	L,G
8 B2	Ipatinga	109	53	214	466	363	---	L,G	L,G	L,G	L,G
24 CR3	Arenal	135	---	---	45	---	---	L,G,M	L,G,M	---	---
52 PA1	Panamá	74	---	---	121	---	---	L,G,Mg	L,G,Mg	G,L,M	G,L,M
26 CU1	Ciq	141	90	349	502	698	1089	G,L	G,L	G,L	G,L
54 PA3	Veraguas	96	199	37	141	287	74	L,G,Mg	L,Mg	G,L,M	G,L,M
13 B7	Rio de Janeiro	266	54	---	754	183	---	L,G	L,G	L,G	L,G
53 PA2	Colón	170	---	---	399	---	---	G,L	G,L	G,L	G,L
10 B4	Cubatao	125	---	85	362	---	368	L,G,M	L,G,M	L,GM	L,M,G
19 CO1	Isia Naval	1150	704	754	327	169	448	L,G,A	L,G,A	---	---
27 CU2	Cojimar	868	190	220	1274	191	---	M,L,G	M,L,G	M,G,L	MG,AL

Mexico these products are present after just 2 years of atmospheric exposure. The presence of greater contents of soluble salts in the corrosion products formed, render them more porous and less protective, and could promote localized active metal conditions or under-deposit corrosion when subjected to the electrochemical test solution, and therefore lower LPR values (San Luis Potosí) [16, 18]. Nevertheless, the electrochemical re-

⁵ L- Lepidocrocite; G- Goethite; M-Magnetite; Mg-Maghemite; A-Akaganeite. Corrosion products are presented from major to minor proportion.

sults obtained suggest a progressing protective nature of the corrosion products formed under these atmospheres. Further evidence is presented in the next section on electrochemical potential noise.

Marine- The following results presented correspond to marine atmospheres (S_1P_0). Variable results were obtained and presented due to the different environmental exposure conditions (Tables 2 and 3). Active corrosion potentials were obtained after one year of exposure in the atmosphere, becoming less active after two and three years. Acapulco presents noble potential for the two and three year samples. The LPR values tend to increase with time, but the numbers are relatively smaller than before (chloride free atmospheres). For the first year the values lie between $0.09 \text{ k}\Omega\cdot\text{cm}^2$ (Acapulco) and $10 \text{ k}\Omega\cdot\text{cm}^2$ (Chiriqui), reaching a high $22 \text{ k}\Omega\cdot\text{cm}^2$ for Acapulco at the end of exposure. Under the electrochemical test conditions considered, only Chiriqui samples present noble potentials from the start, remaining till the end of the atmospheric exposure, while the LPR values were $10 \text{ k}\Omega\cdot\text{cm}^2$ for one and two years, decreasing to $3.7 \text{ k}\Omega\cdot\text{cm}^2$ at the end of exposure. After one year of exposure, lepidocrocite and goethite and even maghemite in different proportions are present simultaneously in the corrosion products formed. Magnetite is present in Acapulco after one year and in Chiriqui after three years. Balanced contents of chloride/sulfate soluble salts were registered in the corrosion products formed and found in Chiriqui and Caratinga samples, where maghemite is present as part of the corrosion products formed after the first year of exposure. The presence of goethite in the corrosion products formed (the greatest proportion in the case of Chiriqui) appears to be related as before, to the characteristic properties of film oxides and the increasing LPR values obtained. The low LPR results obtained for Camet and after three years in Chiriqui could be explained in terms of the presence of layers of porous and/or cracked corrosion products with high contents of soluble salts, promoting localized attack, as observed [16].

Urban-Marine- These atmosphere (S_1P_1) samples, present noble potentials for the one year exposed samples, decreasing to more active potentials the following year and increasing again at the end of the specimens' exposure period. Variable LPR values were registered for the first of atmospheric exposure samples ranging from $1.58 \text{ k}\Omega\cdot\text{cm}^2$ for Panama up to $21.45 \text{ k}\Omega\cdot\text{cm}^2$ for Bauta. Similar results were obtained for the two years exposed samples, presenting variable results as low as $1.15 \text{ k}\Omega\cdot\text{cm}^2$ (Ipatinga) and as high as $25.5 \text{ k}\Omega\cdot\text{cm}^2$ (Bauta). Results were lower for the end of exposure samples, ranging in the order of $1.75 \text{ k}\Omega\cdot\text{cm}^2$ (Panama) to $5.88 \text{ k}\Omega\cdot\text{cm}^2$ (Bauta). The corrosion products formed, present intermediate protective characteristics under the presence of both pollutants (higher contents of chlorides and sulfur dioxide) in the atmosphere. Retained pollutants are responsible for the localized pitting and underdeposit attack, according to the electrochemical parameters registered [16, 19].

The presence of SO_2 in the atmosphere, including chloride containing atmospheres (mixed atmospheres) appears to have a certain beneficial effect in the oxide film formation and its protective characteristics. This was suggested by the results presented above, and also in the following results obtained corresponding to industrial-marine atmospheres (S_1P_2). The overall trend of the electrochemical parameters as a function of time of exposure, is similar for the steel samples of the three test stations considered. Noble corrosion potentials except Cubatao, were obtained for the first year exposure samples. An increase was observed in all two year sample corrosion potentials, decreasing again to less noble

values at the end of exposure samples. LPR values show similar trend, starting for the first year in the range between $2.1 \text{ k}\Omega\cdot\text{cm}^2$ (Colon) to $3.60 \text{ k}\Omega\cdot\text{cm}^2$ (Rio de Janeiro), increasing the second year up to $25.18 \text{ k}\Omega\cdot\text{cm}^2$ in the case of Colon and finally decreasing again to values between $1.95 \text{ k}\Omega\cdot\text{cm}^2$ for Rio de Janeiro, and $9.08 \text{ k}\Omega\cdot\text{cm}^2$ for Cubatao. Variability is less in the case of Rio de Janeiro but the absolute numbers are also lower. These results appear to be related to the presence of soluble salts in the corrosion products formed in Rio de Janeiro which presents almost double the amount of those obtained in Colon and Cubatao. Corrosion products formed consisted of lepidocrocite and goethite, although in Colon goethite is the major constituent and in Cubatao magnetite is also present.

Coastal-Urban- Finally two coastal-urban (S_2P_1) test stations were considered: Isla Naval and Cojimar. Noble corrosion potentials were registered for the different steel exposure samples, between -51 and -330 -mV for Isla Naval and for Cojimar, -330 and -288 mV. The LPR values remained in the same order of magnitude (as the *blank* condition) in both cases; between 2.42 and $2.11 \text{ k}\Omega\cdot\text{cm}^2$ for Isla Naval, and 3.22 and $1.63 \text{ k}\Omega\cdot\text{cm}^2$ for Cojimar. The results suggest that film oxide formed under these conditions is less protective than in the previous cases. High chlorides concentration in the atmosphere, and high soluble salts within corrosion products (higher chlorides than sulfates) appears to affect the corrosion product morphology and reflected in the electrochemical results. The usual lepidocrocite and also goethite were found in the corrosion products formed, but now akaganeite is present in Isla Naval after the first year. In Cojimar, magnetite is the major constituent in the corrosion products formed.

In general terms corrosion potentials registered during electrochemical measurements present noble potentials either from the start or at the end of the experiments. LPR values tend to increase as a function of time of exposure of the steel samples to the atmosphere. The trend is similar to the cumulative weight loss observed under atmospheric conditions as observed [11, 16, 20]. This behavior suggests a growth of the corrosion products formed over the surface, diminishing the corrosion activity and protecting the metal surface. Exceptions to this behavior include: Guayaquil, Chiriqui, Bauta, Ipatinga, Arenal, Panama, Ciq, Veraguas, Rio de Janeiro, Colon, Cubatao, Isla Naval and Cojimar.

Under the electrochemical test conditions considered, potentials above -250 mV are indicative of passivation or more oxide film protective conditions and below that, less protective or more active conditions [21]. The noblest potentials were associated with the formation of more stable and protective oxide films, which were obtained under similar climatic and/or environmental conditions. However, under these circumstances more localized attack can take place [11, 16].

The LPR values for the test samples were associated with overall corrosion and ascribed to the increasing amounts of chlorides and/or sulfur dioxide in the atmosphere. For example, S. L. Potosí contain some sulfur dioxide ($18.9 \text{ mg/m}^2\cdot\text{d}$); Camet contain relatively large amounts of chlorides ($55.1 \text{ mg/m}^2\cdot\text{d}$) and Panama contains both ($9.8 \text{ mg/m}^2\cdot\text{d}$ for Cl and $21.7 \text{ mg/m}^2\cdot\text{d}$ for SO_2). The exceptions are Iguazu and San Juan where very little pollution is present ($<3 \text{ mg/m}^2\cdot\text{d}$ for Cl and $<10 \text{ mg/m}^2\cdot\text{d}$ for SO_2) [10]. Pollutants present in the atmosphere are reflected in the large amounts of soluble salts accumulated in the corrosion products if they are not washed off by rain (see for example S. L. Potosi, Camet, Isla Naval and Cojimar; Table 3).

Pollutants in the atmosphere affect the formation, morphology, stability and protective properties of corrosion products over steel. After one year of atmospheric exposure, steel specimens presenting fewer corrosion products of lepidocrocite (rural S_0P_0 atmospheres, except Cuernavaca and Cotove) present active potentials and very low LPR values which are indicative of overall corrosion activity. The presence of SO_2 in the atmosphere, benefits the protective characteristics of the film oxides [22]. More noble potentials and higher LPR values registered suggest a decreasing corrosion activity due to the growth of more stable corrosion products over the surface in some rural, urban and industrial atmosphere samples (see for example Cuernavaca, Mexico and Sao Paulo; Table 2).

On the contrary, chlorides appears to affect the stability of oxides and provide less protective characteristics in mixed marine atmospheres. The oxides formed are porous, cracked and prone to exfoliation. Particularly at the beginning of layer formation, platelets or scales appear frequently [22, 23]. This is commonly associated with the presence of magnetite in the rust formed in marine atmospheres under high temperature and humid conditions. (see Acapulco, Arenal, Cubatao and Cojimar in Table 3). Variable results were obtained for this condition and associated to the film characteristics. According to the electrochemical results obtained for this chloride condition, the long exposure periods and/or the presence of certain amounts of SO_2 in the atmosphere, improves the stability and protective characteristics of oxides diminishing the overall corrosion activity.

For localized corrosion to occur, a stable homogeneous and protective oxide is needed. The oxide can be damaged by cracking and spalling exposing bare metal transiently, and corrosion can take place as "hot spots" in local areas. If aggressive ions such as chlorides are present, then this localized corrosion will take place in the form of pitting. Alternatively the accumulation of salts underneath the corrosion products layers will promote localized under-deposit attack, decreasing the higher LPR values (Bauta, Ciq and Veraguas) [18]. In coastal-urban atmosphere, high chloride and SO_2 produce fragile, fractured and defective film oxides with poor protective characteristics, as suggested by the electrochemical results obtained for Isla Naval and Cojimar (noble potentials and low LPR).

Another important factor associated to the electrochemical measurements obtained, is the appearance of goethite, specially during the first year of exposure as component of the corrosion products formed, improving and influencing the long term behavior of the protective properties of film oxides. The rust layer develops more readily in sulfur containing atmospheres. Also, crystalline constituents predominate and goethite plays a prominent role in protecting the metal. In addition, a lepidocrocite sublayer is initially formed that reaches a limiting thickness dependent on the particular atmosphere which remains constant while goethite is being formed [17, 22]. This could also explain the electrochemical results obtained for: Cuernavaca, Cotove, S. L. Potosi, Sao Paulo, Caratinga, Chiriqui, Ciq and Cubatao samples.

Electrochemical Noise

The electrochemical noise measurements obtained complement and support the electrochemical results already presented. Figures 2 to 6 illustrate the differences in the noise response and contain EPN time records and corresponding spectral density analysis obtained for samples exposed to different periods and to different atmospheres.

Figure 2 corresponds to a steel plate exposed for one year to a rural atmosphere (Cuernavaca). The EPN response consists basically of a low amplitude, high frequency noise signal superimposed to a low frequency oscillation obtained. This is reflected in its almost flat spectral density plot PSD (independent of frequency) associated to a white noise signal, reflecting general corrosion. The corrosion potential was -554 mV and the standard deviation 1.89 mV.

Figure 3 corresponds to a steel plate exposed for three years to the same atmosphere. The EPN response is a high amplitude, low frequency noise signal with little high frequency components superimposed, as can be seen in the EPN time record. The PSD for these data has a steep smooth slope, indicative of stable oxide film conditions as observed [11]. The corrosion potential was -96 mV and the standard deviation 1.98 mV.

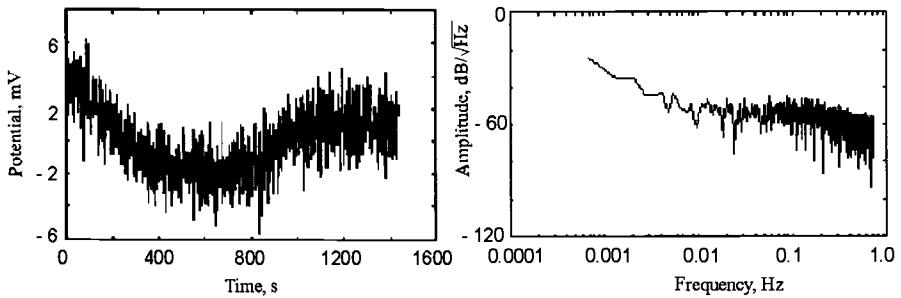


Figure 2- EPN and PSD for samples exposed one year in a rural atmosphere

The low frequency components are associated with the presence of oxides or corrosion products over the surface, and the high frequency components are related to the stability of the oxide film in the passive or protective state [22]. The noise response for a

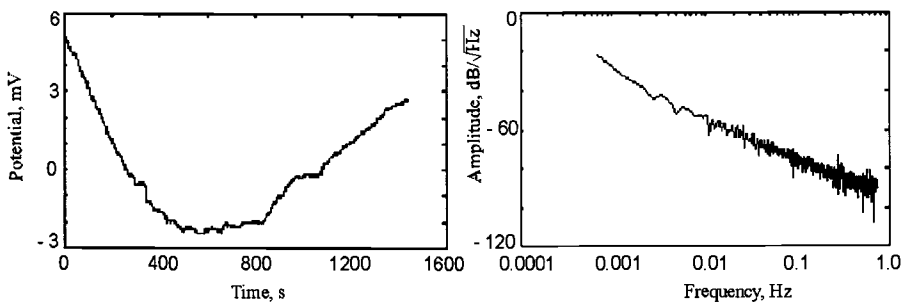


Figure 3- EPN and PSD for samples exposed three years in a rural atmosphere

steel sample exposed for two years to an urban atmosphere (San Luis Potosí) is presented in Fig. 4. The EPN response is similar to the previous case (rural, three years), but presenting an increase in the noise response specially in the high frequency components, reflected in the PSD plot (above 10-mHz). As the corrosion products or oxide film becomes more porous or heterogeneous when formed in a polluted atmosphere, more active

sites will be present for cracks to occur, which are responsible for the observed increase [16, 19, 23]. The spectra are less smooth and more high frequency components of variable intensity (spikes) appear in the spectrum (San Luis Potosí). The corrosion potential and standard deviation registered were -407 and 0.54 mV, respectively.

Figure 5 presents the EPN time records and associated spectra for a 2-year marine (Acapulco) exposure steel plate sample. The noise characteristics observed for 2 years are low frequency oscillations with some sudden potential drops accompanied with exponential recovery transients related to film rupture or localized attack [24]. The PSD

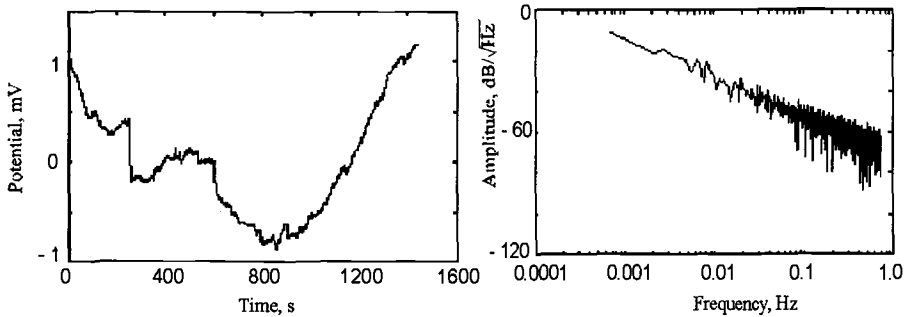


Figure 4- EPN and PSD for samples exposed two years in urban atmosphere

presents a $1/f$ behavior [25]. Nevertheless the attack appears to be of low intensity since the standard deviation is low (0.58 mV) with a corrosion potential of 116 mV. For the 3-year marine exposure, the potential noise characteristics show an increasing transient behavior of high amplitude, high frequency components related to under-deposit localized pitting attack as observed and reflected in the SDP (Fig. 6). As the attack becomes

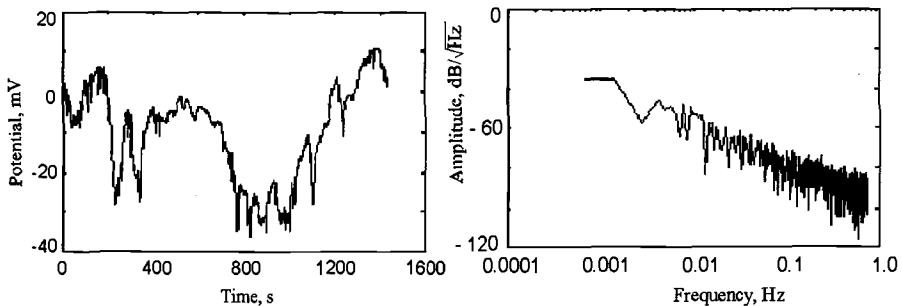


Figure 5- EPN and PSD for samples exposed two years in marine atmosphere

more intense, the spectra thus obtained resemble a white noise spectral (that is, independent of frequency). The standard deviation (1.01 mV) indicative of a more intensive localized attack, increases compared to the previous one (marine, 2-years) with a corrosion potential registered of -125 mV [14, 16].

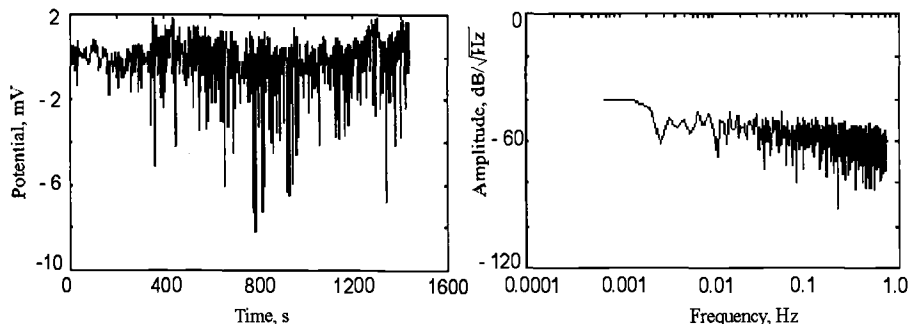


Figure 6- EPN and PSD for samples exposed three years in marine atmosphere

Conclusions

The electrochemical measurements reflect the protective characteristics of steel corrosion products developed during atmospheric corrosion exposure. In general, for rural atmospheres low protection (less than $10 \text{ k}\Omega\cdot\text{cm}^2$) was observed for oxides developed during the first year of exposure improving its characteristics with the time of exposure.

For SO_2 polluted atmospheres, intermediate protection (between 10 and $20 \text{ k}\Omega\cdot\text{cm}^2$) was achieved during the first year improving to good protection (more than $20 \text{ k}\Omega\cdot\text{cm}^2$) conditions with the time of exposure. For chloride and mixed atmospheres poor to intermediate protection conditions were observed improving with the presence of SO_2 in the atmosphere. Finally in highly polluted mixed atmospheres, low protective conditions were found according to the electrochemical measurements obtained.

Acknowledgments

Co-authors of this work for the MICAT Group include: B. Rosales (Argentina), L. Uller and M. Marrocos (Brasil), G. Joseph (Chile), A. Valencia (Colombia), J. F. Alvarez (Costa Rica), A. Cabezas (Cuba), J. Peña (Ecuador), A. de Bosquez (Panama), J. Genesca (Mexico), G. Salas (Peru), E. Almeida and M. Ferreira (Portugal), M. Morcillo (Spain), S. Rivero (Uruguay), and M. R. Prato (Venezuela). The authors wish to express their gratitude to the Programa Iberoamericano de Ciencia y Tecnologia (CYTED) for financial support granted to the research project and to all involved in this task, without whose assistance it would not have been possible to undertake this ambitious project.

To *Mariquita* in loving memory.

References

- [1] Granese, S. L., and Rosales, B. M., "Corrosion Atmosferica de Zinc," *Revista Iberoamericana de Corrosion y Proteccion*, Vol. 17, 1986, p.197.
- [2] Dutra, A. C., and Viana, R. O., "Atmospheric Corrosion Testing in Brazil," *Atmospheric Corrosion*, Ailor, W.H., Ed., John Wiley, New York, 1982, p.755.

- [3] Corvo, F., "Atmospheric Corrosion of Steel in Humid Tropical Climate. Influence of Pollution, Humidity, Temperature, Rainfall and Sun Radiation," *Corrosion*, Vol. 40, No. 4, 1984, p.251.
- [4] Southwell, C.R., and Bultman, J.D., "Corrosion of Metals in Tropical Environments," *Atmospheric Corrosion*, Ailor, W.H., Ed., John Wiley, New York, 1982, p.943.
- [5] Uller L., and Morcillo, M., "The Setting up of an Iberoamerican Map of Atmospheric Corrosión," *Proceedings of the 11th International Corrosion Congress*, Vol. 5, AIM, Florence, 1990, p.2.35.
- [6] Knotkova, D., and Vrobel, L., "ISOCORRAG: The International Testing Program within ISO/TC 156/WG4," *Proceedings of the 11th International Corrosion Congress*, Vol. 5, AIM, Florence, 1990, p.5.581.
- [7] Kucera, V., Coote, A., Henriksen, J., Knotkova, D., Leygraf, C., and Reinhardt, U., "Effects of Acidifying Pollutants on Materials Including Historic and Cultural Monuments," *Proceedings of the 11th International Corrosion Congress*, Vol. 5, AIM, Florence, 1990, p.2.433.
- [8] Tomashov, N. D., *Theory of Corrosion and Protection of Metals*, Ed., Mac Millan Co., New York, 1966, p.367.
- [9] Koppen, W., "Das Geographische System der Klimate," *Handbuch der Klimatologie*, 3, Gebruder, Berlin, 1936.
- [10] Morcillo, M., "Atmospheric Corrosion in Ibero-America: the MICAT Project." *Atmospheric Corrosion, ASTM STP 1239*, Kirk, W. W., and Lawson, H. H., Eds., American Society for Testing and Materials, Philadelphia, 1995. p. 257.
- [11] Almeida, E., Mariaca, L., Rodríguez, A., Uruchurtu, J., Veloz, M. A., "Characterization of Prerusted Steels in Some Iberoamerican Atmospheres by Electrochemical Potential Noise Measurements," *Electrochemical Noise Measurements for Corrosion Applications, ASTM STP 1277*, Kearns, J. R., Scully, J. R., Roberge, P. R., Reichert, D. L., and Dawson, J. L., Eds., American Society for Testing and Materials, Philadelphia, 1996. p. 411.
- [12] Hladky, K., and Dawson, J.L., "The Measurement of Corrosion Using Electrochemical 1/f Noise," *Corrosion Science*, Vol.22, 1982, p. 231.
- [13] Hashimoto, M., Miyajima, S., and Murata, T., "A Stochastic Analysis of Potential Fluctuations During Passive Film Breakdown and Repair on Iron," *Corrosion Science*, Vol. 33, 1992, p. 885.
- [14] Uruchurtu, J., "Electrochemical Investigations of the Activation Mechanism of Aluminium," *Corrosion*, Vol.47, No.6, 1991, p. 472.
- [15] Kihira, H., Ito, S., Murata, T., "Electrochemical Impedance Spectroscopy of Oxide Covered Steels," *Proceedings 10th International Congress in Metallic Corrosion*, 1987, p. 4023.

- [16] *Corrosion y Proteccion de Metales en las Atmosferas de Iberoamerica, Parte I: Mapas de Iberoamerica de Corrosividad Atmosferica*. (Eds. M., Morcillo, E., Almeida, B., Rosales, J., Uruchurtu, and M., Marrocos, CYTED, Madrid, 1999.
- [17] Miranda, L. R. M., "Les Aspects Electrochimiques de la Corrosion Atmospherique des Aciers Patinables," *Ph. D. Thesis*, Universite Libre de Bruxelles, 1974.
- [18] Slarska-Smialoska, Z., "The Pitting Corrosion of Iron in Sodium Sulphate," *Corrosion Science*, Vol. 18, 1978, p. 97.
- [19] Granese, S. L., Rosales, B. M., Ayllon, E. S., Varela, F. E., Gervasi, C. A., and Vilche, J. R., "Characterization of the Atmospheric Corrosion Products," *Proceedings of the 1st Pan American Congress on Corrosion and Protection*, Mar del Plata, 1992.
- [20] Uruchurtu- Chavarin, J., "Evaluacion Electroquimica de Oxidos formados en Diferentes Atmosferas," *V Congreso Ibero-Americano de Corrosión y Proteccion*, Tenerife, 1995, p. 43.
- [21] Pourbaix, M., *Atlas of Electrochemical Equilibria in Aqueous Solutions*, NACE, Houston, 1974.
- [22] Arroyave, C., Morcillo, M., "Atmospheric Corrosion Products in Iron and Steels," *Research Trends*, Vol. 2., 1997, p. 1.
- [23] Ayllon, E. S., Granese, S. L., Bonazzola, C., and Rosales, B., "Corrosion Atmosferica de Fe y Zn en Ambientes Poluidos," *Revista Iberoamericana de Corrosion y Proteccion*, Vol. XVII, 3, 1986, p. 205.
- [24] Uruchurtu, J., "Transient Behavior of Pure Aluminium During Noise Analysis," NACE Conference in Localized Corrosion, *NACE-9*, Orlando, 1987, p. 141.
- [25] Uruchurtu-Chavarin, J., Malo, J. M., "Electrochemical Noise as a Powerful Electrochemical Technique for Corrosion Studies," *Research Trends*, Vol. 2., 1997, p. 49.

George A. King¹ and Peter Norberg²

A Methodology for Quantifying the Atmospheric Corrosion Performance of Fabricated Metal Products in Marine Environments

Reference: King, G. A. and Norberg, P., “A Methodology for Quantifying the Atmospheric Corrosion Performance of Fabricated Metal Products in Marine Environments,” *Marine Corrosion in Tropical Environments, ASTM STP 1399*, S. W. Dean, G. Hernandez-Duque Delgadillo, and J. B. Bushman, Eds., American Society for Testing and Materials, West Conshohocken, PA, 2000.

Abstract: In Australia a long-term project is studying the marine atmospheric corrosion performance of several metals and alloys, and a range of generic classes of coatings and finishes (metallic and organic) on steel and aluminum. Specimens have been exposed for over nine years at three marine sites, both in the open and under a specially designed glass shelter which has greatly accelerated deterioration. The sheet product test pieces include a range of features designed to simulate the types of distress introduced during manufacture and building, and at which corrosion defects initially manifest. A methodology is described for the development of quantitative performance indices for these formed specimens. The general philosophy involves using the collected data to determine appropriate weighting to different types of defects on features, or to the relative contribution of different features to overall defect indices and in turn their relative contribution to a total performance index. A rigorous mathematical procedure was followed to calculate defect indices and total performance indices for all products. Some results for the two-year specimens are discussed.

Keywords: atmospheric corrosion, marine environment, prepainted coated product, coil coating, durability assessment, performance indices, semi-sheltered exposure

Nomenclature

Types of corrosion defect on coated metal products:

WCP	White Corrosion Products
RR	Red Rusting
BL	Blistering
UC	Undercutting

Features in formed specimens – also used for the ratings at those features in equations with subscripts min and max representing the minimum and maximum values:

FS	Flat Surface
ϕt	Flat bend in product through 180 degrees
3t	Bend in product using mandrel of 3× thickness
5t	Bend in product using mandrel of 5× thickness
3mm	Conical bend of 3 mm diameter
20mm	Conical bend of 20 mm diameter

¹Principal Research Scientist, CSIRO BCE, PO Box 56, Highett, Victoria 3190, Australia.

²Royal Institute of Technology, Centre for Built Environment, PO Box 88, SE-801 02 Gävle, Sweden.

ED	Drawn Erichsen Domes (to British Standard 3900: Part E4 Cupping Test)
SC	Scribes
TCE	Top Cut Edge of specimen
BCE	Bottom Cut Edge of specimen
VCE	Vertical Cut Edge of cover plate adjacent to main panel
CH	Circular Hole

Defect indices for features of specimens, viz. a measure of the defect on that specimen feature:

FSI _{WCP/RR}	Flat Surface Index for White Corrosion Product and Red Rusting
BI _{WCP}	Bends Index for White Corrosion Product
BI _{RR}	Bends Index for Red Rusting
CEI _{WCP/RR}	Cut Edge/Scribe Index for White Corrosion Product and Red Rusting
FSI _{BL}	Flat Surface Index for Blistering
BI _{BL}	Bends Index for Blistering

Overall defect indices and product total performance index:

UCI _{TOT}	Total Undercutting Index
WCPI _{TOT}	Total White Corrosion Product Index
RRI _{TOT}	Total Red Rusting Index
BLI _{TOT}	Total Blistering Index
TPI	Total Performance Index

Introduction

Prefinished sheet metal products in roll formed profiles are very widely used in the building and construction industries throughout the world. The majority share of the market is occupied by steel, coated with zinc, 5% aluminum-zinc (Al-Zn), or 55% Al-Zn, either bare or with additional coil painted finishes; however, prepainted aluminum is also extensively used. In 1997 BHP produced 475 000 tonnes of 55% Al-Zn coated steel for the Australian domestic market, with nearly 60% coil painted [1]. Most Australian construction is close to the coast, and the marine environment represents by far the principal corrosion hazard to all metal products. The need for information on the comparative performance of these generic classes of materials and finishes in part led to the initiation of a long-term exposure program in 1991 with international funding. The original joint sponsors of the project were the International Lead Zinc Research Organisation Inc. (ILZRO), BHP Research (Coated Products Division – Research & Technology) and Comalco Aluminium Ltd. ILZRO provided assistance in sourcing coated sheet products from the USA, Japan and Germany, and supplies of zinc (USA) and 5% Al-Zn (Japan) for corrosion rate measurements. BHP provided coated sheet products from Australia and New Zealand, and supplies of 55% Al-Zn for corrosion rate measurements. Comalco provided coated aluminum sheet products from the USA, and an extrusion in a range of finishes from Australia.

The rationale behind the program, including materials and product selection, the specimen design, and the characteristics of the three exposure sites which also feature a novel semi-sheltered exposure system, has been described in detail previously [2]. Twenty commercial sheet products (of four generic types – aluminum, stainless steel with organic topcoat, metallic-coated steel with organic topcoat, and metallic-only-

coated steel) were exposed (with subsequent appraisal to the present methodology) in a program designed to run for 10 years. Only the two-year specimens had been recovered at the time of this evaluation. To give an indication of the very great range in exposure conditions from which the data for this study has been obtained, the levels of chloride deposition (according to ISO 9225 Corrosion of Metals and Alloys – Corrosivity of Atmospheres – Measurement of Pollution) and zinc corrosion rates are given in Table 1. The figures represent a range in severity of conditions by up to a factor of about 17.

The sheltering system has been found to meet its designed purpose as an accelerated test, and has induced extreme deterioration of most metals and coatings compared to those in open exposure, at the severe and moderate marine sites. The test pieces include a range of features designed to simulate the types of distress introduced into sheet products during manufacture and building, and at which corrosion defects initially manifest. This paper describes in detail the progressive development of a methodology for quantifying the atmospheric corrosion performance of the specimens, taking account of the features in the specimens and the different defect types.

The vast majority of studies describing the exposure and appraisal of coated sheet metal products have used simple specimens, generally with a flat surface only and possible scribing. The issue of incorporating a range of features into test specimens and evaluating the corrosion performance at these, has not been addressed adequately by standards organizations worldwide. The ASTM Test Method for Evaluation of Painted or Coated Specimens Subjected to Corrosive Environments (D 1654) describes the scribing of specimens in detail, but leaves the issue of assessment at deformation features and cut edges to be agreed upon between the producer and user. The US National Coil Coaters Association Technical Bulletin No. III-9, Guidelines for Conducting Exterior Exposure Tests, incorporates a reverse drawn dome, scribe and 180° bend. The Australian/New Zealand Standard on Performance Requirements of Prefinished/Prepainted Sheet Metal Products for Interior/Exterior Building Applications (AS/NZS 2728:1997) describes a flat panel with optional shaping (3t and 5t bends) and scribing. However, no requirements for the durability of the organic film at the bends of shaped panels are specified.

Nonetheless, attempts have been made in a few studies of the durability performance of coil-coated materials to account for the influence of various features and defects, and calculate performance indices in an objective way. Work in The Netherlands used panels to the ECCA (European Coil Coaters Association) design and converted all estimates of defects to a percentage of the total area or edge length of the panel [3].

By far the most comprehensive attempt to date was a major study carried out about 20 years ago by Johnson and Marsh of the British Steel Corporation [4]. They

Table 1 – Chloride Deposition Levels and Zinc Corrosion Rates for Exposure Sites

		Chloride Deposition (mg/m ² .d)	One-year Zinc Corrosion Rate (µm/y)
Severe marine	– Open	99	6.2
	– Sheltered	70	15.2
Moderate marine/rural	– Open	33	1.9
	– Sheltered	26	3.9
Mild marine/urban	– Open	6	1.0
	– Sheltered	5	0.9

emphasized two points: "firstly that conventional testing took no account of design features, and published methods for assessing defects from weathering of coatings (ISO and ASTM) are based on the assumption that defects occur uniformly across a surface." They devised formed panel specimens with variable radius bends, cut edges, overlaps, scribing, an Erichsen Dome and fasteners, and also produced "box-type" specimens using these panels which enabled the study of sheltering and orientation. Corrosion products, blistering and flaking were assessed according to the ISO standards, but apparently undercutting from scribes and cut edges was not. Numerical values were assigned to the severity and extent of defects, and these were multiplied by weighting factors for both design feature and defect type. The weighted values were summed to produce a performance index. A deficiency in this procedure though, and one acknowledged by the authors, is that the weighting factors were chosen subjectively. One aim of the current methodology was to attempt to overcome this aspect of determining an objective quantitative measure of performance. The new approach uses the actual outcome of the defect assessments for the various features, as the basis for determining their relative severity in an objective way. This procedure is assumed to be justified by the fact that the present study comprises a very wide range of products, conditions and defect ratings.

Development of a New Methodology for Quantifying Atmospheric Corrosion Performance of Coated Products

The procedure followed involves four stages of calculations:

1. Allocation of numerical ratings to defects on all features of specimens, and generation of a database.
2. Determination of the relative contributions of various individual features within feature types (bends, cut edges) for each of the defect indices.
3. Determination of the relative contributions of the feature type indices to overall defect indices for a product.
4. Determination of the relative contributions of the total defect indices to a total performance index for a product by generic type.

Defects and Features of "Formed" Specimens Used for Assessment

Full details of the formed (bent) specimens have been published previously [2]. A schematic drawing of the specimen showing its features is reproduced here in Figure 1. The product codes from Table 2 of that paper are used here for sake of brevity. The metallic/organic-coated products (I1, I4–I9, B5–B8) were assessed with respect to four types of defect: White Corrosion Products (WCP), Red Rusting (RR), Blistering (BL) and Undercutting (UC). The metallic-only-coated products (I2, I3, B1) were assessed for White Corrosion Products and Red Rusting only. Product B4, fluorocarbon-coated 304 grade stainless steel, was not assessed for White Corrosion Products, and the aluminum products C1–C5 were not assessed for Red Rusting. The numbers of the different types of specimen and the defect assessments performed on them are summarized in Table 2. Two independent (i.e. two observers) assessments were made for appropriate defect/feature combinations for all specimens and the average calculated and used in the mathematical treatment. Assessments of the defect types were made on the specimen features as indicated in Table 3. For the Scribes (SC) and the Erichsen Domes (ED), the worst rating applicable was chosen as representative of the feature.

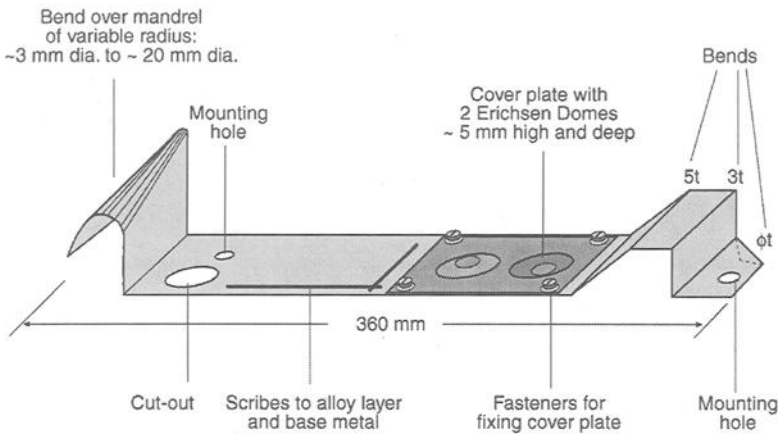


Figure 1 – Schematic of “Formed” Specimen

Table 2 – Numers of Specimens of Different Generic Types and Defect Assessments Performed on Them

Defect Type	Generic Type				Total Assessments for Defect Type
	Metallic-coated Steel + Organic Topcoat	Metallic-only Coated Steel	Stainless Steel + Organic Topcoat	Stainless Steel + Organic Topcoat	
WCP	66	18		30	114
RR	66	18	6		90
BL	66		6	30	102
UC	66		6	30	102

Table 3 – Features of “Formed” Specimens Assessed for Different Defect Types

	White Corrosion Products Red Rusting	Blistering	Undercutting
Flat Surface	FS	FS	
Bends – zero t bend	φt		
– 3 t bend	3t	3t	
– 5 t bend	5t	5t	
– 3 mm diameter conical bend	3mm	3mm	
– 20 mm diameter conical bend	20mm	20mm	
Erichsen Domes	ED	ED	
Scribes	SC		SC
Top Cut Edge	TCE		TCE
Bottom Cut Edge	BCE		BCE
Vertical Cut Edge of cover plate adjacent to main panel	VCE		VCE
Circular Hole			CH

Criteria for Allocation of Numerical Ratings to Defects

A number of systems exist for rating defects on painted metal products. One is the ISO Paints and Varnishes – Evaluation of Degradation of Paint Coatings – Designation of Intensity, Quantity and Size of Common Types of Defect – Part 1: General Principles and Rating Schemes (ISO 4628/1), Part 2: Designation of Degree of Blistering (ISO 4628/2) and Part 3: Designation of Degree of Rusting (ISO 4628/3). ISO 4628/1 “establishes a general system for designating the intensity, quantity, and size of common types of defects in paint coatings...” It adopts a uniform convention for “designating the intensity and quantity of defects by means of ratings on a numerical scale from 0 to 5, 0 denoting no defects and 5 denoting defects so severe that further discrimination has no practical meaning.” The ratings from 1 to 4 “are so defined that they give an optimal discrimination over the whole range of the scale.” Three tables give rating schemes for intensity of uniform deterioration, quantity of scattered defects and size of defects. The numerical ratings developed for this study have adhered to the 5-point ISO principles. As a general rule, the means of the two assessments referred to above with a decimal of 0.5 were rounded up to the next integer.

White Corrosion Products – There being no existing international standard for assessment of the extent of White Corrosion Products, an “in-house” rating system used by BHP Coated Products (Port Kembla, Australia) was adopted. This is in exact accord with Table 1 of ISO 4628/1. The rating number is followed by the description of the extent of the defect: 0 zero, 1 very slight, 2 slight, 3 moderate, 4 considerable, 5 severe.

Red Rusting – ISO 4628/3 has pictorial standards for designating the degree of rusting of paint coatings (combination of rust broken through the coating and apparent under-rust). The area rusted in percent for each rating is as follows: 0 = 0%, 1 = 0.05%, 2 = 0.5%, 3 = 1%, 4 = 8%, 5 = 40–50%. The ASTM Test Method for Evaluating Degree of Rusting on Painted Steel Surfaces (D610–95) has an 11-point scale for degree of rusting which moves in the opposite direction to ISO 4628/3 and allows for greater discrimination also. ISO 4628/3 presumably is defining the percent area rusted as being “up to” that figure, e.g., rating 1 is for no rust up to 0.05% rusted area. Rating 5 would then be from 8% to 40–50%. This does not really enable distinction between say 10% and 50% rust. A slightly modified scale is developed here based principally on ISO 4628/3 but taking account of D610. The term “trace” in an assessment is designated a percent area of 0.05, and is given a rating of 1. Each independent assessment provided a subjective percentage area affected by red rusting (0–100%). In general, the average of these figures was calculated and converted to a 5-point rating as follows: Red Rusting index followed by percentage area of rusting on specimens 0 = 0%, 1 = >0 ≤0.05%, 2 = >0.05 ≤1%, 3 = >1 ≤8%, 4 = >8 ≤40%, 5 = >40%.

Blistering – Blistering was assessed according to the Australian Standard AS 1580.481.1.9–1991 Paints and Related Materials – Methods of Test. Method 481.1.9: Coatings – Exposed to Weathering – Degree of Blistering. The pictorial standards for blister size and density are the same as for ASTM Test Method for Evaluating Degree of Blistering of Paints (D714–87), but in the Australian Standard the numerical rating has been changed to a 5-point scale in accordance with ISO 4628/2. Blistering is appraised in terms of density and size aSb, where a is the index for density and b is the index for size. A single numerical index is required to enable mathematical calculations (statistical analysis etc.) of the data. This was achieved as follows. The averages of the independent

ratings for density and size were evaluated separately and rounded to give a representative rating. These numbers were multiplied together, the square root was taken, and the resulting number was rounded to the nearest integer. Example as follows: rating by operator A is 3S4, by operator B is 4S3. This gives an average rating of 3.5S3.5 which is rounded to 4S4. The average indices for size and density are multiplied together to give 16, the square root is 4; so the blistering index for that feature is 4.

Undercutting – ISO 4628 does not specify a rating scale for Undercutting. However, AS 1580.481.3–1992 Paints and Related Materials – Methods of Test: Method 481.3: Coatings – Exposed to Weathering – Degree of Corrosion of Coated Metal Substrates, has a rating scale for assessment of representative mean creepage of underfilm corrosion from a scribed line and panel edge. This scale is in accord with the ISO principle and has been adopted here for assessment of undercutting. This was assessed as an actual range of depths (minimum and maximum) in millimeters by two independent operators. The arithmetic averages of the two minima and maxima were determined and then converted to ratings (min. and max.) again on the 5-point scale from the Australian Standard as follows: Undercutting rating followed by depth (mm), 0 = 0, 1 = >0 ≤1, 2 = >1 ≤3, 3 = >3 ≤7, 4 = >7 ≤13, 5 = >13.

Database of Numerical Ratings – Based on the above criteria, all specimens recovered after exposure for 2 years 29 days were assessed and the average numerical ratings for each defect on the chosen features were calculated for each of the product/exposure condition combinations (20 products × 3 sites × open/sheltered = 120). The results were entered into an extensive spreadsheet. Table 4 shows part of this spreadsheet, the raw data for six of these combinations, as an example. Three products with similar paint topcoats (polyester or silicon-modified polyester (SMP)) are chosen (I1, B5, C4 – see Ref. 2). They had all been exposed at a severe marine site for 2 years in the open and under the special shelter (1, 2, O and S respectively as the last three characters in the Specimen ID).

Criteria for Determining the Relative Contribution of Each Individual Feature (Within Feature Type) to the Defect Indices

The philosophy on which the development of performance indices is based depends on assigning an appropriate weighting to different types of defects on features, or the relative contribution of different features to an overall defect index. The “severity” of features is reflected in the defect ratings, which have themselves accordingly been used to derive weighting coefficients. A procedure of inverting and normalizing has been adopted to determine appropriate coefficients for each feature on the basis of their severity. A severe feature is more likely to show a defect and its coefficient should accordingly be smaller. The severity of features is reflected in the database (spreadsheet) of all of the ratings (only a part of which is shown in Table 4 here) which has itself accordingly been used to derive weighting coefficients. The mean values of the defect ratings for each of the “features” of the formed specimens are given in Table 5. These mean values have been calculated from all available data for the 120 product/exposure condition combinations.

Non-zero ratings on all or most features were obtained from about 53% of specimens for White Corrosion Products, 13% for Red Rusting, 49% for Blistering and 69% for Undercutting.

Table 4 – Numerical Ratings for Defects on Selected Features of Formed Specimens (This Example is for Three Products with a Polyester or SMP Topcoat Exposed Both in the Open and Sheltered for a Period of Two Years at a Severe Marine Site)

		Specimen ID	I1120	I112S	B5120	B512S	C4120	C412S	
		Base Metal	Steel	Steel	Steel	Steel	Al	Al	
		Alloy Coating	5% Al-Zn	5% Al-Zn	55% Al-Zn	55% Al-Zn	–	–	
		Organic Coating	20 µm SMP	20 µm SMP	20 µm Polyester	20 µm Polyester	20 µm Polyester	20 µm Polyester	
Defect Types	White Corrosion Products WCP	Flat Surface	2	3	0	0	0	0	
		φt bend	5	5	2	5			
		3t bend	2	5	1	2	1	3	
		5t bend	1	5	1	2	0	0	
		Conical 3 mm	1	4	1	2	0	0	
		Conical 20 mm	2	4	1	2	0	2	
		Erichsen Domes	3	5	1	3	0	0	
		Scribes	3	5	1	4	0	3	
		Top Cut Edge	3	5	2	4	3	3	
		Bottom Cut Edge	3	5	3	4	3	3	
		Cover plate/main panel, Vertical Cut Edge	3	5	2	4	2	3	
		Red Rusting RR	Flat Surface	0	0	0	0		
	φt bend		0	5	0	0			
	3t bend		0	0	0	0			
	5t bend		0	3	0	0			
	Conical 3 mm		0	0	0	0			
	Conical 20 mm		0	0	0	0			
	Erichsen Domes		0	3	0	0			
	Scribes		0	5	0	0			
	Top Cut Edge		0	5	0	0			
	Bottom Cut Edge		0	5	1	3			
	Cover plate/main panel, Vertical Cut Edge	0	5	0	2				
	Blistering BL	Rating R	Flat Surface	1S1	2S4	1S2	0	0	1S1
			3t bend	5S1	4S4	0	4S2	1S1	4S3
			5t bend	4S1	3S3	0	4S2	0	0
			Conical 3 mm	2S1	4S3	0	3S2	0	0
			Conical 20 mm	3S1	4S4	0	3S2	0	1S2
			Erichsen Domes	5S1	3S4	2S2	4S2	0	0
		Index I	Flat Surface	1	3	1	0	0	1
			3t bend	2	4	0	3	1	3
			5t bend	2	3	0	3	0	0
			Conical 3 mm	1	3	0	2	0	0
			Conical 20 mm	2	4	0	2	0	1
			Erichsen Domes	2	3	2	3	0	0
	Undercutting UC	Minimum	Top Cut Edge	0	2	0	1	0	0
			Bottom Cut Edge	0	3	0	2	0	0
Cover plate/main panel, Vertical Cut Edge			0	3	0	3	0	0	
Circular Hole			1	2	0	3	0	0	
Scribes			0	2	0	1	0	0	
Maximum		Top Cut Edge	2	3	2	3	1	1	
		Bottom Cut Edge	2	4	3	4	1	1	
		Cover plate/main panel, Vertical Cut Edge	2	5	3	5	1	1	
		Circular Hole	2	3	3	3	1	1	
		Scribes	1	3	2	3	1	2	

Table 5 – Mean Values of Defect Ratings for Features of Formed Specimens (for all Available Data for 120 Product/Exposure Condition Combinations)

Feature	Defect Type				
	WCP	RR	BL	Min. UC	Max. UC
Flat Surface	0.84	0.18	0.55		
φt bend	1.72	0.53			
3t bend	1.27	0.20	1.06		
5t bend	0.89	0.14	0.86		
Conical 3 mm bend	0.89	0.08	0.76		
Conical 20 mm bend	0.83	0.10	0.75		
Erichsen Domes	1.04	0.26	0.97		
Scribes	1.88	0.70		0.30	1.16
Top Cut Edge	2.17	1.18		0.28	1.2
Bottom Cut Edge	2.43	1.53		0.47	1.62
Vertical Cut Edge	2.18	1.40		0.32	1.34
Circular Hole				0.32	1.32

White Corrosion Product/Red Rusting – For White Corrosion Products and Red Rusting the features were considered in three groups: the Flat Surface, the deformed areas (viz. Bends and Erichsen Domes), and the Cut Edges and Scribes (edges of coatings exposed). For each group it was considered that the Feature Index should have a potential maximum value of 100. This criterion determines the value that the sum of the coefficients must have.

(a) Flat Surface Index – For the Flat Surface the maximum value of a rating is 5, there is only one coefficient, and the relationship to develop the Index for White Corrosion Product and Red Rusting is:

$$FSI_{WCP/RR} = 20 * \text{Flat Surface Rating (FS)} \quad (1)$$

(b) Bends Index – For the deformed areas the coefficients for White Corrosion Product to describe the relative importance of each of the bends and the Erichsen Domes were derived by normalizing the mean values of the ratings to the most severe feature (φt bend) as follows. The mean value of the WCP rating for the φt, 3t, 5t, 3mm and 20mm bends and for the Erichsen Domes is divided into 1.72 (the value for the φt bend itself). The sum of the coefficients must add up to 20. This is achieved by multiplying by 2 and then rounding. The procedure is shown in Table 6.

Table 6 – Normalizing Rating Values to Determine WCP Feature Coefficients for Deformed Areas

Feature	Mean Value of WCP Rating	Divide Mean Value of WCP Rating into 1.72	Multiply by 2	Round
φ t bend	1.72	1	2	2
3 t bend	1.27	1.35	2.7	3
5 t bend	0.89	1.92	3.84	4
Conical 3 mm bend	0.89	1.94	3.87	4
Conical 20 mm bend	0.83	2.06	4.12	4
Erichsen Domes	1.04	1.66	3.32	3

The relationship to develop the Bends Index for White Corrosion Product is therefore shown below with the abbreviated parameters standing for that rating, i.e., ϕt is ϕt Rating:

$$BI_{WCP} = (2 * \phi t) + (3 * 3t) + (4 * 5t) + (4 * 3mm) + (4 * 20mm) + (3 * ED) \quad (2)$$

with a potential maximum individual rating at each of the features of 5, the Bends Index also has a maximum value of 100. Note that the coefficient on the most severe feature (the ϕt bend) has the lowest value.

For Red Rusting the mean values of the ratings for each of the features yielded a different set of coefficients (for the bend features) to those obtained for the White Corrosion Product. The actual normalized coefficients were as follows: $\phi t = 1$, $3t = 3$, $5t = 4$, $3mm = 7$, $20mm = 5$, $ED = 2$. However, as these values were derived from a very small data set (about 12 specimens) it was decided to adopt the same coefficients as for the White Corrosion Product. White Corrosion Product is a “precursor” to Red Rusting, providing an additional reason for adopting the same set of coefficients. The relationship to develop the Bends Index for Red Rusting (BI_{RR}) is therefore the same as Equation 2.

(c) Cut Edge/Scribe Index – A similar procedure was followed normalising the mean values of the ratings to the highest value, and the results are given in Table 7.

The mean values for WCP were derived from 114 specimens and the mean values for RR were derived from 90 specimens, a total of 204 assessments. As with the Bends Index, a uniform set of coefficients was desirable to cover both White Corrosion Product and Red Rusting. The coefficients for WCP were multiplied by 114 and added to the coefficients for RR multiplied by 90. The totals were divided by 204 to yield a set of coefficients as follows: Scribes 1.69, Top Cut Edge 1.20, Bottom Cut Edge 1.00, Vertical Cut Edge 1.10. These were rounded to values of 2, 1, 1 and 1 respectively. The relationship to develop the Cut Edge/Scribe Index for both White Corrosion Product and Red Rusting (again with a potential maximum value of 100) is shown in Equation 3.

$$CEI_{WCP/RR} = 4 (2 * SC + TCE + BCE + VCE) \quad (3)$$

Blistering – The same procedure as for White Corrosion Product/Red Rusting is followed. The mean values of the ratings at each of the features of the formed specimens and the normalized coefficients are shown in Table 8.

Table 7 – Normalizing Rating Values to Determine WCP/RR Feature Coefficients at Coating Edges

Feature	Mean Value of WCP Rating	Divide Mean Value of WCP into 2.43	Mean Value of RR Rating	Divide Mean Value of RR into 1.53
Scribes	1.88	1.29	0.70	2.19
Top Cut Edge	2.17	1.12	1.18	1.30
Bottom Cut Edge	2.43	1.00	1.53	1.00
Vertical Cut Edge	2.18	1.11	1.40	1.10

Table 8 – Normalizing Rating Values to Determine Feature Coefficients for Blistering

Feature	Mean Rating	Divide into 1.06	Round
Flat Surface	0.55		
3t bend	1.06	1	1
5t bend	0.86	1.23	1
con 3mm bend	0.76	1.38	1
con 20mm bend	0.75	1.42	1
Erichsen Domes	0.97	1.09	1

(a) Flat Surface Index – For the Flat Surface the maximum value of the rating is again 5, there is again only one coefficient, and the relationship to develop the Flat Surface Index for Blistering is the same as for White Corrosion Products/Red Rusting:

$$FSI_{BL} = 20 * FS \tag{4}$$

(b) Bends Index – The coefficients for the bends and Erichsen Domes are all unity and the relationship to develop the Bends Index for Blistering again with a potential maximum value of 100 is:

$$BI_{BL} = 4 * (3t + 5t + 3mm + 20mm + ED) \tag{5}$$

Undercutting – Again the same procedure as for the previous defects is followed. The mean values of the ratings at each of the features (with a highest rating of 1.62) and the normalized coefficients are given in Table 9.

The sum of all of the rounded coefficients is 20. These values have been used to develop the Total Undercutting Index in one step. As each individual feature can have a maximum rating of 5, the relationship again yields a potential maximum value of 100:

$$UCI_{TOT} = (4 * TCE_{min}) + (2 * BCE_{min}) + (3 * VCE_{min}) + (3 * CH_{min}) + (3 * SC_{min}) + TCE_{max} + BCE_{max} + VCE_{max} + CH_{max} + SC_{max} \tag{6}$$

Table 9 – Normalizing Rating Values to Determine Feature Coefficients for Undercutting

Feature	Minimum Undercutting			Maximum Undercutting		
	Mean Rating	Divide into 1.62 → A	A × 0.65 and Round	Mean Rating	Divide into 1.62 → A	A × 0.65 and Round
Top Cut Edge	0.28	5.69	4	1.20	1.35	1
Bottom Cut Edge	0.47	3.44	2	1.62	1.00	1
Vertical Cut Edge	0.32	5.00	3	1.34	1.20	1
Circular Hole	0.32	5.00	3	1.32	1.22	1
Scribes	0.30	5.32	3	1.16	1.40	1

Determining Relative Contributions of Feature Type Indices to Overall Defect Indices for a Product

White Corrosion Product – Over 114 specimens, the mean WCP indices for the Flat Surfaces, Bends and Cut Edges are respectively 16.8, 20.4 and 42.1. The overall WCP Index is to have a potential maximum value of 100. As incidence of WCP is greatest on the Cut Edges and least on the Flat Surface (the least severe feature), the overall relationship to account for the relative contributions of the features should reflect this and emphasize the occurrence of the WCP defect on the Flat Surface. The same process of normalization is followed as before by dividing each of the mean indices into the highest value to yield coefficients of Flat Surfaces 2.50, Bends 2.06, Cut Edges 1. These coefficients are converted to decimal fractions, maintaining relativity such that their sum equals 1, by multiplying by 0.18 [1/(2.50 + 2.06 + 1.00)]. The overall relationship to determine the relative contributions of the Flat Surfaces, Bends and Cut Edges to the Total White Corrosion Product Index is:

$$WCPI_{TOT} = 0.45 FSI_{WCP} + 0.37 BI_{WCP} + 0.18 CEI_{WCP} \quad (7)$$

Red Rusting – Over 90 specimens, the mean RR indices for the Flat Surfaces, Bends and Cut Edges are respectively 3.6, 3.7 and 22.0. However, it should be noted the Flat Surface Index is based on only 7 non-zero readings, the Bends index on only 17 non-zero readings and the Cut Edge Index on 55 non-zero readings; these are much smaller samples than for the WCP (equivalent numbers Flat Surfaces 45, Bends 79, Cut Edges 114). Normalization is followed as before to yield coefficients for Flat Surfaces 6.20, Bends 5.92, Cut Edges 1. These coefficients are converted to decimal fractions maintaining relativity by multiplying by 0.0762 [1/(6.20 + 5.92 + 1.00)]. The overall relationship to determine the relative contributions of the Flat Surfaces, Bends and Cut Edges to the Total Red Rusting Index is:

$$RRI_{TOT} = 0.47 FSI_{RR} + 0.45 BI_{RR} + 0.08 CEI_{RR} \quad (8)$$

Blistering – Over 102 specimens, the mean BL indices for the Flat Surfaces and the Bends are respectively 11.0 and 17.6. The Flat Surface Index is based on 32 non-zero readings, the Bends Index on 49 non-zero readings. Normalization is followed as before to yield coefficients of 1.60 and 1 which are converted to decimal fractions maintaining relativity such that their sum equals 1 by multiplying by 0.3846 [1/(1.60 + 1)]. The overall relationship to determine the relative contributions of the Flat Surface and Bends to the Total Blistering Index is:

$$BLI_{TOT} = 0.62 FSI_{BL} + 0.38 BI_{BL} \quad (9)$$

Contribution of Features to Total Defect Indices – Using the above relationships, the spreadsheet package was used to calculate the Total Indices for White Corrosion Product, Red Rusting and Blistering. Table 10 gives the component and total indices for the same 6 product/exposure condition combinations as in Table 4.

Table 10 – Calculated Indices for All Defect Types on Individual Features, and Total Defect Indices (Example for 6 Product/Exposure Condition Combinations)

	Specimen ID	I112O	I112S	B512O	B512S	C412O	C412S
White Corrosion Product	WCP FS-Index	40.0	60.0	0	0	0	0
	WCP B-Index	41.0	92.0	22.0	49.0	3.0	17.0
	WCP CE-Index	60.0	100	36.0	80.0	32.0	60.0
	WCP Total Index	44.0	79.0	14.6	32.5	6.9	17.1
Red Rusting	RR FS-Index	0	0	0	0		
	RR B-Index	0	31.0	0	0		
	RR CE-Index	0	100	4.0	20.0		
	RR Total Index	0	22.0	0.3	1.6		
Blistering	BL FS-Index	20.0	60.0	20.0	0	0	20.0
	BL B-Index	36.0	68.0	8.0	52.0	4.0	16.0
	BL Total Index	26.1	63.0	15.4	19.8	1.5	18.5
	UC Total Index	12.0	53.0	13.0	47.0	5.0	6.0

Determination of Relative Contributions of Total Defect Indices to the Product Total Performance Index

Total Performance Index Based on the Data Itself – The premise underlying the development of the Total Performance Index is that the potential maximum value should be the same for all generic types of product. In each case, the sum of the derived decimal fraction coefficients must be unity and the potential maximum value of the Total Performance Index is again 100.

(a) Aluminum specimens – There are three types of defect: White Corrosion Products, Blistering and Undercutting. From the database, the mean overall respective total indices over 30 specimens are as follows: $WCPI_{TOT} = 10.9$, $BLI_{TOT} = 6.4$, $UCI_{TOT} = 4.1$. The same procedure of normalization is followed dividing each of the indices into the highest value (10.9) to yield coefficients of 1.00, 1.70 and 2.68, which are normalized to decimal fractions 0.19, 0.31, 0.50 (adding up to 1) by multiplying by 0.1859 $[1/(1.00 + 1.70 + 2.68)]$. The overall relationship for the Total Performance Index based on the data is:

$$TPI(\text{aluminum}) = 0.19 WCPI_{TOT} + 0.31 BLI_{TOT} + 0.50 UCI_{TOT} \quad (10)$$

(b) Stainless steel + organic topcoat – There are three types of defect: Red Rusting, Blistering and Undercutting. From the database, the mean overall respective total indices (6 specimens) are as follows: $RRI_{TOT} = 2.0$, $BLI_{TOT} = 0$, $UCI_{TOT} = 0.2$. The procedure of normalisation fails in this case as coefficients of 1, ∞ and 10 would be obtained. No blistering occurred on the specimens, and one specimen had an undercutting rating of 1 on one feature. The total index for red rust at the stage as exemplified in Table 10 was used for the total performance index.

(c) Metallic-coated steel + organic topcoat – There are four types of defect: White Corrosion Products, Red Rusting, Blistering and Undercutting. From the database, the mean overall respective total indices over 66 specimens are as follows: $WCPI_{TOT} = 22.5$, $RRI_{TOT} = 4.8$, $BLI_{TOT} = 18.0$, $UCI_{TOT} = 16.0$. The procedure of normalization yields equivalent coefficients of 1.00, 4.68, 1.25 and 1.41 which are normalized to decimal fractions 0.12, 0.56, 0.15 and 0.17 by multiplying by 0.12 [$1/(1.00 + 4.68 + 1.25 + 1.41)$]. The overall relationship for the Total Performance Index based on the data is:

$$TPI (\text{metallic/org-coated steel}) = 0.12 WCPI_{TOT} + 0.56RRI_{TOT} + 0.15 BLI_{TOT} + 0.17 UCI_{TOT} \tag{11}$$

(d) Metallic-only-coated steel – There are two types of defect: White Corrosion Products and Red Rusting. From the database, the mean overall respective total indices over 18 specimens are as follows: $WCPI_{TOT} = 47.5$, $RRI_{TOT} = 10.3$. The procedure of normalization yields coefficients of 1.00 and 4.62 which are normalized to decimal fractions 0.18, 0.82 by multiplying by 0.178 [$1/(1.00 + 4.62)$]. The relationship for the Total Performance Index based on the data is:

$$TPI (\text{metallic-only-coated steel}) = 0.18 WCPI_{TOT} + 0.82 RRI_{TOT} \tag{12}$$

Total Performance Index Based on the Judgments of Industry Representatives – Eleven industry representatives were asked to assign coefficients (between 0 and 1) to describe the relative importance of the four types of defect on each of the four generic types of product. It was stated that no assignment was to be made for Red Rusting on aluminum, White Corrosion Product on stainless steel, or Blistering and Undercutting on metallic-only-coated steel, and also that the sum of the coefficients must be unity. The averages of the values together with the coefficients derived from the data are given in Table 11. The equations based on the 12 sets of coefficients were used to calculate 12 sets of Total Performance Indices using the spreadsheet.

Results and Discussion

Space precludes a detailed presentation and analysis of the results from this project. Table 12 presents as an example the Total Performance Indices for the same 6 product/exposure condition combinations as previously (see Table 4).

Table 11 – *Coefficients for Relative Contribution of Defect Types to Total Performance Index*

Defect Type	Aluminum		Stainless Steel + Organic Topcoat		Metallic-coated Steel + Organic Topcoat		Metallic-only-coated Steel	
	Average of 11 Opinions	Based on Data	Average of 11 Opinions	Based on Data	Average of 11 Opinions	Based on Data	Average of 11 Opinions	Based on Data
WCP	0.336	0.19			0.159	0.12	0.341	0.18
RR			0.541		0.409	0.56	0.659	0.82
BL	0.395	0.31	0.259		0.232	0.15		
UC	0.268	0.50	0.200		0.200	0.17		

Table 12 – Total Performance Indices for 3 Products with Polyester or SMP Topcoats

TPI		I112O	I112S	B512O	B512S	C412O	C412S
Calculated from data		11.2	40.2	6.5	15.8	4.3	12.0
Calculated from	Ave.	15.4	46.2	8.5	19.5	4.3	14.4
11 industry opinions	Min.	10.8	39.0	6.0	12.9	3.3	12.0
	Max.	20.8	55.5	12.6	32.8	5.6	16.5

This data shows that the aluminum-based product (C4) is the best overall performer (TPIs are low) of these three (with polyester paint topcoats). Also, good agreement exists between the TPI calculated from the data and the average TPI for 11 industry opinions. The action of the shelter in markedly accelerating the deterioration of products is apparent, with the sheltered indices being 3 to 4 times those of the open indices.

Agreement Between Performance Indices Calculated from Data and Industry Opinions

Exceptional agreement has been obtained between the total performance indices calculated from the data and those based on the judgments of the 11 industry representatives as to the relative importance of different defect types for each generic class of product. A plot of the average industry opinion TPIs against that calculated from the data is given in Figure 2. A linear regression forced through the origin has a slope of 1.16 (standard error 0.01) and an R-squared value of 0.98. There was great variation in the TPIs among the 11 opinions though. Across the 120 product/exposure condition combinations the ratio of the maximum industry opinion TPI to the corresponding minimum was on average 3.1, with a range of 1.1 to 8. This clearly demonstrates that the procedure developed in this paper to use the data itself has overcome the drawback of one individual subjectively assigning weighting factors to the relative importance of various defects and features.

Comparative Performance of Generic Classes of Products

The performance of individual products or classes of products can be assessed by comparing either the Total Performance Indices (TPIs) or the relative rankings. If the aim is to get an overall assessment across several sites of different severity, the use of rankings may be preferable as all sites and conditions (open and sheltered) will contribute equally. If TPIs are used there is a very great difference between the results from the sheltered severe site and the open benign site and the former results will “skew” an overall assessment. To this end, a file with TPIs calculated from the data was sorted (from low to high) for each of the sites/conditions in turn. A ranking from 1 to 20 was added in each case. These rankings were summed for each of the products, separately for open and sheltered exposures (3 cases, i.e. 3 sites for each). A plot of the summed rankings sheltered versus open is given in Figure 3; again low values represent the best performers. At the bottom left of the plot PVF₂ painted 304 stainless steel (B4), PVF₂ painted (with 25 µm primer) 55% Al-Zn (B7), PVF laminated galvanized steel (I6), and aluminum painted with PVF₂ (C1), polyester (C4) and urethane X link polyester (C3) are performing best considering both open and sheltered exposures. Considering open exposure only, unpainted 55% Al-Zn and polyester painted 55% Al-Zn (B1 and B5 respectively), and polyester painted 5% Al-Zn (I1), are also better performers. See Table 2 of Ref. 2 for full identification and specification details of all products.

The TPIs from the data itself for the severe marine site are shown in Figure 4 grouped into generic classes. Again the stainless steel product and those based on aluminum are performing very well considering both open and sheltered exposures.

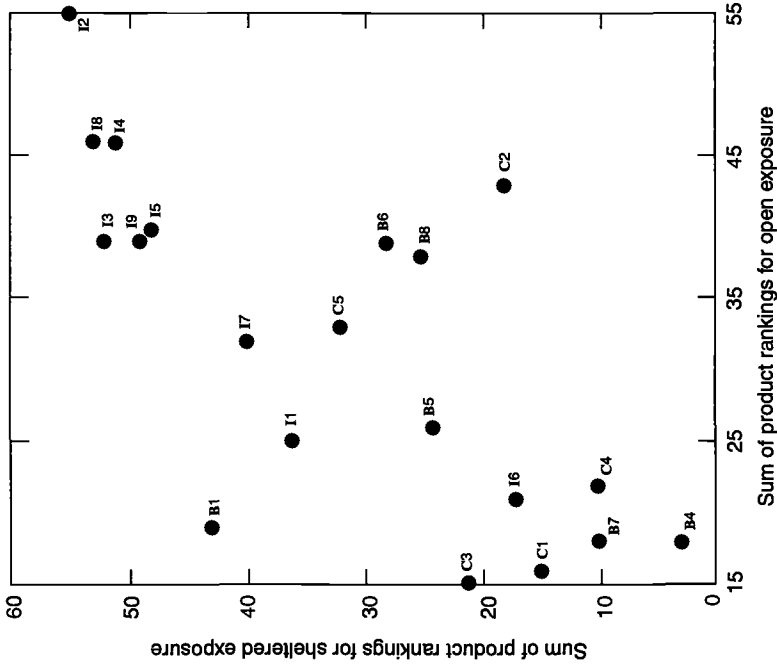


Figure 3 – Sum of Comparative Rankings for Each of 20 Products Exposed at Three Sites for Two Years

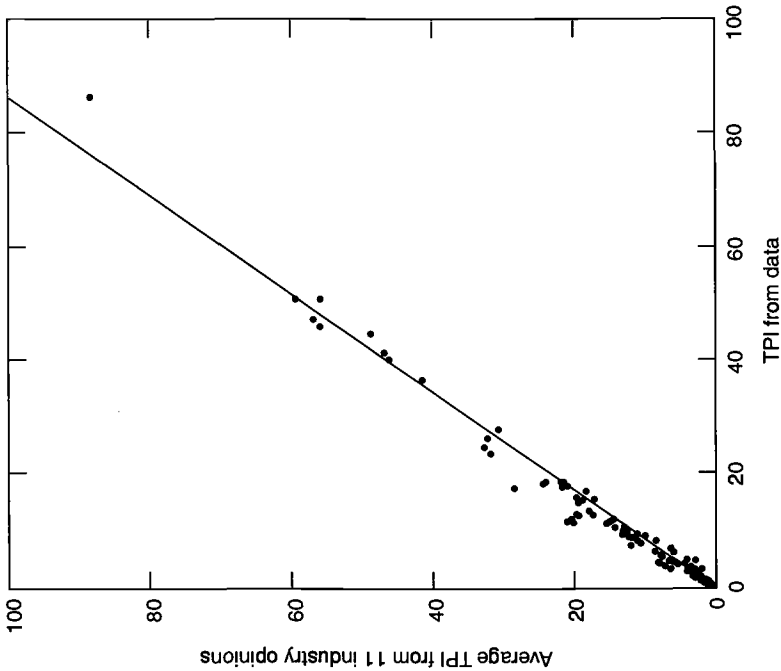


Figure 2 – Total Performance Indices from Average of 11 Industry Opinions Versus that Calculated from the Data (Two-year Data)

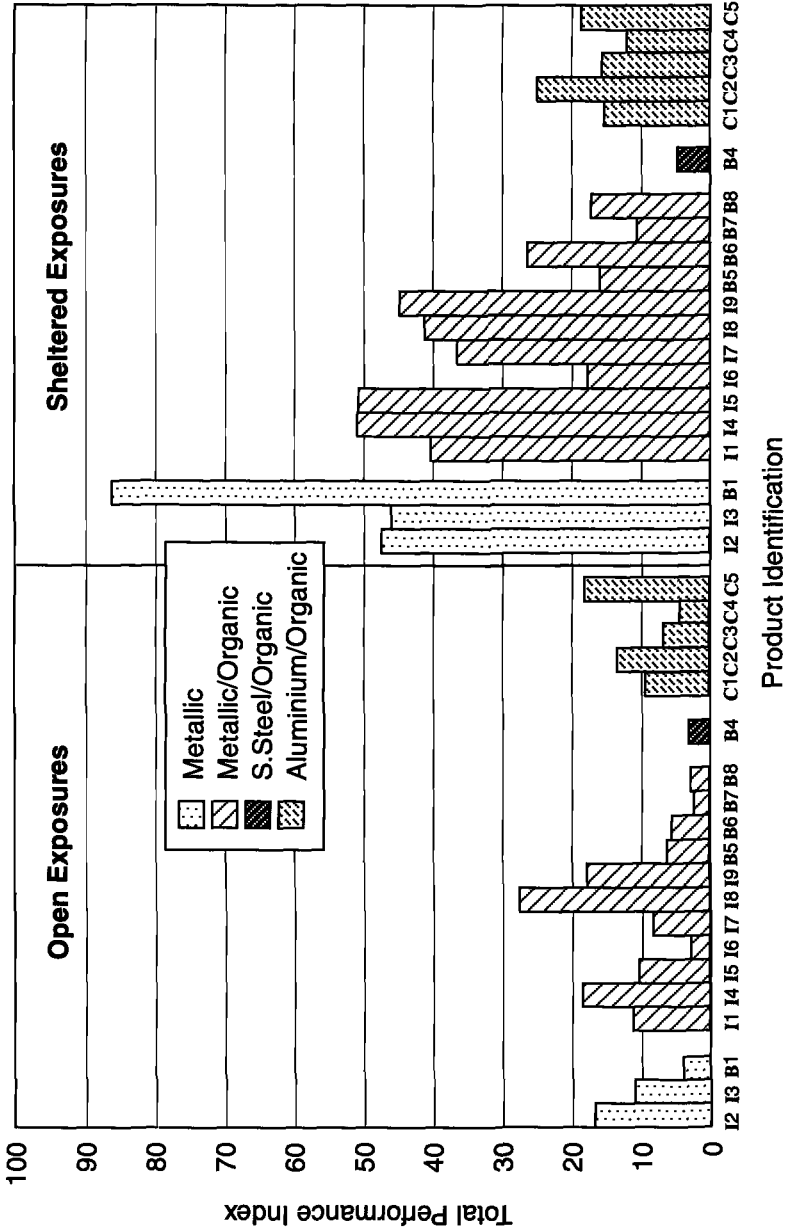


Figure 4 – Total Performance Indices for All Products at Severe Marine Site (Navy Base) Based on Data Only

Action of the Sheltering System in Accelerating Deterioration

For the example given above, the action of the shelters in markedly accelerating the deterioration of products was apparent. Across all of the 20 products the ratios of the sheltered to open TPIs (from the data) were as follows (average followed by min. and max. in parentheses): severe marine site 4.0 (1.0, 20.2), moderate marine/rural site 7.2 (0.6, 21.9), mild marine/urban site 6.0 (1.2, 17.2). These figures represent very significant increases in the rates of deterioration compared to products in open exposure. Future papers will discuss the relationships that exist between sheltered and open exposures in terms of defect types as well as total performance, and compare the results from different exposure periods to determine how well sheltered short-term exposures predict the performance for longer term open exposures.

Measurements of air temperature and relative humidity, and also estimates of time of wetness according to ISO 9223 Corrosion of Metals and Alloys – Corrosivity of Atmospheres – Classification, have shown that at the severe marine sites no significant differences exist between the conditions prevailing in the open and those under the specially designed shelter [5]. In contrast, direct measurements of time of wetness and surface temperature using the Scandinavian WETCORR technique [6] have revealed that the actual time of wetness is much longer under the shelter. This is consistent with the observed differences in corrosion rates between the open and sheltered exposures. The mechanism is not yet fully understood but definitely involves the fact that deposited sea salt accumulates with time and never gets an opportunity to be washed off during rain periods [5].

Conclusions

A methodology for determining objective quantitative indices to describe the atmospheric corrosion performance of coated metal sheet products has been developed. Analysis of the indices in conjunction with those produced by using subjective opinions from industry representatives, has demonstrated that the new technique can accurately describe and quantify performance. A means is available for a more rigorous and numerical analysis of corrosion performance in an area hitherto often descriptive. A novel semi-sheltered exposure system has been shown to induce highly accelerated deterioration of sheet products, with factors on average from four to seven times comparing indices for sheltered and open exposures.

Acknowledgments

BHP Research (Coated Products Division) and the International Lead Zinc Research Organisation Inc. (ILZRO) for ongoing financial support and Comalco Aluminium Ltd for prior support of the project. RAN HMAS Cerberus and Mornington Peninsula and District Water Boards for their cooperation in establishing exposure racks within their grounds. David O'Brien, Natalie Sherman and Pon Kao of CSIRO for technical assistance. Mary Cope of CSIRO for the word processing of this document, Cathy Bowditch of CSIRO for editorial and Marie Scott of CSIRO for the figures.

References

- [1] Willis, D. J., "Performance of 55% Al-Zn Coated Steel Sheets Used for Residential Houses in Australia," Proc. 4th Int. Conf. on Zinc and Zinc Alloy Coated Steel Sheet (GALVATECH '98), The Iron and Steel Inst. of Japan, Chiba, Japan, 1998.
- [2] King, G. A., and O'Brien, D. J., "The Influence of Marine Environments on Metals and Fabricated Coated Metal Products, Freely Exposed and Partially Sheltered," *Atmospheric Corrosion, ASTM STP 1239*, W. W. Kirk and H. H. Lawson, Eds., American Society for Testing and Materials, West Conshohocken, PA, 1995, pp. 167–192.
- [3] Tiemens, J. J., and Hoeflaak, M., "The Performance Level of Some Commercial Coil-Coated Materials," *Construction and Building Materials*, Vol. 8, No. 4, pp. 243–259, 1994.
- [4] Johnson, K., and Marsh, E., "A Study of Relationships Between Design of Precoated Steel Cladding and its Environmental Behaviour in Service," Report EUR10715EN, Commission of the European Communities, 1987.
- [5] Norberg, P., King, G., and O'Brien, D., "Corrosivity Studies and Microclimate Measurements in Marine Environments," Proc. 35th Conf. of the Australasian Corrosion Association (Corrosion & Prevention 95), Perth, Australia, 12–16 November 1995, Paper 36.
- [6] Norberg, P., Proc. 6th Int. Conf. on Durability of Building Materials and Components, Omiya, 26–29 October 1993, pp. 637–646.

Concrete Deterioration

André T. C. Guimarães and Paulo R. L. Helene²

The Moisture Effect on the Diffusion of Chloride Ion in Hydrated Cement Paste

Reference: Guimarães, A. T. C. and Helene, P. R. L., “The Moisture Effect on the Diffusion of Chloride Ion in Hydrated Cement Paste,” *Marine Corrosion in Tropical Environments, ASTM STP 1399*, S. W. Dean, G. Hernandez-Duque Delgadillo, and J. B. Bushman, Eds., American Society for Testing and Materials, West Conshohocken, PA, 2000.

Abstract: Previous research [1] showed high chloride concentrations (2% / cement) on the outside surface of reinforced concrete structures in the mist zone of marine environments. However, the chloride penetration reaches low depths for the concrete class used. Observed data have raised suspicions as to the effect of moisture content on the diffusion of chlorides. A test method was developed to assess the changes in the chloride diffusion coefficient with changes in moisture content in cement paste. It was concluded that the saturation degree (SD) (percentage of moisture content in the cement paste in relation to maximum water absorption of the cement paste) has a large influence in the chloride diffusion properties of the hardened cement paste, and this factor must be taken into consideration when predicting the service life of a reinforced concrete structure.

Keywords: concrete, chloride, durability, marine environment

Nomenclature:

SD: saturation degree - percentage of moisture content in the mass of the test specimen in relation to the water absorption after immersion and boiling according to Brazilian Standard NBR 9778 – Hardened Mortars and Concretes – Determination of Water Absorption by Immersion – Porosity Index and Specific Mass

TS: test specimen

Introduction

In the mist zone, high concentrations of chloride ions can be found in the outermost layer of concrete. This can be observed both in the dry [1] and wet seasons.

¹ PhD Student, University of São Paulo, Civil Construction Engineering Department
PCC/USP, São Paulo, SP, Brazil.

² Professor, University of São Paulo, Civil Construction Engineering Department
PCC/USP, PO Box 61.548, São Paulo, SP, Brazil, CEP 05424-970.

Guimarães [7] describes concentrations of 2% in relation to the cement mass, i.e., a higher value than those indicated by the literature examined [2,3].

The penetration depths of chloride ions found in this research also show lower values than those indicated when using diffusion coefficients mentioned in the literature [3,4] and the equations obtained from the Fick Second Law.

Several chloride ion penetration tests are currently used [3, 4, 5, 6] but nearly all of those found in the literature are performed with water-saturated test specimens. Only the test shown by Mehta et al [7] correlate the direction of the water vapor flow with the diffusion coefficient, using unsaturated TSs.

What is seen in reality is a variation of moisture content in the outermost layer of the concrete (wetting and drying process), and this layer is the penetration medium for the external agents that attack concrete, chloride in this case, eventually reach the steel bars and depassivate them. This brought about the need to research the influence of the changes in moisture contents in the chloride penetration speed in the hardened cement paste. A test was thus developed to confirm whether the influence of the moisture content in the cement paste is a significant factor in the penetration of chloride ions by diffusion.

Objective

The aim of this test is to analyze changes in the diffusion coefficient of chlorides as a function of the moisture contents in the cement paste.

Material Characteristics

Test specimens prepared with cement paste were used in the development of this test. The cement used was the CPV-ARI type (Brazilian Standard NBR-5733 - portland cement for high early strength) because of its faster hydration properties in relation to other cement types. In this way, possible differences in cement hydration have a smaller influence when submitted to the different moisture contents throughout the test. A paste was prepared using this cement at 0.5 w/c ratio. Fifty test specimens (TSs) measuring 30 mm diameter and 45 mm long were molded in plastic molds, and 5 TSs measuring 50 mm diameter and 100 mm long for characterization tests were prepared in metallic molds.

The TS were removed from their molds after 24 hours and the small TSs had their top surface sand-papered to eliminate the top layer, which usually has a very poor quality because of exudation (Figure 1a). Afterwards, they were placed in a curing bath for 14 days and then stored in a lab environment to the age of 28 days.

Compressive strength tests were run on the paste according to NBR 5739 – compressive strength test for cylindrical concrete test specimens. The absorption index after immersion and boiling and specific mass (NBR 9778) of 50 mm x 100 mm TSs were determined after 28 days of age.

In order to estimate the dried mass of 30 mm x 45 mm TSs, 6 samples were selected at random (it is not convenient to dry all TS in an oven) to obtain their dried mass that were used to monitor moisture contents during the test, since cracks may appear and these would interfere with the results. The TS were dried in an oven at 105 °C +/- 5 °C for 72 hours. The results of these tests are shown in Tables 1 and 2.

Table 1 – *Dry mass of cement paste test specimens (30 mm x 45 mm) (NBR 9778)*

TS	Test specimens 30 mm x 45 mm					
	1	2	3	4	5	6
Dried mass (g)	47.9	48.4	48.9	48.5	48.7	47.3
Mean dried mass	48.3 g					
Standard deviation	0.58 g					
Confidence Interval (95% confidence)	48.3 ± 0.61 g					

Table 2 – *Specific mass and absorption after immersion and boiling (NBR 9778/1987) and compressive strength (NBR 5739/1980) of 50 mm x 100 mm cylinders*

Test specimens 50 mm x 100 mm				
TS	I	II	III	Mean
Dried mass in oven, g	281.0	278.4	280.8	280.1
Mass after saturation with dried surface, g	361.5	361.6	361.1	361.4
Mass after saturation and boiling with dried surface, g	362.9	363.7	363.0	363.2
Mass after saturation and immersion in water, g	173.0	171.5	172.9	172.5
Absorption after immersion and boiling, %	29.1	30.6	29.3	29.7
Specific mass, g/cm ³	1.480	1.448	1.477	1.468
TS	IV		V	
Compressive strength - f_{c28} , MPa	27.0		31.1	
Mean f_{c28} , MPa	29.0			

Experimental Methods

A layer of paste with 5% of NaCl in relation to the cement mass was spread on the top of the 30 mm x 45 mm TSs (and were called contamination coats) (Figure 1c). After moisture contents had stabilized, a profile of chloride penetration was obtained by sectioning half of the TSs and by testing chloride ion concentration in the paste. This profile could refer to chloride penetration caused mainly by capillary absorption, particularly in the low-moisture TSs. After approximately 3 months, with TSs showing little or no changes in the SD (saturation degree), the remaining TSs were sectioned and new tests on chloride ion concentration were performed in the paste to obtain a second profile for each group of TSs (or groups of SD). The profiles were analyzed to obtain a diffusion coefficient for each SD.

SD values of 55%, 75%, 90% and 100% were selected for the test. The TSs were randomly split into 4 groups of 10 samples each, and their moisture contents were allowed to stabilize. The 100 % group had only 9 TSs because a few specimens were damaged when removed from their molds or showed cracks caused by contraction.

A silicone rubber ring was placed along the top edge of the TSs to prevent spilling of the chloride contaminated paste over the edge and the contamination of the lateral surface of the TSs (Figure 1b).

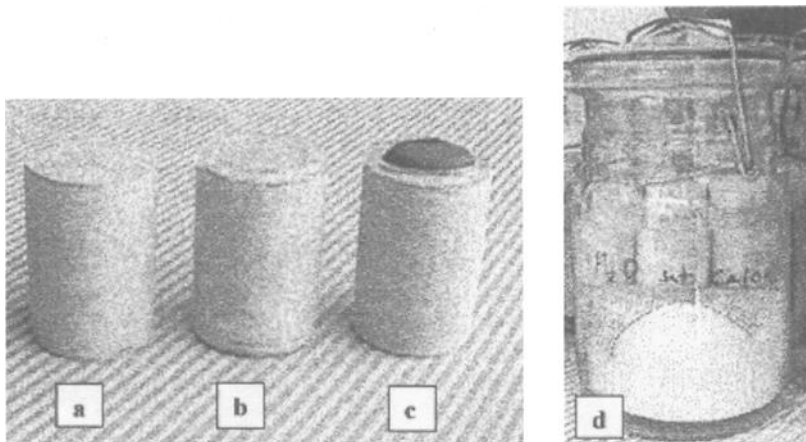


Figure.1 – Test specimen preparation a) TS with sand-papered top; b) TS with silicone ring; c) TS with contamination coat; d) TSs of the 100 % SD group, partly immersed in a saturated solution of $\text{Ca}(\text{OH})_2$

The SDs around 55%, 75% and 90% were achieved by allowing the TSs to dry or by moistening them with distilled water after 28 days of age. The 100% SD was achieved by partially immersing the TSs to the height of 30 mm in a saturated solution of $\text{Ca}(\text{OH})_2$ in a sealed glass container (Figure 1d). As the slicing was no deeper than 1.2 mm from the top, this solution was not expected to interfere in the diffusion process after moisture contents in the TSs had stabilized.

After moisture contents prescribed for each group were reached, the contamination coats was prepared (Figure 1c). Once again, stabilization was necessary to achieve SDs of 55%, 75% and 90%.

After the TSs had stabilized, 5 samples in each group were sliced at 2-mm intervals to a depth of 8 mm (4 layers about 1,5 mm of thickness). These TSs were sliced at 76 days of age and 30 days after the NaCl paste had been applied. Layers from the same group and depth were mixed and ground for the test of total chloride ion concentration in the mass of the paste, according to ASTM Test Method for Acid-Soluble Chloride in Mortar and Concrete (C 1152).

The deepest layers were also tested for free chloride ion concentration in relation to the mass of the paste according to ASTM Test Method for Water-Soluble Chloride in Mortar and Concrete (C 1218). The contamination coats were prepared in the same way they were for the test of water-soluble chloride ion concentration in relation to the mass of the paste (ASTM C 1218).

To keep moisture contents within each group as stable as possible, the remaining TSs in each group were placed inside a plastic bag where the air had been removed to the maximum possible extent. This was the most practical method that was found to maintain and control moisture contents in each group. As the weight of the plastic bag was known, each group could be weighed as a whole more often, and before slicing the TSs to obtain the second profile, each TS could also be weighed separately. The TSs were placed horizontally inside each bag (lengthwise). Approximately every 7 days, the TSs in the

bags were rotated to alternate their positions. These precautions were taken to keep moisture contents as homogeneous as possible inside the TSs. Only the 100 % SD group was placed in a glass container as described above. It was found in this group that small amounts of water had accumulated on the top of the TSs. When the coats and silicone rings were removed, those that were not damaged were weighed to monitor moisture contents in the TSs. The contaminated coats were dried in an oven at 105 °C ± 5 °C for 72 hours (Table 3).

Table 3 – Mean mass of silicone rings and contamination coats

	Individual Masses, g	Mean, g	Standard Deviation, g	Confidence Interval (95% confidence)
Silicone rings	0.26/0.25/0.40/0.44/0.21/0.24/ 0.63/0.38/0.42/0.21/0.46/0.53/ 0.30/0.22/0.23/0.44/0.48/0.19/ 0.34	0.35	0.13	0.35±0.06
Contaminated coats	1.9/1.7/1.5/1.4/1.7/1.4/1.6	1.6	0.18	1.6±0.17

The remaining TSs were sliced, and the resulting same-depth slices in each group of TSs were placed together. 74 days had elapsed between the slicing of the first and the remaining TSs. The SD values for each TS group are shown in Table 4.

Table 4 – Degree of saturation (SD) in each group of TSs

	SD anticipated, %	SD obtained, %
Group I	55	57.2±9.8
Group II	75	74.8±9.8
Group III	90	90.2±9.8
Group IV	100	97.7±9.8

The confidence interval of the SDs of the TSs in Groups I, II, III e IV was calculated from the average mass of the 30mm x 45mm TSs (48.3±0.61g), the mass of the silicone rings (0.35±0.06g), the mass of the contamination coats (1.6±0.17g) and absorption after immersion and boiling (29.7±1.21%). To calculate SD maximum , the lowest values for the mass of TSs, silicone rings, contamination coats and the lowest absorption after immersion were used. To calculate SD minimum, the highest mass values and absorption after immersion were used. In this way, a 95% confidence value was obtained for SDs within the range of ± 9.8%.

The chloride ion concentration tests (Table 5) were performed in the Laboratory of Materials Chemistry at the Instituto de Pesquisas Tecnológicas de São Paulo S.A.

Table 5 – Chloride ion concentrations

Profiles time T ₁			Profiles time T ₂		
Identification tag	Water-soluble Cl, %		Identification tag	water-soluble Cl, %	
Group I CP-1 coat	0.93		Group I CP-2 coat	0.68	
Group II CP-4 coat	0.79		Group II CP-3 coat	0.53	
Group III CP-6 coat	0.49		Group III CP-5 coat	0.28	
Group IV CP-7 coat	0.36		Group IV CP-8 coat	0.19	
Identification tag	Totals %	water-soluble, %	Identification tag	Totals, %	water-soluble, %
Group I CP 1a	0.39	--	Group I CP 2 a	0.29	--
Group I CP 1b	0.26	--	Group I CP 2 b	0.28	--
Group I CP 1c	0.09	--	Group I CP 2 c	0.11	--
Group I CP 1d	0.02	0.02	Group I CP 2 d	0.04	0.05
--	--	--	Group I CP 2 e	0.00	0.02
--	--	--	Group I CP 2 f	0.00	--
Group II CP 4a	0.39	--	Group II CP 3 a	0.24	--
Group II CP 4b	0.35	--	Group II CP 3 b	0.26	--
Group II CP 4c	0.20	--	Group II CP 3 c	0.18	--
Group II CP 4d	0.07	0.05	Group II CP 3 d	0.12	0.11
--	--	--	Group II CP 3 e	0.07	0.06
--	--	--	Group II CP 3 f	0.03	--
Group III CP 6a	0.33	--	Group III CP 5 a	0.25	--
Group III CP 6b	0.27	--	Group III CP 5 b	0.24	--
Group III CP 6c	0.17	--	Group III CP 5 c	0.18	--
Group III CP 6d	0.08	0.02	Group III CP 5 d	0.12	0.09
--	--	--	Group III CP 5 e	0.08	0.07
--	--	--	Group III CP 5 f	0.06	--
Group IV CP 7a	0.28	--	Group IV CP 8 a	0.20	--
Group IV CP 7b	0.24	--	Group IV CP 8 b	0.15	--
Group IV CP 7c	0.17	--	Group IV CP 8 c	0.09	--
Group IV CP 7d	0.10	0.07	Group IV CP 8 d	0.08	0.06
--	--	--	Group IV CP 8 e	0.06	0.05
--	--	--	Group IV CP 8 f	0.04	--

Figures 2-5 show the profiles for the mean concentrations of chloride ions at times T₁ and T₂ in the TSs of Groups I, II, III e IV, respectively.

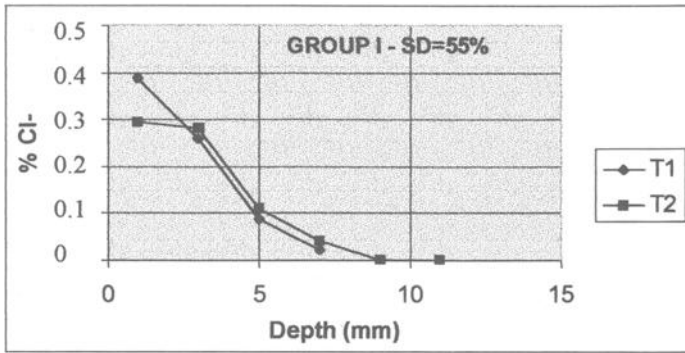


Figure 2 -Profiles for mean concentrations of total chlorides at times T_1 and T_2 - Group I

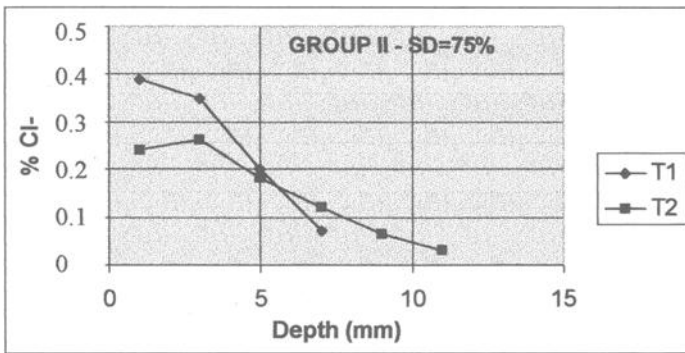


Figure 3 -Profiles for mean concentrations of total chlorides at times T_1 and T_2 - Group II

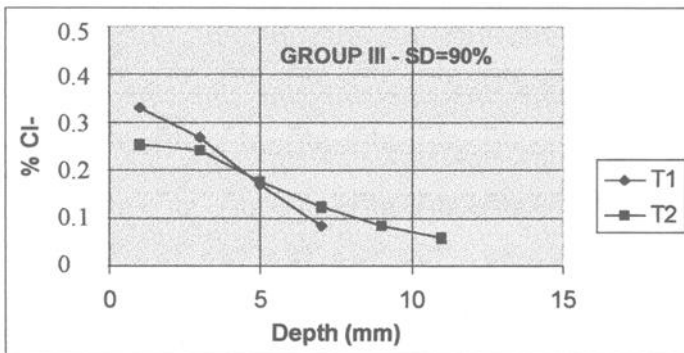


Figure 4 - Profiles for mean concentrations of total chlorides at times T_1 and T_2 - Group III

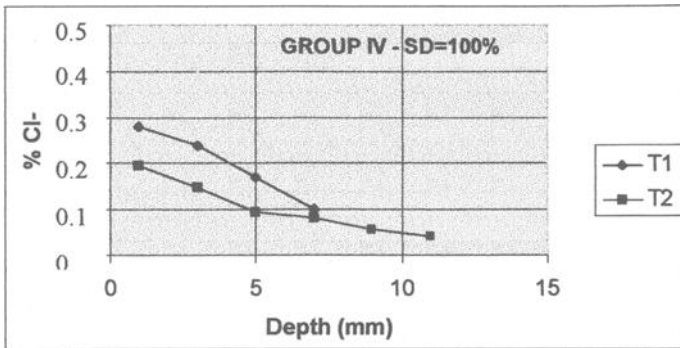


Figure 5 - Profiles for mean concentrations of total chlorides at times T_1 and T_2 – Group IV

Evaluation of Results

As Table 5 shows, each group displayed changes in the concentration of free chlorides in the contamination coat during the test, with each group showing a different value. This was caused mainly by the different moisture contents in each group.

From the T_1 profiles (Figure 2 – 5) and the concentrations of the contaminated coats of each TS group at T_1 (Table 5), it can be observed that ion diffusion was more intense than the penetration of ions via capillary absorption because the chloride ions penetrated more deeply in the TSs with higher SD.

Since the contaminated coats were applied after moisture contents had already stabilized, it was expected that those chloride ions would penetrate those TSs with a lower SD more readily because of capillary absorption, but the reverse was observed.

A quantitative evaluation show a great difference in the diffusion of chlorides between Group I and Group IV because the profiles T_1 and T_2 in Group I practically overlap at depths greater than 7.5 mm. It is also observed the inclination of the curves decrease from Group I to Group IV, indicating that chloride ion penetration increases as the SD increases.

There was apparently a greater diffusion of ions in the first 5 mm, and this effect decreases as the SD increases. This may be caused by the hygroscopic nature of the chlorides. Adding chlorides to the water used to prepare the paste could minimize this effect.

The following equation was used to calculate the diffusion coefficient for each group of SD:

$$J = \frac{D_{ef}}{l} \cdot (C_1 - C_2) \tag{1}$$

where

J = chloride ion flow ($\text{g} \cdot \text{cm}^{-2} \cdot \text{s}^{-1}$);

D_{ef} = effective diffusion coefficient of the chloride ions ($\text{cm}^2 \cdot \text{s}^{-1}$);

l = layer thickness where the flow is measured (cm);

C_1 and C_2 = chloride ion concentrations on the top surface and the last layer (g/cm^3) (mean values for free chloride will be used). Figure 6 shows how the TSs was sliced.

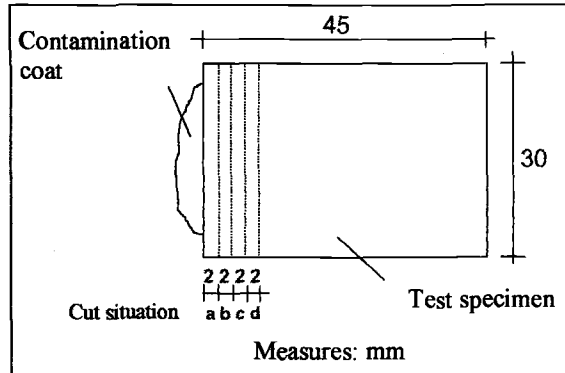


Figure 6 - Slicing the Test Specimens

The J value was calculated by the balance of the chloride ion mass in the first 8 mm of the TSs. The mass of the ions that cross this thickness was divided by the cross-section and by the time elapsed between the data collection of the first (T_1) and last (T_2) profiles. The mass of the chlorides at T_1 and T_2 was calculated as a function of both the mean mass of the contamination coat and TS layers (assumed to be 2 mm thick and with specific mass determined by testing), and the concentrations of chloride ions measured in each layer (assuming mean values for these layers).

The mean concentration of the solution of free chlorides in the contamination coat (C_1) was calculated as a function of the moisture contents measured between T_1 and T_2 and the mass of free chlorides at T_1 and T_2 . Two values were obtained and the mean value was calculated. The mean concentration of the solution in the layer between 6 and 8 mm was calculated in the same way. The value of D_{ef} was calculated with the values of J , l , C_1 and C_2 . The values for the diffusion coefficients in each group are shown in Table 6.

Table 6 – Values for the effective diffusion coefficient as a function of the SD

Group	$D_{ef} - \text{cm}^2/\text{s}$	SD - %
Group I	18.3×10^{-10}	57.2 ± 9.8
Group II	56.6×10^{-10}	74.8 ± 9.8
Group III	65.1×10^{-10}	90.2 ± 9.8
Group IV	203.8×10^{-10}	97.7 ± 9.8

These results are shown in a graph (Figure 7). In this graph, results are shown in an exponential equation and show the zone where SD values can change. It can be observed that the diffusion coefficient values obtained by the mean curve are slightly higher than those obtained by the exponential curve for SD below 80 %. The difference

in the diffusion coefficient found in the mean value curve and the lower limit line is small for SD values below 85 %, and the mean value curve has lower values.

The ratio between the largest diffusion coefficient (Group IV – SD = 100 %) and the other values is 0.09 for Group I, 0.28 for Group II and 0.32 for Group III. These ratios show very marked differences, and indicate that the SD of the concrete is a factor that should be taken into account when analyzing ion diffusion.

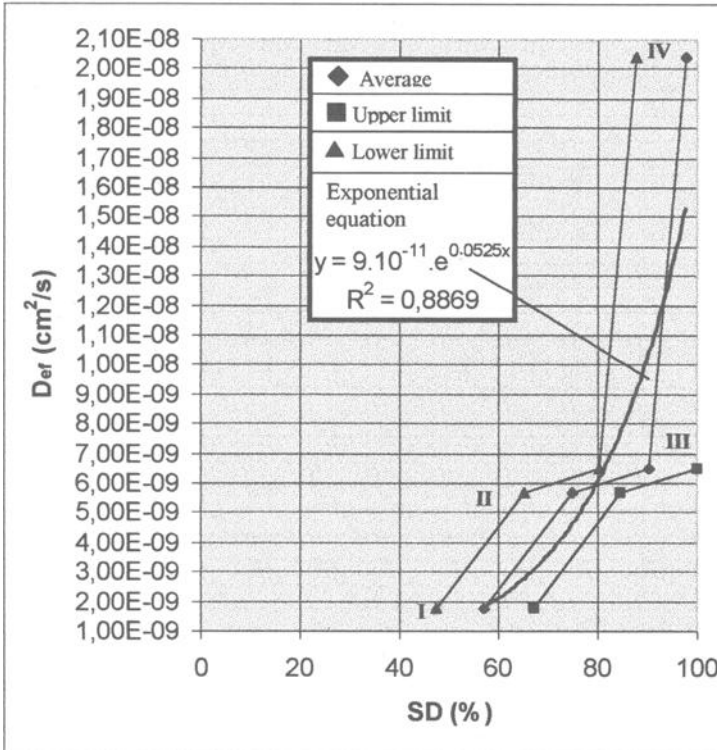


Figure 7 - Values for the effective diffusion coefficient as a function of the SD

Interpretation of results

Test results underscore the importance of taking the moisture content of the concrete into consideration when trying to estimate the coefficient of chloride ion diffusion. To better understand the role of water in this process it is necessary to describe its behavior inside the pore network found in the hardened cement paste. A very important parameter for mass transport in the cement paste is the so-called critical diameter, which is the smallest pore size which allows an interconnected pore network to form, thus allowing mass transport to take place through a sample. According to Mehta and Manmohan [8], large pore sizes have a more important effect on compressive strength and diffusion properties and small pore sizes affect shrinkage and creep properties.

In Figure 8 the pore distribution in the cement paste can be seen [8]. The inflection points in the curves show the critical diameter for pastes with different w/c ratios.

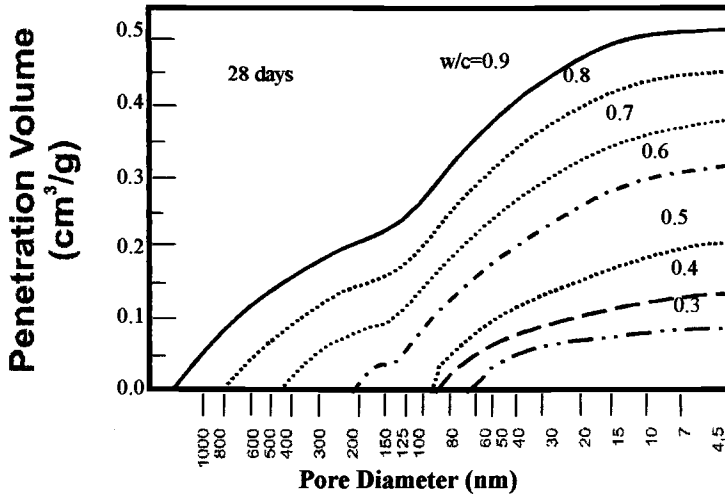


Figure 8 - Pore distribution in cement paste [8]

The following considerations attempt to describe a possible mechanism to explain the influence of the SD in the diffusion of chloride ions in the hardened cement paste.

- In saturated hardened cement paste (Figure 9a) all pores with sizes above the critical diameter are filled with water and this facilitates ion diffusion. The cross-section of these pores is the cross-section where the ions undergo diffusion.
- According to Mehta and Manmohan [8] (Figure 8), the critical diameter is the same for the cement paste with w/c ratios from 0.9 to 0.6, but the percentage of pores with diameters above the critical diameter decreases from w/c ratio 0.9 to 0.6. The number of pores above the critical diameter is around 15 % for the cement paste with a 0.6 w/c ratio. If this is true, the percentage of pores above than the critical diameter for cement paste with a w/c ratio must be lower than 15 % of the total pore volume. So, a reduction of the SD from 100 % to 85 % should reduce more dramatically the water content in that pore network that is larger than in the critical network (Figure 9b). Thus, the cross-section for ion diffusion falls sharply, as can be seen in Figure 7 between points IV and III. Figure 8 shows that the critical diameter for a paste with a 0.5 w/c ratio is approximately 80 nm, and condensation in pores of this size happens with RH above 95 % [9]. Therefore, if the RH falls below 95 %, these pores tend to become filled with water vapor and a water layer adsorbed in their walls, with a thickness of approximately 0.2 nm, 0.45 nm and 0.9 nm for RH of 10 %, 50 % and 90 %, respectively (Figure 10). In this way, pores above the critical diameter tend to reduce water condensation to the point that only a thin layer of adsorbed water remains. When the SD drops to approximately 85 %, all the

interconnected pore network (pore diameter > critical diameter) will show only adsorbed water (Figure 9c). Therefore, the pore cross-section available for ion diffusion can be greatly reduced. In this case, the ions also have to travel greater distances because they have to bypass the pore to overtake them. For small adsorbed water thickness (≤ 0.9 nm) it is to be expected that the precipitated elements, such as $\text{Ca}(\text{OH})_2$ may become obstacles that block the passage of chloride ions, which measure 0.36 nm wide.

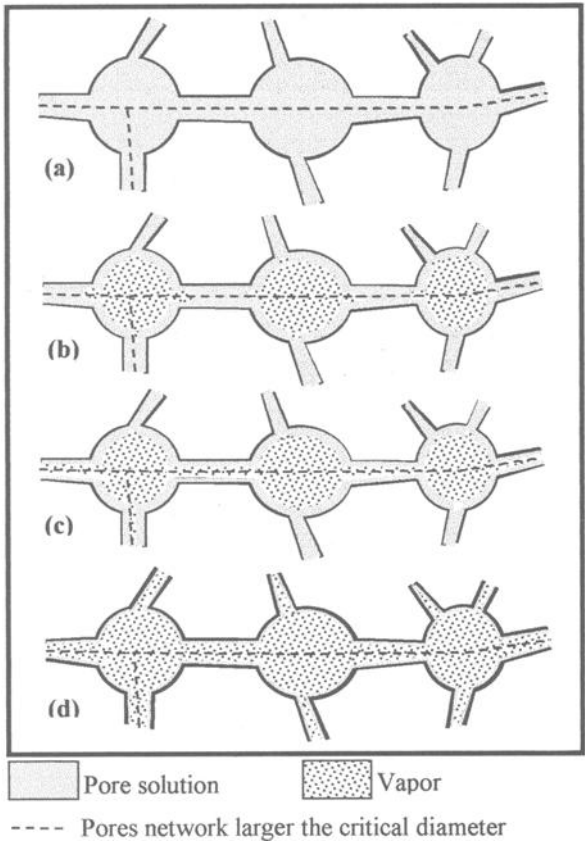


Figure 9 – Pore network in hardened cement paste with different moisture contents: a) $SD = 100\%$; b) $85\% < SD < 100\%$; c) $SD = 85\%$; d) $SD < 75\%$

▪ For SD below 85% , the diffusion coefficient should drop less dramatically. This probably happens because loss of water begins to happen in those pores below the critical diameter and which have less influence on mass transport. This is expected to occur up to the moment when the thickness of the adsorbed water layer in the walls of those pores above than the critical diameter starts to decrease, as shown in (Figure 7) between the point III and II.

- The diffusion coefficient should again drop sharply (Figure 7, between points II and I) when the thickness of the water layer adsorbed in the walls of those pores above the critical diameter begins to decrease (Figure 9d).

There are strong indications that this process occurs when the Mehta and Manmohan [8] graph is compared with the results of the influence of the moisture effect on chloride diffusion on the cement paste. It can be observed that the inflection in the paste with a 0.6 w/c ratio takes place when approximately 15 % of the pore volume is filled with mercury (measurement taken with mercury-intrusion) (Figure 9), which is equivalent to a SD of 85 % (Figure 7, between points II and III).

If this is the case, it seems wiser to use the mean curve of Figure 7, even though a good correlation has obtained with the exponential curve ($R^2 = 0.88$), particularly for those SDs below 80 %, where higher diffusion coefficients are found in the mean curve. Tests shown by Mehta et al. [7] seem to corroborate the results found in thus test. These researchers performed tests to correlate the direction of water vapor with the diffusion coefficient, and showed that when the vapor moved in the same direction as the chloride ions, the diffusion coefficient was much greater than when the reverse situation was observed. It can be seen in Figure 11 that when the vapor follows the same direction as the chloride ions, the first layers that they cross have a higher moisture content than when the vapor moves in the opposite direction.

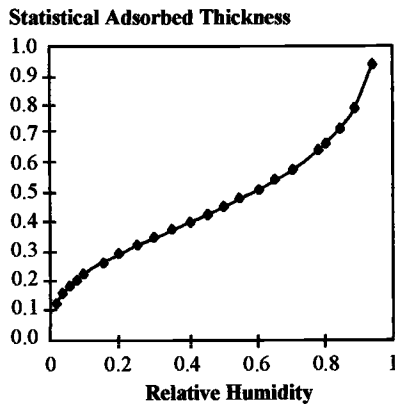


Figure 10 - Thickness of adsorbed water layer on pore walls as a function of RH [10]

A steady-state flow of chloride ions was assumed when determining the diffusion coefficients in this study, taking into consideration the mean values between the profiles at times T_1 and T_2 on the TSs surface and in the fourth layer. To make the determination of the diffusion coefficient according to Fick's Second law easier, i.e., under a unsteady-state flow, the chloride ion concentration can be kept constant on the surface of the TSs throughout the test. To do so, the concentration of NaCl added to the contamination layer should be increased above the saturation level of the pore solution. This allows the calculation of water-soluble chloride concentrations for each SD, because as the

dissolved chlorides undergo diffusion, new chlorides which had been thus far precipitated as NaCl are dissolved.

Therefore, because of the final considerations made during the analysis of this test, the diffusion coefficients thus calculated must show some divergence, but the correlation between the changes in the diffusion coefficients and the SDs should be good because the same considerations were taken into account in the analysis of all groups with different SDs.

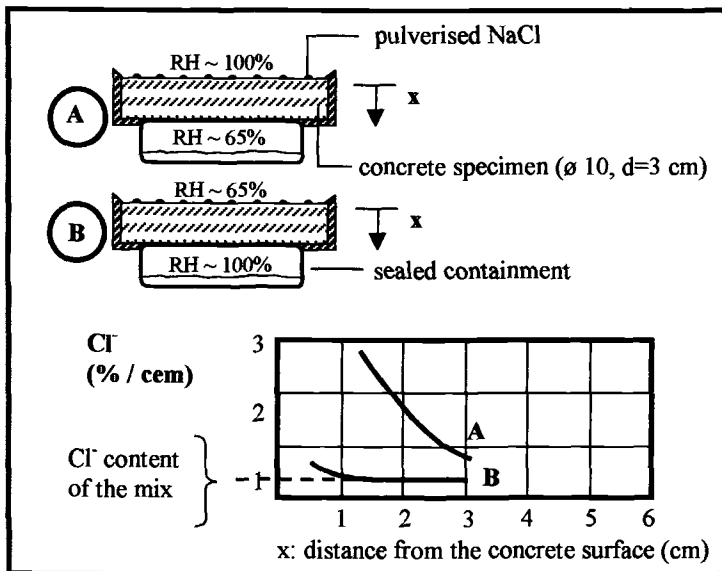


Figure 11 - Test correlating the direction of water vapor and the diffusion coefficient [7]

Conclusions

The tests carried out in this study point to the great influence of the SD of the hardened cement paste. The SD of the hardened cement paste has a more decisive effect on the intensity of chloride ion penetration than the moisture content does, just as pore interconnection is more important than pore content. Consequently, this factor must be taken into account when estimating the service life of any reinforced concrete structure that is subject to a chloride environment.

Therefore, this research must be developed further, since some changes must be implemented in the methodology adopted here to allow the calculation of the diffusion coefficient under an unsteady-state flow (Fick's Second Law).

Acknowledgements

The authors would like to thank FAPESP (The Office of Support to Research in the State of São Paulo - Brazil) for their support which was essential to the development of this research.

References

- [1] Guimarães, A. T. C., "Desempenho do concreto em ambiente marítimo na região do extremo sul do Brasil," Dissertação (mestrado), Fundação Universidade do Rio Grande, Rio Grande, 1997.
- [2] Helene, P. R. L., "Contribuição à normalização: A resistência sob carga mantida e a idade de estimativa da resistência característica; Durabilidade e vida útil das estruturas de concreto armado," Monografias, Universidade de São Paulo, São Paulo 1994.
- [3] Prudêncio, L. R., Jr., "Durabilidade de concreto frente ao ataque de cloretos e sulfatos," *Qualidade e Durabilidade das Estruturas de Concreto, Seminário NORIE-UFRGS*, Universidade Federal do Rio Grande do Sul, Porto Alegre, 1993, pp. 1-12.
- [4] Page, C. L., Short, N. R., and El Tarras, A., "Diffusion of chloride ions in hardened cement pastes," *Cement and Concrete Research*, Vol. 11, 1981, pp.395-406.
- [5] Andrade, M.C., "Calculation of chloride diffusion coefficients in concrete from ionic migration measurements," *Cement and Concrete Research*, Vol. 23, 1993, pp.724-742.
- [6] Gjrv, O. E., Tan, K., and Zhang, M., "Diffusivity of chlorides from seawater into high-strength lightweight concrete," *ACI Materials Journal*, Vol. 91, 1994, pp 447-452.
- [7] Mehta, P. K., Schiessl, P., and Raupach, M., "Performance and Durability of Concrete Systems," *International Congress on the Chemistry of Cement, 9*, New Delhi, 1992.
- [8] Mehta, P. K., and Manmohan, D., "Pore size distribution and permeability of hardened cement paste," *7th International Congress on the Chemistry of Cement*, Paris, 1980, Vol. III, pp. VII-1 - VII-5.
- [9] Qunard, D., and Salle, H., "Le transfert isotherme de la vapeur d'eau condensable dans les matriaux microporeux du btiment," *Cahiers du CSTB, Livraison 323, Cahier 2525*, 1991.
- [10] Qunard, D., and Salle, H., "Water vapour adsorption and transfer in cement-base materials: a network simulation," *Materials and Structures*, Vol. 25, 1992, pp. 515-522.

Luis Maldonado¹

Electrical Conductivity of Concrete and Mortar Prepared with Calcareous Aggregates for Construction in the Gulf of Mexico

Reference: Maldonado, L., “Electrical Conductivity of Concrete and Mortar Prepared with Calcareous Aggregates for Construction in the Gulf of Mexico,” *Marine Corrosion in Tropical Environments, ASTM STP 1399*, S. W. Dean, G. Hernandez-Duque Delgadillo, and J. B. Bushman, Eds., American Society for Testing and Materials, West Conshohocken, PA, 2000.

Abstract: The electrical conductivity of mortar and concrete samples was measured. Series of samples were prepared with crushed limestone (approximately 95-98% calcium carbonate), water-to-cement ratios of 0.53, 0.59, 0.70 and 0.76 and cured at 7 and 28 days. The conductivity, for both mortar and concrete, in chloride solution of concentration 1M, 2M, 3M and 4M, increases as the chloride concentration in the solution increases. The conductivity of mortar specimens take values between 0.60 and 2.18 mS/cm, while the concrete samples have values in the range from 2.10 to 5.44 mS/cm. For concrete samples, the conductivity decreases with curing time, which indicates that the conduction is, in such a case, due mainly to capillar porosity. The conductivity values of mortar increase, when the curing time increases. It is suggested that such behavior is due to the hydration process of the paste in the mortar and the water transport in the pore gel structure resulting thereafter.

Keywords: mortar, concrete, water-to-cement ratio, curing time, electrical conductivity, Yucatan Peninsula

Introduction

The corrosion of reinforcing bars in concrete is a major problem in marine environments worldwide. The literature gives numerous examples of research devoted to elucidate the corrosion mechanisms, with the aim of contributing to the solution of the problem [1-18]. This concern exists also in the Gulf of Mexico [19-26], where harsh tropical conditions enhance the corrosivity of the atmosphere [24]. Marine corrosion in the coastal regions of Mexico is observed over almost 10 000 km, where tourism or industrial facilities exist [22, 23]. A survey at the Caribbean zone, conducted by the

¹ Department of Applied Physics, CINVESTAV-Mérida, A.P. 73 Cordemex, C.P. 97310, Mérida, Yuc., México.

corrosion group at CINVESTAV-Mérida, has shown that most buildings suffer corrosion problems after 5 to 10 years. That is because they had been sprayed by, or overflowed with, seawater during hurricanes such as Gilbert, Opalo or Roxana. Constructions exhibit huge cracks and delamination of concrete exposing the reinforcing bars to atmospheric corrosion. On the northern coastline of the Yucatan Peninsula, buildings are suffering corrosion also because their foundations are located in sea or brackish water [20, 21]. Bridges and docks show serious corrosion damage before 20 years of service, and after 30 or 40 years are completely destroyed by corrosion [19].

In order to assess corrosion of the infrastructure along the Gulf of Mexico at the Yucatan Peninsula, electrical resistivity of concrete is being used to indirectly evaluate relevant properties such as chloride ion content, its diffusivity (or permeability) or to characterize the pore water composition. Moreover, resistivity values of concrete in service may be an indicator of the possible extent of corrosion macrocell currents and an important parameter in cathodic protection design. Care must be exercised in relating electric properties of the concrete to other quality performance parameters. However, the non-destructive nature, speed, and ease of conducting resistivity measurements make them an attractive addition to the set of techniques that can be performed to characterize concrete. For example, rapid chloride tests have been used to compare the mechanical resistance of different concrete types to chloride ingress. This has proved very useful in finding economical mixes for high durability applications, and also for understanding the factors that improve the resistance of concrete to chloride ingress. Whiting [27], Dhir [28], and Tang [29] proposed rapid methods for measuring chloride in concrete. Such methods are conduction tests with negligible diffusion. However other authors have proposed the replacement of the AASHTO T 227, which is based on the Whiting recommendation, with a resistivity method [30, 31].

The published literature shows that the electrical conductivity of concrete and mortars depends on various factors such as the measuring technique [32, 33], the age of the concrete, curing treatment, chemical composition of the cement, temperature, relative humidity, concrete design parameters and aggregates [34, 35].

Aggregates used in the Yucatan Peninsula for concrete structures are mainly calcium carbonate (approximately 95-98%). They are essentially crushed rock from limestone quarries of ancient marine sediments and contain high porosity levels due to the crushing process and its origin. Concrete and mortars used for construction or repair in the Yucatan Peninsula result with high porosity levels due to the aggregate characteristics and, to the high water to cement ratios used in this region. When concrete and mortars are exposed to high relative humidity and high chloride deposition rates, due to airborne salinity or marine spray, the electrical conductivity values increase, resulting in the development of corrosion macrocells and rapid corrosion damage in infrastructure. However, no data exist of the electrical conductivity of concrete or mortars used in the Mexican region of the Gulf of Mexico. This research represents a first attempt to assess the electrical conductivity of fresh mortars and concrete as a function of the chloride content in the solution, the water to cement ratio and the curing time.

Experimental Procedure

Test Apparatus

The test apparatus was constructed according to a design proposed in the literature [31], for rapid chloride test. It consisted (Fig. 1) of two glass containers. A lateral wall of each cell had a circular aperture with a neoprene collar, in which the sample was positioned. A constant potential difference was established between a carbon anode and a stainless steel cathode by a dc source. Saturated calomel electrodes (SCE) were used to construct two halfcell, each one containing a Luggin capillar, where only the potential difference across the sample was measured.

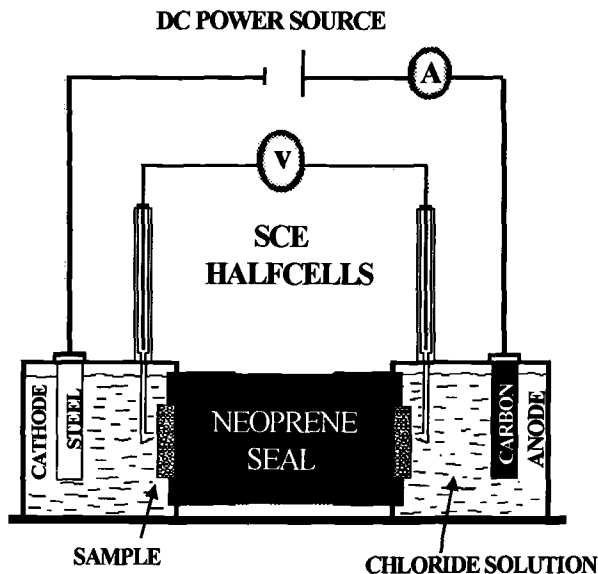


Figure 1 - Conduction Test Apparatus Diagram, after Reference [31].

Samples Preparation and Conductivity Measurements

The test apparatus was designed for testing cylindrical samples of 40 mm diameter. Four water to cement ratios, w/c, (0.53, 0.59, 0.67, 0.76) and two curing times, t_c , (7 and 28 days) were tested for concrete and mortar samples. An additional set of cylinders (dimensions of 30 x 15 cm) for determination of the concrete strength was used. The specimens were immersed in saturated limewater and allowed to cure at room temperature of 24°C, in accordance with ASTM Method for Making and Curing Concrete Test Specimens in the Field. Subsequently, the cylinders were dried at 50°C for a week and the corresponding series of specimens were immersed in NaCl solutions of concentration 1M,

2M, 3M and 4M. The conductivity test on the mortar samples was performed in conductivity cells containing solutions with similar concentration than the solution used in the sample saturation process. From each mix and condition three samples were measured.

The conductivity experiments were performed by applying a potential difference of 2 volts (dc) between anode and cathode, and recording the current in the cell, when the steady state was established, which occurred about 1200 seconds after application of the potential.

The measured potential and current in steady state condition was used to calculate the conductivity, using the relation:

$$\sigma = \frac{i}{V} \frac{L}{A}$$

where,

σ = conductivity of the the mortar in millisiemens per centimeter

i = electric current, in milliamperes

V = potential difference, in volts and

L = sample thickness, in cm.

A = sample area, in square centimeter

Experimental Results and Discussion

Tables 1 and 2 show the mortar and concrete strength after 7 and 28 days curing, respectively.

The electrical conductivity (Table 3) for both mortar and concrete ranges from 0.57 to 5.44 mS/cm, for NaCl content between 1M and 4M in the solution. For the same NaCl content, w/c ratio and t_c , the conductivity values of concrete are a factor several times larger than the values obtained for mortar. Such behavior was expected due to the high porosity of the aggregate type used in the samples. The pore structure of mortar is quite different than that of concrete due to the aggregate-paste interface, which has a definite effect on the pore size distribution. The considerably higher porosity of the calcareous aggregates from the Yucatan Peninsula, produces interfaces or transition zones that influence the transport properties. Concrete containing similar or higher amount of aggregates with higher porosity than the mortar samples exhibit higher conductivity values because the transition zones overlap and consequently the conductivity increases.

Concrete, cured 7 days, showed higher conductivity values than those cured during 28 days. This behavior is due to quantity and characteristics of the various types of pores in the concrete, which denotes a capillary pore fragmentation as a result of the process of curing. Nevertheless, mortars cured 7 days result in conductivity values higher than those obtained for mortar cured during 28 days, which means that the curing time is irrelevant in this case. Such behavior is probably due to the mechanism of transport through the gel porosity. Mortar contains less capillar porosity than concrete. The volume size and continuity of the pores are especially important in case of conductivity. The structure of porosity of the material within, is essentially due to the initial w/c ratio, the

degree of compaction and the degree of hydration. The w/c determines the initial porosity, while the degree of hydration determines the extent to which the original pores become filled with new solid. When water is mixed with cement, the clinker grains begin to hydrate. The hydrate is approximately 1.6 times absolute volume of its constituents [36].

Table 1 - Water-to-Cement Ratio and Mechanical Resistance of Mortar Samples used for Electrical Conductivity Measurements

w/a ratio	Water (kg/m ³)	Cement (kg/m ³)	Strength (kg/cm ²)	
			Curing time (d)	
			7	28
0.53	329	621	269	345
0.59	372	631	228	317
0.67	362	540	215	274
0.76	401	528	187	246

Table 2 - Water to Cement Ratio and Mechanical Resistance of Concrete Samples used for Electrical Conductivity Measurements

w/a ratio	Water (kg/m ³)	Cement (kg/m ³)	Strength (kg/cm ²)	
			Curing time (d)	
			7	28
0.53	211	401	255	270
0.59	228	383	215	230
0.67	221	328	160	175
0.76	234	307	147	165

The hydration process results in a formation of capillary and gel pores. Due to its small size, the gel pore contributes little to the permeability. The larger capillary pores cause the transport to be dependent on the initial w/c ratio. The hydration process results in segmentation of the capillaries. The segmentation of pores implies impermeability, even in the case of concrete of high w/c ratios. The dependence of concrete on the conductivity may mean that enough capillary pores built up during the mix and that they segment during the curing process.

High values of conductivity for mortar samples, may be associated to a higher amount of cement paste in relation to the aggregate volume, which reduces the hydration process due to the gel porosity. As discussed previously, the gel porosity formed during the mix process may impinge or delay water incorporation, delaying or impeding further formation of capillary porosity and especially their fragmentation. A network of non-fragmented capillary pores at 28 days curing, would increase conductivity.

Table 3 - *Electrical Conductivity of Mortar and Concrete Saturated in Solution of Different NaCl Concentration.*

W/c And (tc)	Molar Content of NaCl in Solution							
	1		2		3		4	
	Conductivity (mS/cm)		Conductivity (mS/cm)		Conductivity (mS/cm)		Conductivity (mS/cm)	
	Mortar	Concrete	Mortar	Concrete	Mortar	Concrete	Mortar	Concrete
0.53 (7)	0.60	2.10	0.80	3.0	0.81	3.93	0.85	4.32
0.59 (7)	0.72	2.35	0.95	3.02	1.29	4.06	1.42	4.42
0.70 (7)	0.79	2.46	0.85	3.48	1.29	4.52	2.06	5.44
0.76 (7)	0.80	2.42	0.79	3.39	1.65	4.20	1.69	5.13
0.53 (28)	0.78	1.51	0.80	2.13	1.27	3.15	1.24	3.26
0.59 (28)	1.01	1.56	1.30	2.51	1.59	3.44	1.55	4.28
0.70 (28)	1.10	2.34	1.93	3.38	2.07	4.09	1.94	4.61
0.76 (28)	1.19	2.14	1.89	3.24	2.18	3.93	2.17	4.83

Conclusion

The electrical conductivity of mortar and concrete samples has been determined in chloride solutions of concentration 1, 2, 3 and 4 molar. Mortars prepared with calcareous stone result in smaller conductivity values than similar concrete samples. This behavior agrees with models based on interfacial zones with larger capillar porosity due to aggregate additions to the cement paste. The curing time decreases the conductivity of concrete samples, as expected from some models for the hydration process described in the literature. Nevertheless, the conductivity of mortars is higher for mortars cured seven days than of those cured for 28 days. It is suggested that this behavior is due to the difficulty of water transport in the gel pore structure.

References

- [1] Rasheeduzzafar, Dakhil, F. H., Bader, M. A., and Khan, M. M., "Performance of Corrosion Resisting Steels in Chloride-Bearing Concrete," *ACI Materials Journal*, Vol. 89, No. 5, 1992, pp. 439-448.
- [2] Treadaway, K.W. J., Cox, R. N., Brown, B. L., "Durability of Corrosion Resisting Steels in Concrete," *Proceedings of Institution of Civil Engineers (London) Part 1 -Design and Construction*, 1989, pp. 305-331.

- [3] Turgeon, R., "Evaluation of Epoxy and Galvanized Reinforcing Bars in Pennsylvania Bridge Decks," *Corrosion* 87, National Association of Corrosion Engineers, Paper 140, 1987, Houston, TX, USA.
- [4] Hazan, J., and Yahalom, J., "Corrosion of Protected Aluminum and Zinc," *Corrosion Science*, Vol. 35, Nos. 1-4, 1993, pp. 223-229.
- [5] MacDowell III, L. G., "Protective Coating Systems for Carbon Steel Exposed to an Acid-Marine Environment," *Materials Performance*, Vol. 31, No. 4, 1992, pp.33.
- [6] Vincent, L. D., "Inorganic Zincs-A Love/Hate Relationship," *Materials Performance*, Vol. 33, No. 9, 1994, pp. 35-38.
- [7] Faidi, S. E., Scantlebury, J. D., Bullivant, P., Whittle, N. T., and Savin, R., "An Electrochemical Study of Zinc-Containing Epoxy Coatings on Mild Steel," *Corrosion Science*, Vol. 35, No. 5-8, 1993, pp. 1319-1328.
- [8] Rodríguez-Gómez, F. J., Rodríguez-Urbina, R., Rodríguez, H. P., and Genescá-Llongueras, J., "Protección del Acero Galvanizado en Atmósferas Marinas," *Memoria del XVI Congreso, Academia Nacional de Ingeniería, A.C.*, 1990, pp. 193-197.
- [9] González, J. A., Vázquez, A. J., Jáuregui, G., and Andrade, C., "Effect of Four Coating Structures on Corrosion Kinetic of Galvanized Reinforcement in Concrete," *Matériaux et Constructions*, Vol. 17, No. 102, 1984, pp. 409-414.
- [10] Yeomans, S. R., "Considerations of the Characteristics and Use of Coated Steel Reinforcement in Concrete," Report No. NISTIR 5211, National Institute of Standards and Technology, U.S. Department of Commerce, Gaithersburg, MD, 20899, USA, 1993.
- [11] Yeomans, S. R., "Corrosion of the Zinc alloy Coating in Galvanized Reinforced Concrete," *Corrosion* 98, National Association of Corrosion Engineers, Paper 653, 1992, Houston TX., USA.
- [12] Yeomans, S. R., "Performance of Black, Galvanized, and Epoxy-Coated Reinforcing Steels in Chloride-Contaminated Concrete," *Corrosion*, Vol. 50, No. 1, 1994, pp. 72-81.
- [13] Hime, W. G., and Machin, M., "Performance Variances of Galvanized Steel in Mortar and Concrete," *Corrosion*, Vol. 49, No 10, 1993, pp. 858-860.
- [14] Andrade, C., Jáuregui, G., and González, J. A., "Influence of Mortar Mix Proportions on Corrosion of Bare and Galvanized Reinforcements Causes by Penetration of Chlorides," *8th. Int. Cong. on Metallic Corrosion*, 1981, pp. 1372-1377.
- [15] Macías, A., and Andrade, C., "Galvanized Steel Behaviour in $\text{Ca}(\text{OH})_2$ Saturated Solutions Containing SO_4 Ions," *Cement and Concrete Research*, Vol. 17, 1987, pp. 307-316.
- [16] Macías, A., and Andrade, C., "Corrosion rate of Galvanized Steel Immersed in Saturated Solutions of $\text{Ca}(\text{OH})_2$ in the pH Range 12-13.8," *British Corrosion Journal*, Vol. 18, No. 2, 1983, pp. 82.
- [17] Roberge, R., and Zheng, W., "Hydrogen Embrittlement Susceptibility of Galvanized 4135 Steel in Cement Environment," *Corrosion Science*, Vol. 35, No. 1-4, 1993, pp. 507-514.

- [18] Wilcox, G. D., and Gabe, D. R., "Electrodeposited Zinc Alloy Coatings," *Corrosion Science*, Vol. 35, No. 5-8, 1993, pp. 1251-1258.
- [19] Vázquez, D. "Diagnóstico de Corrosión del Puente de Celestún, Yuc. Mex.," Tesis de Maestría, Fac. de Ing. Civil. UADY, 1997.
- [20] Castro, P., and Maldonado, L., "Penetration of Chlorides and Rebars Corrosion in Concrete Columns of two Schools at a Marine Site," *Corrosion 96*, National Association of Corrosion Engineers, Paper 321, 1996, Houston TX., USA.
- [21] Castro, P., and Maldonado, L., "Initial Efforts to Evaluate the Corrosion Problems in the Infrastructure of the Mexican Southeast Coastal Zone," *Corrosion 95*, National Association of Corrosion Engineers, Paper 21, 1995, Houston, TX., USA.
- [22] Castro, P., Veleva, L., and Balancán M., "Corrosion of Reinforced Concrete in a Tropical Marine Environment and in Accelerated Tests," *Construction and Buildings Materials*, Vol. 11, 1997, No 2, pp. 75-81.
- [23] Veleva, L., Castro, P., Hernández-Duque G., and Schorr, M., "The Corrosion Performance of Steel and Reinforced Concrete in a Tropical Humid Climate," *Corrosion Reviews*, Vol. 16, No. 3, 1998, pp. 235-284.
- [24] Maldonado L., and Veleva, L., "Corrosivity Category Maps of a Humid Tropical Atmosphere: The Yucatan Peninsula, Mexico," *Materials and Corrosion* Vol. 50, 1999, pp. 261-266.
- [25] Maldonado, L., Castro P., and Echeverría, M., "A Comparative Study of Atmospheric Corrosion in the Caribbean Area," *Corrosion 95*, National Association of Corrosion Engineers, Paper 237, 1995, Houston, TX, USA.
- [26] Corvo, F., Haces, C., Betancourt, N., Maldonado, L., Véleva, L., Echeverría, M., de Rincón O. T., and Rincón, A., "Atmospheric Corrosivity in the Caribbean Area," *Corrosion Science*, Vol. 39, No. 5, 1997, pp. 823-833.
- [27] Whiting, D., "Rapid Chloride Determination of the Chloride Ion Permeability of Concrete," Final Report No. FHWA/RD-81/119, Federal Highway Administration, Washington D. C., 1981.
- [28] Dhir, R. K., Jones, M. R., Ahmed, H. E. H., and Seneviratne, A. M. G., *Magazine of Concrete Research*, Vol. 42, 1990, pp. 177-185,
- [29] Tang L., and L. O., Nilsson, *ACI Materials Journal*, Vol. 89, 1992, pp. 49-53.
- [30] Feldman, R. F., Gordon W. C., Brosseau R. J., and Tumidajski, J., *ACI Materials Journal*, Vol. 91, 1994, pp. 246-255.
- [31] Streicher P. E., and Alexander, M. G., "A Chloride Conduction Test for Concrete," *Cement and Concrete Research*, Vol. 25, 1995, pp. 1284-1294.
- [32] Hansson I. L. H., and Hansson C. M., "Ion-Conduction in Cement-Based Materials," *Cement and Concrete Research*, Vol. 15, 1985, pp. 201-212.
- [33] Morris, W., Moreno E. I., and Sagués, A. A., "Practical Evaluation of Concrete Test Cylinders Using a Wenner Array Probe," *Cement and Concrete Research*, Vol. 26, 1996, pp. 1779-1787.
- [34] Hansson I. L. H., and Hansson, C. M., "Electrical Resistivity Measurements of Portland Cement Based Materials," *Cement and Concrete Research*, Vol. 13, 1983, pp. 675-683.

- [35] Tumidajski, P. J., "Electrical conductivity of Portland Cement Mortars," *Cement and Concrete Research*, Vol. 26, 1996, pp. 529-534.
- [36] Nataliya H., Hooton R. D., and Mills R. H., "Pore Structure and Permeability," reprint from the STP 169 C of the American Society for Testing Materials, pp. 240-260, ASTM, Philadelphia, 1994.

Pedro Castro¹ and Lucién P. Véleva¹

Time of Wetness and Temperature as Tools to Evaluate Corrosion Risk in Concrete Blocks Exposed to a Humid Tropical Environment

Reference: Castro, P. and Véleva, L. P., “Time of Wetness and Temperature as Tools to Evaluate Corrosion Risk in Concrete Blocks Exposed to a Humid Tropical Environment,” *Marine Corrosion in Tropical Environments, ASTM STP 1399*, S. W. Dean, G. Hernandez-Duque Delgadillo, and J. B. Bushman, Eds., American Society for Testing and Materials, West Conshohocken, PA, 2000.

Abstract: The internal relative humidity (RH) during the setting, curing and service life is one of the factors that influences on the durability of any concrete structure. However, it does not show evidence of rebar deterioration since local corrosion products formed change the critical RH value. For this reason, the measurements of the RH in concrete, as many authors have stated in the literature, are not accurate enough to predict the development of the corrosion process. The time of wetness (TOW) and the moisture content are, however, more acceptable parameters to survey the structure durability. This paper discusses the information that the concrete internal temperature (T) and the TOW provide regarding durability, when changes in the external environmental parameters, the geometry of the structure and its orientation with respect to the sun take place. The monitored data are from concrete exposed to humid tropical atmosphere of Yucatan Peninsula, southeast of Mexico. Some of the results indicated that there are specific tendencies regarding geometry and orientation of the specimens. The TOW distribution found in this work would allow the structure designers to define the concrete thickness over the steel bars based on the orientation and geometry of the structural element and in terms of the direction in which the environmental parameters act.

Keywords: moisture, relative humidity, temperature, time of wetness, corrosion, durability, concrete

¹ Research Professors, Applied Physics Department, Corrosion Group, Centro de Investigación y de Estudios Avanzados (CINVESTAV- IPN), Unidad Mérida, A.P. 73, C.P. 97310, Mérida, Yucatán, México.

Introduction

Moisture content and internal relative humidity (RH) are two of the most influential parameters on the durability of concrete structures. The moisture distribution is determined, mainly, by the concrete composition, the curing and the micro-climate in its different parts [1]. When the structure is new, the internal moisture governs the concrete hardening and curing. As a consequence, it controls the permeability to gases, water and aggressive ions. A lack of moisture at early ages produces not only reduced and defective cement hydration, but also a porous surface and drying shrinkage that will have a latter influence on the penetration of aggressive agents [2]. Also, the cement hydration can cease if the RH falls below 80% [3].

On the other hand, the moisture availability at intermediate to advanced ages can produce concrete deterioration. The pore saturation is one of the factors that control the oxygen availability and, therefore the corrosion rate. For example, when the moisture content saturates the pores, the entrance of gases like CO₂ is avoided but the chlorides access by diffusion is favored. However, a carbonation process together with a chloride entrance can take place simultaneously if the pores are partially saturated and produce a loss of alkalinity together with a higher tendency to corrosion deterioration [4]. The carbonation can affect the permeability through the concrete cover because the involved reaction modifies the pore structure of the cement paste matrix [2]. In general, moisture plays a significant role in concrete chemical reactions and, therefore in the processes associated with its deterioration [1].

The above circumstances have led to several studies on the RH distribution within concrete with the objective of correlating them not only with that of the environmental conditions, but with the corrosion onset and other durability properties. For example, attempts to measure moisture profiles in situ (concrete structures immersed in seawater at depths from 20 to 50 mm) have been done in different ways [1]. It was recognized that the moisture penetration mechanism for indoor concrete is different from that of a structure exposed to seawater and that further studies are needed. In this way, partially sealed 100 mm concrete cubes specimens under laboratory exposure have shown that the curing time and the water/cement (w/c) ratio have little influence on the internal RH profiles [6]. The existence of a critical RH at which corrosion starts has also been suggested [3] (80% for laboratory conditions and 70% for field conditions) and it has been recognized that the external RH is lower than the internal one when chlorides are present in concrete [5].

Despite the above findings, the difficulty of correlating the internal RH with the corrosion rate and the external RH is recognized [5]. There are also authors who express the inability to find correlation between the internal and environmental RH under their test conditions [6].

The works mentioned represent a substantial effort and the results suggest that not only the internal RH but the time of wetness (TOW) should be used as a more accurate parameter to represent the deterioration process (for example rebar corrosion).

The RH can be defined as the percentage ratio of the water vapour pressure in the atmosphere compared with that, which would saturate the atmosphere at the same temperature:

$$RH = \frac{\text{Saturated vapour pressure of H}_2\text{O at dew point temperature}}{\text{Saturated vapour pressure of H}_2\text{O at ambient temperature}} \times 100 \quad (1)$$

However, the same RH value can result in several levels of saturation. Instead, the TOW takes into consideration all the means by which an electrolyte solution is maintained on a metal surface. Therefore, it really determines the duration of the electrochemical corrosion process [7] and denotes explicitly when the mass transport, charge transfer or electrochemical corrosion are possible.

This work shows the influence of several environmental parameters associated with a humid tropical climate (T, RH, rain, sun) on the T and TOW registered at different depths in a concrete block. Also, the influences of the concrete block orientation with respect to the sun and its geometry on the T and TOW are discussed.

Experimental

Specimen Design

The Fig. 1 represents a general view of the concrete sample and data acquisition system in use.

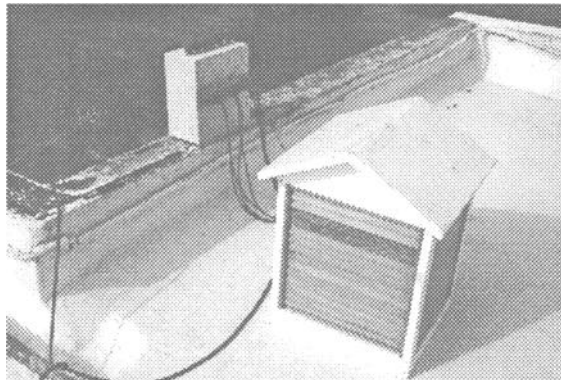


Figure 1 - General view of the concrete block and data acquisition system

The specimen consisted of a 300 x 300 x 150 mm concrete block as illustrated in Fig. 2. An ASTM Type I portland cement, crushed aggregates, tap water and a common w/c ratio of 0.5 were used to construct the block. Several PVC fittings, as used in other works [3,6], were embedded in different positions with the objective of using them to introduce the sensors for continuing monitoring of T and TOW. Six

PVC fittings were positioned at 75 mm depth from the thinnest block face (section A-A' from Fig. 2). This was made in order to observe the influence of the T and RH from the external environment, as well as that of the sun exposure effect during the day in the concrete internal T and TOW values. This configuration also allowed the observation of the influence of the environment on the concrete edges. The other six PVC fittings were embedded at different depths (15, 25, 40, 65 and 75 mm) in order to observe the influence of the concrete permeability on the T and TOW. One of the differences between this block and others [6] was that none of the concrete faces was sealed in order to examine the environment effects in all directions. The block was cured in a humidity chamber (approx. 95% RH and T of 23°C) according to ASTM Practice for Making and Curing Concrete Test Specimens in the Field (C31-91).

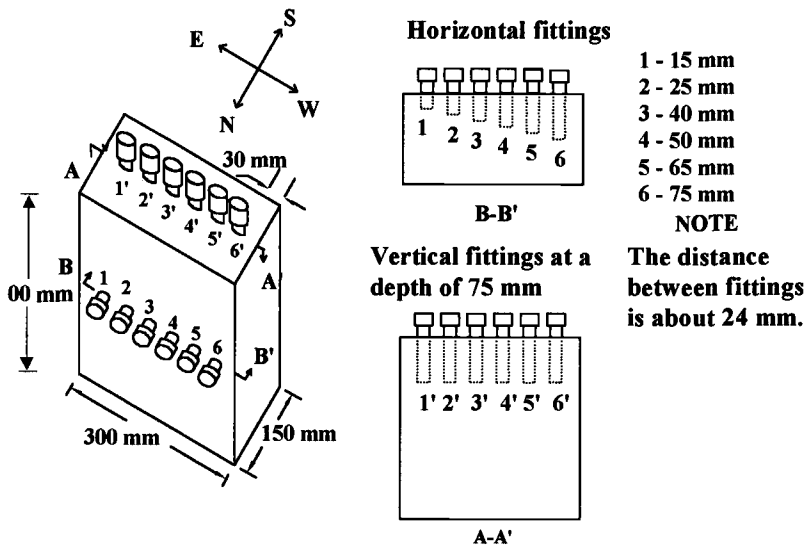


Figure 2- Scheme of concrete specimen.

Test Site Characterisation

The specimen was exposed in a rural-urban test station (CINVESTAV-IPN Merida Unit) after curing. The test station is located at 30 km from the Gulf of Mexico in the tropical humid climate of the Yucatan Peninsula. This environment was chosen due to its low chloride level contamination [8]. In this manner, the measured TOW would not be influenced by the deposition of chloride and its hygroscopy. Another ongoing stage of the project involves exposure at marine sites. The concrete block was oriented in a north-east direction in such a way that its thinnest faces would receive the first and last sun contact, respectively, as observed in Figs. 1 and 2.

It is well known that the humid tropical climate is very aggressive and it is characterized by high annual T and RH values. It has two marked seasons: dry winter

period and summer rainy season. The first one corresponds to the winter months when the airborne salinity increases due to the prevailing north winds that cross the Gulf of Mexico, and it is followed by the summer rainy period with low atmospheric contamination. During this latter season, the rain washes the concrete surface and prevents salt accumulation. The calculated annual TOW (TOW_{calc}) of the rural-urban station according ISO Corrosion of Metals and Alloys. Corrosivity of Atmospheres. Classification (9223-1992) is about 4 840 h [9] is based on the external T and RH. Besides, it occurs in high temperature ranges. For example, 54% to 64% of TOW is in the interval of 20°C to 25°C.

Sensors and Data Acquisition Device

An electronic device with software (patent pending) was designed and constructed to acquire, store and transmit the T and TOW data to a computer. The device stores data continuously over a period of 20 days. Fig. 3 shows a flow diagram of the apparatus. It has possibilities of connecting up to eight independent channels (4 for T and 4 for TOW). The T and TOW were measured using specific electronic components and appropriated capacitive Cu/Au TOW sensor, according to ASTM Practice for Measurements of Time of Wetness of Surfaces (G84-89). The data were acquired hourly and processed through commercial spreadsheets. The selection of the fittings, in which the sensors were going to be located, was based on previous finding [10], made with a portable T/RH meter. The results of that research indicated that the depths of 15, 40, 65 and 75 mm were the most representatives to illustrate the environmental effects on the internal T and TOW. Measurements through portable T/RH meters made the TOW calculation impractical [10].

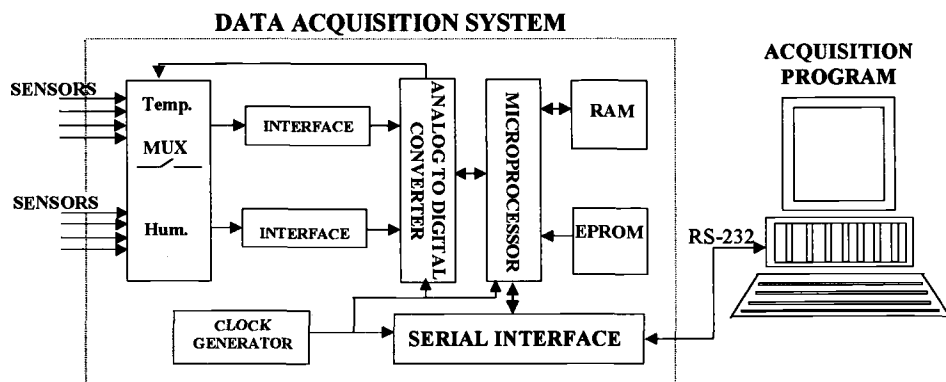


Figure 3 -Flow diagram for acquiring, storing and transmitting T and TOW data from concrete block.

Results

The data presented here are only a few examples of those obtained during a year of exposure and they correspond to comparisons between the external and the internal concrete T and TOW. Comparisons in corrosion terms will be presented elsewhere.

Fig. 4 shows an example of the daily T and TOW records of the external environment and four different concrete block depths.

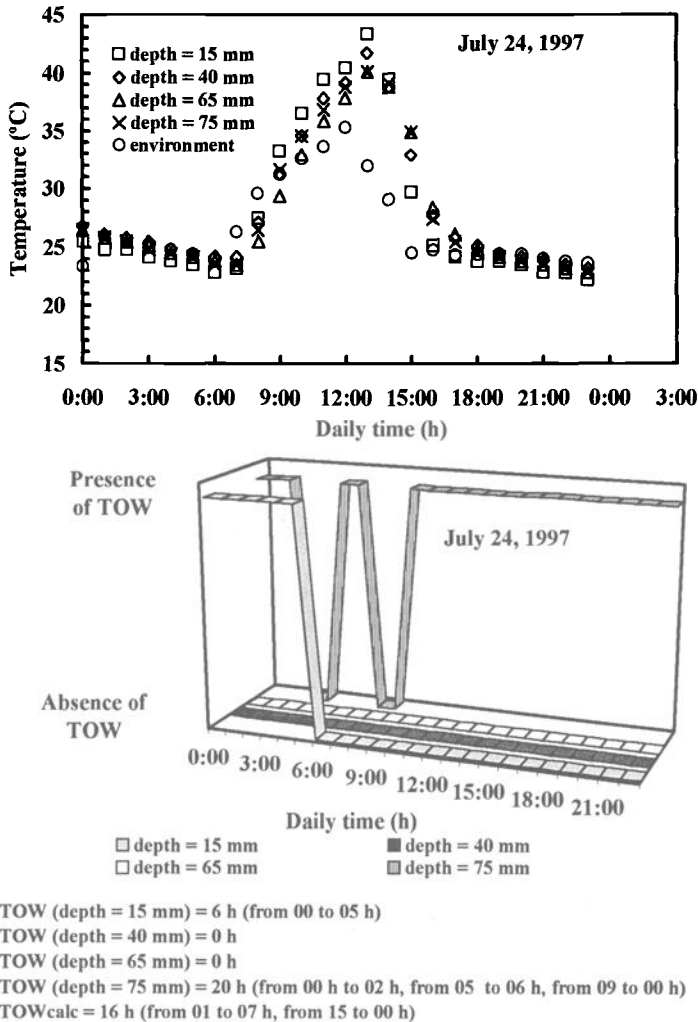


Figure 4 - Daily data of T and TOW recorded at different depths of concrete exposed to a humid tropical climate during rainy day of the summer period.

The day of the measurement (July 24) is part of the summer rainy period and precipitation occurred from 15:00 h to 18:20 h. The daily changes in the internal concrete T value followed those of the external environment. However, the external T becomes out of phase during the period with the greater sun incidence. A small but clear difference among the T values at different concrete depths is observed in this period only. From midnight to sunrise (00:00 h to 07:00 h) and after sunset (18:00 h to 23:59 h) the concrete T at all depths is similar to that of the external environment (only 2°C to 3°C hotter). This behavior was repeated during all the days of the experiments and demonstrated that the concrete internal T and TOW are a clear logical response to that of the external environment.

On the other hand, in the concrete block the TOW showed no presence of moisture at 40 mm and 65 mm depths despite being a rainy day. However, TOW values were observed at 15 mm and 75 mm, the latter being the greatest (20 h). This latter observation was due to the wind driven rain that blew on the south concrete block face. The external TOW_{calc} was 16 h. These data show that not only the depth at which a reinforcing bar is placed, but its position in the structural element, as well as the concrete thickness, and the rain direction, are the determinant factors for the internal dampening.

The TOW_{calc} of dry summer days is about 12 h as shown in Fig. 5 (July 29). The changes of T at different depths in the concrete follows that of the environment, with the concrete being hotter at superficial depths with temperatures ranging from 43°C to 44°C. The east-west oriented faces are hotter during the day (15 mm and 40 mm depths) than those north-south oriented (65 mm and 75 mm). As a consequence, the west face that has accumulated less sunshine becomes cool faster than the east one and that is the reason that the TOW was detected there first.

Discussion

The critical RH (RH_{crit}) is a value under which corrosion will not occur [3]. However, it is important to know if such RH_{crit} refers to a clean bar or to one containing corrosion products [11]. There is a second RH_{crit} if the bar has corrosion products and it is due to their hygroscopic nature or that of the chlorides having a role in the process. A third RH_{crit} has also been detected in the steel [12]. In this way, for example, an atmospherically exposed metal can start to corrode at a very low rate at 60% RH [13], but a sharp corrosion increase can take place at 75% to 80% RH, due to the capillary moisture condensation within the rust [11, 14]. There is further increase in the corrosion rate above 90% RH that may correspond to the vapour pressure of saturated ferrous sulfates in solution [15]. It is generally accepted that the first RH_{crit} is common for all the metals without corrosion but the secondary and tertiary values depend on the circumstances. The same phenomena may occur in reinforced concrete. Results of RH inside concrete during a year of exposure [5] show how the reinforcing steel corrodes from negligible values (0.06 $\mu\text{A}/\text{cm}^2$) to significant ones (0.7 $\mu\text{A}/\text{cm}^2$); this is two orders of magnitude.

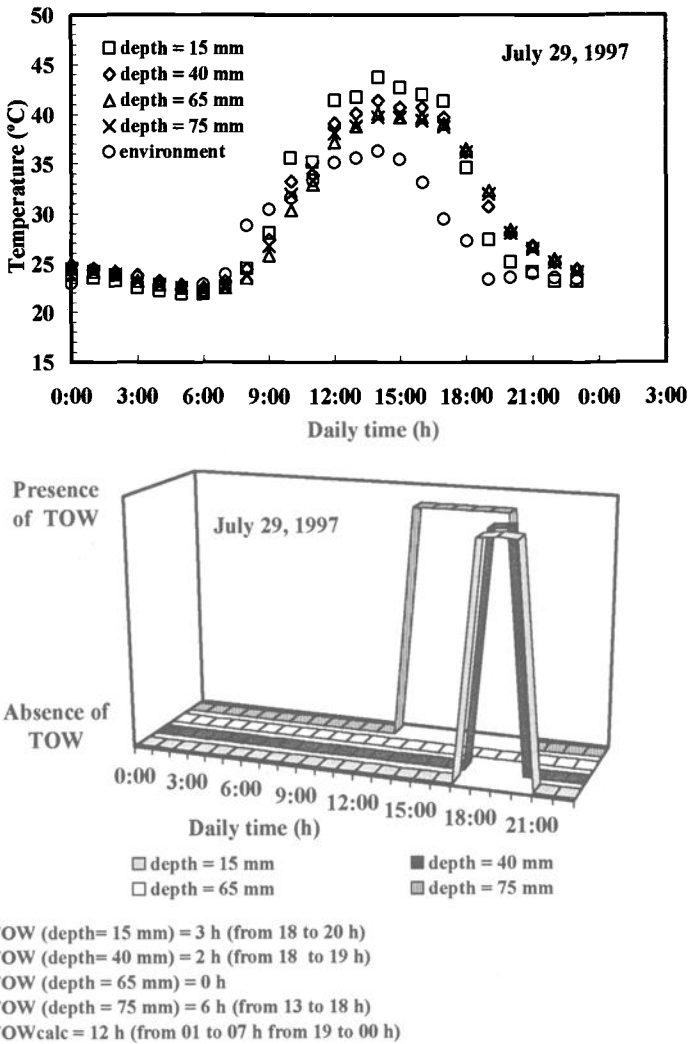


Figure 5 - Daily data of T and TOW recorded at different depths of concrete exposed to a humid tropical climate during a dry day of the summer period.

However, these results show also that different values of RH can give rise to different instantaneous corrosion rates (for example, data from Ref. 5 show that a 0.1 $\mu\text{A}/\text{cm}^2$ corrosion rate value can be obtained with RH from 55% to 90%). This behavior confirms the existence of several RH_{crit} values at which a significant corrosion rate can take place, and it is due to the changing steel surface conditions with time and according to the aggressive agents action and the corrosion products

layers modification. Other authors [3] have found critical RH values of 80% that are valid only for their conditions (2% chloride contaminated mortars in laboratory conditions) and recognize the need for confirming the results in the field. The existence of different RH_{crit} values will always make the correlation with other parameters difficult. This leads to use of a more accurate parameter, such as the time of wetness, that takes into account the duration of the electrolyte and therefore the corrosion process only [7]

On the other hand, the susceptibility to the initiation and propagation of the corrosion process is varied and should be studied according to the conditions of each particular environment. The results presented in this work allowed the observation of how the environmental parameters of a humid tropical climate influence the concrete internal T and TOW distribution.

The information registered in the concrete block is important to concrete structure designers and shows that, at least for the conditions of this exposure, the concrete cover on the structure's west side should be thicker than those oriented toward the east. This is due to the TOW, which is longer in the west than in the east face. The existence of a greater TOW will cause a higher possibility of gases to react, such as the CO_2 that can cause the concrete carbonation. More research is needed in order to find possible correlations between TOW and the overall corrosion process of steel in concrete.

Conclusions

The TOW is a tool that allows investigators to understand the phenomena related to the reinforced concrete durability with more clarity than the RH. The TOW distribution found in this work will allow structure designers to define the concrete thickness over the steel bars, based on the orientation and geometry of the structural element and in terms of the direction in which the environmental parameters act.

Acknowledgments

The authors are indebted to CONACyT (contracts 2667 PA and 2186 PA) and CINVESTAV-IPN Unidad Mérida for partial support for this research. The authors are grateful to the G-01 ASTM Committee for fruitful comments (Dr. Neal S. Berke). The opinions expressed in this work are those of the authors and not necessarily of the supporting organisations. The authors also recognise the technical support of M. Balancán, F. Kantún and J. Bante.

References

- [1] Nilsson, L. O., "Moisture in Marine Concrete Structures," 7th International Conference on Durability of Building Materials and Components, Stockholm, 1996, pp. 23-45.
- [2] Parrott, L. J., "Moisture Profiles in Drying Concrete", *Advances in Cement Research*, Vol. 1, 1988, pp. 164 – 170.
- [3] Enevoldsen, J. N., Hansson C. M., and Hope, B. B., "The Influence of Internal Relative Humidity on the Rate of Corrosion of Steel Embedded in Concrete and Mortar," *Cement and Concrete Research*, Vol. 24, 1994, pp. 1373-1382.
- [4] Andrade, C., *Inspección de Obras Dañadas por Corrosión de Armaduras*, Ed. ACUR.CSIC, 1989.
- [5] Andrade, C., Sarria, J., and Alonso, C., "Statistical Study on Simultaneous Monitoring of Rebar Corrosion Rate and Internal Relative Humidity in Concrete Structures Exposed to the Atmosphere", 4th International Symposium on Corrosion of Reinforcement in Concrete Construction, Cambridge, UK, 1996, pp. 233-242.
- [6] Parrott, L. J., "Factors Influencing Relative Humidity in Concrete," *Magazine of Concrete Research*, Vol. 43, 1991, pp. 45-42.
- [7] Shreir, L. L., Jarman, R. A. and Burstein, G. T., 1994a, *Corrosion*, Vol. I, Butterworth-Heinemann, Ltd., Oxford, England.
- [8] Corvo, F., Haces, C., Betancourt, N., Maldonado, L., Véleva, L., Echeverría, M., Rincón, O., and Rincón, A., "Atmospheric Corrosivity in the Caribbean Area," *Corrosion Science*, Vol. 39, 1997, pp. 823-833.
- [9] Véleva, L., Pérez, G., and Acosta, M., "Statistical Analysis of the Temperature-Humidity Complex and Time of Wetness of a Tropical Climate in the Yucatán Peninsula," *Atmospheric Environment*, Vol. 31, 1997, pp. 773-776.
- [10] Castro, P., Véleva, L., and García, J., "Distribution of Relative Humidity and Temperature in Concrete Exposed to a Rural-Urban Atmosphere," (in Spanish), XII Congreso Nacional de la SME, 1997, pp. 42-50.
- [11] Weiss, J., "Investigation on the Radical HO₂ in Solution," *Transaction of the Faraday Society*, Vol. 31, 1935, pp.668-681.

- [12] Schikorr, G., "Die Bedeutung des Schwefeldioxyds für die Atmosphärische Korrosion der Metalle," *Werkstoffe und Korrosion - Materials and Corrosion*, Vol. 15, No. 6, 1964, pp.457-463.
- [13] Skorchel'eti, V. V. and Tukachinsky, S. E. "Atmospheric Corrosion of Metals at Relative Humidities Below 100% Adsorption Structure of Rust," *Journal Applied Chemistry (URSS)*, Vol. 28, 1955, pp. 651-655.
- [14] Barton, K. and Bartonova, Z., "Concept of Critical Humidity in the Atmospheric Corrosion of Steel," *Werkstoffe und Korrosion - Materials and Corrosion*, Vol. 21, No. 2, 1970, pp. 85-88.
- [15] Schikorr, G. "Ueber die Nachahmung des Atmosphärischen Rostens in Laboratorium," *Werkstoffe und Korrosion - Materials and Corrosion*, Vol. 18, No. 6, 1967, pp. 514-521.

Lucien P. Véleva¹ and Maria C. Cebada²

Model Solutions of Concrete Environment and Effect of Chloride Ions on the Electrochemical Corrosion Behavior of Reinforcing Mild Steel

Reference: Véleva, L. P. and Cebada, M. C., “**Model Solutions of Concrete Environment and Effect of Chloride Ions on the Electrochemical Corrosion Behavior of Reinforcing Mild Steel,**” *Marine Corrosion in Tropical Environments, ASTM STP 1399*, S. W. Dean, G. Hernandez-Duque Delgadillo, and J. B. Bushman, Eds., American Society for Testing and Materials, West Conshohocken, PA, 2000.

Abstract: Two model solutions have been used in this study in order to simulate the corrosion behavior of mild steel rebars in the pore concrete environment. The first one is based on saturated calcium hydroxide ($\text{Ca}(\text{OH})_2$, $\text{pH } 12.7 \pm 2$) and cement (portland Type I) extract solution ($\text{pH } 12.7 \pm 2$) in open air, at room temperature ($24 \pm 1^\circ\text{C}$). The effect of chloride ions (5g/l and 10g/l NaCl) was studied in both model solutions. Electrochemical techniques such as potentiodynamic polarization curves and electrochemical impedance spectroscopy (EIS) have been performed in a classical three-electrode cell. Also additional information was obtained by SEM and EDAX analysis. It seems that there is a difference in the way each solution simulates the behavior of steel, because the passive films formed show dissimilar topography, composition and anticorrosion protectiveness. The presence of chloride ions allows one to see more clearly the difference between the model solutions and the way each one interacts with the reinforcing steel. In this case the cement solution provides a more protective film for the reinforcing steel.

Keywords: model solution, concrete environment, reinforcing steel, chloride effect, electrochemical impedance spectroscopy (EIS), polarization curves, SEM, EDAX

Introduction

Steel-reinforced concrete is a widely used and durable construction material [1], because the steel is usually protected from corrosion by a passivating layer, which forms

¹ Research Professor, Applied Physics Department, CINVESTAV-IPN, Unidad Mérida, Km 6 Carretera a Progreso, C.P. 97310, Mérida, Yucatán, México.

² Master Degree Student, UADY, F.Q., C.P. 97150, Mérida, Yucatán, México.

in alkaline conditions prevailing in the concrete.

Chemically, the hydration products of the cement (calcium hydroxide -Ca(OH)_2 - in combination with small quantities of sodium or potassium ions) present in the moisture of the concrete pores, are highly alkaline and that is what assures a complete electrochemical passivation of the steel embedded in it, due to the formation of a protective film of an iron oxide (Fe_3O_4 or $\gamma\text{-Fe}_2\text{O}_3$) on the surface of the metal [2-4]. However, it is well known worldwide that the deterioration of the reinforced concrete caused by the corrosion of the steel rebars [5], due mainly to the presence of chloride ions in combination with the wetness (electrolyte), is typical for the tropical climate in a coastal zone Southeast of Mexico. Therefore, the lifespan of structures (hotels, bridges, dock piles, etc.) in such a climate is great by [6, 7].

The corrosion resistance of the reinforced concrete can be studied by a) field test in natural conditions, or b) accelerated tests carried out in different artificial atmospheres (model solutions and weathering chamber). The first group provides very confident results, although it is necessary a very long period of time to get data. In the past few years, the use of concrete model solutions (simulating the environment of the pore) applying electrochemical techniques, is gaining attention [8, 9]. Generally, the most common model solution is based on Ca(OH)_2 and sometimes with addition of sodium and potassium hydroxide [10, 11]. The pore solution of the concrete has a complex composition [12] that includes a variety of compounds besides Ca(OH)_2 , therefore a cement extract also has been proposed as a model solution. Those kind of model solutions allow one to obtain comparative results on metals behavior and to control some parameters that otherwise would be very difficult to achieve, like in natural and *in situ* tests. The effect of adding chlorides to such solutions has been employed in mechanistic studies [10, 13].

The data presented in this study are part of a wider investigation of mild and stainless steels in concrete pore model solutions, using electrochemical techniques such as polarization curves and electrochemical impedance spectroscopy, in order to obtain rapid and comparative information on the corrosion behavior of those steels in the presence of chloride ions.

Experimental

Model Solutions

Two kind of model solutions were used in this study:

- a) Saturated Ca(OH)_2 solution ($\text{pH } 12.7 \pm 0.2$) without and with the addition of 5 g/l and 10 g/l sodium chloride.
- b) Extract of cement solution ($\text{pH } 12.7 \pm 0.2$) without and with the addition of 5 g/l and 10 g/l sodium chloride. The cement used was ordinary portland cement (Type I, ASTM-C-150), produced in Mexico and the water-cement (w:c) ratio was 1:1 [12]. The mixture was left 24 hours for hydration and filtered. The pH measurements were performed with a Corning pH-meter.

All the reactants were analytical grade and the water used was deionized quality. All the solutions were kept in closed recipients to prevent carbonation by the atmosphere.

The composition of the cement and the cement solution is given in Table 1. The conductivity of the saturated $\text{Ca}(\text{OH})_2$ solution is 5.53×10^{-3} S/cm, whereas the cement solution is 12.6×10^{-3} S/cm.

Table 1 - *Composition of cement and cement solution according to the producer's chemical analysis.*

Compound	% per weight in the cement	Present in the cement solution
SiO₂	19.96	-
Al₂O₃	4.87	as Al ³⁺
Fe₂O₃	2.89	as Fe ³⁺
CaO	66.84	as Ca ²⁺
K₂O	0.39	-
Na₂O	0.08	-
SO₃	2.42	-
MgO	1.16	as Mg ²⁺
Silicates	72.00	-
Aluminosilicates	5.00	-
Fluorosilicates	13.00	-

Electrochemical Measurements

The electrochemical techniques were performed in a standard electrochemical three-electrodes cell. The steel specimens used as working electrodes (0.9 cm of diameter) were cut from mild steel bar having the following composition (by mass percentage, %): C = 0.40, Mn = 0.97, S = 0.035, P = 0.014, Si = 0.15, Cr = 0.10, Ni = 0.08, Cu = 0.37, Sn = 0.03, Mo = 0.03. All steel samples (circular shape with an area of 0.64 cm²) were consecutively polished with wet emery paper (100, 400, 600 grit), rinsed with water, degreased and dried before use. A saturated Calomel electrode (Corning) was employed as a reference electrode while a platinum cylinder sheet (30 cm²) as auxiliary electrode. All the measurements were carried out in open air (in the presence of oxygen) at room temperature (24 ± 1 °C).

Potentiodynamic polarization curves were registered in a potential range from -0.35 to 1.5 V at a scanning rate of 0.1 mV/s, using a Gamry Electrochemical Measurement System CMS100. The electrochemical impedance spectra (EIS) were obtained with Gamry Electrochemical Impedance System CMS300, the sine-wave amplitude was 10 mV and the frequency range was 10kHz to 1mHz. The EIS tests were performed without and with the application of d.c. external polarization corresponding to the active and passive regions of the steel polarization curves in the given solutions.

At the beginning of the measurements all the working electrodes were left immersed in each solution for 45 minutes without the application of potential, to stabilize the open circuit potential and allow a uniform passive film formation on the surface.

Surface Analysis

JSM-6300 Scanning Microscope coupled with EDAX equipment were used to obtain additional information about the topography and composition of the films formed on the reinforcing steel surface after 21 days of immersion in each of the model solutions.

Results and Discussions

Potentiodynamic Polarization Curves

Figures 1 and 2 show the potentiodynamic polarization curves registered at different times of immersion in saturated $\text{Ca}(\text{OH})_2$ and cement solutions, respectively.

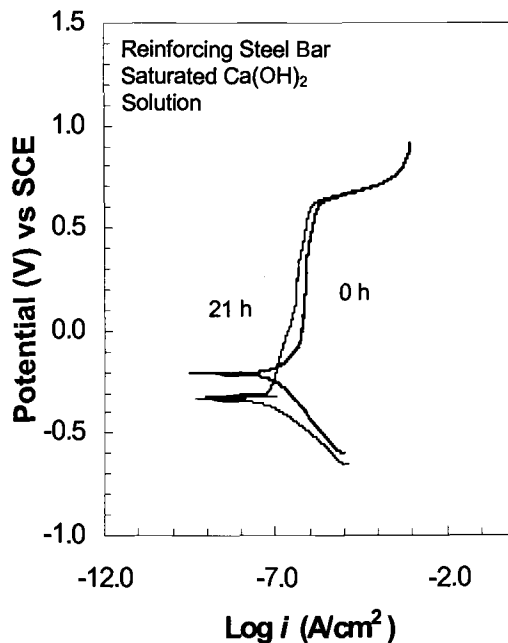


Figure 1 – Potentiodynamic polarization curves for the mild steel rebar at different times of immersion in the saturated $\text{Ca}(\text{OH})_2$.

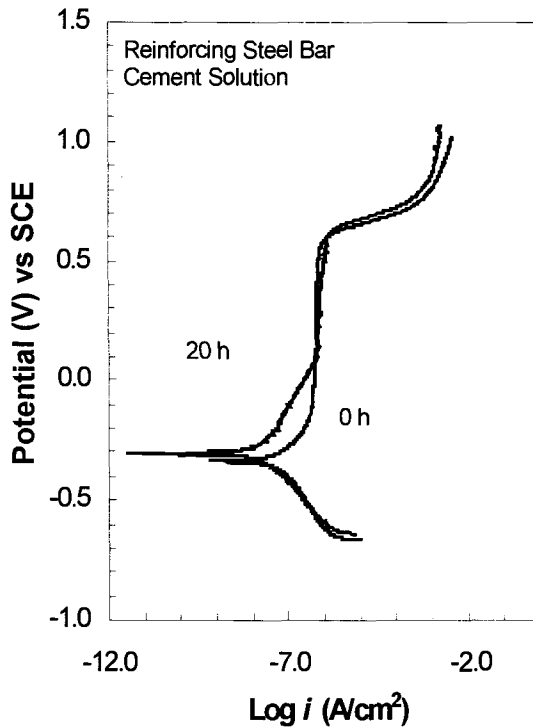


Figure 2 – Potentiodynamic polarization curves for the mild steel rebar at different times of immersion in the cement extract solution.

The observed passive region appears after a small active one. The reinforcing steel presents a similar passive behavior in both model solutions: saturated $\text{Ca}(\text{OH})_2$ (Figure 1) and cement solution (Figure 2). The passive region shows a tendency to decrease its amplitude while the immersion time increases, keeping a current density of about 10^{-6} A/cm^2 and shifting the open circuit potential towards a little more positive values in the cement solution and to more negative in the saturated $\text{Ca}(\text{OH})_2$ solution. With the increasing of immersion time the passive layer formed in each of the model solutions seems to be dissimilar. An Auger electron spectroscopy (AES) and X-ray photoelectron spectroscopy (XPS) study [12] have showed that the passive films formed in $\text{Ca}(\text{OH})_2$ solutions revealed differences in composition and thickness when compared to films formed in the paste (cement) solutions. It has been also reported [14-16], using the ellipsometric technique, that the passive film formed in calcium hydroxide $\text{Ca}(\text{OH})_2$ solution is closer to an iron oxyhydroxide (FeOOH) than to Fe_3O_4 or Fe_2O_3 . According to [12], the outermost layers of the passive film formed on the steel in cement paste

solutions are composed essentially of FeOOH . In aerated solutions Fe_3O_4 was the intermediate oxidation product on the steel surface [13], for periods longer than 2 s the composition of the film formed on steel in basic solution (pH 12) corresponds to FeOOH that covers the inner layer identified as Fe_3O_4 [15]. The concentration of that compound increases with the concentration of chloride in the solution (0.5 wt% and 1.0 wt%, pH ~13) [12]. It has been also reported [14-16] that the presence of chlorides in $\text{Ca}(\text{OH})_2$ solution seemed to change the composition, thickness, and density of the passive film. Using X-ray photoelectron spectroscopy (XPS) and secondary ion mass spectrometry (SIMS) it was found that water was incorporated in the passive film. Those authors conclude that this fact decreases the protective nature of the film because the water "paths" facilitate chloride ion penetration and consequent breakdown of the passive film. Those confirmations could be a good explanation for the differences observed above detected by the polarization curves.

In the presence of chloride ions (5 and 10 g/l) the initial potential (0 hours) shifts abruptly to more negative values as the concentration of those ions increases (Figures 3 and 4), with a more significant changes in the $\text{Ca}(\text{OH})_2$ model solution (Figure 3).

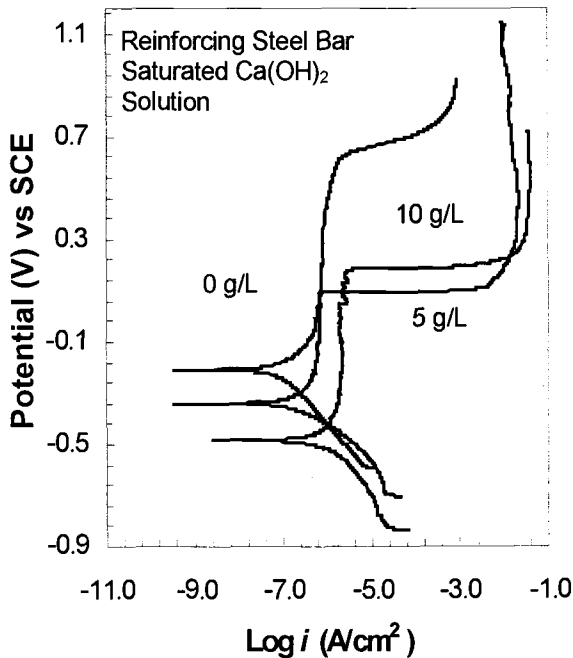


Figure 3 – Potentiodynamic polarization curves for the mild steel rebar in saturated $\text{Ca}(\text{OH})_2$ with 0, 5 and 10 g/l chlorides.

It can be seen, that in the cement solution (Figure 4) the passive region and its current density stay practically the same with the addition of 5 g/l NaCl, but it is markedly shortened in the presence of 10 g/l NaCl. These facts mean possibly that the film formed on the metal in the absence of chloride is enough resistant to provide a good corrosion protection even in the presence of 5 g/l, but at 10 g/l its effectiveness diminishes significantly. On the other hand, in the saturated model $\text{Ca}(\text{OH})_2$ solution (Figure 3) the reinforcing steel displays a dissimilar behavior: in the presence of 5 g/l NaCl, can be seen that the amplitude of the passive region decreases abruptly, shifting to more negative potential with the addition of chloride (5 g/l) and with a higher current density in the presence of 10 g/l. This fact confirms again that in this model solution the passive layer formed in absence of chloride is less protective than the one formed in cement extract solution and could be due to their different characteristics.

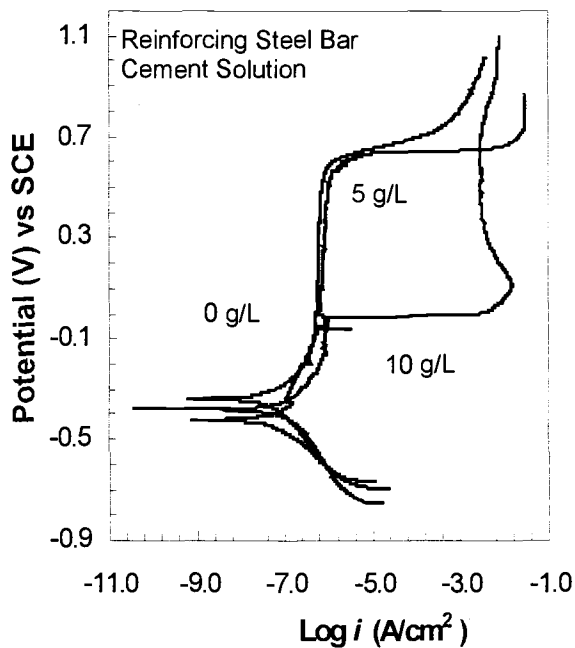


Figure 4 – Potentiodynamic polarization curves for the mild steel rebar in cement extract solution with 0, 5 and 10 g/l chlorides.

Electrochemical Impedance Spectra (EIS)

In order to obtain more information about the real state of steel, immersed in both model solutions, impedance spectroscopy measurements were performed without and with the application of polarization corresponding to the active and passive states, using the information provided by polarization curves. Figures 5-8 present the impedance spectra in the Nyquist type for the reinforcing steel bar in both model solutions without and with chlorides.

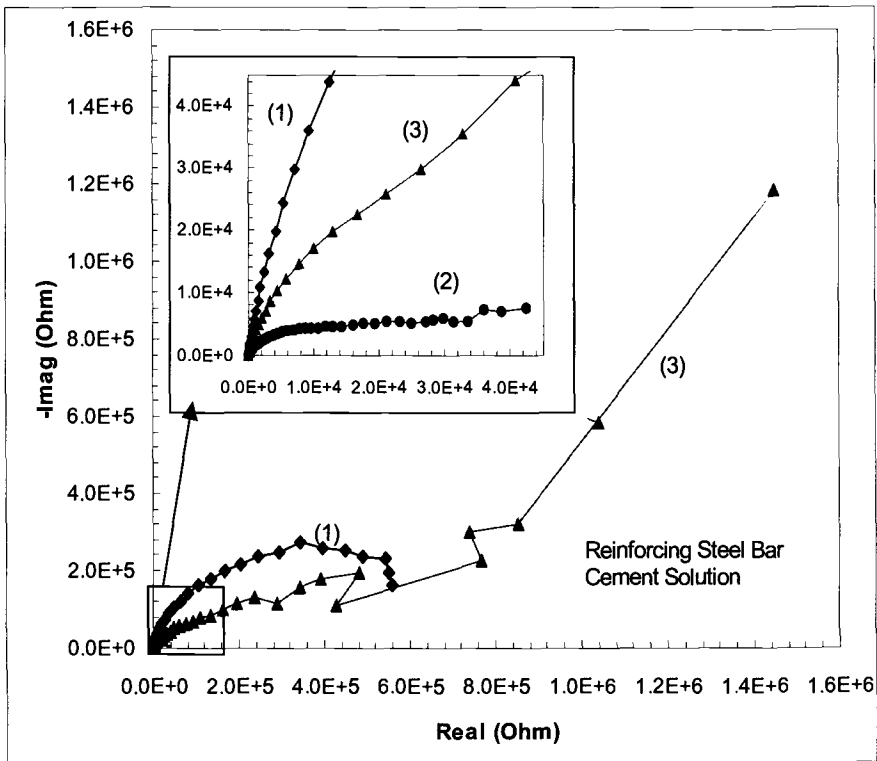


Figure 5 – EIS Nyquist diagram for mild steel in cement solution: (1) without polarization; (2) polarization in the active and passive regions (3).

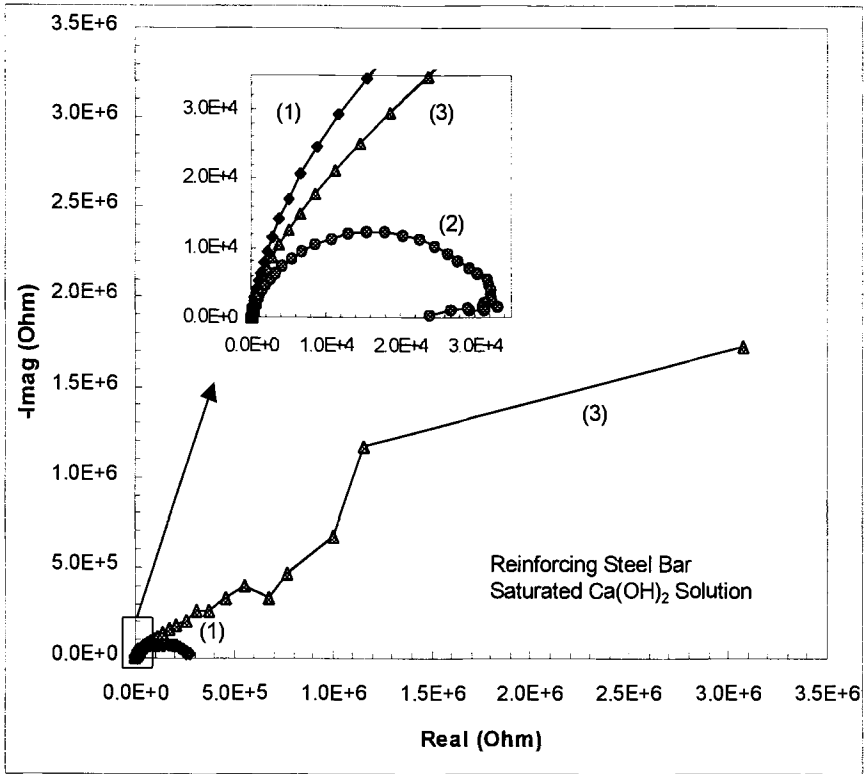


Figure 6 – EIS Nyquist diagram for mild steel in saturated $\text{Ca}(\text{OH})_2$ solution: (1) without polarization; (2) polarization in the active and passive regions (3).

It can be seen, in all Nyquist plots, that the spectra (1) and (3) are different, even though they both correspond to passive behavior: the spectra (1) represents the natural formation of the passive layer without application of polarization, while the spectra (3) represents the formation of the passive film induced by polarization. Also the results show that all the spectra (3) display a more capacitive behavior than all spectra (1). Therefore, there is a difference between the passive films because of the way they are formed in each of the model solutions, and it is more evident when the impedance spectra in the Bode type (Figures 9-14) are observed. Generally, three stages can be seen in the Bode diagrams: a) resistive behavior at very high frequencies; b) capacitive behavior in the majority of the frequency range; and c) a little resistive behavior at very low frequencies.

For the reinforcing steel in cement extract solution (Figures 9,11 and 13) the spectra (3), with polarization, exhibit a behavior that goes like this: in the solution free of

chlorides (Figure 9) the steel shows a capacitive behavior that stays the same in the presence of NaCl 5g/l (Figure 11), but with the addition of NaCl 10 g/l (Figure 13) the impedance value is smaller than the other two. This kind of behavior matches with the one observed in the polarization curves (Figure 4) for the passive regions.

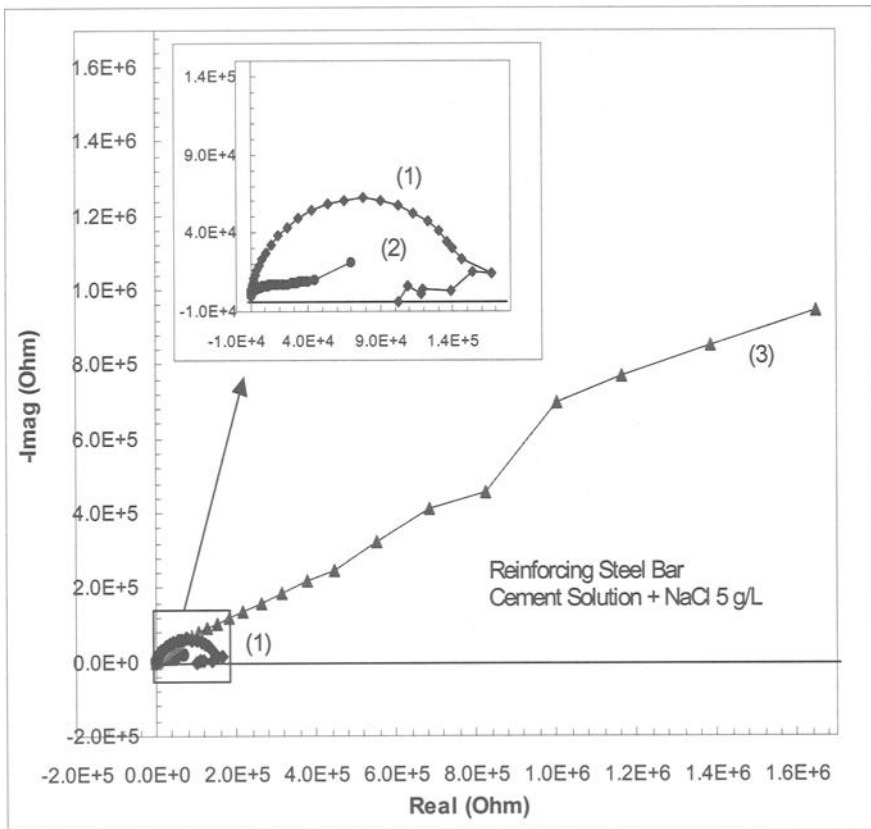


Figure 7 – EIS Nyquist diagram for mild steel in cement solution with 5 g/l NaCl: (1) without polarization; (2) polarization in the active and passive regions (3).

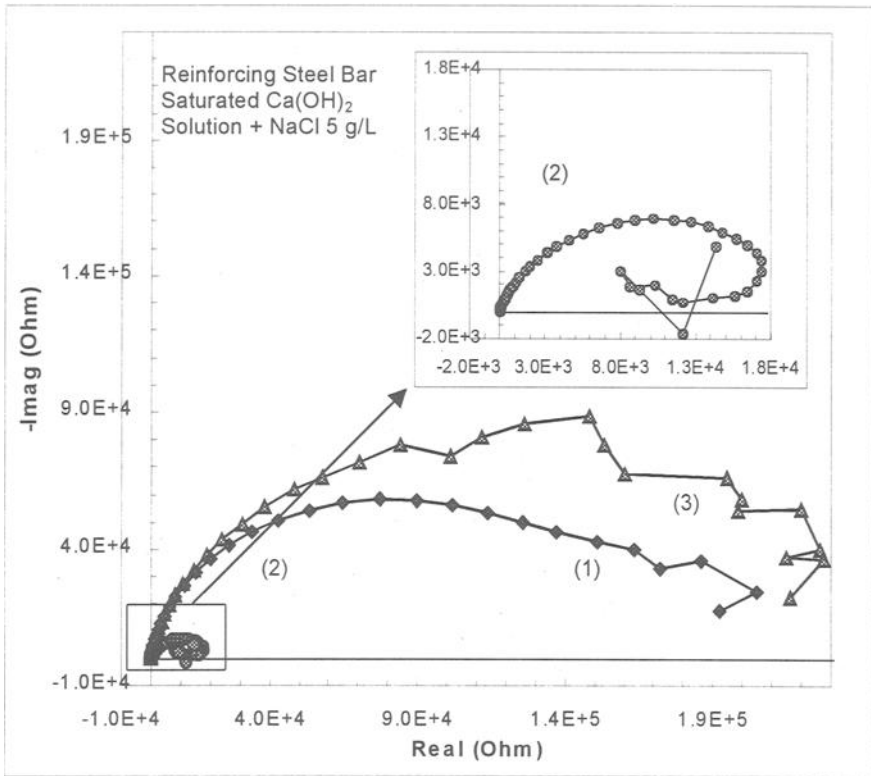


Figure 8 – EIS Nyquist diagram for mild steel in saturated $\text{Ca}(\text{OH})_2$ solution with 5 g/l NaCl: (1) without polarization; (2) polarization in the active and passive regions (3).

In the saturated $\text{Ca}(\text{OH})_2$ solution the Bode spectra (3) (Figures 10,12 and 14) show that in the presence of 5 g/l (Figure 12) chloride ions the capacitive behavior of steel diminishes abruptly its impedance value compare with the one obtain in the absence of chloride ions (Figure 10). With the addition of 10 g/l NaCl (Figure 14) the impedance value increases slightly compared with the one for 5 g/l. In the same way as before, this behavior matches with the one displays in the corresponding polarization curve (Figure 3).

The passive behavior of the reinforcing steel without the external polarization is shown in the Figures 9-14, spectra (1). The capacitive behavior (impedance value) of the steel in cement solution with the addition of 5g/l NaCl (Figure 11) can be seen to be decreased compared with the one observed in the absence of chloride ions (Figure 9),

but exhibits no change with the addition of 10 g/l NaCl (Figure 13). For the steel in the saturated $\text{Ca}(\text{OH})_2$ solution the impedance value stays the same without (Figure 10) and with 5 g/l NaCl (Figure 12), but with 10 g/l NaCl (Figure 14) the value drops markedly. These behaviors are contrary to the ones observed in spectra (3) (Figures 9-14) and in the polarization curves (Figures 3 and 4).

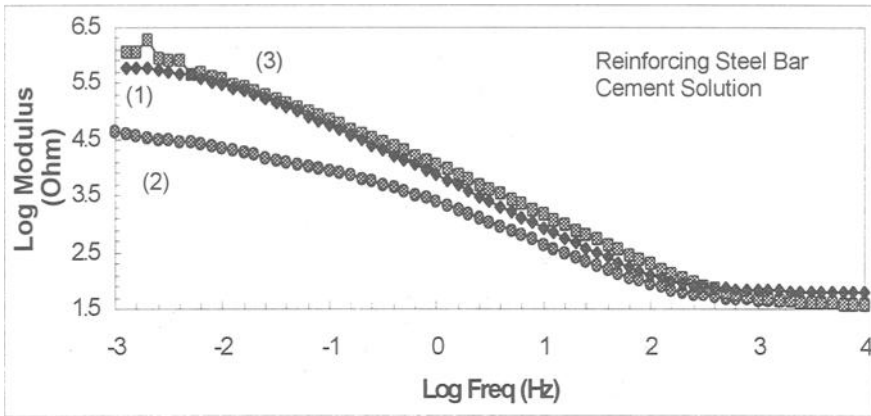


Figure 9 – EIS Bode diagram for mild steel in cement solution: (1) without polarization; (2) polarization in the active and passive regions (3).

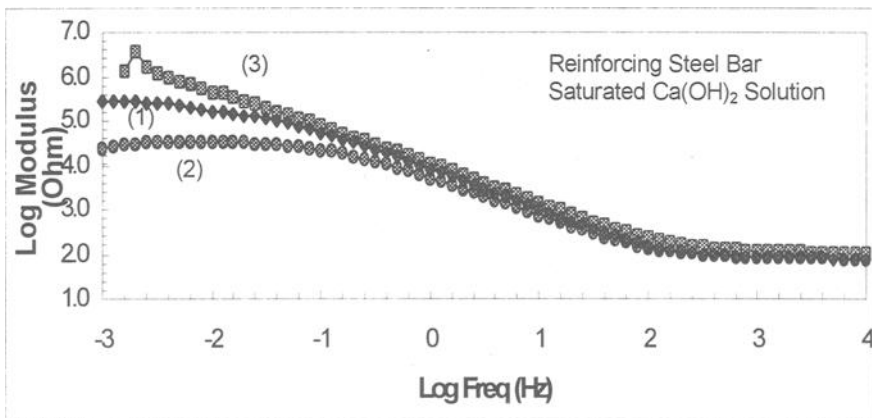


Figure 10 – EIS Bode diagram for mild steel in saturated $\text{Ca}(\text{OH})_2$ solution: (1) without polarization; (2) polarization in the active and passive regions (3).

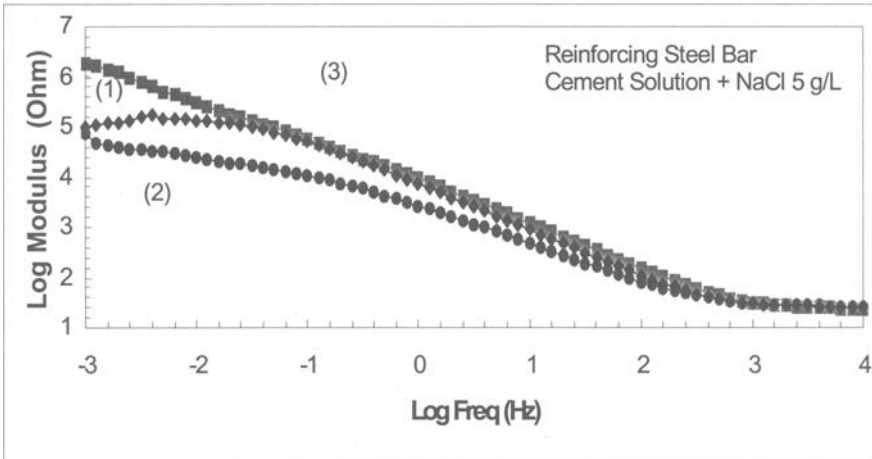


Figure 11 – EIS Bode diagram for mild steel in cement solution with 5 g/l NaCl: (1) without polarization; (2) polarization in the active and passive regions (3).

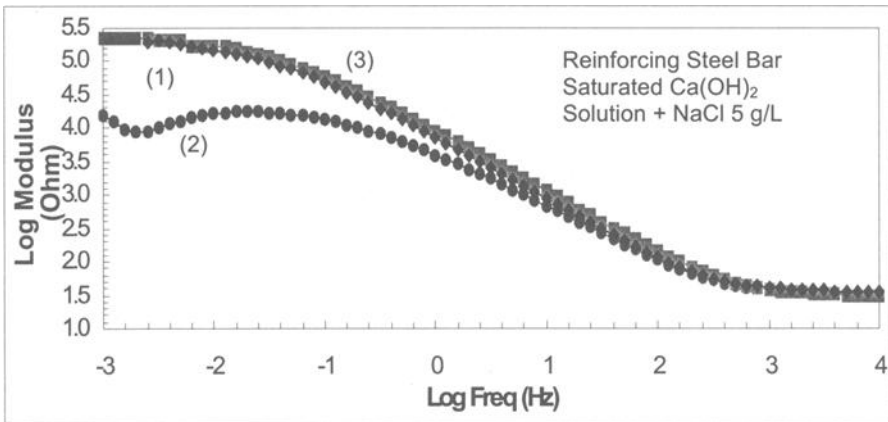


Figure 12 – EIS Bode diagram for mild steel in saturated Ca(OH)₂ solution with 5 g/l NaCl: (1) without polarization; (2) polarization in the active and passive regions (3).

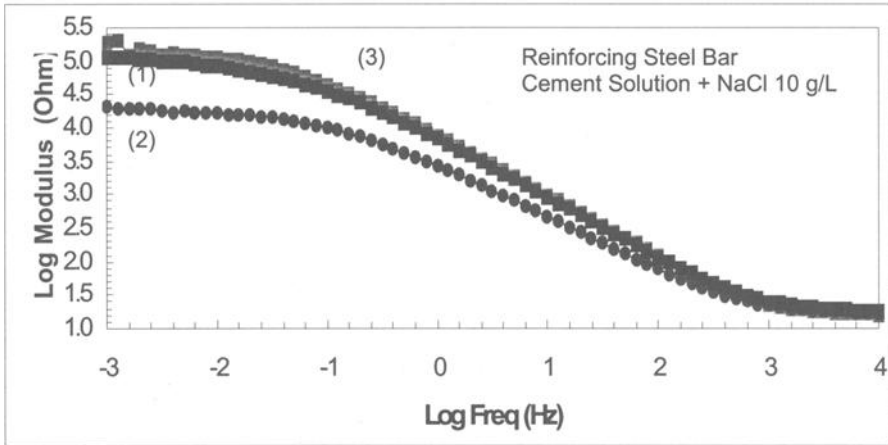


Figure 13 – EIS Bode diagram for mild steel in cement solution with 10 g/l NaCl: (1) without polarization; (2) polarization in the active and passive regions (3).

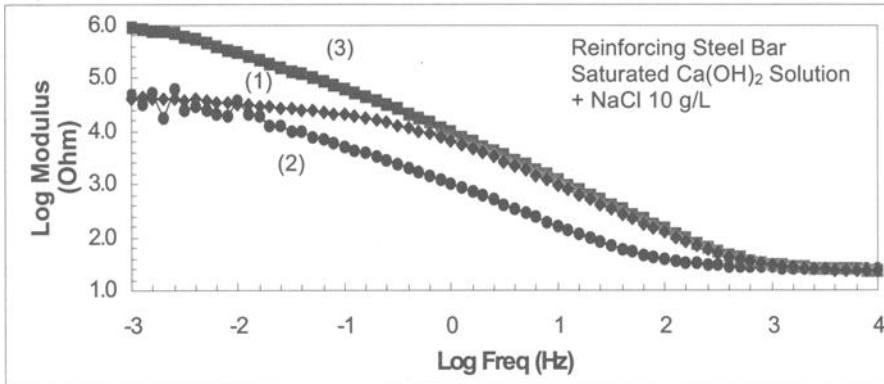


Figure 14 – EIS Bode diagram for mild steel in saturated Ca(OH)₂ solution with 10 g/l NaCl: (1) without polarization; (2) polarization in the active and passive regions (3).

Figures 15-17 show the SEM topography images of the layer formed on the reinforcing steel surface in both model solutions with the addition of 10 g/l NaCl (Figures 16, 17), and SEM of the control specimen surface immersed in no solution at all (Figure 15). The film formed in the cement solution (Figure 16) is apparently more homogeneous than the one formed in saturated $\text{Ca}(\text{OH})_2$ (Figure 17) and its appearance is different. Also can be seen from the EDAX film surface analysis that the peaks for Ca, Si, C, Cr and oxygen are higher in the cement solution (Figure 18) than the ones for the steel in saturated $\text{Ca}(\text{OH})_2$ (Figure 19). Therefore, the passive film formed in each one of the model solutions is different in composition, homogeneity, anticorrosion protectiveness and perhaps thickness. All those observations explain why the two model solutions do not produce similar behavior of steel.

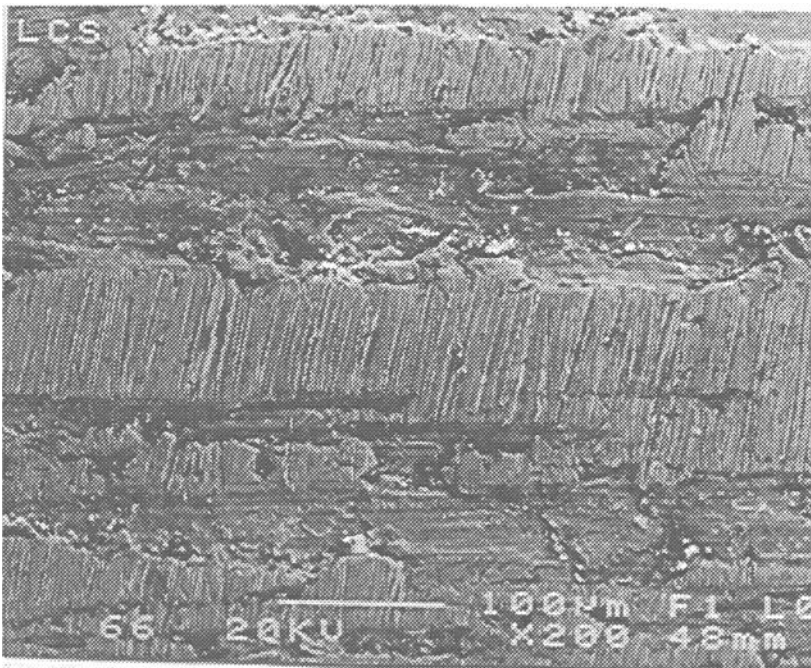


Figure 15 – SEM image of the reinforcing steel surface without being immersed in any solution.

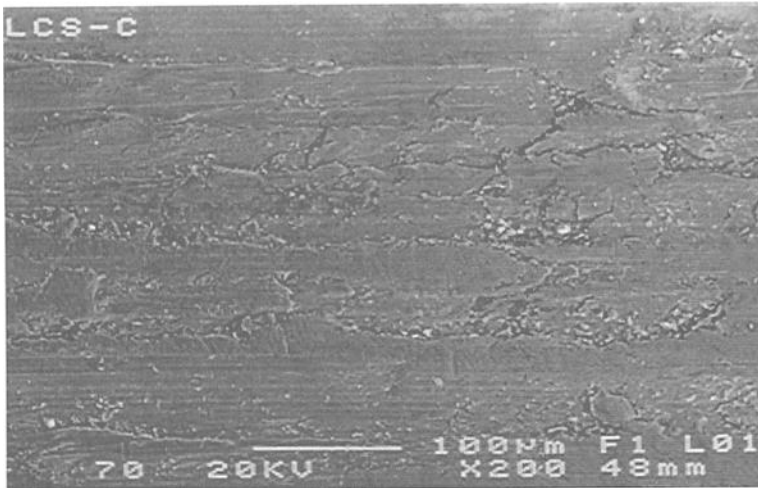


Figure 16 – SEM image of the passive layer formed on the reinforcing steel surface in the cement extract solution with NaCl 10 g/l, after 21 days of immersion.

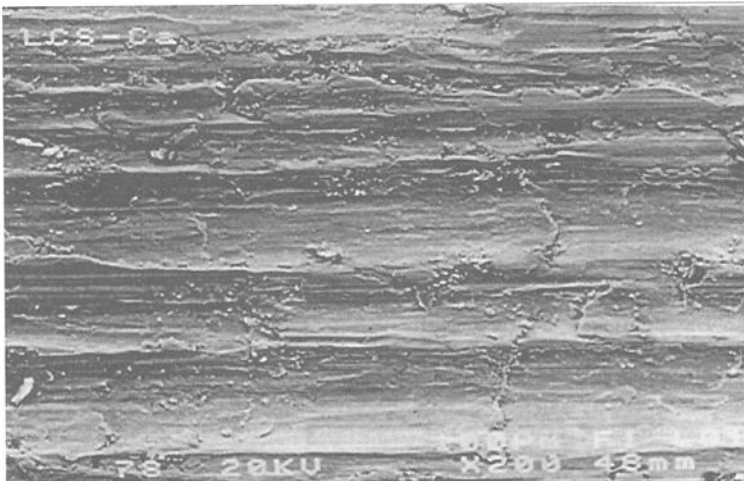


Figure 17 – SEM image of the passive layer formed on the reinforcing steel surface in the saturated Ca(OH)_2 solution with NaCl 10 g/l, after 21 days of immersion.

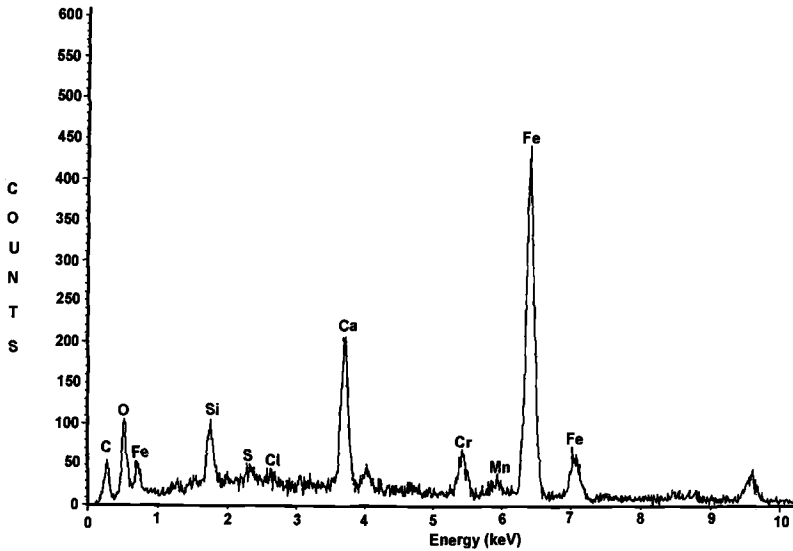


Figure 18 – EDAX analysis of the passive layer formed on the reinforcing steel surface in the cement extract solution with NaCl 10 g/l, after 21 days of immersion.

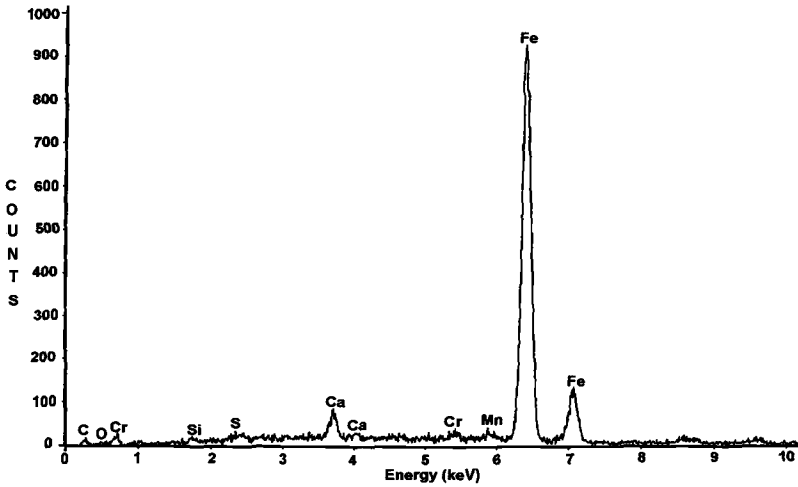


Figure 19 – EDAX analysis of the passive layer formed on the reinforcing steel surface in the saturated $\text{Ca}(\text{OH})_2$ solution with NaCl 10 g/l, after 21 days of immersion.

Therefore, our future investigation is directed towards further study of the topography and composition of the layers formed on the metal surface immersed in both solutions, at different values of polarization corresponding to the passive state of the metal. On the other hand, EIS circuit equivalent simulation could be done in the cases where it is possible, because of the very complex system metal-interface-model solutions.

Summary

Reinforcing steel bars (mild steel) were studying using electrochemical techniques, in two model alkaline solutions (12.7 ± 0.2 , at $24 \pm 1^\circ\text{C}$): saturated calcium hydroxide ($\text{Ca}(\text{OH})_2$) and cement extract (ordinary portland cement, Type I), as such and with the addition of 5 g/l and 10 g/l NaCl. The use of electrochemical techniques, such as polarization curves and impedance spectroscopy (EIS), provides a very powerful information related to real corrosion state of the metal immersed in model solutions. Also some additional SEM and EDAX information is presented about the topography and composition of the films formed on the metal surface in both model solutions.

Conclusions

According to the polarization curves, in the absence of chloride ions, both model solutions (cement extract and saturated $\text{Ca}(\text{OH})_2$) show similar behavior of reinforcing steel. However, the open circuit potential in the cement solution shows a slightly shift to more positive values with the increasing of the immersion time, that indicates distinct film characteristics in both model solutions. This fact is more pronounce in the presence of chloride ions (5 and 10 g/l).

The impedance spectra obtained with the application of external polarization (corresponding to the passive region of the polarization curves), are in agreement with the behavior of the steel displayed by the polarization curves in the same region, although these measurements do not show the real behavior exhibited by the metal in natural conditions (without external polarization). Therefore the EIS spectra registered at open circuit (without external polarization) provide more confident information.

The SEM and EDX surface analysis confirm that there are topography and composition differences in the passive layers formed in each of the model solutions. It seems that the cement extract solution allows the metal to develop a more protective film than the saturated $\text{Ca}(\text{OH})_2$.

All the results presented above show that the two model solutions do not produce similar behavior of steel.

Acknowledgments

The authors wish to recognize the financial support provided by Mexican CONACyT grant project 29649U, and also for the scholarship to M. C. Cebada. We appreciate also CINVESTAV-IPN, Unidad Mérida, for allowing us to carry out this research work. Finally, the authors are very grateful to CINVESTAV-IPN, Unidad Saltillo, especially to Dr. Cecilia Montero Ocampo for performing the SEM and EDAX analysis.

References

- [1] Berke, N.S. and Hicks, M.C., "Electrochemical Methods of Determining the Corrosivity of Steel in Concrete," *Corrosion Testing and Evaluation: Silver Anniversary Volume, ASTM STP 1000*, R. Baboian and S.W. Dean, Eds., American Society for Testing and Materials, Philadelphia, 1990, pp.425-440.
- [2] Callaghan, B.G., "The Performance of a 12% Chromium Steel in Concrete in Severe Marine Environments," *Corrosion Science*, Vol. 35, 1993, p. 1535.
- [3] Nagayama, M. and Cohen, M., "The Anodic Oxidation of Iron in a Neutral Solution," *Journal of Electrochemical Society*, Vol. 110, 1963, p. 670.
- [4] Kruger, J. and Calvert, J.P., "Ellipsometric-Potentiostatic Studies of Iron Passivity," *Journal of Electrochemical Society*, Vol. 114, 1967, p.43.
- [5] Stainless Steel Rebar International Bulletin, Tullmin Coonsulting, Ontario, Canadá, 1999.
- [6] Castro, P., Veleva, L. and Balancán, M., "Corrosion of reinforced concrete in a tropical marine environment and accelerated tests," *Construction and Building Materials*, Vol. 11, 1997, pp. 75-81.
- [7] Veleva, L, Castro, P., Hernandez-Duque, G. and Schorr, M., "The Corrosion Performance of Steel and Reinforced Concrete in a Tropical Humid Climate," *Corrosion Reviews, ISSN 0048-7538*, M. Schorr, Ed., Freund Publishing House, London, England, 1998, pp. 235-284.
- [8] Andrade, C., et al., "Cement Paste Hardening Process Studied by Impedance Spectroscopy," *Electrochimica Acta*, Vol. 44, 1999, pp. 4313-4318.
- [9] Dawson, J.L. and Langford, P.E., "The Electrochemistry of Steel Corrosion in Concrete Compared to Its Response in Pore Solution," *The Use of Synthetic Environments for Corrosion Testing, ASTM STP 970*, P.E. Francis and T.S.

- Lee, Eds., American Society for Testing and Materials, Philadelphia, 1988, pp. 264 -273.
- [10] Berman, H.A., "The Effect of Sodium Chloride on the Corrosion of Concrete Reinforcing Steel and the pH of Calcium Hydroxide Solution," FHWA-RD-74-1, Federal Highway Administration, Washington, DC, 1974.
- [11] Ftikos, C.L. y Parissakis, G., "The combined Action of Magnesium (2+) and Chloride Ions in Cement Pastes," *Cement and Concrete Research*, Vol. 15, 1985, p. 593.
- [12] Montemor, M.F., Simões, A.M. y Ferreira, M.G., "Analytical Characterization of Passive Film Formed on Steel in Solutions Simulating the Concrete Interstitial Electrolyte," *Corrosion*, Vol. 54, 1998, pp. 347-353.
- [13] Gouda, V.K., "Corrosion and Corrosion Inhibition of Reinforced Steel. I. Immersed in Alkaline Solutions," *British Corrosion Journal*, Vol. 5, 1970, p. 198.
- [14] Oranowska, H. and Szklarska-Smialowska, Z., "An Electrochemical and Elipsometric Investigation of Surface Films Grown on Iron in Saturated Calcium Hydroxide Solutions with or without Chloride Ions," *Corrosion Science*, Vol. 21, 1981, p. 735.
- [15] Zakroczymski, T., Fan, C.J., Szklarska-Smialowska, Z., "Kinetics and Mechanism of Passive Film Formation on Iron in 0.05M Sodium Hydroxide," *Journal of Electrochemical Society*, Vol. 132, 1985, p. 2,862.

Ruby de Gutiérrez,¹ Silvio Delvasto,¹ and Rafael Talero²

Permeability Properties of Cement Mortars Blended with Silica Fume, Fly Ash, and Blast Furnace Slag

Reference: de Gutiérrez, R., Delvasto, S., and Talero, R., “**Permeability Properties of Cement Mortars Blended with Silica Fume, Fly Ash, and Blast Furnace Slag**,” *Marine Corrosion in Tropical Environments, ASTM STP 1399*, S. W. Dean, G. Hernandez-Duque Delgadillo, and J. B. Bushman, Eds., American Society for Testing and Materials, West Conshohocken, PA, 2000.

Abstract: Deterioration of concrete structures due to reinforcement corrosion because of chloride ingress is a growing problem in many countries throughout the world. Partial replacement of portland cement by mineral additions, such as ground granulated blast furnace (GGBS), silica fume and fly ash influences the resistance of the pastes and mortars to the chloride environments. The rate of chloride ingress into mortar depends on the pore structure and the capacity of the hydration products to bind chlorides

This paper reports the comparative results of mechanical and permeability properties of blended mortars. Mortar specimens were made with slag replacement levels of 60%, 70%, and 80%, fly ash replacement levels of 20%, 30%, 40%, and 50% and silica fume replacement levels of 5%, 10%, 15%, and 20%. The following tests were performed: compressive strength, water absorption, rapid chloride permeability, mercury intrusion porosimetry, and X-ray diffraction.

Mortars with fly ash and slag reported lower strengths than silica fume mortars. The silica fume mortars show a 50% pore size of that for the mortar without addition. The densifying effect of these materials on the microstructure is attributed to the sealing of pore openings and the narrowing of pore channels by the hydration products of pozzolanic reactions. This results in a reduction in permeability. In general, the use of these admixtures improves the resistance of portland cement mortars against chloride attack. The slag added mortar obtained the best performance.

Keywords: blast furnace slag, fly ash, silica fume, pozzolans, blended cement, chlorides, durability

The major form of concrete deterioration is corrosion of reinforcing material. The increased volume of corrosion products causes cracking and spalling of the concrete.

¹Titular Professors, Materials Engineering Department, Universidad del Valle, Cali, Colombia.

²Research Scientist, Institute “Eduardo Torroja” of Construction Sciences, CSIC, Madrid, Spain.

Chloride and carbon dioxide can diffuse through concrete and cause corrosion of the steel reinforcement, leading to its deterioration and to an eventual reduction of a concrete structure load-carrying capacity [1]. The levels of chlorides required to initiate steel corrosion are extremely low. The chloride limits in international codes vary widely. Based on the present state of knowledge the following chloride limits in concrete used in new construction, expressed as a percentage by weight of portland cement, are recommended (ACI 222, 1997): 0.08% in prestressed concrete, 0.10 for reinforced concrete in wet conditions and 0.2% for reinforced concrete in dry conditions. Since moisture and oxygen are always necessary for electrochemical corrosion, there are some exposure conditions where the chloride levels may exceed these values without corrosion occurrence. Hence, structures continuously submerged in seawater or where concrete is continuously dry present a little risk of corrosion. However, those structures partially in air and partially submerged in a chloride medium are at greatest risk of corrosion.

The ingress of aggressive ions into concrete can principally be controlled by using a good quality concrete. For example, the chloride resistance of concrete can be improved when using additives than modify the concrete pore structure and additionally bind chlorides into concrete [2].

The objective of this paper is to compare the resistance and durability properties of blended cement mortars and relating these results with the corrosion resistance of steel embedded in different types of mortars.

Materials and Experimental Procedure

The materials used in this study were an Ordinary Portland Cement (OPC) and three types of supplementary cementitious materials, Fly Ash (FA), Ground Granulated Blast Furnace Slag (GGBS) and Silica Fume (SF). The chemical characteristics of these materials are shown in Table 1.

Table 1 - *Chemical Properties of the Raw Materials*

Material	I.L. %	SiO ₂ %	Fe ₂ O ₃ %	Al ₂ O ₃ %	CaO %	MgO %	SO ₃ %	Na ₂ O + K ₂ O, %
OPC	2.51	20.11	1.75	6.66	62.40	1.27	3.72	1.40
SF	6.28	92.02	0.39	0.70	0.00	0.00	0.60	0.00
FA	1.75	51.54	9.28	27.15	3.52	1.52	0.82	4.30
GGBS	0.00	38.32	0.92	15.90	39.34	2.47	0.31	2.50

50.8 mm cubic mortar specimens were prepared. The mix proportions of the mortars consisted of one part by weight of cement with and without addition, and three parts by weight of sand. The water – cementitious ratio was 0.50. Mortar specimens were made with slag replacement of 60%, 70% and 80% by weight, fly ash replacement of 20%, 30%, 40% and 50 % by weight and silica fume replacement of 5%, 10%, 15%, and 20 %

by weight of cement. A control mortar is named that without addition of any supplementary material. The specimens were wet cured for 24 hours after casting, then demoulded and continuously cured in water until the tests were run. The hardened mortars were tested for compressive strength, pore structure, water absorption, and chloride permeability.

Results and Discussion

Activity Test

The activities of the pozzolans, SF and FA, and the slag, GGBS, were determined following the ASTM Specification for Silica Fume for Use in Hydraulic – Cement Concrete and Mortar (C1240), the Specification for Fly Ash and Raw or Calcined Natural Pozzolan for Use as a Mineral Admixture in Portland Cement Concrete (C618) and the Specification for GGBS for Use in Concrete and Mortars (C989). Activity indexes of 90.6% and 87.3% were obtained for the addition of SF, and FA respectively. These results are higher than the minimum specified pozzolanic activity index in C1240 and C618. The GGBS activity index was 93.0%; by this reason it is classified by C989 as Slag Grade 100.

Mortar Strength

Fig. 1 shows the 28-day compressive strength for all the mortars tested. In general, mortars with fly ash and slag incorporations reported lower strengths than SF added mortars.

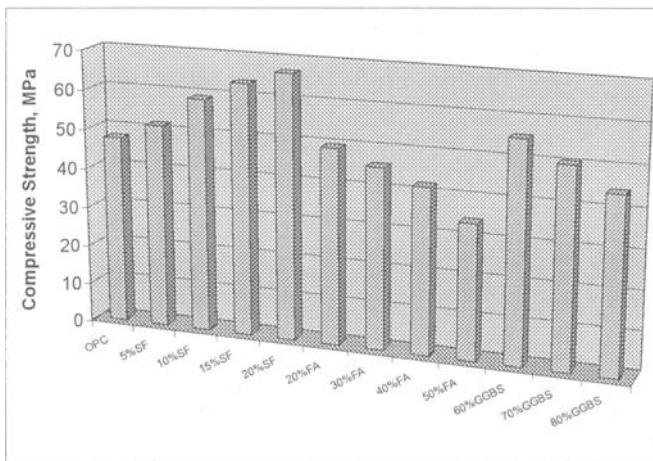


Figure 1 – *Compressive Strength (MPa) of Blended Cement Mortars*

The addition of silica fume (SF) increased the strength up to 40% for 20% of SF when is compared with the control mortar. The addition of 60% of GGBS increased strength by 20%. The lowest values were those for 40% and 50% FA additions. The maximum compressive strength achieved by these mortars was 68 MPa corresponding to 20% of SF addition. At 90 days the fly ash mortars had strengths comparable to or significantly greater than the control mortar. These results are in agreement with those obtained by Ozyildirim and Halstead [3]

Pore Structure

A mercury – intrusion porosimetry technique was employed to measure the porosity and pore structure of the various mortars. The average pore diameter is presented in Table 2 and the pore size distribution of blended mortars is also shown in Fig. 2. The pores, whose diameter is greater than 0.1 μm are considered as large pores. On the contrary, when the diameter of the pores is less than 0.1 μm the pores are small. It is found that the pore structure of the cementitious matrix is changed through the reaction of the pozzolan and slag with the calcium hydroxide released during the portland cement hydration. The large pores occupy 28.5%, 33.0% and 51.5% of the total pore volume in the SF, GGBS and FA blended mortar respectively. The FA mortar presents a larger pore size than SF and GGBS mortar.

Table 2 – Pore Diameter in Blended Cement Mortars

Material	OPC	OPC+SF(15%)	OPC+FA(20%)	OPC+GGBS(70%)
Mean Diameter, μm	0.0543	0.0260	0.0445	0.0150

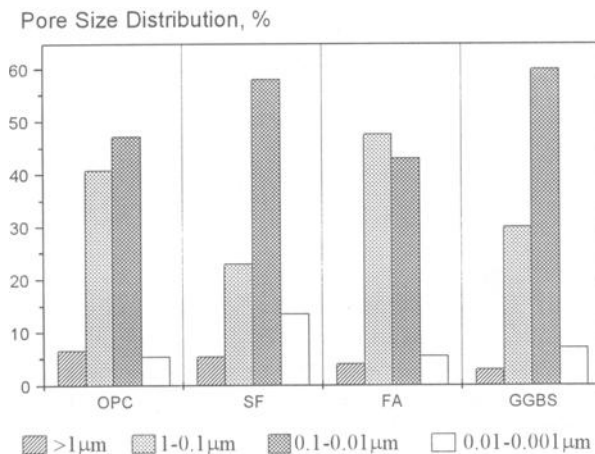


Figure 2 - Pore Distribution in Blended Mortars

Water Absorption

A test method of water absorption by capillarity proposed by Fagerlund [4] was used. It is based in the monitoring of the increase in weight of the specimen by time because of the absorbed water. The specimen mortars were pre-dried at 50 °C during three days before the test. The total amount of water that was taken out per unit suction surface was plotted over the square root of time and the resistance to water penetration (s/m^2) was calculated (Fig. 3). In general the resistance to water penetration increases with the content of addition indicating that the mortar became more impervious. Thus, the reduced water absorption results primarily from the effective interruption of the capillary pore system and the refinement of the pore structure because of the pozzolanic reactions and consequent filling of the matrix with the hydration products.

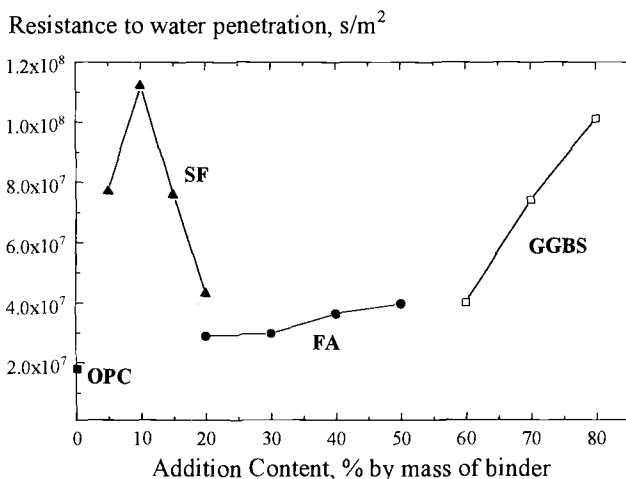


Figure 3 - *Effect of pozzolan and slag content on the resistance to water absorption*

Chloride Ion Penetration

The 28 day test results of the resistance to penetration of chloride ions into mortar, measured in terms of the electric charge passed through the specimens in coulombs in accordance to ASTM Electrical Indication of Concrete's Ability to Resist Chloride Ion Penetration (C1202), are given in Fig. 4. The chloride permeability of a mortar containing any active addition is greatly reduced when it is compared with a mortar without addition. This property is related to its porosity and pore size distribution [5]. GGBS and SF blended mortars showed very significant improvements, over the portland cement control mortar, in reducing chloride permeability. The resistance to chloride intrusion increases as the level of these additions increases in the mortar mixture [6]. Additionally, other factor of special importance, for the chloride resistance, is the capacity of the cement to bind chemically the chloride. When GGBS and FA additions are used,

these materials are able to bind chloride in the form of the Friedel salt, which has been proved by X-ray diffraction [7–10].

An alternative method of evaluate ion diffusion involves placing a thin slice of the material under test between the source of chloride ions and a neutral solution (limewater). This technique is known as diffusion cell method. Based on the increase of the chloride concentration and using Fick's law, the coefficient of diffusion of the blended mortars was calculated. The best result was obtained by the 80% slag added mortar with a diffusion coefficient of $1.2 \cdot 10^{-13} \text{ m}^2/\text{s}$.

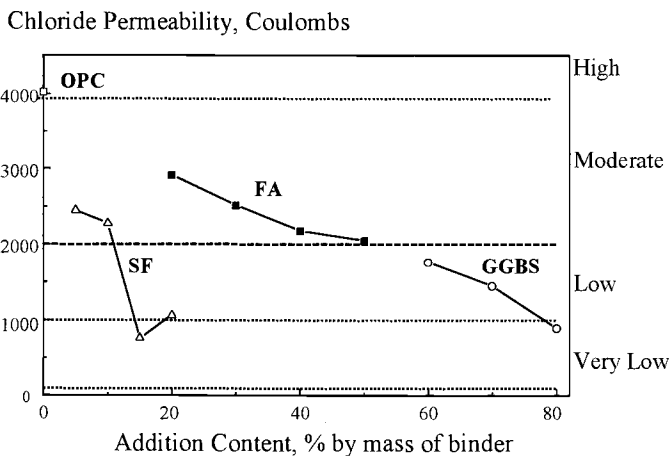


Figure 4 - Chloride Permeability of blended mortars

Conclusions

The results of the presented experimental work indicate:

1. Mortars with fly ash and slag incorporations reported lower early strengths than silica fume added mortars. The addition of SF increased the strength up to 40% for 20% of SF when it is compared with the control mortar.
2. These blending materials showed a higher resistance to water penetration. The densifying effect on the microstructure of these materials is accountable to the sealing of pore openings and the narrowing of pore channels by the hydration products and pozzolanic reactions.
3. In general, the blending of portland cements with appropriate quantities of a high quality pozzolan, such as fly ash and silica fume, or a ground granulated blast furnace Slag improves the resistance of portland cement mortars against chloride attack. The reduction in the case of FA and GGBS added mortars is mainly attributed to the binding of chloride ions, but in the case of SF additions the reduction is possibly due, in a higher grade, to the change in the pore size distribution.

References

- [1] Ibrahim, M. et al., "Use of Surface Treatment Materials to Improve Concrete Durability," *Journal of Materials in Civil Engineering*, Feb. 1999, pp. 36-40.
- [2] Mackechnie, J. R., Alexander, M. G., and Stevenson, C. E. "Predicting Chloride levels in Marine Concrete," *Proceedings International Conference on Corrosion and Rehabilitation of Reinforced Concrete Structures*, Section 3B, Orlando, Dec. 1998.
- [3] Ozyildirim, C., and Halstead, W., "Resistance to Chloride Ion Penetration of Concretes Containing Fly Ash, Silica Fume or Slag," *Permeability of Concrete, ACI, SP 108-3*, Detroit, 1988, pp. 35-61.
- [4] Fagerlund, G., "On the Capillarity of Concrete," *Nordic Concrete Research No 1*, Oslo, Paper No 6, 1982, pp. 1-20.
- [5] Metha, P. K., "Durability of Concrete in Marine Environment - A Review," *Performance of Concrete in Marine Environment, ACI, SP65*. Detroit, 1980, pp. 1-20.
- [6] Ellis, W. E., Riggs, E. H., and Butler, W. B., "Comparative Results of Utilization of Fly Ash, Silica Fume and GGBS in Reducing the Chloride Permeability of Concrete," *Durability of Concrete, International Conference ACI, SP 126-23*, Detroit, 1991, pp. 443-458.
- [7] De Gutiérrez, R., Delvasto, S., and Talero, R., "Chloride Binding Capacity of Blended Cements," *7th Ibero-American Congress of Corrosion and Protection, Corrosion Control as a Base for a Suitable Development*, Cartagena, Colombia, September 2000 (in press).
- [8] Dhir, R. H., et al., "Chloride Binding in GGBS Concrete," *Cement and Concrete Research*, Vol. 26, N° 12, 1996, pp. 1767-1773.
- [9] De Gutiérrez, R., Delvasto, S., and Talero, R., "Metakaolinite Pozzolan for High Performance Cementitious Materials," *Rehabilitation of Corrosion Damaged Infrastructure, Chapter V: Cement, Mortar and Concrete*, Edited by P. Castro, O. Troconis, C. Andrade, NACE International, Houston, 1998.
- [10] Wiens, U., and Schiessl, P., "Chloride Binding of Cement Paste Containing Fly Ash," *Proceedings of the International Congress on the Chemistry of Cement, ICC-97*, Trodheim, 1997.

Ruby de Gutiérrez,¹ Lina A. Calderón,² and Silvio Delvasto¹

Degradation of Fiber Reinforced Mortar in a Marine Environment

Reference: de Gutiérrez, R., Calderón, L. A., and Delvasto, S., “**Degradation of Fiber Reinforced Mortar in a Marine Environment,**” *Marine Corrosion in Tropical Environments, ASTM STP 1399*, S. W. Dean, G. Hernandez-Duque Delgadillo, and J. B. Bushman, Eds., American Society for Testing and Materials, West Conshohocken, PA, 2000.

Abstract: Concrete is a brittle material with a relatively low tensile strength compared to its compressive strength. Reinforcement with randomly distributed short fibers could improve the ductility and tensile strength of concrete and permits the stabilization of the crack system. These products could be used in marine applications, but several chemical reactions must be controlled to generate durable materials. Sulfates and chlorides presented in seawater are especially dangerous ions for the concrete and the reinforcing steel.

The main objective of this research was to determine the effects of a marine environment on the properties of fiber reinforced mortars. Different types of natural and synthetic fibers such as sisal (S), fique (F), coconut (C), glass (G), polypropylene (PP) and steel (St) were used. The physical, mechanical and durability properties of the mortar made with each type of fiber were determined. The mortar matrix included additions such as silica fume (SF), and a superplasticizer (SP). Durability properties under marine environments were evaluated by measuring chloride ion penetration and water absorption.

The test results indicate an increase in the matrix porosity due to fiber application, but the blended cement matrix showed superior performance compared to the portland cement under marine service conditions. The utilization of mineral additions and additives in fiber reinforced mortars under severe environments was recommended.

Keywords: fiber reinforced mortar, natural and synthetic fibers, silica fume, durability.

Concrete is the most widely used man-made construction material in the world. Low cost, versatility, and adequate compressive strength are reasons for its popular use. The main disadvantages are low tensile strength and brittleness [1]. One of the main roles of the randomly oriented, discrete, discontinuous fibers which are added to produce fiber

¹Titular Professors, Materials Engineering Department, Universidad del Valle, Cali, Colombia.

²Chemical Engineer, Materials Engineering Department, Universidad del Valle, Cali, Colombia.

reinforced concrete is to bridge across the cracks that develop in concrete either as it is loaded or as it is subjected to environmental changes [2].

The first widely used to manufactured composite in modern times was asbestos cement, which was developed one century ago with the invention of the Hatschek process. Since the early use of asbestos fibers, a wide variety of other fibers have been used with hydraulic cements: conventional fibers such as steel and glass; new fibers such as carbon or kevlar; and low modulus fibers, either man-made (polypropylene, nylon) or natural (cellulose, sisal, jute), which are derived from vegetables and wood. These types of fibers vary considerably in properties, effectiveness and cost [3].

The applications of fiber reinforced composites are as diverse as the types of reinforcing fibers. Steel fibers have been used in pavements, in shotcrete (tunnel linings), and a variety of other structures. Fibrillated polypropylene fibers are being used as secondary reinforcement to control plastic shrinkage cracking. Asbestos and wood fibers have long been used in pipes and corrugated or flat roofing sheets. Glass and carbon fibers are used primarily in precast panels (non-structural) [3].

Quality and performance of concrete have traditionally been assessed by its compressive strength. However in a marine environment, problems associated with poor durability such as corrosion of steel reinforcement and subsequent spalling are more important than problems related to strength [4]. Here, several chemical reactions must be controlled in order to generate durable materials. For example, sulfates present in seawater are especially aggressive to concrete, they react with tricalcium aluminate (C_3A) in the cement paste to yield calcium sulfoaluminate hydrate (ettringite) which is an expansive product and can cause swelling and cracking [1].

It is considered that the chloride-induced corrosion of the steel embedded in concrete is the most important factor determining durability of reinforced concrete structures in a marine environment. In general, the most effective method of preventing chloride-induced corrosion of reinforcing steel is to have sufficient concrete cover and "high quality" concrete. The use of cementitious and pozzolanic material such as silica fume, slag and fly ash have been widely reported to reduce the chloride penetration of the concrete [4-6].

The main objective of this research was to determine the effects of a simulated marine environment on the properties of fiber reinforced mortars. Different types of natural and synthetic fibers were used and silica fume was incorporated into the matrix in order to improve its performance. In this paper, the mechanical properties, the water absorption and the chloride permeability of the different mixtures are shown.

Materials and Tests

The materials used in this research included an ASTM type V portland cement, a standard siliceous sand, and different types of natural and synthetic fibers such as sisal, fique, coconut, glass, polypropylene and flattened steel Dramix fibers. 2.5% (by weight) of each type of fiber, with a length between 10 – 15 mm, were added to mortar mixes with cement: sand ratio of 1:3. Sisal and coconut fibers were received from Brazil, and the fique is a Colombian native fiber. A SEM micrograph of the fique fiber is shown in Fig. 1. The characteristics of the tried fibers are presented in Table 1.

The different series of fiber reinforced mortars were prepared, cast, and cured in water following standardized procedures. As expected, the addition of fibers caused loss of workability. For this reason, it was necessary to incorporate between 1.5 to 3% (with respect to the portland cement) of a superplasticizer. In order to improve the performance of the fiber reinforced material 15% of silica fume was used. Reference mortars were prepared in order to compare the effect of pozzolan, superplasticizer or fiber incorporation. Compressive strength, water absorption and chloride permeability of the different series were determined.

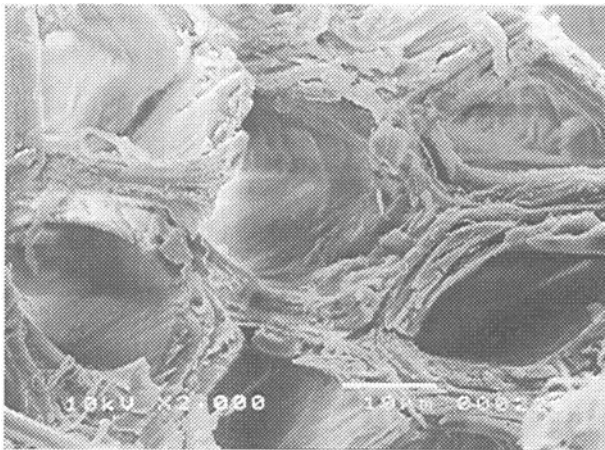


Figure 1 - Tubular form of fique fiber filaments [7]

Table 1 - Characteristics of the reinforcing fibers

Characteristic	Fiber					
	Fique [8]	Sisal [9]	Coconut [9]	PP [10]	Steel [10]	Glass [11]
Equivalent diameter, mm	0.16-0.42	0.28-0.40	0.21-0.37	0.1 - 0.2	0.4	0.09-0.015
Apparent density, kg/m ³	723	564	638	-	-	-
Specific gravity, kg/m ³	1 470	1 370	1 140	910	786	254
Water absorption, %	60.0	65.0	155	-	-	-
Cellulose, %	70.0	66	50	-	-	-
Lignin, %	10.1	9.9	43	-	-	-
Tensile strength, MPa	43-571	275-350	99-116	394	1380	2800
Ultimate elongation, %	6	5	3-13	21	2.0	4.8
Elastic modulus, GPa	8.2	15.2	22.5	4.93	197	72.5

Results and Discussion

Compressive Strength

The tests for uniaxial compressive strength (R_c) were made up to 90 days using 50.8 mm cubic mortar specimens. The water – cement ratio (w/c) used in this study was 0.56, and it was constant for all the series. In order to achieve this w/c and adequate workability a superplasticizer was used. The compressive strength results demonstrate:

1. Notable increase of the strength at all the curing ages because of the SP incorporation (Fig. 2).
2. Besides the increase of the compressive strength due to the reduction of the water content, the compressive strength at 90 days after mortars mixing reported to be 23% higher when 15% of SF was added.
3. The compressive strength is reduced because of fiber incorporation. The greatest reduction was produced by the addition of sisal fiber. The mortars containing steel fibers almost reach the same level of strength of the mortar alone (Table 2).
4. When fibers are added to mortars containing silica fume (Fig. 3), the compressive strengths are reduced at lower curing ages, but at ages as longer as 90 days after mixing, the series with high elastic modulus (steel and glass fibers) do increase the

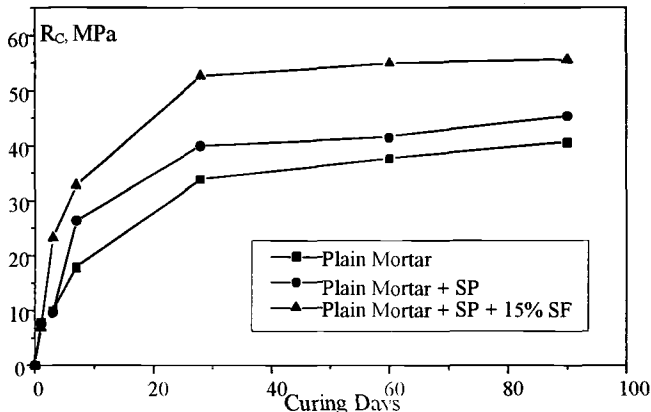


Figure 2 - *Compressive strength behavior of plain mortars without fiber additions*

Table 2 – *Effect of fiber incorporation on the strength of the 90 days old material*

Reduction in Compressive Strength, % Fiber (Mixes without Silica Fume)					
Steel	Glass	Polypropylene	Fique	Coconut	Sisal
6.7	23.2	29.7	18.9	7.8	30.9

resistances by at least 5%. On the contrary, the compressive strength of the mortar is reduced with the addition of coconut, fique, polypropylene, and sisal in 9, 19, 18, and 21%, respectively.

5. The addition of 15% of SF generates a notable increase in strength of the fiber reinforced material, principally when the mortar is reinforced with glass fibers (Table 3). That effect also is observed in the series with other fibers, although in a lesser degree.

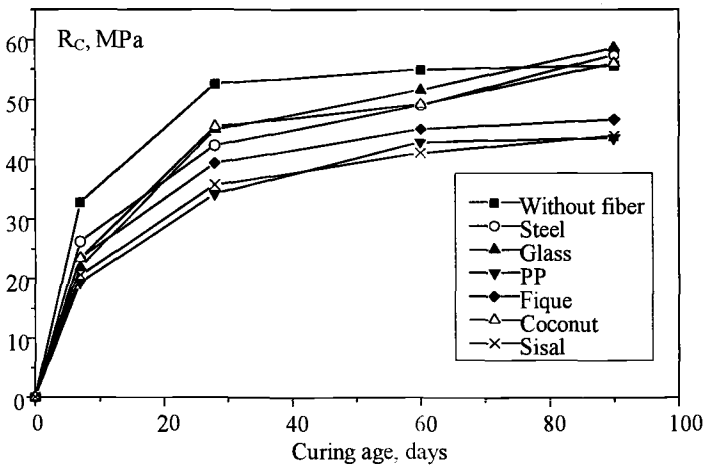


Figure 3 - Compressive strength of series containing silica fume

Table 3 - Effect of the incorporation of silica fume on the compressive strength at 90 curing days

Fiber	Matrix with 0% SF (MPa)	Matrix with 15% SF (MPa)	Strength increase (%)
Without Fiber	45.4	55.6	22.5
Steel	42.3	57.4	35.7
Glass	34.8	58.6	68.4
Polypropylene	31.9	43.5	36.4
Fique	36.8	46.6	26.6
Coconut	41.8	50.7	21.3
Sisal	31.3	43.8	39.9

The reported results indicate that the silica fume addition contributes a densification of the matrix (plain mortar) which is manifested by the higher resistance of the material added with respect to the mortar without silica fume. This densification is essential to obtain reduction in permeability. Additionally, the loss of resistance due to embedding of

steel fiber or glass fiber is compensated by the augmentation of strength caused by silica fume addition to the mortar.

Durability Properties

Absorption Behavior - The water absorption was determined following the procedure established by ASTM Test Method for Specific Gravity, Absorption and Voids in Hardened Concrete (C642), using specimens aged 30 days. The results of this characteristic (Fig. 4) match with the compressive strength obtained. The addition of silica fume reduces the absorption of the hardened matrix. This effect is very important to attenuate the great increment of absorption induced by the incorporation of the natural fibers, as coconut, sisal, and fique.

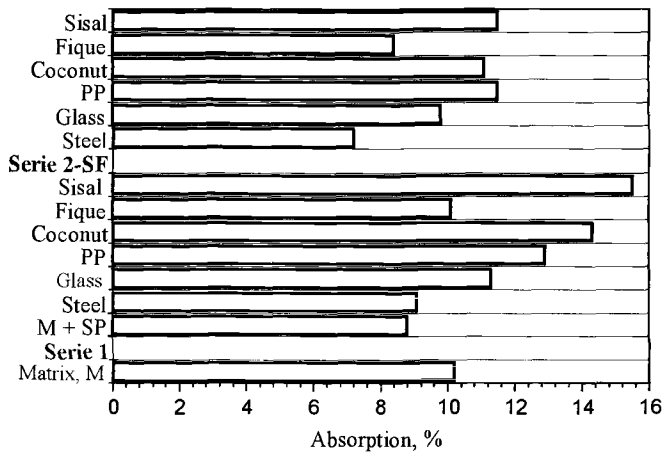


Figure 4 - Water absorption (%) reported by the mortars series (ASTM C642)

Complementary absorption properties were also determined following the method proposed by Fagerlund [12] called the capillary suction technique. The specimens tested, aged 45 days, were conditioned by drying them at 50°C prior to their testing. It was observed that:

1. The incorporation of a superplasticizer and 15% of silica fume do decrease the capacity of water absorption in the capillary pores of a mortar due to the densification of the matrix which reduces its permeability. The water absorption of specimens exposed to water for 24 hours, reported 9.2, 6.4, and 2.1 kg/m² for the plain mortar, mortar with superplasticizer, and mortar with the superplasticizer and silica fume respectively.
2. The coefficient of capillary absorption was reduced and the resistance to water penetration was increased because of the silica fume addition to the mortars (Table 4). For this reason, today most of the shotcrete used for repair and rehabilitation often

contains supplementary cementing materials, such as fly ash and silica fume, in order to improve its performance [5, 13].

3. The water absorption of the fiber-reinforced specimens when they were placed on a “coarse porous” sponge that is kept saturated with water [12] for 24 hours, is generally higher than that reported for the plain mortar matrix. The specimens with glass fiber and silica fume yield comparable results to the matrix alone (Table 4). These results are in accord with the results reported here for mechanical resistance and are in agreement with other reports [14].

Table 4- *Capillary absorption results*

Matrix % SF	Fiber Type	Absorption Coefficient, $\text{kg/m}^2\text{s}^{1/2}$	Resistance to Water Penetration, S/m^2	Water Absorption, (24 hours) kg/m^2
0	Steel	0.0219	$3.9 \cdot 10^7$	5.5
	Glass	0.0264	$3.6 \cdot 10^7$	7.5
	Polypropylene	0.0239	$5.4 \cdot 10^7$	5.6
	Coconut	0.0166	$9.2 \cdot 10^7$	4.8
	Fique	0.0249	$5.4 \cdot 10^7$	7.2
	Sisal	0.0220	$4.9 \cdot 10^7$	5.9
15	Without Fiber	0.0043	-	2.1
	Steel	0.0124	$12.7 \cdot 10^7$	3.7
	Glass	0.0062	$6.1 \cdot 10^7$	1.6
	Polypropylene	0.0148	-	3.4
	Coconut	0.0165	$14.4 \cdot 10^7$	4.1
	Fique	0.0137	$8.5 \cdot 10^7$	4.7
	Sisal	0.0103	$8.7 \cdot 10^7$	3.0

Chloride Penetration – Cylindrical specimens were specially made for the rapid chloride permeability test according to ASTM C1202. This test method provides a rapid indication of the resistance to the penetration of chloride ions. The relation between the total charge (coulombs) of the fiber reinforced mortar and the charge of the matrix without fiber for each of the series is shown in Fig. 5.

For all of the reinforced mortars of series 2 (matrix with 15% SF) the charge is reduced remarkably. This performance has been attributed to a reduction in the permeability resulting from a finer and discontinuous pore structure because the SF addition [15].

Conclusions

The results of this investigation show that:

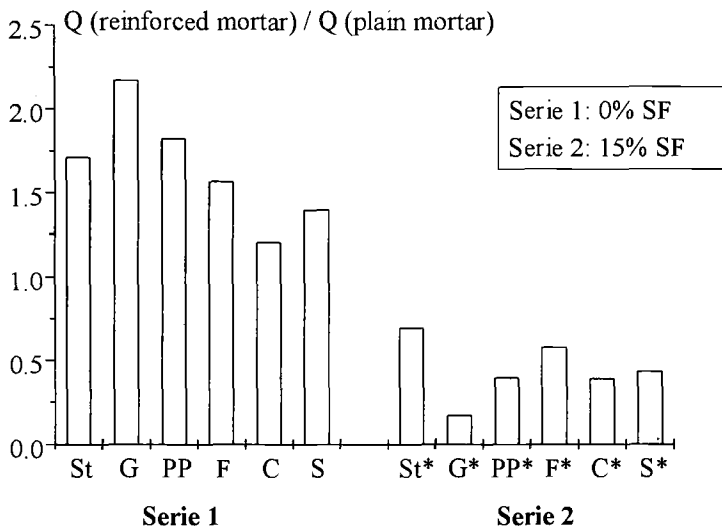


Figure 5 – Resistance to the penetration of chloride ions

- Incorporation of fibers into a cementitious matrix, generally, reduces the compressive strength. The greatest decrease was produced by the addition of sisal fiber. The mortars containing steel fibers almost reach the same level of strength of the mortar alone.
- The strength behavior of the fiber-reinforced mortars improves with the addition of silica fume. This could be due to a barrier effect around the fiber created by the SF pozzolanic reaction products.
 - The polymeric and natural fibers reinforced mortars increase their compressive strength with 15% SF addition however the level of strength is much lesser than the matrix with SF.
 - There is a great accordance between the results of the compressive strength and the absorption properties. In general, the silica fume addition reduces the matrix permeability. This effect is very important to attenuate the great increment of absorption induced by the incorporation of the natural fibers.
 - Resistance to chloride penetration is remarkably diminished when fibers are embedded in a based cement matrix. This resistance is increased when it is incorporated with SF in the fiber-reinforced materials.
 - In general, silica fume has a significant positive influence on the compressive strength of the mix and at the same time can yield a denser, more durable hardened matrix.
 - Utilization of mineral additions such as silica fume and additives in fiber reinforced mortars is recommended, especially in severe environments.

References

- [1] Rider, R. and Heidersbach, R., "Degradation of Metal-Fiber-Reinforced Concrete Exposed to a Marine Environment," *Corrosion of Reinforcing Steel in Concrete, ASTM STP 713*, W. R. Grace, Ed., American Society for Testing and Materials, Philadelphia, 1984, pp.75-92.
- [2] Mindess, S., "Fibre Reinforced Concrete, Challenges and Prospects," *Fiber Reinforced Concrete*, Banthia and Mindess, Ed., Univ. of British Columbia, 1993, pp. 1-11.
- [3] Shah, S. P., and Marikunte, S. S., "Fiber Reinforced Concrete," *Proceedings of ACBM Faculty Enhancement Workshop*, 1993, pp. 226-252.
- [4] Baweja, D., Sirivivatnanon, V., and Gross, W., "High-Performance Australian Concretes for Marine Applications," *High Performance Concrete: Proceedings ACI International Conference, ACI, SP-149*, Detroit, 1994, pp. 363-377.
- [5] Bentur, A., "Fiber Reinforced Cementitious Materials," *Materials Science of Concrete*, American Chemical Society, 1989, pp. 223-283.
- [6] De Gutiérrez, R., Delvasto, S., and Talero, R., "Performance of GGBS Cements," *Journal of Solid Waste Technology and Management*, Vol. 25, No. 2, 1998, pp. 112-115.
- [7] Perdomo, F., "Composites de matriz polimérica y fibra natural de fique," *Tesis Doctoral en Nuevos Materiales y sus Tecnologías de Fabricación*, Universidad Politécnica de Valencia, España (in progress).
- [8] Delvasto, S., "Investigación de los Mecanismos de Adherencia en la Interfase del Material Compuesto Hormigón-Fibra Natural de Fique y de la Optimización de su Comportamiento a la Tenacidad en Servicio," *Tesis Doctoral en Nuevos Materiales y sus Tecnologías de Fabricación*, Universidad Politécnica de Valencia, España, 1997.
- [9] John, V. M., and Agopyan, V., "Materiais Reforcados con Fibras Vegetais," *Simposio Internacional sobre Materiales Reforzados con fibras para Construcción Civil*, Anais, Sao Paulo, EP-USP, 1993, pp. 29-38.
- [10] Bentur, A., et al., "Fiber matrix Interface," *Second International Workshop: High Performance Fiber Reinforced Cement Composites II (HPFRCC)*, Ann Arbor, Michigan, Edited by A. E. Naaman and H. W. Reinhart, 1996.
- [11] Balaguru, P. and Shah, S., "Fiber Reinforced Cement Composites," McGraw Hill Ed., 1992, 313 p.

- [12] Fagerlund, G., "On the Capillarity of Concrete," *Nordic Concrete Research No. 1*, Oslo, Paper No. 6, 1982, pp. 1-20.
- [13] Morgan, D. R., "Developments in Shotcrete for Repairs and Rehabilitation," *CANMET International Symposium on Advances in Concrete Technology*, Athens, Greece, 1992.
- [14] Aguilar, M. T. P., et al., "Mechanical Properties of Synthetic Fibers Reinforced Plaster with Silica Fume or Slag," *II International Conference in High Performance Concrete SP-58*, Performance and Quality of Concrete Structures, Granada, Brasil, June 1999.
- [15] Saricimen, H., "Research to Improve Durability of Reinforced Concrete in Agressive Environments" *Controlling Concrete Degradation*, Dhir R. K. and Newlands M. D., Eds., UK, 1999.

John L. Piazza II¹

Corrosion Control on Concrete Structures: Zinc-Hydrogel Technology

Reference: Piazza, J. L., II, “Corrosion Control on Concrete Structures: Zinc-Hydrogel Technology,” *Marine Corrosion in Tropical Environments, ASTM STP 1399*, S. W. Dean, G. Hernandez-Duque Delgadillo, and J. B. Bushman, Eds., American Society for Testing and Materials, West Conshohocken, PA, 2000.

Abstract: A discussion of the various deterioration mechanisms on concrete structures including conventional reinforced structures, post-tensioned structures, and prestressed structures in tropical environments will be presented. Corrosion mitigation systems will be reviewed, and new protection methods will be discussed. Key issues in evaluating the performance of different corrosion protection systems on concrete structures will be described. The effectiveness of the different protection methods for corrosion control used historically will be reviewed. Case histories of both failures and successes of the various methods will be discussed. Cathodic protection systems using impressed current and galvanic designs will also be reviewed, and various limitations and advantages of each method will be presented and compared with other corrosion mitigation systems. A new zinc-hydrogel system for cathodic protection of concrete structures which has been used successfully on reinforced, post-tensioned, and prestressed steel structures will be discussed. The design parameters for the different applications of the zinc-hydrogel cathodic protection system will be described, and the effectiveness of this system will be evaluated based on different operating characteristics for each type of structure. The research data used in developing the zinc-hydrogel material will be presented and compared with actual data from commercial installations to verify the long-term operating characteristics. The cost effectiveness of the zinc-hydrogel system will be compared with other cathodic protection systems as well as other corrosion mitigation systems.

Keywords: corrosion, corrosion control, cathodic protection, zinc-hydrogel, concrete structures, reinforced concrete structures, prestressed steel structures, post-tensioned structures, chlorides, carbonation

Introduction

Reinforced concrete has enjoyed enormous success as a construction material

¹ Principal Engineer, Southern Cathodic Protection Company, 1100 Johnson Ferry Road, Suite 108, Atlanta, GA 30342.

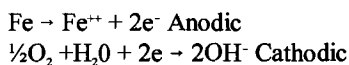
during the twentieth century. Designers and builders have used the combination of concrete and steel for building construction in tropical environments extensively because of expected long-term performance and structural and mechanical strength. In most environments, concrete provides the steel with a relatively high degree of protection against corrosion, and the steel is an excellent reinforcement for the concrete. Concrete is strong in compression but relatively weak in tension and shear, and steel is strong in tension, compression and shear. Concrete reinforced with steel is a durable construction product and should provide many years of maintenance free use if properly designed and constructed. A major factor affecting the longevity of the concrete structure is depth of concrete cover on the steel. The concrete produces a protective passivating film on the surface of the steel. This passive film is created by the high alkalinity of the concrete. Typically, the pH of the concrete is approximately 13. As long as this passivating film is not disrupted, the corrosion reaction on the steel will be minimum.

However, in this millennium, an increasing population of reinforced concrete structures will be faced with huge repairs due to the deterioration of the concrete caused by electrochemical activity in tropical environments — in particular the corrosive action of salt water spray. The most common durability problem of reinforcing concrete is corrosion of steel in concrete.

The three general types of concrete construction are conventional reinforcing bars, post-tensioned, and prestressed. A combination of these types may be used in the same structure. Steel for reinforced concrete is usually deformed bars, which may vary from 0.38 in (0.97 cm) to 2.25 in (5.72 cm) in diameter. Welded wire fabric, plain or deformed, with wire areas from 0.014 in² (0.09 cm²) to 0.45 in² (2.90 cm²) and tendons for post-tensioning are also used in combination with rebar. Reinforced concrete building construction usually consists of bearing walls and columns supporting roof and floor systems. Depending on the type of construction, many different steel components are used throughout the structure — each offering a possible unique corrosion problem. This paper will address corrosion control on commercial or residential building construction; however, the same theories and practices would apply to other types of steel reinforced concrete structures such as bridges and overpasses.

Corrosion Mechanisms of Steel in Concrete

Corrosion can be defined as the destruction of a metal by chemical or electrochemical reaction with its environment. The corrosion of steel in concrete is an electrochemical process. The electrochemical reactions that occur in this process are known as anodic, which involves iron going to the ferrous ion, and cathodic, which involves reduction of oxygen. The reactions are as follows:



Note: For the corrosion reaction to start and continue, oxygen must be present; however, in concrete structures located in tropical environments, oxygen is generally

available. The corrosion current will flow from the anode to the cathode, and any interruption will stop the corrosion process. The deterioration of the metal will occur at the anodic location as the iron atoms are converted to ferrous ions as indicated in (Figure 1).

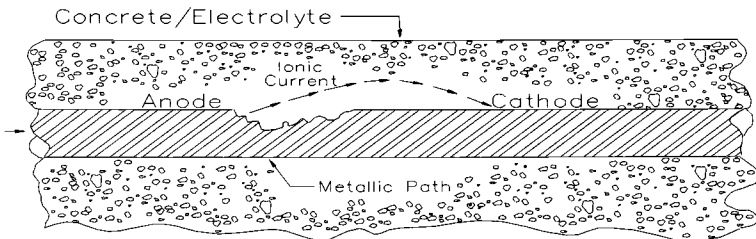


FIGURE 1

As the steel deteriorates at the anode, there will be a loss of structure integrity of the metal by the reduction in size of the steel member which will result in failure if allowed to continue. However, an even more significant problem of the corrosion process is the deterioration of the concrete due to cracking and spalling created by the corrosion products formed at the anode. The volume of corrosion products produced in a corrosion reaction is much larger than the original volume of steel. With the exception of the steel that is dissolved, the majority of corrosion products are confined in the concrete in an area (anodic) around the steel, and this creates stresses within the concrete. The stresses created by expansion of the corrosion products causes longitudinal cracks which ultimately cause spalling and delaminating of the concrete as in (Figure 2). As these cracks grow, additional saltwater and oxygen enter the concrete to steel depth accelerating the corrosion rate.

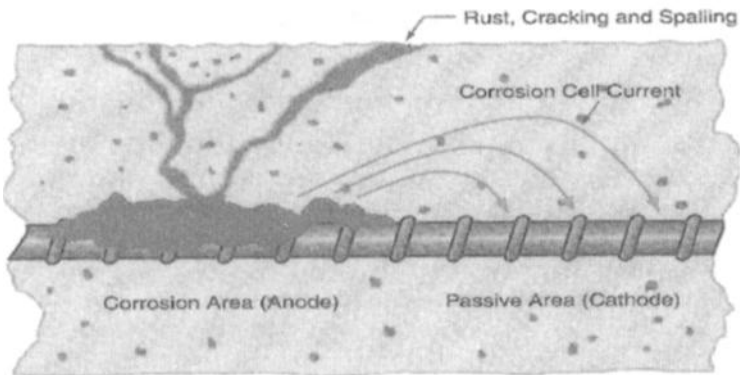


FIGURE 2

Corrosion of Steel in Concrete: Depassivation

As previously mentioned, the high alkalinity of the concrete provides a protective oxide film on the steel. This film is dependent on maintaining the alkalinity or pH of the environment. "However, in practice this favourable state of affairs may change and depassivation may occur under two specific sets of conditions: (1) reduction of the pH level due to reaction with atmospheric CO₂ (carbonation); and (2) penetration of chloride ions into the concrete pore solution around the steel" [1].

Carbon dioxide will react with the hydroxides in the pore solutions to form carbonates and water. As a result of this reaction, the alkalinity of the pore solution decreases lowering the pH to approximately 8, and the steel corrodes in this environment. The electrochemical activity in the hardened concrete depends on the depth of concrete cover and the rate of diffusion of CO₂. The rate of diffusion depends on the partial pressure of CO₂ and the pore structure of the concrete.

When chloride ions penetrate the protective film on the steel surface, the passive condition is broken, and corrosion may start. It is generally agreed that there is a threshold concentration of chloride ions that must be exceeded before corrosion occurs. This threshold concentration is a function of pH. The American Concrete Institute Committee Reference, Ref.4.10, offers specifications for chloride content for prestressed and conventionally reinforced concrete as shown in (Table 1).

Table 1 — *Chloride Limits for Portland Cement Mixes (% wt.)*

1.	Prestressed concrete	0.06
2.	Conventionally reinforced concrete in a moist environment and exposed to external sources of chloride	0.10
3.	Conventionally reinforced concrete in a moist environment but not exposed to external sources of chloride	0.15
4.	Above ground building construction where the construction will stay dry	No limit

The chloride ions will diffuse through the concrete from external sources such as sea water in tropical environments (salt spray) or deicing salts used in temperate climates to melt ice on concrete surfaces. In some cases the chloride ion is added to the concrete inadvertently as part of the water or aggregate mix. It can also be added in calcium chloride used as an admixture component.

There are many measurement techniques available to determine the corrosion activity of steel in concrete. The following organizations offer information on various techniques and methods: NACE International, American Concrete Institute, International Concrete Repair Institute, American Society for Testing and Materials, and Federal Highway Administration. It is not the intent of this paper to offer detailed information on various measurement techniques, but rather to discuss the corrosion mitigation systems.

Corrosion Mitigation in New Construction

If it is assumed that the chlorides were not incorporated in the original concrete mix, then the depth of cover and properties of the concrete offer the first line of defense against corrosion. The time required for corrosion to begin and the rate of corrosion are dependent on concrete cover. There are British [British Standard BS8110 (8.6)] and American specifications available for concrete cover including quality and thickness. One source of these specifications is The American Concrete Institute, Farmington Hills, MI 48333-9094. However, the minimum requirements for depth of cover and quality of concrete are in many cases not sufficient to offer long life for structures in tropical environments due to the extreme corrosivity of saltwater spray. In new construction, high-strength concrete may be used to reduce the permeability in order to reduce the rate of chloride diffusion or carbonation of the concrete. There are various mineral admixtures such as fly-ash and silica fume which offer additional protection for chloride contamination by reducing the rate of diffusion and increasing the electrical resistivity. Also, there are various corrosion inhibitors available that can be added to the concrete mix that offer additional corrosion protection. The most common corrosion inhibitor is calcium nitrite, and it has been used successfully for over twenty years. It is important to use caution in the use of inhibitors to insure that they have no effects on the integrity of the concrete. In summary, properly designed reinforced concrete can offer years of corrosion free performance.

Material selection can also play an important role in corrosion mitigation of new reinforced concrete structures by the use of non metallic reinforcing. Coated steel products utilizing sacrificial coatings or epoxy coatings may offer additional corrosion protection. The use of coatings should not be used as a substitute for proper concrete cover and quality.

Corrosion Mitigation in Existing Structures

After the concrete has been contaminated with chlorides or after carbonation has occurred, it is necessary to investigate other methods for corrosion mitigation. Historically, the concrete repair industry has used the "patch and repair" method for corrosion control. The emphasis was on developing materials that would give long term performance in the patch area without addressing what was happening in the macro corrosion environment. "The concrete construction industry does not pay adequate attention to the three primary issues related to premature corrosion in repaired concrete structures, namely: cracking as a result of drying shrinkage, electrochemical incompatibility, and changes in interior environment caused by the repair "[2]. "Although a tremendous amount of information exists in the literature on corrosion of steel in concrete, comparatively very little work has been done that specifically addresses the mechanisms of corrosion involved with the repair of concrete structures. Theoretical analysis of corrosion processes involved in repaired concrete structures has traditionally focused on potential differences between the patched areas and the surrounding substrate. This analysis has led to repair practices that suggest using repair materials that have the same permeability as the substrate concrete. A different analysis including both

potential theory as well as kinetic theory suggests that repair materials that are less permeable should have less impact on the surrounding substrate, as well as provide a higher level of protection in the patched area. Unfortunately sufficient experimental data supporting either approach is still needed”[3]. It is obvious from the historical data that “patch and repair” should not be considered a corrosion mitigation solution for carbonation and chloride contamination, but only as a method to repair the concrete damage of the structure with corrosion mitigation required in addition. Further, the components used in the repair should be compatible with the corrosion mitigation system.

Sealers and membranes can provide some degree of corrosion protection for reinforced concrete structures by reducing the penetration of chlorides and carbonation and by minimizing water entry into the concrete thereby slowing the corrosion process. Caution should be used in applying sealers and membranes to concrete structures that are already contaminated with chlorides as the corrosion process will continue even if at a slower rate, and deterioration of the concrete will occur. Many reinforced concrete structures have been repaired in the past where “patch and repair” and waterproofing were used. However, not all of the chloride contamination was located and removed, and the structures failed in a fairly short cycle.

A relatively new concept for corrosion mitigation is electrochemical treatment of the reinforced concrete. This technique removes the chloride by electrochemical extraction and can be used to realkalise carbonated concrete. Chloride extraction and realkalisation will mitigate corrosion by returning the reinforcing steel to a passive state. This method, unlike “patch and repair” methods, treats the entire concrete member and returns the entire member to a passive condition. If this technique is used in a tropical environment where chlorides are continuously available (salt water spray), it may be necessary to use sealers or membranes to prevent contamination after the concrete is passivated in order to achieve the long term protection required. This technique may offer the best results if applied on chloride contaminated concrete in which the threshold concentration of chloride at the steel has not been exceeded and before there is concrete damage requiring major repairs of cracked, spalled, and delaminated areas. When considering the life cycle cost analysis of electrochemical extraction versus “patch and repair” for chloride contaminated reinforced concrete structures, the electrochemical treatment methods are often the most cost effective [4].

Migrating corrosion inhibitors for existing concrete structures have appeared in the marketplace recently. These claim corrosion protection at both the anode and cathode. However, until more field data are available on the performance of this corrosion mitigation method the effectiveness can not be determined. The laboratory tests indicate an overall reduction in corrosion activity [5].

Cathodic Protection as a Corrosion Mitigation System

Cathodic protection has been used to prevent corrosion of steel for over two hundred years [6]. It has more than a twenty-year history of effectiveness in mitigating corrosion of steel in concrete on U.S. highway structures utilizing impressed current systems and galvanic systems. A major advantage of cathodic protection is the ability to measure its

effectiveness in real time measurements using an accepted national criteria (NACE International RP290-90). A recent survey found that of all the cathodic protection systems installed by state highway agencies eighty percent were still functional, again indicating long term effectiveness [7]. Cathodic protection, if applied properly, can prevent corrosion of steel in concrete, and stop corrosion that is in progress [8].

The two types of cathodic protection systems are impressed current and galvanic. The impressed current system uses an external power source to energize anodes to supply the protective current. The galvanic system's current is supplied by connecting the steel to a metal which is higher in the electrochemical series, resulting in current flow from the anode to the steel. The anode dissolves as it oxidizes, and it supplies electrons to the steel. It is sometimes referred to as a "sacrificial anode."

The following are comparisons of the advantages and disadvantages of impressed current and galvanic cathodic protection systems:

Advantages of Impressed Current Systems:

- No voltage or current limitations
- Adjustable over wide ranges
- Long design life anode systems
- Effectiveness measured in real time

Disadvantages of Impressed Current Systems:

- High installation cost
- Higher maintenance cost
- Continuous AC power required
- Possible hydrogen embrittlement [9]
- Relatively complex systems

Advantages of Galvanic Systems:

- Low installation cost
- Low maintenance
- No external AC power required
- Adaptable to aesthetics of structure
- Relatively simple and reliable systems
- Effectiveness measured in real time
- Anode systems adaptable to impressed current
- Flexible designs for multi-function
- Self-regulating

Disadvantages of Galvanic Systems:

- Limited current capacity
- Limited driving voltage

Cathodic protection offers a cost effective method for reinforced concrete structures that are contaminated with chlorides or are corroding due to carbonation. The selection of the type of cathodic protection is dependent on the system design parameters with both types offering advantages over other corrosion mitigation methods. In order for a cathodic protection system to be effective, all of the steel structure in the concrete must

be electrically continuous. There are many impressed current systems available today; however, they are relatively complex and expensive to service and maintain.

Metallized zinc sprayed directly onto the concrete surface has been generally successful; however, to maintain adequate current flow, metallized zinc requires periodic wetting of the anode surface. In addition, due to environmental and safety concerns related to thermal spraying during installation, enclosures and waste recovery systems are required in order to comply with various codes and standards which result in increased costs. The joint study by Florida DOT and the University of South Florida demonstrated that the metallized zinc anode was not capable of maintaining an adequate flow of galvanic current without periodic wetting of the anode surface [10]. Therefore, the long term use of this type of system for corrosion control on building type construction is limited.

The concept of a galvanic system that could offer long term performance while maintaining sufficient current flow to achieve the requirements for corrosion control of reinforced concrete building components led to the concept of galvanic anodes with an ionically conductive adhesive [11]. Laboratory tests indicated that aluminum alloys were not suitable for use in contact with hydrogel adhesives, and the best anode is pure zinc. The hydrogels absorb water and remain conductive even in relatively low humidity environments, offering a long term solution for maintaining adequate current flow for cathodic protection.

Galvanic cathodic protection systems have been installed on various reinforced concrete balconies of ocean front condominiums in Florida for approximately five years. Test data indicates that they are providing sufficient current to polarize the reinforcing steel to a minimum of 100 millivolts polarization. The average operating current density for the balcony installations was 0.08 ma/ft (0.86 ma/m²). The estimated life of these original systems is in excess of 12 years. The test data for one of these installations are given in (Table 2).

Table 2 — *Depolarization and Current Density Data, Ocean Front Condominium, Florida*

Date	Initial "On" Reading (mvs)	4-Hr. Depolarization Reading (mvs)	Current Density ma/sf --- ma/m ²
9/94	-800	-220	3.50 (initial*)37.67
9/95	-850	-240	0.17 1.83
10/96	-760	-200	0.07 0.75
11/97	-900	-290	0.05 0.54
5/98	-850	-200	0.06 0.65
4/99	-870	-210	0.06 0.6

*The initial current density was recorded immediately after energizing the system.

The zinc hydrogel anodes have been commercially available for approximately three years and over 200000 ft² (18580 m²) have been installed as galvanic systems. The zinc hydrogel cathodic protection systems have been installed on conventional rebar type

construction as well as prestressed and post-tensioned structures.

One of the first galvanic cathodic protection systems utilizing the zinc-hydrogel anode was installed on a post-tensioned structure (a five story condominium) located on the Gulf of Mexico in Florida in 1997. The cathodic protection system was designed to mitigate corrosion on the post-tensioned cable anchors and the breakout rebars. A minimum 100 millivolt depolarization was achieved on 100 percent of the test locations. The average current density was 0.15 mA/ft² (1.61 ma/m²). The estimated system life was in excess of 15 years.

The zinc hydrogel anode was used to furnish cathodic protection on a combination prestressed and conventional rebar condominium structure in south Florida in 1998. The balconies on this structure were constructed of prestressed concrete slabs which were supported by reinforced concrete beams and columns. The corrosion data indicated that the chloride content was generally above the threshold level in the balconies and the support structure. After the system was installed the effectiveness of the cathodic protection system was checked using the four hour depolarization criteria of a minimum of 100 millivolts. The test results indicated a minimum of 188 millivolts depolarization at an average current density of 0.10 ma/ft² (1.08 ma/m²). The estimated life of the cathodic protection system is in excess of 20 years.

The zinc hydrogel material historical operating data indicates that the galvanic anodes will furnish the required current to mitigate corrosion of steel in concrete structures. The potential and current data from operating commercial systems compares very favorably to the research data obtained in the development of the anode system. The galvanic anode systems should be designed for optimum operating characteristics of the zinc hydrogel material. The anode systems can be installed on the top, bottom, or side surfaces of concrete members, allowing for flexible designs on complex structures and for aesthetic considerations.

Conclusions

Cathodic protection of reinforced concrete structures using galvanic anode systems offers a cost effective method of corrosion mitigation in tropical environments [12]. When using the total life-cycle cost analysis for corrosion control systems for reinforced concrete structures which includes initial costs, maintenance, and repair costs, the benefits of corrosion mitigation systems are evident [13]. Zinc hydrogel galvanic cathodic protection systems used in tropical environments have sufficient current capacity to achieve the 100 millivolt depolarization criteria. The zinc hydrogel system offers major advantages over other corrosion control systems for existing buildings that are corroding due to chloride contamination or carbonation because of its lower initial cost, low maintenance, and minimum operating costs. The zinc-hydrogel system offers flexibility and simplicity in design giving the engineer many choices in anode layout and building compatibility. After approximately five years of operation in various locations in Florida, the zinc hydrogel anodes are operating in accordance with the design parameters, and test data indicates a life in excess of fifteen years for most installations.

As we enter the next century, our existing aging infrastructure will continue to deteriorate at an accelerated rate due to corrosion of reinforcing steel. Cathodic

protection has been proven to be an effective and economical method of corrosion remediation on reinforced concrete structures in tropical environments. In the future, installation of corrosion control systems on new reinforced concrete structures in tropical environments could eliminate the staggering costs associated with concrete restoration and corrosion remediation and mitigation. Prevention of corrosion on reinforced concrete structures in tropical environments would certainly be more cost effective than concrete repair and restoration.

References

- [1] Bentur, A., Diamond, S., Berke, N. S., *Steel Corrosion in Concrete*, E & FN SPON, New York, 1997, p. 26.
- [2] Emmons, Peter H., Vaysburd, Alexander M., "Corrosion Protection in Concrete Repair: Retrospect and Prospect," ICRI Workshop Manual, Houston, 3/21/98.
- [3] Hanley, B., Coverdale, T., Miltenberger, M., Nmai, C., "Electrochemical Compatibility in Concrete Repair," ICRI Workshop Manual, Houston, 3/21/98.
- [4] Whitmore, David W., "Electrochemical Treatment of Concrete: A New Approach to Extend the Service Life of Chloride Contaminated or Carbonated Concrete Structures," ICRI Workshop Manual, Houston, 3/21/98.
- [5] Scannell, W. T., M. Islan, and A. A. Sohanguhpurwala, "Status Report on Long Term Field Evaluation of Corrosion Inhibitors in Repair of Reinforced Concrete Structures," paper presented at the ACI Annual Convention, Atlanta, GA, November 9-14, 1997.
- [6] Burns, R. and W. Bradley, *Protective Coatings for Metals*, 3rd edition, Reinhold, New York, 1967, pp. 104-106.
- [7] U.S. Department of Transportation, Federal Highway Administration, "Galvanic Cathodic Protection of Reinforced Concrete Bridge Members Using Sacrificial Anodes Attached by Conductive Adhesives," Publication No. FHWA-RD-99-112, (September 1999).
- [8] Bentur, A., Diamond, S., Berke, N. S., *Steel Corrosion in Concrete*, E & FN SPON, New York, 1997, pp. 139-140.
- [9] Bentur, A., Diamond, S., Berke, N. S., *Steel Corrosion in Concrete*, E & FN SPON, New York, 1997, p. 141.
- [10] Powers, R. G. and Sagues, A. A., *Sprayed Zinc Galvanic Anodes for Concrete Marine Bridge Substructures*, Report No. SHRP-S-405, Strategic Highway

Research Program, Washington, D.C., 1994.

- [11] U.S. Department of Transportation, Federal Highway Administration, *Galvanic Cathodic Protection of Reinforced Concrete Bridge Members Using Sacrificial Anodes Attached by Conductive Adhesives*, Publication No. FHWA-RD-99-112, (September 1999).
- [12] Pullar-Strecker, Peter, *Corrosion Damaged Concrete, Assessment and Repair*, CIRIA, Butterworths, Kent, England, 1996, p. 76.
- [13] Jones, M., "A Solution for Deteriorating Concrete Balconies, 3M, St. Paul, Minnesota, 1998.

Zia Chaudhary¹

Design and Protection Criteria for Cathodic Protection of Seawater Intake Structures in Petrochemical Plants

Reference: Chaudhary, Z., “**Design and Protection Criteria for Cathodic Protection of Seawater Intake Structures in Petrochemical Plants,**” *Marine Corrosion in Tropical Environments, ASTM STP 1399*, S. W. Dean, G. Hernandez-Duque Delgadillo, and J. B. Bushman, Eds., American Society for Testing and Materials, West Conshohocken, PA, 2000.

Abstract: Impressed current cathodic protection (ICCP) and sacrificial anode cathodic protection (SACP) systems were designed and installed to control chloride-induced corrosion of the steel reinforcement in the atmospherically exposed and submerged parts of the seawater structures, respectively. The design and long-term performance assessment of these systems are described and discussed. The monitoring data collected have suggested that all ICCP systems are performing satisfactorily and meeting the design objectives in controlling the corrosion of the steel reinforcement. The SACP systems generally did not meet the specified criterion of -800 mV Ag/AgCl current-on steel potentials; however, there have been no signs of corrosion or concrete distress in submerged areas since application of SACP system.

The results showed that a steel current density ranging between 8 and 14 mA/m² was sufficient to afford required protection to the steel reinforcement in different structures. The protection afforded to these structures has residual effect and could last up to 2 months or so when the CP system is turned off. As a result of CP application, the corrosion potentials of the steel reinforcement have been shifted by some 100 to 200 mV in the positive direction.

Keywords: impressed current cathodic protection, sacrificial anode cathodic protection, design steel current density, 100 mV decay criterion

Introduction

Saudi Basic Industries Corporation (SABIC) operates some 15 world-scale plants in the industrial cities of Jubail and Yanbu. The plants produce more than 20 million metric tons per year of petrochemicals, chemicals, fertilizers, plastics, steel products and industrial gases. In petrochemical plants, removal of exothermic heat generated in the reactors is essential to the process. In SABIC plants this is achieved using seawater

¹Corrosion Advisor, Saudi Basic Industries Corporation (SABIC), SABIC Technology Center Jubail, P.O. Box 10040, Al-Jubail 31961, Saudi Arabia.

supplied from the Royal Commission (RC) canal network. Seawater is used because a large quantity of water is needed for cooling and fresh water is not available. Large and massive reinforced concrete structures, i.e., intake and return reservoirs, were constructed in the plants to form and provide the cooling system to the plant. In general, seawater gravitates from the canal network through large-diameter underground lines (usually 1600 mm dia.) to the seawater intake structure. The water flows through trash screens to the pump basin from which it is pumped through a pipe loop (normally underground) to the consumer areas. The heated effluent is returned to the seawater return structure, where the water flows over an elevated weir and gravitates back through pipelines to the outgoing RC canal.

Most of the plants came on-stream in the early 1980s. After only a few years of service, many of the seawater structures started showing signs of distress in the form of cracking and spalling of concrete. The extent of deterioration varied from one structure to another. Since the structures are critical for the operation of plants and in any event significant failure could result in complete shutdown of the plant, rehabilitation of these structures and also a long-term solution was necessary for the protection of the repaired structures against further concrete deterioration. Repairs were undertaken to restore the lost strength of these structures and CP systems were installed to control further corrosion of the steel reinforcement.

The CP system design philosophy and performance assessment since commissioning is described and discussed in terms of controlling corrosion of steel reinforcement in these structures.

Cathodic Protection System Design

Pre-Design Survey

A systematic and detailed condition survey was conducted on each structure to identify the form, cause and extent of concrete deterioration and establish the feasibility of the CP system. It consisted of delamination survey, potential mapping, electrical continuity testing of the rebar cage, concrete chemistry analysis of cored samples and electrical resistivity testing. The results showed that chloride levels were significantly higher than the threshold limit (0.4% by wt. of cement) for chloride-induced corrosion of steel reinforcement [1] and had penetrated in sufficient levels to cause corrosion of both the inner and outer layers of the steel reinforcement. Electrical resistivity measurements revealed that more than 80% of the readings were below 10000 ohm-cm. The steel reinforcement was found to be generally continuous in each structure.

Design Philosophy

The exposure conditions were different for internal and external concrete surfaces in each intake and outtake structure. Visible damage to submerged areas was significantly less as compared to atmospherically exposed areas. This was attributed to a lower corrosion rate in the low oxygen, water saturated concrete, and to the less voluminous ferrous corrosion product formation. Taking this into account, plus the installation constraints and cost implications, impressed current cathodic protection (ICCP) system

type was selected for the atmospherically exposed concrete surfaces and sacrificial anode cathodic protection (SACP) system type for the submerged areas.

ICCP System

The anode system comprised expanded mixed-metal oxide-coated titanium mesh anodes and a titanium conductor bar, which were fixed onto the appropriately prepared concrete surfaces using plastic fasteners and then embedded in shotcrete overlay. Multiple anode feeder cable connections were installed to have good current distribution and some level of redundancy. The anode system was designed to provide a 40 years service life with minimum maintenance.

SACP System

The SACP system consisted of aluminum anodes installed on "A" frame or steel channels. The anodes were then lowered in the water and connected to the steel reinforcement with cable connections. The anode system was designed to provide a minimum life of 10 years and to be easily replaceable.

Anode Zone Configuration

The large size structures were divided into discrete anode zones in order to acquire sufficient and uniform protection in areas that were different in terms of geometry, resistivity, steel density and exposure such as splash zone, etc. Each anode zone was powered by an independent transformer rectifier, which had a separate anode, structure connection, and multiple reference electrodes for monitoring the potential.

Design Steel Current Density

According to British, "Code of Practice for Cathodic Protection" (BS7361: Part 1: 1991) and NACE recommended practice "Cathodic Protection of Reinforced Steel in Atmospherically Exposed Concrete Structures" (RP0290-90), typical recommended current densities for protection of atmospherically exposed reinforced concrete structures range between 10 and 20 mA/m² of steel. Based on the condition survey results, (i.e. the chloride concentration at the reinforcing steel, extent of corrosion and concrete deterioration) and considering the hot and humid aggressive environment, to which the structures are exposed, each CP system was designed using the following criteria:

ICCP System

Atmospherically exposed sections: 20 mA/m² of steel surface area
 Buried sections: 20 mA/m² of steel surface area
 The maximum anode current density used was 110 mA/m² of anode.

SACP System

For steel embedded in concrete: 20 mA/m² of steel surface area
 For steel exposed to seawater: 60 mA/m² of steel surface area

Protection Criteria

The specified protection criterion for the areas protected by ICCP system was a shift of -100 mV (IR free) in the corrosion potential of the steel throughout the structure (subject to a most negative limit of -1.10 volts relative Ag/AgCl). It is commonly known as “100 mV decay” criterion, as it is measured when the current is interrupted for a given period of time. This criterion was based on the NACE RP0290-90 and Technical Report no. 36 of the Concrete Society of Corrosion Engineering Association [2].

The specified protection criterion for the submerged areas (protected by SACP system) was to maintain a “Current-On” potential of -800 mV relative to Ag/AgCl at all rebar surfaces in accordance with NACE recommended practice “Control of External Corrosion on Underground or Submerged Metallic Piping Systems-item #21001” (RP0169-90-92).

System Monitoring

In order to monitor and assess the performance of CP systems, embeddable Ag/AgCl reference electrodes were embedded into the concrete at representative locations of each structure. About 15 to 20 reference electrodes were installed in each structure, i.e., each electrode covering approximately an area of 150 to 200 m². For an ICCP system, potential measurements were made at the location of each embedded reference electrode to determine the potential decay after current interruption. Applied current and driving voltage of each independent anode zone were also recorded.

For an SACP system, only current-on potentials were measured and recorded at the location of each reference electrode embedded in submerged areas. There was no provision or facility provided to interrupt the current flowing between the sacrificial anode and the steel reinforcement, to measure instant-off steel potentials.

Performance Assessment Of CP Systems

ICCP System

The “100mV Potential Decay” criterion is the most commonly used criterion and recommended practice for performance assessment of CP systems of atmospherically exposed structures. The time allowed for such measurements is usually between 4 and 24 hours after current interruption. Based on theory and experiment, it is considered that a shift of 100 to 150 mV reduces the corrosion rate by an order of magnitude [3]. The potential decay (measured after 24-hour current interruption) results collected during monitoring of the systems are summarized in Figs. 1-4.

The results show that the specified criterion was met at most of the monitoring locations (representing the entire structure) for the seawater structure #1 and #2 of SABIC Plants as shown in Figs. 1 and 2. This observation was consistent throughout the monitoring of those CP systems over the last few years. This implies that the corrosion rate of the steel reinforcement was significantly reduced throughout the structures and the CP systems are meeting the design objectives.

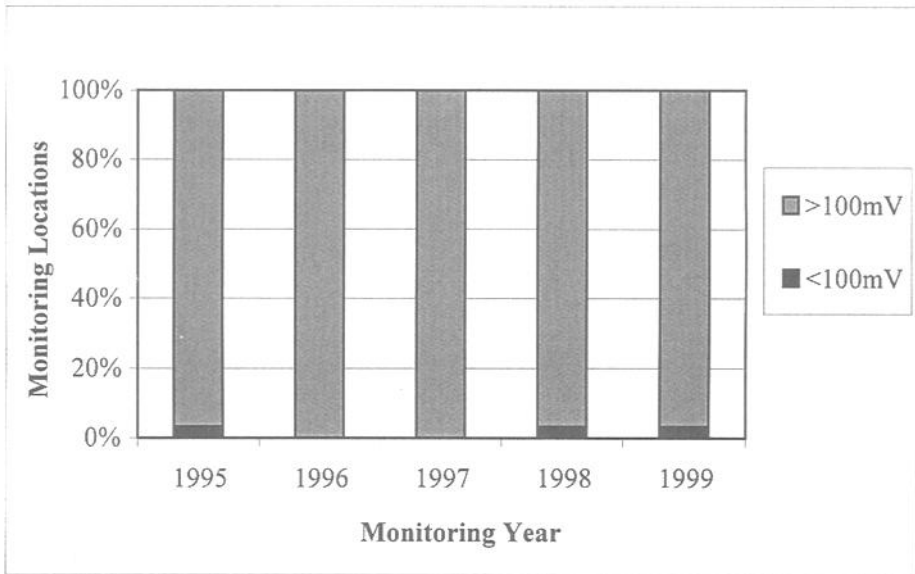


Figure 1- Potential decay assessment in the Seawater Structure #1.

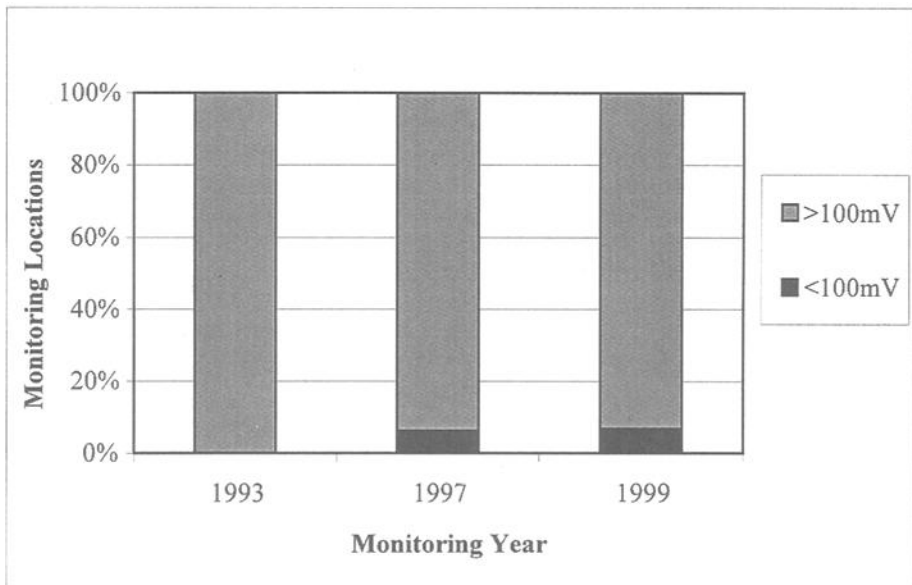


Figure 2- Potential decay assessment in the Seawater Structure #2.

For the structures #3 and #4 located at two different plants, the results appear to be less promising in meeting the specified criterion (see Figs. 3 and 4). The results show that approximately 60% concrete surface area of each structure was sufficiently protected. In the remaining 40% approximately 10% had protection levels just below the established criterion (i.e. ranging between 75 and 100 mV) and the remaining 30% fell well below the required criterion.

For structure #3, this was attributed to poor applied current adjustments and poor or non-uniform current distribution. The monitoring data showed that the initial applied current density was less than 5 mA/m^2 . In 1996, the applied current density was increased to approximately 7 mA/m^2 , which improved performance of the system as indicated by the 1997 data. However, this lasted only for a year or two and the protection level in some areas was again reduced. In 1998, a further increase in the applied current was made, which appeared to have improved the performance of the CP system. In addition, it was noticed that some parts of the structure were relatively more wet than others, resulting in more polarization in wet areas than dry areas.

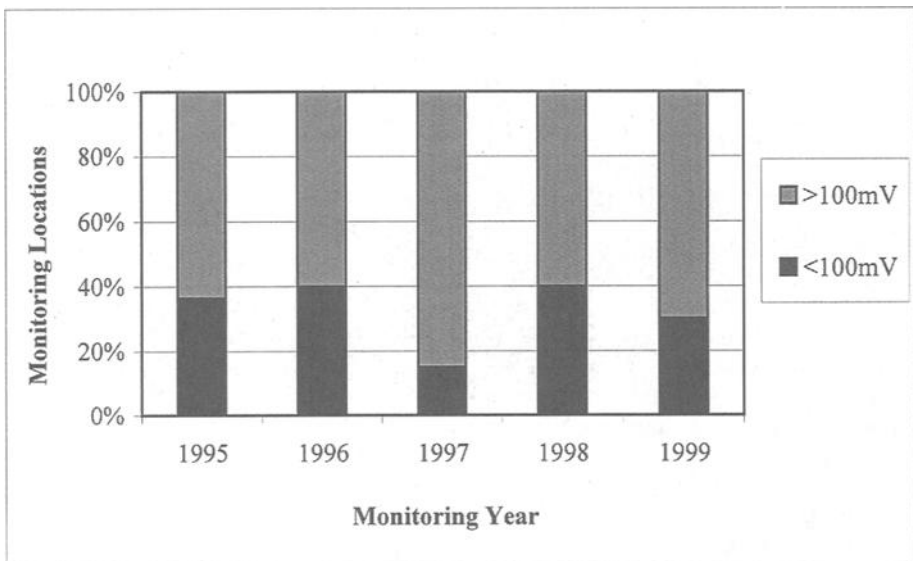


Figure 3- Potential decay assessment in the Seawater Structure #3.

For structure #4, the rate of polarization had been relatively slower in some areas than others (Fig. 4). The CP system was designed to protect the entire structure (approximately 800 m^2 of concrete surface area) using only one anode zone. Normally, it is recommended to have anode zone size not more than 500 m^2 [3-4]. It appears that the slower polarization in some areas was due to non-uniform and inadequate current distribution.

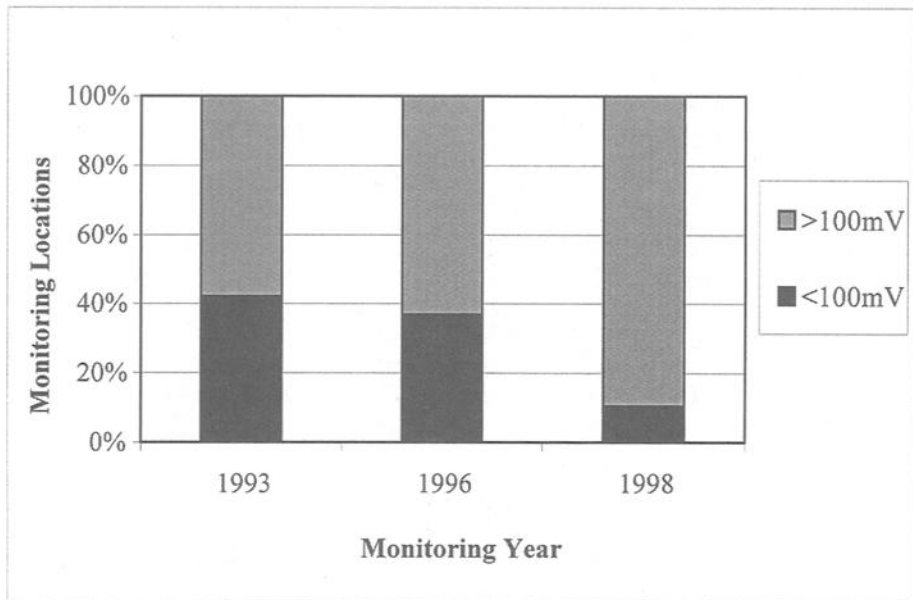


Figure 4- Potential decay assessment in the Seawater Structure #4.

Cathodic protection of steel in concrete produces alkalinity at the steel/concrete interface due to cathodic reaction and also removes chlorides away from the rebar by electric field. This phenomenon can result in restoring passive film on rebar, thus shifting steel corrosion potential towards less negative potentials. In order to assess the long-term effect of CP on the steel reinforcement, power of the CP system was turned off for a period of a month or so and the changes in the open circuit potentials were observed. A comparison of steel corrosion potentials before and after the application of CP for a few years is illustrated in Figs. 5-8.

It is evident from these results that as a result of CP application, free corrosion steel potentials had shifted towards less negative potentials at most of the monitoring locations. At many locations, corrosion potentials had been shifted in the range of -10 mV to -100 mV Ag/AgCl, indicating the restoration of passive conditions on the rebars. There was either no shift or it moved slightly towards more negative potentials at only a few locations. The results indicate that environment around the steel reinforcement has been improved in removing the chlorides and increasing the alkalinity due to application of cathodic protection. This implies and supports the statements that CP is the most appropriate repair method for chloride contaminated structure [3,5].

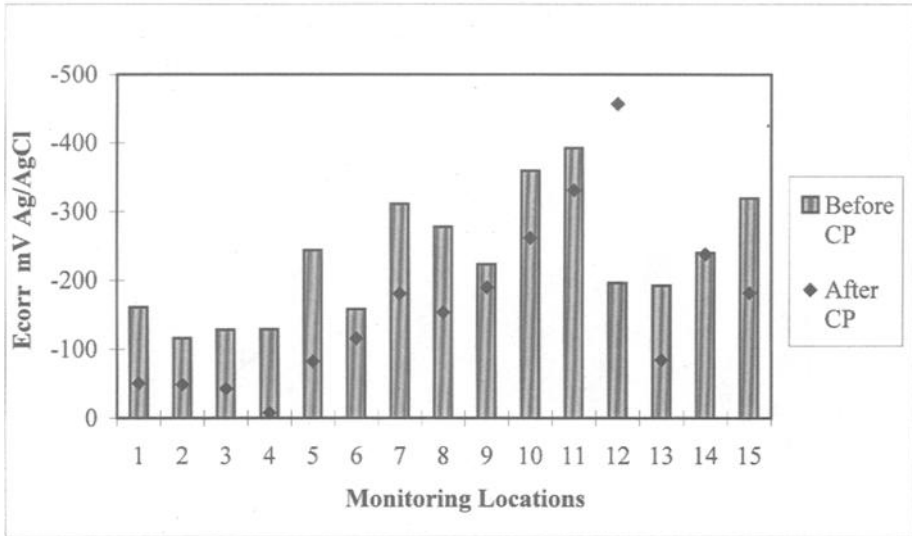


Figure 5-Changes in free corrosion steel potentials as a result of CP application in Seawater Structure #1 .

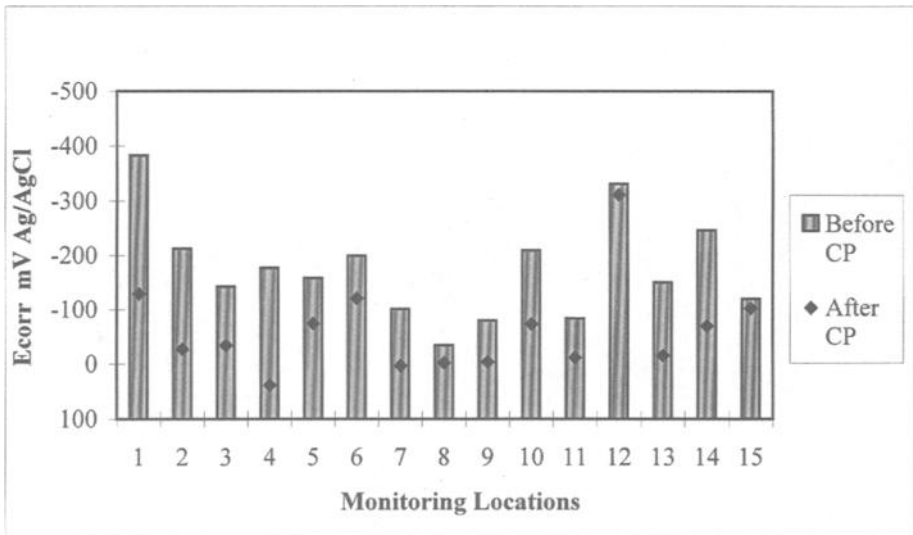


Figure 6-Changes in free corrosion steel potentials as a result of CP application in Seawater Structure #2 .

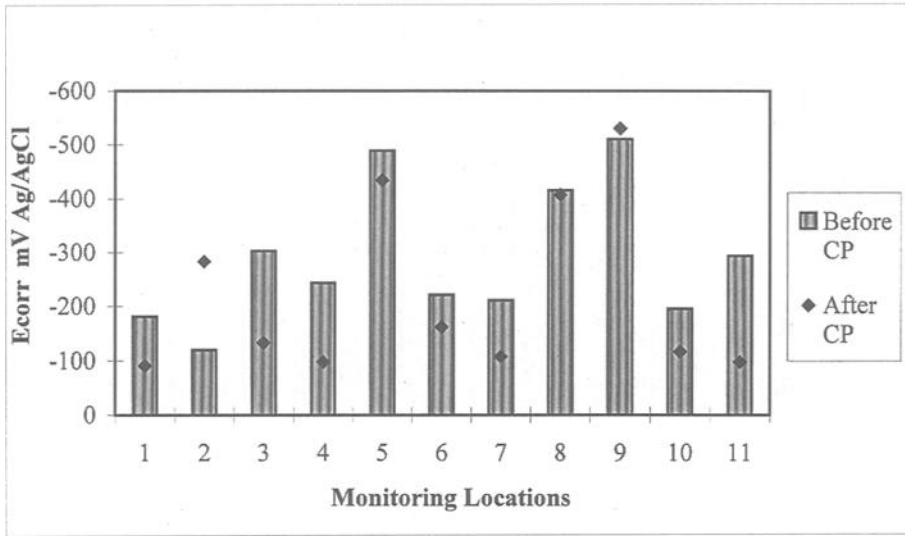


Figure 7-Changes in free corrosion steel potentials as a result of CP application in Seawater Structure #3.

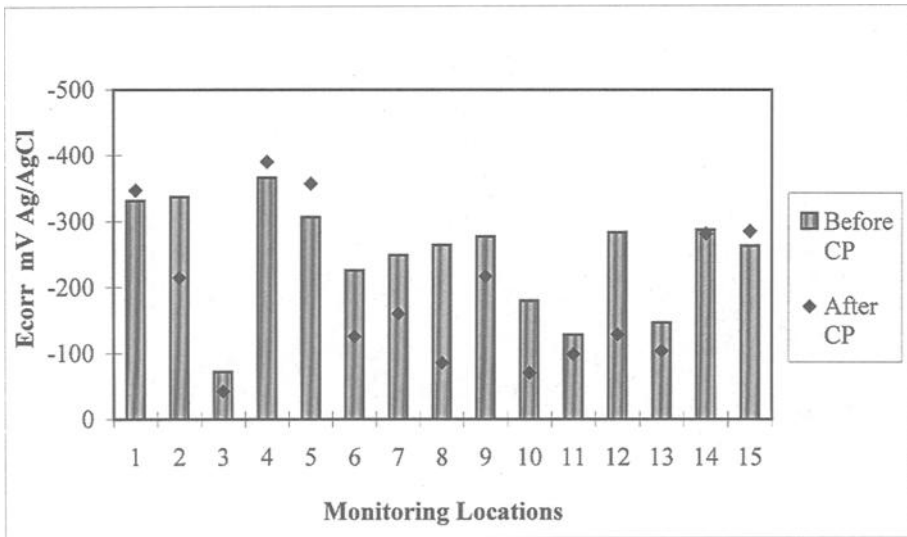


Figure 8-Changes in free corrosion steel potentials as a result of CP application in Seawater Structure #4.

The design and operating (average) parameters of the CP systems are shown in Fig. 9. The results show that the steel current density ranging between 8 and 14 mA/m² was sufficient to afford the required protection.

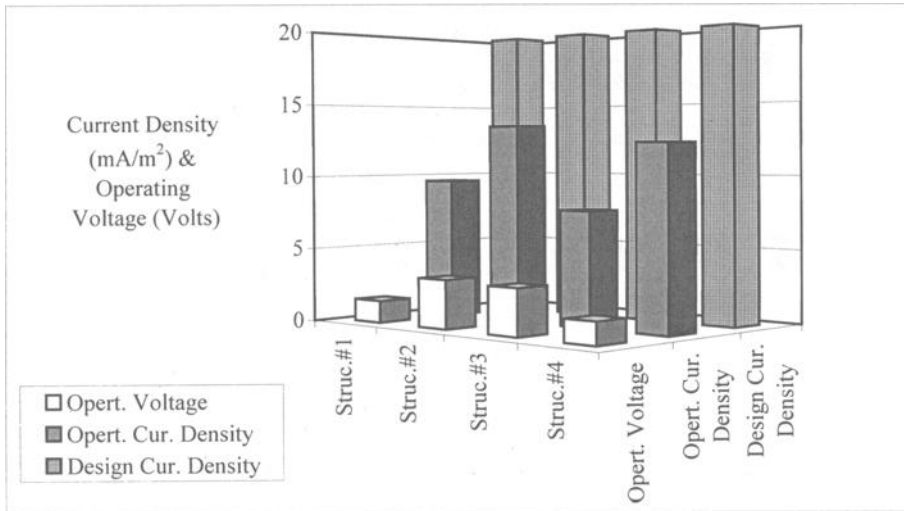


Figure 9-Design and Operating parameters of the CP Systems.

This suggests that a design current density of 15 mA/m² of steel surface area would be sufficient for such structures. Similarly, the operating voltage of the CP systems was very low and ranged between 1.4 and 3.5 volts. No significant increase in the operating voltage of all systems was noticed since commissioning, suggesting that mesh anode systems offer very low circuit resistance which do not change much with time.

SACP System

It is evident from current-on potentials that the specified criterion of -800 mV Ag/AgCl was not generally met at most parts of the two structures (see Figs. 10 and 11). It appears that the SACP systems were not able to deliver sufficient current to achieve the required potentials in those areas. Since drive voltage in such systems is limited and small, this may well be due to incapability of anodes to distribute current adequately to remote areas.

No visible damage was detected in submerged areas, except at seawater structure #2. The water level in that structure was lowered by some 150 cm probably due to drop in canal water level. As a result of this, there was no current flow to these exposed areas. This resulted in significant cracking of concrete but only in exposed and unprotected areas as shown in Fig. 12.

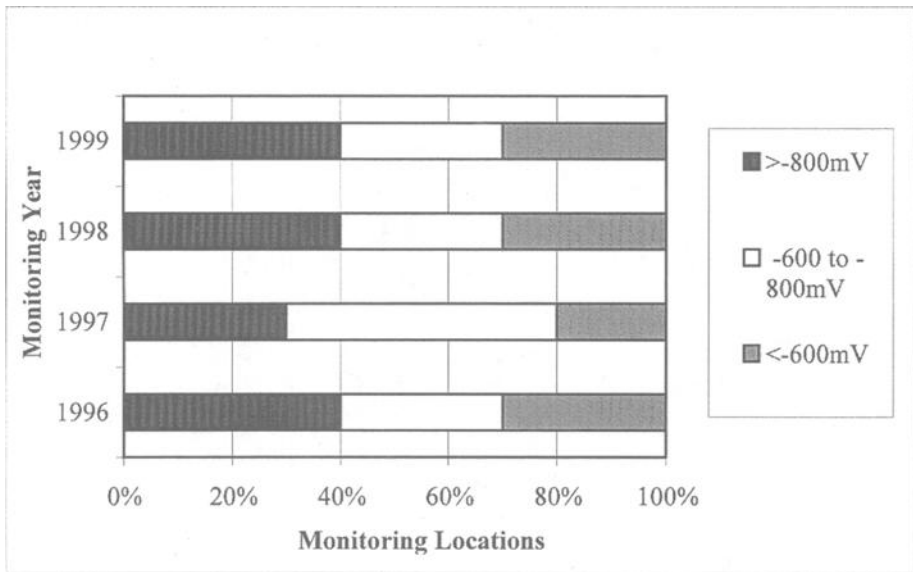


Figure 10-Current-on steel potentials in submerged areas of Seawater Structure #3 after application of SACP system.

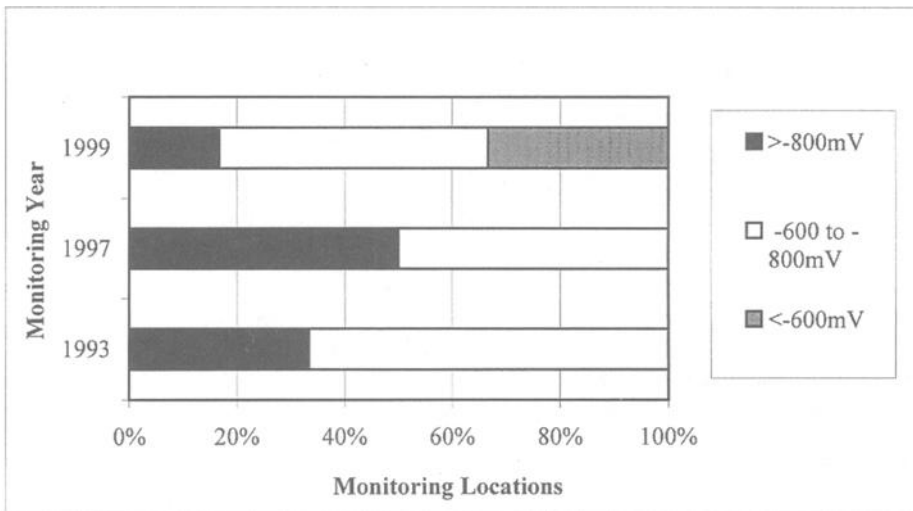


Figure 11-Current-on steel potentials in submerged areas of Seawater Structure #2 after application of SACP system.

This suggests that although the specified criterion was not met, SACP system was probably able to control corrosion of the steel reinforcement sufficiently in the submerged areas. The -800 mV criterion is normally recommended for bare steel structures and pipelines in submerged and below ground conditions. For concrete structures, it is not essential to shift the steel potential to that criterion value. Normally, a negative shift of 300 mV can be considered sufficient to control corrosion of the steel reinforcement. Better conclusions related to this criterion could be drawn if there were provisions as part of the installation to interrupt the applied current and measure the instant-off and current-off steel potentials.



Figure 12-*Spalling of concrete due to corrosion of steel reinforcement in the unprotected areas of seawater structure #2.*

Conclusions

1. In ICCP systems, the specified criterion was generally met at most of the monitoring locations, hence showing satisfactory performance in arresting or controlling corrosion of the steel reinforcement.
2. The long-term application of the CP systems has resulted in restoring the passive conditions on the steel reinforcement. Visually, no distress signs have been observed since CP application. This implies that CP is a more effective and durable repair method in controlling corrosion of steel in chloride-contaminated concrete than conventional structural or patch repairs.
3. A steel current density of 15 mA/m^2 is sufficient to provide adequate protection in reinforced concrete seawater structures.
4. In SACP systems, -800 mV Ag/AgCl current-on potential criterion was not met at most of the monitoring locations. However, so far it has not resulted in any visible damage in submerged areas. In future designs, a facility should be provided to interrupt the applied current and measure instant-off potentials.

5. New seawater structures should be constructed with a built-in ICCP system, which would not only be economical but also prevent corrosion of the steel reinforcement from day one, providing a safe design life of >50 years.

References

1. "The Durability of Steel in Concrete" Parts 1, 2 and 3, digests 263-5, Building Research Establishment, U.K. (1982).
2. "Cathodic Protection of Reinforced Concrete" Concrete Society/CEA Technical Report 36. Corrosion Engineering Association, U.K. (1989).
3. Broomfield J.P., *Corrosion of Steel in Concrete, Understanding, Investigation and Repair*, Published by E & FN Spon, U.K. 1997.
4. Chess, P.M., *Cathodic Protection of Steel in Concrete*, Published by E & FN Spon, U.K. 1998.
5. Pedefferri, P. "Cathodic Protection and Cathodic Prevention," *Construction and Building Materials*, Vol. 5, 1996, pp 391-402.

Leonel Tula and Paulo R. L. Helene¹

Methodology for Service Life Prediction of Stainless Steel Reinforced Structures Based on the Correlation between Electrochemical and Mechanical Manifestations of Corrosion

Reference: Tula, L. and Helene, P. R. L., “Methodology for Service Life Prediction of Stainless Steel Reinforced Structures Based on Correlation between Electrochemical and Mechanical Manifestations of Corrosion,” *Marine Corrosion in Tropical Environments, ASTM STP 1399*, S. W. Dean, G. Hernandez-Duque Delgadillo, and J. B. Bushman, Eds., American Society for Testing and Materials, West Conshohocken, PA, 2000.

Abstract: The use of stainless steel reinforcement is recommended for structures exposed to chloride contamination. Concrete structures reinforced with stainless steel are more durable than common carbon steel reinforced structures. In some projects, service lives of 120 and 200 years have been projected. Long-term field experience, which confirms these predictions, is not available. It would be very useful to obtain an acceptable approach to service life prediction. This paper proposes a methodology using the integration of electrochemical and mechanical behavior of the stainless steel rebar corroding in accelerated tests. The studied material is a 10 mm diameter 316L stainless steel bar. The carbon steel bar was included as part of the comparative performance study. The first part of the study analyzes corrosion potential data and potentiodynamic curves. The other part of the study is dedicated to the physical-mechanical consequences of the corrosion in the bars: the bond and tensile strength losses. Integrating both parts of the study and with the aid of some models allowed an approach to the service life prediction of structures reinforced with stainless steel rebars. Some questions for future work are presented.

Keywords: concrete, durability, reinforcement, service life prediction, stainless steel

¹ Ph.D. Researcher and Titular Professor, respectively, Department of Civil Construction Engineer, University of São Paulo (PCC / USP), Caixa Postal 61.548, São Paulo, SP 05424-970, Brazil.

Introduction

The last two decades were characterized by an increasing interest in service life prediction. When including design codes for durability in concrete structures, at least, four prediction techniques are available: previous experience or practice, accelerated tests², deterministic approach, and stochastic approach.

Some deterministic methods based on test results may become probabilistic since the compilation of an experimental database permits obtaining a good statistically based correlation. A very important fact is the determination of the adjusting coefficients between laboratory and field experiences.

The Tuutti model [1] performed by Helene [2] (Fig. 1) continues to be the simplest model for service life estimation of concrete structures affected by corrosion. This model considers an initiation period (t_0), and a propagation period (t_1).

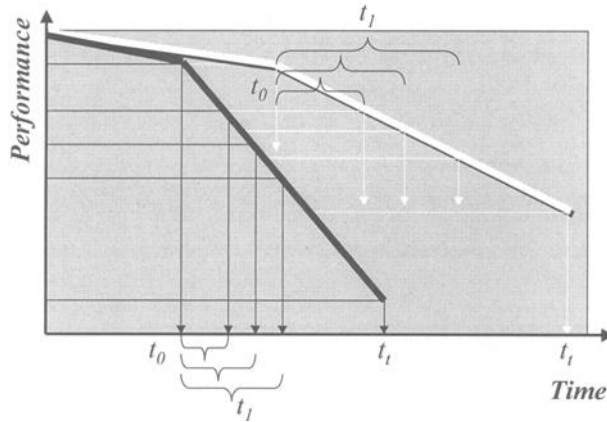


Figure 1 – *Service Life Model of Structures Reinforced with Bars of Two Types of Steel* [t_i – total service life].

From the electrochemical point of view, the initiation period is characterized by the thermodynamic conditions, which cause the loss of passivity of steel. It depends on the corrosion resistance of the steel, on the aggressiveness of the environment and on the protective properties of the concrete (acting as a physical-chemical barrier). The propagation period is characterized by the kinetics of the corrosion process, which depends on the contamination regime (above the tolerable threshold) and on the corrosion resistance of the steel. The initiation period (t_0) defines a *designing service life*, and the propagation period defines a *serviceability service life* ($t_0 + t_1$) of structures which may be limited by some corrosion damage with varying incidence in the concrete structure.

² For example, ASTM E 632-88, “Standard Practice for Developing Accelerated Tests to Aid Prediction of the Service Life of Building Components and Materials.”

Damage such as spots and cracks affect the visual performance of structures. Other damage such loss of bond and tensile strength affects the load bearing capacity of structural elements and in very advancing stages may define the *total service life* (t_t) of concrete structures. These damages can be studied as physical-mechanical manifestations of corrosion. It is possible to correlate them with the corrosion resistance of the steel.

The highly criticized accelerated tests, developed for performance studies, are encouraged as the main way of obtaining the necessary answers to the durability problems of new materials. Accelerated tests with impressed current are currently used for evaluation of physical-mechanical manifestations of corrosion.

Long term periodical measurement of the electrochemical potential and the corrosion current density (determined directly or indirectly) is now being used for electrochemical determinations.

The principal aim of this paper is to present the methodology proposed for a laboratory approach to the prediction of the service life of concrete structures exposed to an aggressive chloride environment. This methodology was implemented in an experimental research using stainless steel 316L rebars and carbon steel CA50³ rebars.

Experimental

The different studies involved in the research were:

Study 1. Evaluation of the electrochemical performance [3]. The experimental program was oriented to study the thermodynamic and kinetic behavior of metallic bars in concretes with different levels of chloride contamination.

Study 2. Evaluation of the physical-mechanical performance [4-6]. The experiments intended to study the relationship between corrosion grade and the deterioration of load bearing capacity - loss of bond and tensile strength. The process of crack formation at concrete surface due to corrosion was also studied but will not be discussed in this paper.

Study 1. Electrochemical Behavior of Reinforcements Corroded by Chloride.

Study 1.a. - Determination of average electrochemical potentials (E_{corr}^m) for different levels of chloride contamination. The electrochemical potentials were determined following ASTM C876:1990, "Standard Test Method for Half-cell Potentials of Uncoated Reinforcing Steel in Concrete."

Study 1.b. - Determination of average corrosion current densities (i_{corr}^m) for different levels of chloride contamination using potentiodynamic polarization technique. The parameters adopted for the tests were: polarization rate of 0.25 mV/s, starting polarization at open-circuit potential (E_{oc}) or at -250 mV of E_{oc} , final polarization at +800 mV_{SCE} (related to saturated calomel electrode). The polarization began only after the stabilization of E_{oc} . Some care was taken during the tests in order to maintain the internal moisture content⁴ (IMC) and temperature (T) of concrete specimens.

³ Brazilian Code, NBR 7480:1985, "Steel Bars and Wires for Reinforcement of Reinforced Concrete."

⁴ Relation, in percentage, between the actual moisture content and the moisture content in saturate condition.

Study 2. Mechanical Behavior of Reinforcements Corroded by Chloride.

Study 2.a. - Determination of bond strength of reinforcements (τ) with different corrosion grades. The τ was determined by pull-out tests as recommended by RILEM/CEB/FIP RC 6 (1978): Essais Portant sur L'adhérence des Armatures du Béton.

Study 2.b. - Determination of tensile strength of reinforcements (f_s) with different corrosion grades. The f_s was determined by stress-strain tests as recommended by NBR 6152:1987 Test Method for Determination of Mechanical Properties in Tension of Metallic Materials.

Independent Variables:

Study 1 - type of steel [carbon and stainless steel], concrete chloride content by cement mass (Cl_{cc}) [0%, 0.4%, 1% and 5%], tensile condition [relaxed and tensioned bars].

Study 2 – type of steel [carbon and stainless steel], time of impressed current [0, 3, 6, 12 and 20 days].

Dependent Variables:

Study 1 – electrochemical potential (E_{corr}), visual observation, polarization curves, corrosion current density (i_{corr}).

Study 2 - weight loss (Δm), bond stress-displacement diagram, ultimate bond strength (τ_u), stress-strain diagram, ultimate tensile strength (f_u) and yield strength (f_y).

Calculated or Graphically Determined Parameters:

Study 1 – E_{corr}^m , Average Anodic Polarization Curves (AAPC); i_{corr}^m .

The E_{corr}^m is calculated from measurement E_{corr} of specimens of 20 to 65 weeks.

The i_{corr}^m was determined graphically by evaluating E_{corr}^m in AAPC. The specimens used for potentiodynamic polarization were of 45 to 65 weeks.

Study 2 – average bond strength (τ_m) calculated by equation (1) [7].

$$\tau_m = \frac{\tau_{10} + \tau_{100} + \tau_{1000}}{3} \tag{1}$$

where: τ_{10} , τ_{100} , and τ_{1000} = Bond strength at 10, 100 and 1000 μm displacement.

Materials:

The materials of reinforced concrete specimens are described in (Tables 1 to 4).

Table 1 – Bars. Chemical Composition [% by mass].

Steel	C	Si	Mn	Cr	Ni	Mo	Cu	N	P	S
Carbon	0.20	0.15	0.55	0.04	0.02	<0.01	0.03	0	0.032	0.028
316L	0.0224	0.33	1.86	16.16	10.12	2.14	0.33	0.089	0.033	0.0255

Table 2 - Bars. Tensile Properties.

Steel	Yield strength [MPa]	Ultimate strength [MPa]	Ductility [%] (to 5 ϕ)	Area reduction [%]
carbon	640	760	12	74
316L	725	860	25	65

Table 3 - Bars. Geometric Characteristics.

Steel	ϕ nominal [mm]	ϕ real [mm]	Surface area [mm ² /cm]
carbon	10	9.89	379.8
316L	10	10.29	373.3

Table 4 - Concrete. Mix and Reological Properties.

Concrete	Concrete components [kg/m ³]			In relation to cement mass		Slump [mm]	Fresh unit weight [kg/m ³]	Average Compressive strength at 28 day [MPa]
	C	S	G	W/C	CI			
c0					0	174	2367	34.6
c04	310	775	1085	0.65	0.004	161	2353	34.5
c1					0.01	132	2335	34.7
c5					0.05	140	2337	33.5

Exposure Conditions:

Study 1 – Specimens inside laboratory, in partial moisture condition for 65 weeks, $IMC = 86\%$, $T = 22^{\circ}C$.

Study 2 – Specimens inside laboratory, in partial moisture condition, corrosion was accelerated by impressed current of $50 \mu A/cm^2$, $IMC = 86\%$, $T = 22^{\circ}C$.

Specimens:

Study 1 – The specimens of relaxed bars (“R”) shown in Fig. 2 were those commonly studied in electrochemical research. The specimens of tensioned bars (“T”) were flexural beams as shown in Fig. 3. Each specimen “R” and “T” had 4 bars with only 5 cm exposed to corrosion.

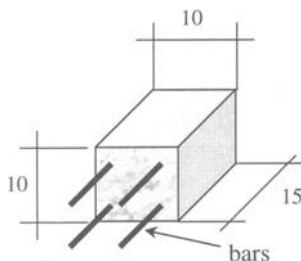


Figure 2 – Specimens of Relaxed Bars, Type “R” [in cm].

More than 3 specimens “R” or “T” are recommended for potentiodynamic tests. At least 6 bars must be used for polarization curves starting at ($E_{oc} - 250$) mV, and 6 bars for curves starting at E_{oc} .

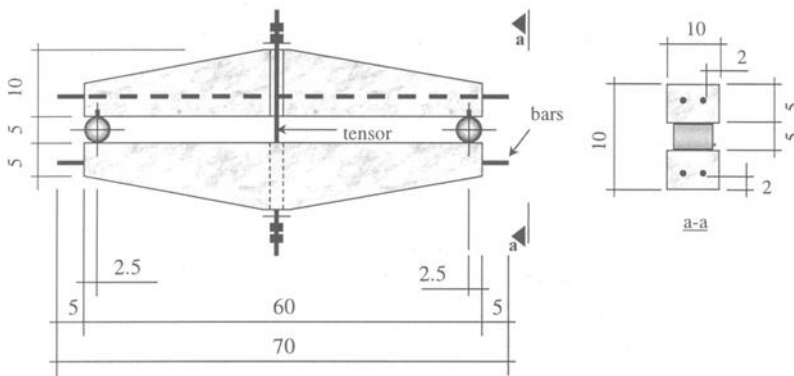


Figure 3 – Flexural Specimens of Tensioned Bars, Type “T” [in cm].

Study 2 – The specimens for pull-out tests follow RILEM/CEB/FIP RC 6 recommendations. The specimens for stress-strain tests (“S”) are shown in Fig. 4. For “S” specimens the exposed area of the bars reached 10 cm in length. All specimens were cured for 28 days in a moisture chamber ($RH = 95 \pm 5\%$ and $T = 22^\circ\text{C}$).

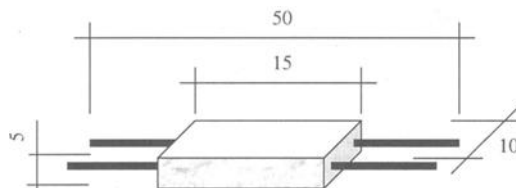


Figure 4 - Specimens Type “S” [in cm].

Specifications for Calculation of Average Anodic Polarization Curves (AAPC) [8].

- 1) Curves that present an extremely different profile when compared with the common profile of the group of curves obtained from specimens of the same case study (same chloride content and same tensile condition) must be rejected;
- 2) Every segment of calculated AAPC should be the result of more than three accepted individual polarization curves of the same case study;
- 3) The lowest potential of AAPC has to be lower than E_{corr}^m ;
- 4) It is useful for graphical determinations to obtain at least one curve with starting potential near (± 50 mV) of E_{corr}^m .

Results and Discussion

Study 1 – Table 5 shows the calculated E_{corr}^m . Based on E_{corr} measurements, visual observation and analysis of polarization curves by Evans and Pourbaix diagrams [8], it was possible to recommend a thermodynamic interpretation of E_{corr} measurement of stainless steel rebars, as shown in Table 6.

Table 5 - Calculated E_{corr}^m [mV_{SCE}] of Specimens in Partial Moisture for 65 Weeks.

		Cl_{CC}			
		0%	0.4%	1%	5%
Carbon steel	Relaxed	-183 ± 58	-226 ± 67	-385 ± 65	-564 ± 61
	Tensioned	-227 ± 62	-275 ± 91	-355 ± 118	-415 ± 165
316L	Relaxed	-98 ± 44	-90 ± 44	-102 ± 57	-140 ± 65
	Tensioned	-140 ± 49	-165 ± 64	-167 ± 61	-208 ± 93

Table 6- Proposed Thermodynamic Interpretation of E_{corr} Measurement for Stainless Steel.

E_{corr} [mV _{SCE}]	E_{corr} [mV _{Cu/CuSO4}]	Thermodynamic interpretation
> 0	> -60	Dissolution of passive film
-180 to 0	-240 to -60	Perfect passivity
-400 to -180	-460 to -240	Imperfect passivity
< -400	< -460	Possible pits formation

Between the accepted curves of each case study, an *AAPC* was calculated. As an example, Figs 5 and 6 show the *AAPC* obtained from relaxed bars of carbon and stainless steel bars.

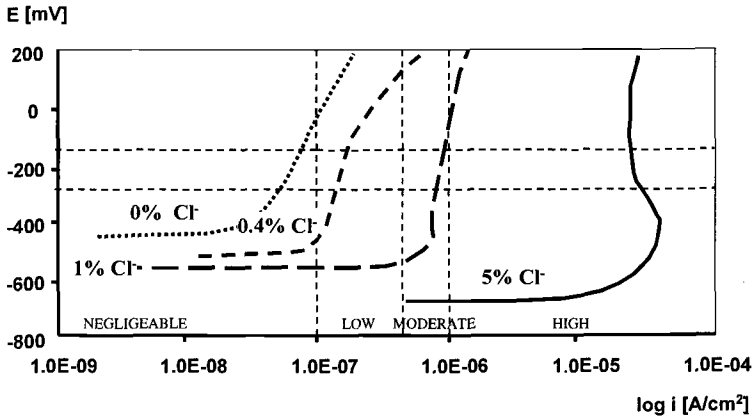


Figure 5 - *AAPC* of Relaxed Bars of Carbon Steel in Concretes with Different Cl_{CC} .

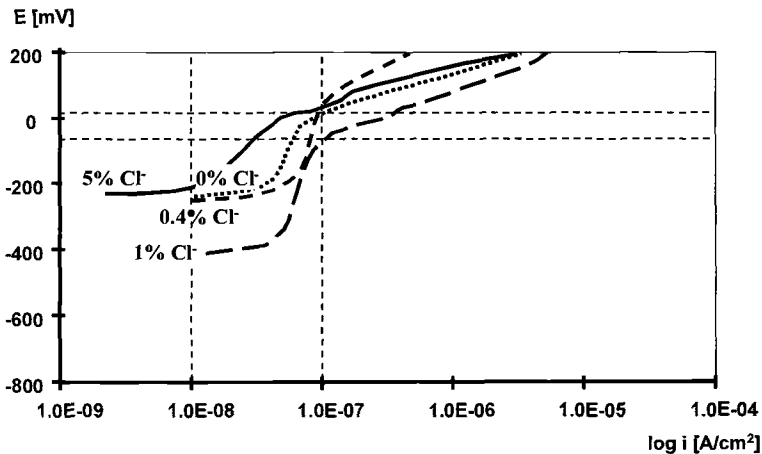


Figure 6 - APC of Relaxed Bars of Stainless Steel in Concretes with Different Cl_{CC} .

Electrochemical instability and determined i_{corr}^m confirm the loss of passivity of carbon and stainless steel bars. Proposed chloride thresholds in Table 7 are conservative.

Table 7 - Laboratory Determined Chloride Content Corresponding with the Loss of Passivity, Recommended as Chloride Threshold [in % of cement mass].

		Loss of passivity [%]	Recommended chloride threshold [%]
Carbon steel	Relaxed bars	at 0.4	0.4
	Tensioned bars	between 0 and 0.4	0.2
Stainless steel	Relaxed bars	between 1 and 5 (near 5%)	1.0
	Tensioned bars	between 0.4 and 1 (near 1%)	0.4

The corrosion current densities recommended for the service life estimation (i_{corr}') for each case study are shown in Table 8. These i_{corr}' are determined from integral analysis of i_{corr}^m data, visual observations and analysis of polarization curves aided by Evans and Pourbaix diagrams. Tensioned bars of carbon and 316L stainless steel showed approximately one order of magnitude higher corrosion current densities than relaxed steel bars [3].

Table 8 – The Recommended Corrosion Current Densities for the Service Life Estimation of Each Case Study [i_{corr}' – in $\mu A/cm^2$].

		Cl_{CC} [%]			
		0 to 0.2	0.2 to 0.4	0.4 to 1	1 to 5
Carbon steel	Relaxed bars	Negligible *			0.025 to 0.30
	Tensioned bars	Negligible *	0.80 to 1.40	1.40 to 2.50	2.50 to 10.0
Stainless steel	Relaxed bars	Negligible *			0.05 to 0.30
	Tensioned bars	Negligible *	0.20 to 0.30	0.30 to 10.0	

* Verified passivity of steel.

The correlation between chloride contamination grade (Cl_{CC}) and corrosion current density (i_{corr}') for each case study was determined. The equations shown in Table 9 may

be properly applied for service life calculation of structures with the same materials and conditions (normal concrete of 35 MPa, W/C = 0.65, IMC = 86% and T = 22°C) used in present study.

Table 9 - Correlation between i_{corr}' and Chloride Contamination Grades [in $\mu A/cm^2$]

		Chloride content [by cement mass]	Relation
Carbon steel	Relaxed bars	0.4%	$i_{corr}' = 0.432 \cdot Cl_{CC}^2 - 0.1324 \cdot Cl_{CC} + 0.0354$
	Tensioned bars	0.2%	$i_{corr}' = 0.0106 \cdot Cl_{CC}^2 + 2.0533 \cdot Cl_{CC} + 0.4676$
Stainless steel	Relaxed bars	1%	$i_{corr}' = 0.0625 \cdot Cl_{CC} - 0.0125$
	Tensioned bars	0.4%	$i_{corr}' = 0.4909 \cdot Cl_{CC}^2 - 0.5207 \cdot Cl_{CC} + 0.3297$

A good correlation between physical-mechanical manifestation and current transferred charge (c_{corr}) by expression (2) was determined. The formation of cracks at concrete surface may be characterized by the determined value of c_{corr} . The loss of tensile and bond strength with corrosion progression may be characterized by determining the value of c_{corr} (Fig. 7 and 8). The values of current transferred charge of interest for service life calculation (c_{corr}') are shown in Table 10.

$$c_{corr} = i_{corr} \cdot time \tag{2}$$

Table 10 - Corrosion Transferred Charges of Interest for Service Life Calculation (c_{corr}').

	Load-bearing capacity loss	
	Bond loss c_{corr}' [$\mu A/cm^2$ year] *	Strength loss c_{corr}' [$\mu A/cm^2$ year] *
Carbon steel	0.41 (25% of loss)	0.87
Stainless steel	0.53 (30% of loss)	0.68

* Negligible bond and strength losses happen with $c_{corr} > c_{corr}'$

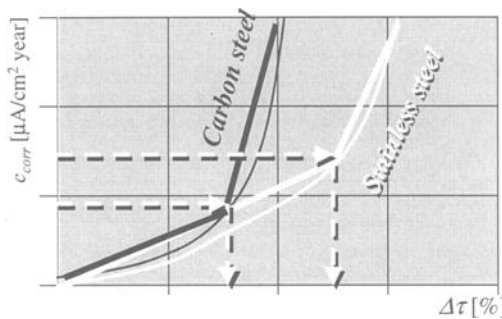


Figure 7 - Expressive Changes of Loss of Bond Strength ($\Delta\tau$) with Corrosion of Carbon and Stainless Steels.

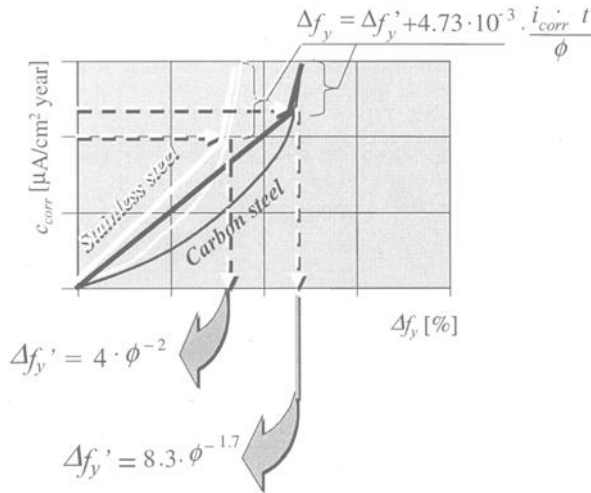


Figure 8 - Expressive Changes of Loss of Yield Strength (Δf_y) with Corrosion of Carbon and Stainless Steel (ϕ - nominal diameter of the bars; $\Delta f_y' = \Delta f_y$ at inflexion point).

The study of ultimate bond strength resulted in identification of three different behaviors depending on corrosion grade: the pre-cracking stage, the micro-cracking stage, and the lubrication stage (Fig. 9). With respect to tensile strength, three stages were described: initiation of pits, development of pits and saturation of pits (Fig. 10).

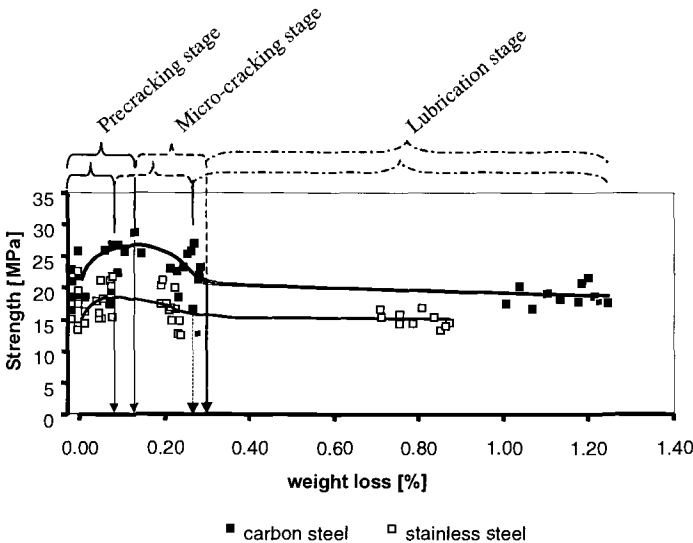


Figure 9 - Relation between Ultimate Bond Strength and Weight Loss for Carbon and Stainless Steel Bars. Identification of Corrosion Stages.

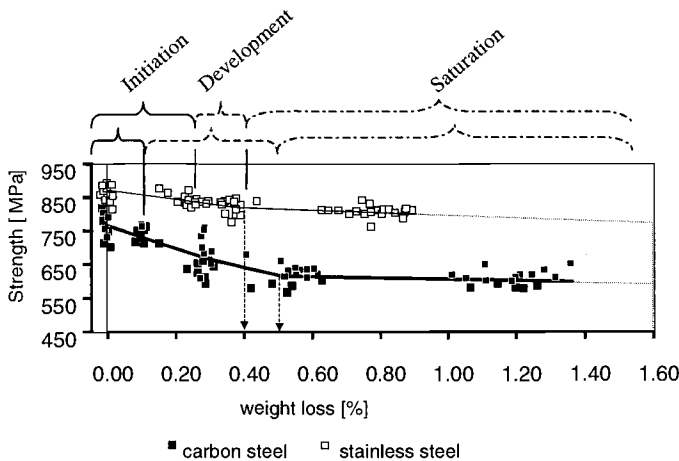


Figure 10 - Relation between Yield Strength and Weight Loss for Carbon and Stainless Steel Bars. Identification of Pit's Stages.

Correlation between Electrochemical and Mechanical Manifestation of Corrosion for Service Life Prediction

A methodology was adopted to correlate the results of Study 1 and 2.

Methodology for Service Life Prediction

Designing Service Life Prediction –Fick’s Second Law or other recently developed probabilistic methods may be used for predicting the chloride penetration process. It is important to know the environmental conditions and the concrete properties.

1) It is possible to predict the contamination regime (CI_{CC} versus **time**).

Serviceability Service Life Prediction – A laboratory approach based on accelerated models may be estimated as follows:

- 2) Predict the corrosion current densities by time, based on predicted contamination regime and on found relation (i_{corr} versus CI_{CC});
- 3) Determine the corrosion regime (c_{corr} versus **time**);
- 4) Predict the physical-mechanical behavior (c_{corr} versus $\Delta\tau$), (c_{corr} versus Δf_y) or (c_{corr} versus **crack appearing**);
- 5) Determine the serviceability by considering maximum tolerable damage.

Total service life prediction – The collapse of structure may occur when the loss of load bearing capacity reaches maximum admissible level:

- 6) Determine the total life of structures by maximum admissible damage.

Adjusting coefficients – The adjusting coefficients are necessary for correlation between laboratory and field experiments. It is very important to obtain a consistent and systematic database of experimental results and of *on site* observations.

The serviceability of more critical locals of structure ($t_{local.serv.}$) is:

$$t_{local.serv.} = (t_0 K_0 + t_1 K_1) \cdot K_g \tag{3}$$

where: K_0, K_1, K_g = adjusting coefficients of initial period, propagation period and global adjusting coefficient, respectively.

The serviceability of structural piece ($t_{general\ serv.}$) also depends on its function, which defines the tolerable grade of incidence of specific damages. For example: It may be possible to limit the incidence of cracks due to corrosion in 15% of concrete surface of pier column. However, for an industrial tank of chloride solution this type of damage should be restricted to 5% or less.

$$t_{general\ serv.} = t_{local\ serv.} \cdot \rho \quad (4)$$

where: ρ = Coefficient that considers the tolerable grade of incidence of observed damage

Calculated Example

The service lives of two structures were calculated with adopted methodology: marine pier and industrial chloride solution tank. Table 11 shows how many times the stainless steel rebars will increase the service life of structures. For this example some adjusting coefficients were used, based on subjective criteria.

Table 11 – *Increased Service Life Length of Stainless Steel Variant in the Case of Two Hypothetical Examples.*

Structure	Elements	Designing service life	Serviceability service life	Final service life
Marine pier	Column and beam	47	36	5
Reservoir (14% Cl)	Wall	3	2.5	2
	Slab	8	11	8

Future Work

- Define more exactly the chloride threshold of stainless steel bars, relaxed and tensioned, using different types of cements, different W/C ratio and different exposure conditions.
- Extend the corrosion *versus* contamination correlation to other case studies.
- Study the relation between laboratory and field experiences to better define the adjusting coefficients.

Conclusions

Based on the experimental results, the following conclusions may be drawn:

- The average electrochemical potentials observed for carbon and for stainless steel bars are in accordance with other investigations [9, 10].
- A thermodynamic interpretation for electrochemical potential measurements of stainless steel rebars was proposed.
- Service life prediction of stainless steel rebars must consider: chloride threshold, and corrosion current densities as functions of chloride contamination (i_{corr} *versus* Cl_{CC}), and the electrochemical transferred charges (C_{corr}).
- A proposed methodology for service life calculation of structures exposed to chloride environments was tested satisfactorily.

Acknowledgment

The experimental work described in this paper was performed in the Construction Materials Laboratory of the University of São Paulo, with the financial support of the Foundation for Aid Research of São Paulo State (FAPESP) and Villares Metals S.A.

References

- [1] Tuutti, K., "Corrosion of Steel in Concrete," Swedish Cement and Concrete Institute (CIB) N. 4-82, Stockholm, 1982.
- [2] Helene, P., "Contribution to Study of Corrosion of Reinforcement in Concrete," São Paulo, 1993, Free-docent Thesis, University of São Paulo (in Portuguese).
- [3] Tula, L., Helene, P., and Panossian, Z., "Evaluation of Stainless Steel Bars for Concrete Structures by Analysis of Potentiodynamic Polarization Curves," In Proceedings: 3th NACE Latin American Region Corrosion Congress, Ref. 9838S3, 1998, pp. 1-12.
- [4] Tula, L., and Helene, P., "Bond Reduction in Stainless Steel Bars Caused by Corrosion in Concrete," In Proceedings: 3th Colloquia '98, São Jose dos Campos, Fev., 1999, 8p. (in Portuguese).
- [5] Tula, L., and Helene, P., "Tensile Strength Reduction of Stainless Steel Bars Caused by Corrosion in Concrete," In Proceedings: CONPAT '99, Montevideo, Oct. 1999, 10p. (in Spanish).
- [6] Ticianelli, F., Helene, P., and Tula, L., "Evaluation of Expansive Effect of Corrosion in Concrete of Stainless Steel Bars," Second Report to FAPESP, São Paulo, 1998, University of São Paulo. (in Portuguese).
- [7] Isa, M. M., "Concrete-Rebar Bond: The Influence of Corrosion and Cathodic Protection," PhD Thesis, São Paulo, 1997, University of São Paulo. (in Portuguese)
- [8] Tula, L., Helene, P., and Panossian, Z., "Study of Electrochemical Performance of Ordinary Black and Stainless Steel Reinforcing Bars in Chloride Contaminated Concrete," In Proceedings: 2nd NACE Brazil Regional Congress, São Paulo, Oct. 1999, 13p.
- [9] Pedefferri, P., "Behavior of Stainless Steel in the Rehabilitation of Corrosion Damaged Infrastructures and Effects of Galvanic Coupling between Carbon Steel and Stainless Steel," In Proceedings: 3th NACE Latin American Region Corrosion Congress, Ref. 9802S3, 1998, pp. 1-11.
- [10] Leckie, H. P., and Uhlig, H. H., "Environmental Factors Affecting the Critical Potential for Pitting in 18-8 Stainless Steel," *Journal of Electrochemical Society*, No. 12, Dec., 1966, pp. 1262-1267.

Cathodic Protection, Microbiological Influenced Corrosion, and Seawater

Edgar W. Dreyman¹

Cathodic Protection of Structures in Coral Sands in the Presence of Salt Water

Reference: Dreyman, E. W., “**Cathodic Protection of Structures in Coral Sands in the Presence of Salt Water**,” *Marine Corrosion in Tropical Environments*, ASTM STP 1399, S. W. Dean, G. Hernandez-Duque Delgadillo, and J. B. Bushman, Eds., American Society for Testing and Materials, West Conshohocken, PA, 2000.

Abstract: This paper covers the use of cathodic protection in saline muds and soils to protect steel and aluminum structures such as tanks and piping. The history of this type of corrosion control in the Caribbean Islands is covered, as well as developments over time in this part of the world. The conditions encountered with saline muds and sands are unique to these areas and lend themselves to specialized application of galvanic and impressed current corrosion control.

Keywords: Marine corrosion, tropical seawater corrosion, saline muds, cathodic protection, saline environments

Introduction:

As has been well established, 2 corrosion loss to infrastructures in tropical saline environments has been extensive and is an ongoing phenomenon. A unique segment of this activity is corrosion of steel and other metals, such as aluminum, in coral sands and mud.

The location of this type of specific activity naturally occurs in areas of coral growth, present and past. Consequently, this paper deals with geographical areas such as the Caribbean Islands and the beach areas of Central America and northern South America.

The importance of corrosion in these countries is not only the loss of structure, but also the cost of such failures to a developing country. For this reason, not only is remedial action mandatory, but must also be of a practical and cost-effective mode.

Additionally, since tourism is a primary source of income in most of the areas mentioned above, the loss of petroleum products from pipelines and storage tanks is completely unacceptable. The fouling of recreational beaches can shut down tourism permanently. The oil companies servicing these islands and small countries have been aware of this situation since they have been providing product by ship or from small "pocket" refineries.

¹Retired Engineer, 4321 Hunters Pass, Brooksville, FL 34606

²West, Howard, Esso Oil Co., Coral Gables, FL (1970)

Cathodic protection engineering has been prevalent since World War II, starting in Panama with its U.S. Naval stores and Panama Canal locks. With the development of refineries in Panama, Curacao, Aruba, Guatemala, Trinidad, Honduras, Costa Rica, and Puerto Rico, the engineering departments of these oil companies not only protected refinery equipment, but also docks, pipelines, and storage tanks.

Ultimately, the value of this work became apparent to the host countries, so today we find cathodic protection being employed to protect underground water and gas lines, water tanks and fuel lines, as well as storage tanks.

The Environment:

The conditions prevalent at these locations entail the following:

- Sea water
- Brackish water
- Coral mud
- Coral sand
- Combinations of the above

The latter are the usual situations that are encountered and can be under quiescent or turbulent highly oxygenated conditions.

Electrolyte resistivity can vary from clean seawater at 20.5 ohm-cm to saline muds of 300-500 ohm-cm to brackish water conditions with resistivity up to 5000 ohm-cm.

Oxygen content can vary from high level in the splash zone, to areas supporting sulfate-reducing bacteria in the complete absence of oxygen. Furthermore, in many developing countries frequently occurring pollution by sewage is common which further complicates remedial measures.

A unique condition encountered on land that has been built up from coral deposits is the presence of blowholes, fissures, and caves which augments the penetration of seawater to areas remote from the actual seashore. Knowing that seawater makes for a very extensive, uniform, low resistivity "ground bed" for cathodic protection anodes, the above condition facilitates the design of unique cathodic protection systems.

In the presence of seawater penetration augmented by tidal action, the normal limited drying out of ground beds does not occur. Furthermore, due to the granular nature of coral sands, a gas blockage is not a factor. Consequently, "remote" ground beds of high efficiency can be readily achieved with anodes placed in seawater for protecting structures a considerable distance from such locations.

Typical Infrastructures:

Typical structures encountered in coral sand and mud are as follows:

Petroleum Product Lines

These can run from several inches in diameter to a 24"/30" diameter and from

hundreds of feet up to 29 miles in length. Smaller pipe can be bare, galvanized, or poorly coated with coal tar mastic; also, epoxy or polyethylene tape which can be field or factory applied.

Larger pipe is usually factory coated and shipped to the site. In most cases, this is as "deck cargo," resulting in mechanical damage to the coating. Consequently, when installed in coral sands in salt water intrusion areas, corrosion can be expected.

Typical installations using cathodic protection are:

- 7 miles, 8" steel pipe - Bahamas;
- 11 miles, 8" steel pipe- Bermuda, and
- hydrant fueling systems at airports in Trinidad, Bahamas, Barbados, Puerto Rico, Bermuda and Jamaica in pipe sizes to 24" with C-2007, polyethylene tape systems, fusion bonded epoxy or coal tar epoxy coating.

In many instances, the cathodic protection design entailed the use of shallow "deep wells," approximately 50 feet deep, sunk in coral caves full of seawater. Alternate ground beds were employed in sea beds adjacent to airport locations. In all cases, very uniform current densities were generally achieved along the entire pipe lengths.

In some island situations, where deep water is not available at the shore line, offshore moorings are necessary to off-load product and pump it ashore. This may vary from 1000 feet to as much as half a mile from shore, requiring piping laid in the seabed. This requires trenching the line into place or allowing the seabed to cover the lines from natural movement due to water activity that can be promoted by storms.

A common cathodic protection design is the use of bracelet anodes that originally were zinc, but now with improved alloys are usually aluminum. Alternately high silicon cast iron anodes, mounted on sleds, buried in the sea bed 250 feet from a given pipeline and midway between shore and the spar buoy ship connection have performed well. Anode return cables can be a maintenance problem unless properly secured to the pipelines and buried at least 5 feet into the sea bed between the pipelines and the anode sled. Anode beds can also be installed in the beach itself, but must be deep enough to be in the saltwater intrusion area.

High silicon cast iron anodes must be of the chromium-containing alloy due to chlorine evolution and preferably be of tubular construction. Extreme care must be exercised in protecting cable connections and employing cable jacketing that will stand abrasion. In protected areas, high molecular weight polyethylene will work, but in more aggressive areas, special dual jacketing may be required.

In open seawater, platinum clad niobium or dimensionally stable anodes may be readily employed but must be secured properly and in a sturdy manner. In coral holes or caves, shallow deep wells can employ 1/4" rod anodes of the above types.

When considering developing nations' economies, the use of scrap steel must not be overlooked. Pipelines in Guatemala and Honduras have successfully used scrap rails with power connections being made above grade; bearing in mind that the consumption rate of steel is 20 pounds per amp year and, consequently, a 10-amp ground bed requires only 200 pounds per amp year so that a ton of scrap steel can provide a ten-year ground bed life span.

Molasses Production

As sugar cane production has increased for these island economies, the export of molasses has become a cash product. In most cases, steel lines are run from shore to deep water (30 feet) so that a similar situation exists as fuel delivery to shore in reverse.

A problem persists since these lines must be kept full of product or water to prevent floating of the lines. The logical fluid would be fresh water but with its scarcity, salt water is commonly employed. This leads to internal corrosion of these lines. Some firms, such as Bacardi, have used stainless steel lines; others have tried internal coatings, but with costs involved, many are still bare steel. Needless to say, the exterior of these lines must still be cathodically protected as previously described.

Aluminum Lines

In the early 1970's, Reynolds Metals Company pipe group, 3 working with Shell Oil (London), developed a unique method of joining aluminum pipe. Aluminum pipe had been employed in many industries to prevent product contamination, but with limited experience by most welders, the welding of aluminum pipe had not become an accepted practice. Jointly, these companies developed, tested, and put into service a small crawler type vehicle that could swage a slip fit collar over two butting sections of pipe. This eliminated welding and, furthermore, provided a light weight system whereby a technician and two helpers could easily join more than 1000 feet of pipe per day.

In developing countries, this was a cost-saving procedure especially in assembling aviation fuel hydrant systems. Installations in Bermuda, Bahamas, and Barbados were installed in areas of coral rock. However, concern over the corrosion of aluminum pipe under ground was a valid consideration, and protective measures were instigated. The pipe was coated with fusion-bonded epoxy or polyethylene jacketing (yellow jacket). The swaged sleeves were epoxy cemented, and the joints were wrapped with polyethylene tape.

In most cases, the pipe had to be installed in coral rock trenches and backfilled with coral sand of unknown chloride content. With a good coating and minimum "holidays," the current demand for pipe protection is minimal. Consequently, small zinc anodes (1.4" x 1.4" x 9") were successfully employed.

These were installed in gypsum backfill that was well wet down for proper operation. Pipe to soil potentials of around -1.00 volt were readily obtained and maintained thus being well within the range of not experiencing cathodic corrosion of the aluminum.

The aluminum pipe must be isolated from steel pipe, or galvanic attack may occur in the aluminum. To attain this isolation, double isolation flanges were employed above grade where the aluminum tied into the steel pipe.

With annual corrosion surveys conducted by outside engineers and monthly testing by resident staff, this system performed properly for some time.

Aluminum Pipe Problems

The first indication of problems, after several years of service, was the lowering of pipe potentials at some locations but not uniformly. It was established that in the coral sands in the Caribbean, the anode backfill was drying out and required periodic "wetting" during the dry season. The use of copper/copper sulfate reference cells also required adding water to the soil at reference cell/soil contact to obtain accurate readings even with high impedance meters. Care must also be maintained to make actual contact with soil. Matted vegetation also promotes high resistivity contact of a reference cell.

In saline soils, when aluminum pipe coating shows evidence of porosity, it was noticed that in the proximity of steel water lines, even without a direct short, some reduction (less electronegative) in potential was noted. Use of dielectric shielding of the steel pipe generally solved this condition.

Proximity of metal clad electrical cable also can be a problem. Furthermore, with aluminum being a "soft" metal, care must be exercised to prevent sharp stone from being in direct contact with the pipe if the pipe can vibrate during pumping. This type of failure has occurred at several installations.

The primary area of concern has been at the hand wrapped joints when saltwater has penetrated the wrapping with time. This corrosion has been augmented by cathodic corrosion from interference by impressed current cathodic protection systems. Since these aluminum pipe installations have been adjacent to steel pipe systems which are under cathodic protection, they have been affected by being in the potential gradient produced by the ground bed.

As the coatings show some deterioration with time, the current demand of the structures shows a need for more current. Where the above systems are adjacent to each other, this current increase has resulted in increasing the electronegative potential of the aluminum. As we have mentioned, zinc anodes, having an open circuit potential of approximately -1.0 volt, were ideal in protecting aluminum and ensuring that potentials never exceeded -1.0 volt; however, in the presence of impressed current, this was not the case, and corrosion of the aluminum was taking place.

The first action to be taken was to employ resistance bonds between the two piping systems and, with proper adjustment, prevented over-protection of the aluminum. Also we encountered an IR drop phenomenon, so that "instant off" potentials becomes the norm in evaluating actual pipe to soil potentials.

As mentioned, accidental contact with steel was the main problem, resulting in the aluminum becoming under protected. Another problem was encountered at airports where copper grounding rods were driven in close proximity to the aluminum line. Also, filters may become necessary to prevent rust deposits in steel tanks from migrating into aluminum lines. With jet fuels being mostly free of moisture, electrolytic action is minimal, but should be considered.

The overall use of these lines has been cost effective, but with internally coated steel and FRP piping, the cleanliness factor of aviation grade fuels has been assured without using aluminum.

On-Ground Tanks

Fuel storage on coral islands that are small but sufficiently separated from each other so that barging of product from one common location is not cost effective, dictates that each location have its own storage facilities. These are generally small-diameter (20-60 feet), but in the case of transshipment facilities (Aruba, St. Croix, Zaire, Curacao and Puerto Rico) may run up to 400 feet in diameter.

Foundations for these tanks vary from the tank bottoms being in oiled sand to being perched on sand foundations as much as five feet above grade. For installation on well drained sand pads, many installations do not employ cathodic protection at all. However, leakage from soil side plate corrosion of tank bottoms has been reported. This situation has occurred when mill scale has been prevalent on the plate.

Two factors have contributed to this condition; firstly, salt laden air has penetrated the underside of the tank due to floor movement of the tank bottom with variations in the amount of product in the tank. Then, the presence of this mill scale creates a small anode/larger cathode condition where the mill scale has cracked at the weld and, with time, allowed penetration at this weld. This, coupled with the reduction in soil resistivity from the chlorides in the air and undertank condensation, augments galvanic corrosion at the break in the mill scale.

This occurred after 7 years where a polyethylene liner had been installed 3" below the tank bottom. This liner was held in place with a padding of coral sand dust high in chlorides, and in the presence of condensation, created numerous galvanic cells. With the small clearance to the dielectric liner, a cathodic protection retrofit was not feasible.

At many island facilities, the original cathodic protection system had been carbon anodes, 10-15 feet below grade about 5 feet from the tank edge. These had a tendency to dry out, increasing the ground bed resistance, and resulting in loss of protection. As the nature of porous salt water caves under the tank forms become better understood, the use of shallow deep anode bed design became accepted. Several deep wells (50 feet) could readily protect an entire tank form, excluding any underground piping.

Although the salt-water-saturated sands provide a well-distributed current source, care must be exercised to locate areas of shielding due to true rock outcropping. This condition is more prevalent where higher resistance soils may exist from volcanic debris or basalt deposit. At times, these current "starved" areas can be treated with high potential magnesium anodes to provide "hot spot" protection. For larger diameter tanks this is not effective, and separate close coupled impressed current anode strings have been employed.

Monitoring of tank bottom steel had been done with copper/copper sulfate reference cells at the tank edge. Maintaining up to -2.0 volt at the tank edge usually guaranteed a -0.85 volt center potential, with ultimate tank bottom polarization. However, with the construction of larger diameter tanks this was no longer true.

The initial response to this situation was to install reference cells (during construction) at the center of the tank with lead wires terminating at the tank edge to monitor this area.

More recently, with the regulatory agencies calling for liners under tanks for

spill prevention, cathodic protection is being installed between the liner and the tank bottom. Consequently, a minimum of 6" of soil must be available for this purpose especially if the tank bottom slopes to a center drain.

With the advent of directional drilling, installation of anodes and reference cells can be retrofitted to existing tanks. With a shortage of chloride-free sand in many islands, sand has been imported from South America to provide proper sand beds for larger tanks (Panama).

Cathodic Protection Hardware:

Rectifiers

Power supply systems generally employed are rectifiers, with occasionally solar power use.^[1] The latter system costs continue to be reduced, so that the future for this type of equipment is promising, especially with "pulsed" D.C. current.

The most cost effective rectifiers seeing service are oil immersed units employing 110/220 volt A.C. input. Some locations have only 50 cycle A.C., so this should be established before ordering equipment. These units have no moving parts, with the main area of concern being the cases. Galvanized cases top coated with epoxy coating provide the best life. In some areas, sunshades are recommended.

Aluminum cases have been used, but if too close to the ocean, "white" rusting may occur. For small air-cooled units, F.R.P. cases are commonly employed as well as junction boxes.

Auto potential or constant current rectifiers are feasible, but must be considered in relation to specific designs. Bear in mind that more complicated systems have components that may be more difficult to replace on short notice or tie up capital in special spares.

Cable

Normally, 600 volt jacketing of HMWPE insulation is adequate. When abrasion may be a problem, placing cable in PVC conduit is helpful. Of more concern is the proper sizing of cable ampacity. With seawater or saturated coral sands and muds, one has a low voltage "system." If wire sizes are too small, the extra cable resistance can impact the efficiency of the system. Consequently, slightly oversized cable and redundant grounding connections become a part of good basic design.

Cable connections must be "robust" and be adequately insulated. Shrink sleeves and multiple tape layers are mandatory. Sufficient slack must be employed to prevent excessive stress on cable connections.

Anodes - Impressed Current

As discussed, materials from scrap steel to platinum clad titanium can be employed as anode materials. Since chlorine can be liberated, care must be exercised

that gas blockage is avoided. Any accumulation of chlorine will lead to anode-to-cable connection failures.

In moving seawater or coral muds, anodes may require support structures. Anode sleds have been used successfully for dock structure and ground beds in the sea floor. This latter application is applied to the protection of pipelines in the seabed.

Anodes - Galvanic

Zinc anodes have been used for many years in this environment, in free flowing seawater as well as buried in silts and sand. These anodes are low in cost and with well-coated structures will provide extended life of up to 20 years.

The use of long (4" x 4" x 60") zinc anodes works well for corrugated sheet piling and the internal webs of steel "H" piles. With weld-on rebar-to-anode cores, it provides anodes that can be welded to structures above mean low water.

In the last 20 years, new aluminum alloys have been developed that perform at 7.5 lb./amp year, compared to 23 lb./amp year for zinc. Depending on the metal market prices, this can equate to being the most cost effective alloy. One area of caution must be considered in that aluminum in mud, especially hot saline mud, may become inactive in a relatively short time. Consequently, these conditions must be avoided.

Galvanic bracelet anodes work well on pipelines and eliminate the possibility of cable failures experienced with impressed current systems. However, good welded connections to the pipes are mandatory or properly clad welded cable must be employed.

Cathodic Protection Monitoring:

A given cathodic protection system is no better than the monitoring system employed to ensure that the structure is properly polarized and maintained under protective potentials.

For soil conditions, copper/copper sulfate reference cells are used to monitor such systems. In mud or seawater situations, silver/silver chloride cells work best, since copper cells can be contaminated by seawater. Also, zinc reference cells used in seawater and of the proper alloy, will give years of reliable service.

Design Parameters:

The less exposed metal surface, the easier it is to protect a given structure. Consequently, a well-coated structure lends itself to fairly rapid polarization at minimum cost.

Although this is a different subject, with many variables, choice of coatings is very important. Alkyd or other coatings prone to alkali attack must not be used, since the cathodic surfaces will have an alkaline pH.

Protective potentials, free of IR drop, are generally -0.85 volt to a copper/copper sulfate cell and -0.80 to a silver/silver chloride cell. Other criteria, such as an electronegative shift of 300 mv or polarization with a potential shift of no more

than 100 mv upon current cut-off are also used. NACE standards are available that cover this criteria. (NACE Standard #RP 0169-96, *Control of External Corrosion on Underground or Submerged Metallic Piping Systems*).

A lot of work has been done on minimum current densities to achieve and maintain protection. These call for 10-12 ma/sq. feet of bare steel area initially to as low as 2 ma/sq. feet to maintain the protection after polarization. Typical corrosion rates in tropical seawater are 4 to 6 mils per year.^[2] This value drops off with time, since rust film and calcareous coatings are partially protective.

Variations in corrosion rates are affected by temperature (minimal), oxygen content of the seawater, rate of water movement, and the amount of abrasive material in the water. Closer to the equator, the tidal effects are less prevalent so that the pronounced effects in the tidal zone do not compare with northern conditions.

Furthermore, average corrosion rate should not be confused with pitting and maximum pit depths under specific conditions. Pit depths can readily be five times the average corrosion rate.^[3] Good practice generally calls for designing to 10 to 20% bare area of submerged metal, since with coated pipe being shipped as "deck cargo" and the presence of "sharp" coral backfill, greater coating damage can be experienced.

Conclusions:

In locations involving coral sands with salt water intrusion, a unique situation exists for low resistance ground beds that can provide cathodic protection over extensive areas. This applies to pipe, tank bottoms, and dock structures.

Properly coated aluminum pipe has performed well in this environment for over 40 years. This alloy requires active monitoring, but the added benefits of low-cost installation and lack of product contamination provide cost-effective systems.

Coral sands and muds lend themselves to standard cathodic protection materials, resulting in the use of low-cost components for either galvanic or impressed current systems. In such marine environments in semiarid areas, consideration must be given to atmospheric corrosion of components as well as proper monitoring procedures.

With good training programs for operators and moderate vigilance, these systems and the structures being protected will provide owners with an expected longevity for their structures.

References:

- [1] Kessler, R. J., Lasa, I. R., and Powers R. G. "Solar Power for Cathodic Protection," *Materials Protection*, Dec., 1998, 37 (12), pp. 14-19.
- [2] Hoe, K. H. Ray, SK, "Current Density for Cathodic Protection of Steel in Tropical Sea Water," *British Corrosion Journal*, 1998, 33 (3), pp. 206-210.
- [3] Alexander, A. L., Forgeson, B.W., and Southwell, C.P., "Corrosion of Metals in Tropical Environments," *Corrosion*, March, 1960, 19 (2), pp. 87-98.

Brenda J. Little,¹ Robert K. Pope,¹ and Richard I. Ray¹

An Evaluation of Fungal-Influenced Corrosion of Aircraft Operating in Marine Tropical Environments

Reference: Little, B. J., Pope, R. K., and Ray, R. I., “An Evaluation of Fungal-Influenced Corrosion of Aircraft Operating in Marine Tropical Environments,” *Marine Corrosion in Tropical Environments, ASTM STP 1399*, S. W. Dean, G. Hernandez-Duque Delgadillo, and J. B. Bushman, Eds., American Society for Testing and Materials, West Conshohocken, PA, 2000.

Abstract: Fungi were isolated and identified in ten aircraft that had been operating in marine tropical environments. Distribution and growth of fungi depended on availability of water and nutrients. Laboratory experiments demonstrated that surface washes, including the approved military maintenance procedure, were ineffective in removing fungal hyphae embedded in polyurethane coatings. Surface cleaning removed spores and discoloration associated with fungi, but fragments of the hyphae remained and grew as soon as conditions were favorable. Aged coatings fouled more rapidly than new coatings. Fungicides incorporated into the topcoats produced mixed results. Bare aluminum suffered localized corrosion when colonized by fungi.

Keywords: corrosion, fungi, marine atmosphere

Introduction

The presence of fungi on painted and bare surfaces of airframe components poses a potential problem for the structural integrity of the airframe. Fungal contamination is typically visible as brown and black patches of fungal hyphae and spores (Fig. 1-2). Hyphae undergo fruiting/development (reproduction) producing pigmented spores that make fungal colonies easily visible. Fungi are nonphotosynthetic microorganisms that grow by elongation of thread-like hyphae with average diameters of 5 μm . Hyphae contain a mass of cytoplasm and many nuclei. Fungi are classified by the structure of the spore package, spore ornamentation, motility, and sexuality of the spores.

Fungi are typically found inside aircraft operating in humid marine environments. Extreme cases of growth form thick masses, especially in areas of the aircraft not regularly cleaned, such as the bilge, behind sound insulation blankets, within tight spaces in the overhead, and behind fixed equipment, including electronics racks.

¹Naval Research Laboratory, Bldg. 1009, Stennis Space Center, MS 39529-5004.

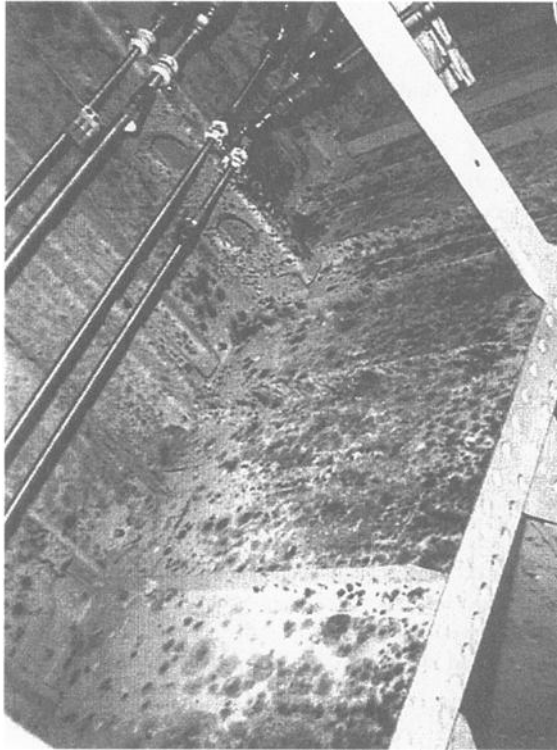


Figure 1 - Surface inside aircraft containing numerous fungal colonies. Brown colonies appear light gray, and black colonies, black.

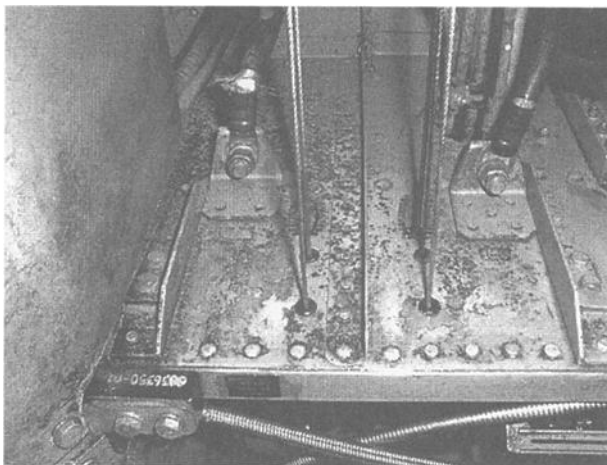


Figure 2 - Surface inside aircraft showing numerous fungal colonies. Brown colonies appear light gray, and black colonies, black.

Numerous reports document fungal growth in passenger compartments of in-service aircraft. Depot personnel report instances of refurbished helicopters being returned to depot for cleaning because of heavy fungal growth during storage periods between maintenance and first use. A report by Lavoie and Little documented the following 8 fungal genera associated with H-53 aircraft: *Pestalotia*, *Trichoderma*, *Epicoccum*, *Phoma*, *Stemphylium*, *Hormodendrum* (also known as *Cladosporium*), *Penicillium*, and *Aureobasidium* [1]. At least one of the isolates can degrade paint [2], and other studies report that fungi of the same class are capable of causing deterioration of polyester-based urethane coatings currently used on interiors of military helicopters [3,4].

Methods

Identification of Fungi

Ten helicopters at various stages of depot-level maintenance were examined and the interiors photographed. Walls, floors, and fluids were sampled for fungal contamination by direct contact plates of potato dextrose agar (PDA) (Fig. 3) and nutrient agar (NA). Plates were incubated in the laboratory at room temperature until colonies could be picked for isolation and maintenance. Fungal isolates were identified by characteristic growth on Sabourauds Medium, PDA, or cornmeal agar (CMA) and by microscopic examination of spore-bearing bodies. The gross appearance of a fungus growing on any particular surface depends on several variables, including available nutrients, colony age, physiological state, and growth environment. For this reason, fungi encountered outside the laboratory must be cultured under standard conditions to make reliable identifications.

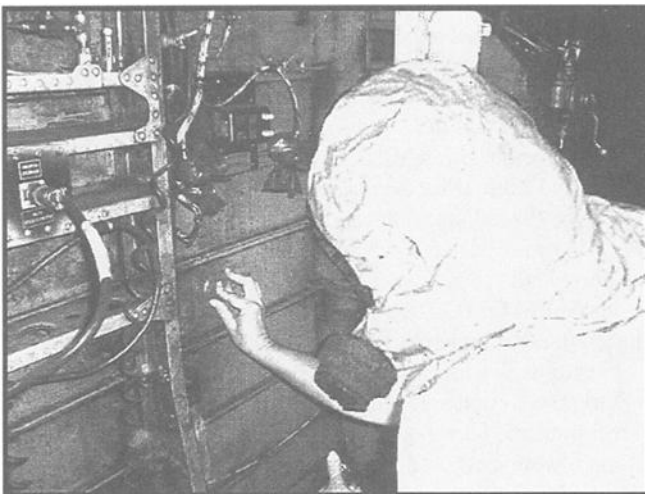


Figure 3 - Sampling of aircraft wall surface with a PDA direct contact plate, prior to cleaning of the wall.

Fungicide/Fungistat Evaluation

Test coupons of 25.4 X 25.4 mm aluminum alloy 2024-T3 were prepared according to standard protocols for repainting helicopter interiors. Coupons were cleaned with MIL-C-85570 detergent and water; pretreated with MIL-C-5541, Class 1A, chromate conversion coating; primed with one coat of MIL-P-85582, Type 1 waterborne epoxy and painted with two coats of MIL-C-85285, Type 1 polyurethane coating. One series of test coupons was coated with a flat version (currently used on all H-53 aircraft) of the topcoat paint per FED-STD-595B, color 36231, while another series was coated with gloss (color 16251). Three candidate fungicides/fungistats were added to the topcoats to make three series of coupons. A fourth series of controls contained no biocidal additive. The fungicides/fungistats included the following: Deft[®] X, a proprietary compound manufactured by the Deft[®] Paint Company (Park Ridge, IL), omacide, a 40% solution in high-flash naphtha of 3-iodo-2-propynyl butylcarbamate (IPBC), Olin Chemicals[®] (Stamford, CT) and zinc omadine, a powder consisting of 95% zinc pyrrithione (zinc 2-pyridinemethiol-1-oxide) and 5% inert ingredients, Olin Chemicals.[®] Final concentration of omacide in the paint was 2.5% by weight and zinc omadine, 1.0%. Each coupon was first cleaned with 100% isopropanol and divided into three areas for surface treatment. One portion was swabbed with lanolin-based preservative used as a surface treatment for long-term storage; another portion was swabbed with MIL-H-83282 hydraulic fluid which sprays from leakage in the gearbox and subsequently contaminates the interior of these aircraft during operation; the remaining portion was not treated further. The three surface treatments simulated the condition of helicopter interiors during field operations (before and after cleaning) and during storage. Coupons made from in-service painted (color 36231) aluminum pieces were scrubbed with MIL-C-85570 detergent, wiped with 100% isopropanol and used to approximate an aged painted surface as opposed to the other freshly painted surfaces. The age of the coating was estimated to be a minimum of 2 years.

The effect of fungi on synthetic polymeric materials was analyzed according to ASTM Standard Practice for Determining Resistance of Synthetic Polymeric Materials to Fungi (G21-90). The method was modified for bare and painted aluminum coupons. Aseptic microbiological techniques were used for all inoculations and transfers. Eight fungi isolated by Lavoie and Little (*Pestalotia*, *Trichoderma*, *Epicoccum*, *Phoma*, *Stemphylium*, *Hormoconis*, *Penicillium*, and *Aureobasidium*) [1] and two other isolates (*Fusarium* and *Aspergillus*) were used to prepare the inoculum. Isolates were grown on PDA plates to verify purity and produce a quantity of spores. After separating fungal spores from hyphae per ASTM G21-90, the concentration of the resulting spore suspension was adjusted to approximately 10⁶ spores per ml. The suspension was sprayed on coupons in petri dishes using a sterilized atomizer per ASTM G21-90 to deliver 10⁶ spores. Petri dishes contained a layer of PDA to maintain relative humidity within or above the recommended level during incubation.

Inoculated specimens were incubated in a sterile polyethylene disposable glove bag (ISI, Groten, CT) set on a low-heat electric pad maintained with filtered moist air passed through the bag for the first week. Bag openings were tightly closed to maintain humidity (polyethylene is permeable to oxygen). Relative humidity within the bag

remained at 85% or more and temperature stayed about 29°C, as measured with a combination thermometer/hygrometer kept inside the bag. Actual humidity within petri plates was greater than 85% as indicated by condensed moisture on plate covers. Coupons were examined periodically and the experiment terminated after 110 days.

Cleaning Experiments

Laboratory and field experiments were designed to evaluate the effectiveness of the following cleaning procedures: Approved military cleaning procedure of 100% isopropanol, Biofinish[®] (applied per manufacturers instructions), alcohol (100% isopropanol) + Biofinish[®] and So-Sure[®] (per MIL-C-81309E, Type III), a corrosion preventative compound. Effectiveness was evaluated by using PDA contact plates to quantify fungi on the surface immediately before and after swabbing the surface. In the case of alcohol + Biofinish[®] the surface was allowed to dry after the alcohol wash prior to application of Biofinish[®]. Environmental scanning electron microscopy (ESEM), a technique especially useful in the study of fungi [5], was used to document surfaces after swabbing with 100% isopropanol in the laboratory.

Results and Discussion

Surveys of Fungi From MH-53J Aircraft

Fungi could be cultured from all surfaces of all platforms. Distribution of organisms was not limited to standing water/fluids, but could be cultured from virtually all interior helicopter surfaces, including primer-coated and polyurethane coated aluminum, fiberglass structural members, caulking, synthetic fabrics, wiring, air-conditioning ducts, cockpits and bay areas. Concentration of organisms did depend on the availability of nutrients and water. Fungi were more numerous in low areas and occluded spaces holding water or hydraulic fluid (Fig. 4). The topcoat of a piece of peeling paint was uniformly colonized by fungi (Fig. 5a). Patches of fungi were also located on the primer side (Fig. 5b). It appears that the fungi penetrated the coating combination, but that can not be conclusively determined from the single piece of paint. Laboratory analysis of freshly collected MIL-H-83282 hydraulic fluid from a reservoir indicated no problems with fungal contamination. Isolates varied among the platforms. Little species diversity was observed among the platforms despite their operation in different locations and their repair and overhaul maintenance at the depot (Table 1). In all cases *Aureobasidium* sp., *Aspergillus* and *Hormoconis* were present.

Fungicide/Fungistat Studies

The inoculum prepared from the fungal isolates was viable and produced black colonies on PDA after 67 hours. Aged coatings were the first to be colonized, and colonies were evident on the cleaned, lanolin coated, and sections coated with MIL-H-83282 hydraulic fluid by 18 days (Fig. 6). Bare 2024-T3 aluminum coupons were colonized by 110 days in areas coated with lanolin and hydraulic fluid (Fig. 7), and

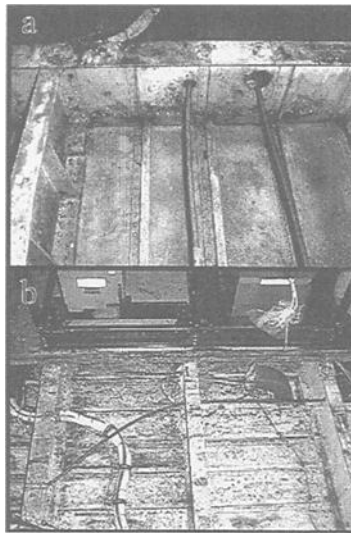


Figure 4 - (a,b) Areas under floorboards of aircraft containing numerous fungal colonies.

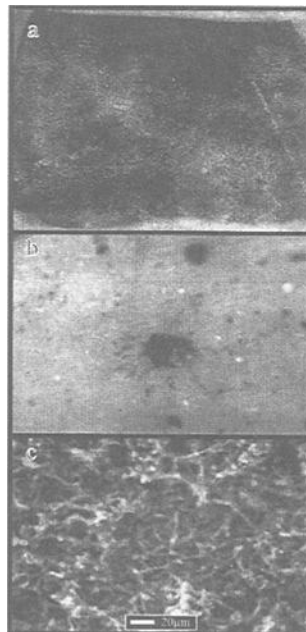


Figure 5 - Paint chip removed from an aircraft. (a) Polyurethane outer coating with complete coverage by fungi; (b) low mag. micrograph of primer side of paint chip showing fungal growth on the underside of the paint (between primer and base metal); and (c) ESEM micrograph of fungi from panel A.

TABLE 1	
AIRCRAFT NUMBER	FUNGI
1	<i>Alternaria</i> <i>Alternaria/Penicillium</i> <i>Alternaria/Fusarium</i>
2	<i>Alternaria</i> <i>Alternaria/Aspergillus/Fusarium/Trichoderma</i> <i>Alternaria/Hormoconis/Penicillium</i>
3	<i>Epicoccum</i>
4	<i>Penicillium</i> <i>Alternaria/Fusarium</i>
5	<i>Epicoccum</i> <i>Alternaria/Fusarium</i> <i>Alternaria/Fusarium</i>
6	<i>Alternaria/Hormoconis/Penicillium</i> <i>Alternaris/Hormoconis</i>
7	<i>Penicillium</i> <i>Penicillium</i> <i>Penicillium</i> <i>Trichoderma</i> <i>Aspergillus</i> <i>Fusarium</i>
8	<i>Hormoconis</i> <i>Penicillium</i>
9	<i>Phoma</i> <i>Mucor</i> <i>Epicoccum</i> <i>Hormoconis</i> <i>Alternaria</i> <i>Alternaria</i>
10	<i>Alternaria</i> <i>Aspergillus</i> <i>Bispora</i> <i>Hormoconis</i> <i>Pestalotia</i> <i>Phialomyces</i> <i>Alternaria</i> <i>Pestalotia</i> <i>Phialomyces</i> <i>Stemphylium</i> <i>Fusarium</i>

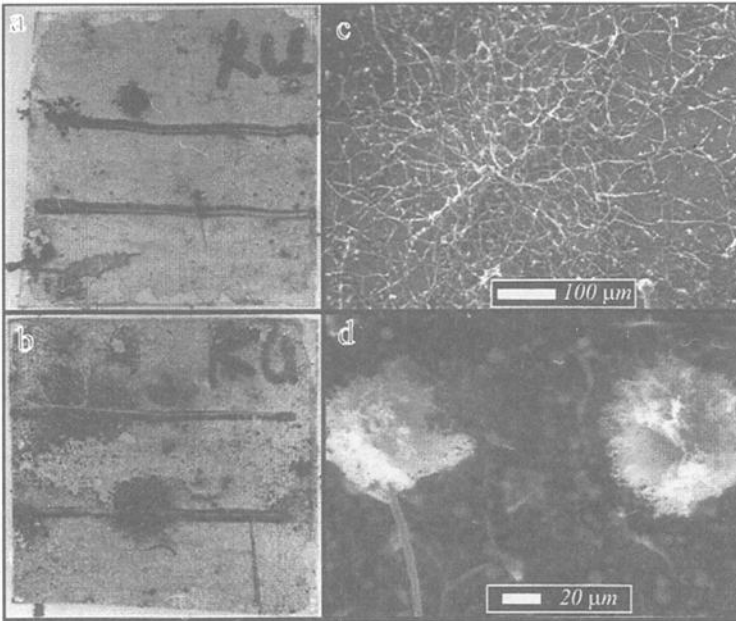


Figure 6 - (a,b) Aluminum panels (25.4 x 25.4 mm) containing aged paint with a flat finish. (c) ESEM micrograph of fungi from the top untreated portion of B. (d) ESEM micrograph of fungi from lower lanolin treated portion of B.

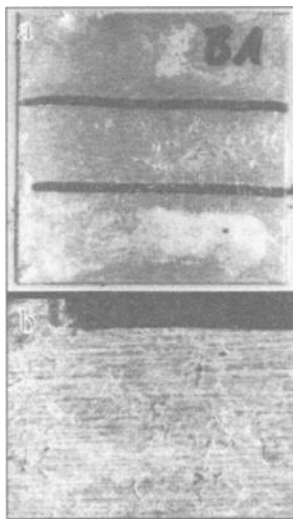


Figure 7 - (a) Bare aluminum panel (25.4 x 25.4 mm) with no urethane coating. (b) Micrograph (7 mm vertical scale) showing fungal growth on the lower lanolin treated surface of the coupon.

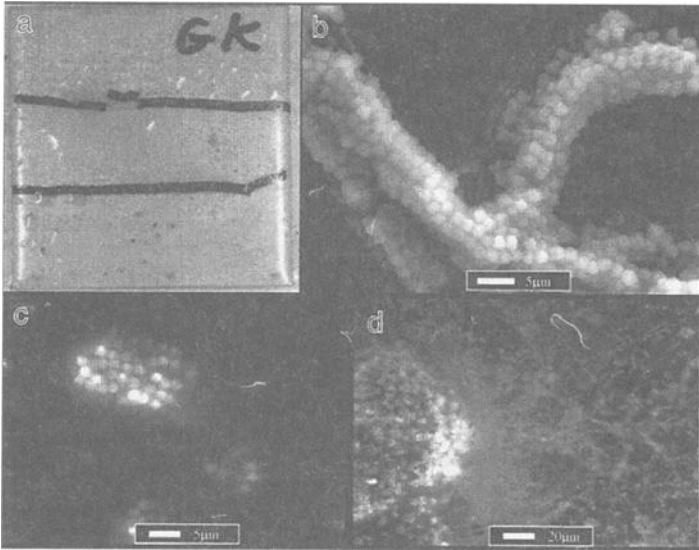


Figure 8 - (a) Aluminum panel (25.4 x 25.4 mm) with a glossy topcoat. (b) ESEM micrograph of fungi growing on the top untreated portion of the panel. (c) ESEM micrograph of fungi growing on the central hydraulic fluid treated portion of the panel. (d) ESEM micrograph of fungi growing on the lower lanolin treated portion of the panel.

localized corrosion was obvious. Fungi in the presence of water and salts can cause direct corrosion of aluminum alloys through the production of acidic metabolic by-products [6]. Control glossy polyurethane coated coupons were colonized by fungi between 27 and 44 days (Fig. 8). Fungi appeared to degrade the glossy polyurethane along the length of the hyphae (Fig. 8b). Flat finish control coupons (without fungicide or fungistat) did not show any signs of colonization until 110 days (Fig. 9). Growth was limited to sections coated with lanolin or hydraulic fluid (Fig. 9 b-c). The Deft® additive did not improve the fungal resistance of the glossy polyurethane (Fig. 10). Growth was observed on all sections of the coupon after 31 days (Fig. 10 d-f). Both omacide and zinc omadine were effective in preventing fungal growth for 110 days in glossy polyurethane (Fig. 11).

Evaluation of Cleaning Procedures

The heavily fouled coupon coated with gloss gray (color 16251) polyurethane containing Deft® X (Fig. 12a) was used for a cleaning experiment. The coupon was washed with warm water and (MIL-C-85570) detergent followed by a rinse with 100% isopropanol. ESEM micrographs demonstrate that the washes removed most of the fungal spores, but many of the hyphae remained (Fig. 12b). After 45 days, regrowth of hyphae left on the surface and the presence of spores could be demonstrated (Fig. 12c). Regrowth was found in the immediate area of cleaning and from contaminated adjacent areas that had not been cleaned. In laboratory tests using the ESEM to obtain images

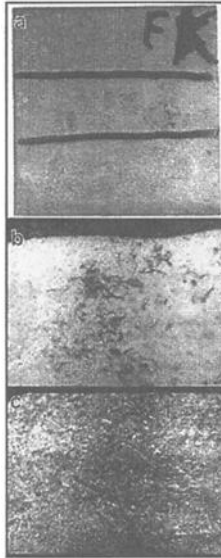


Figure 9 - (a) Aluminum panel (25.4 x 25.4 mm) with a flat topcoat. (b) Micrograph showing fungi growing on the central hydraulic fluid treated portion of the panel. (c) Micrograph showing fungi growing on the lower lanolin treated portion of the panel. Vertical scale of b-c, 5 mm.

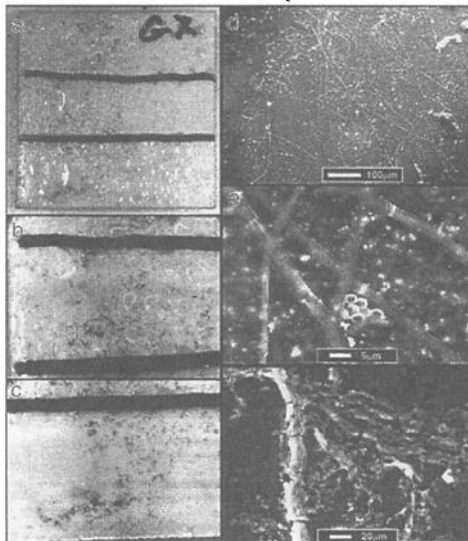


Figure 10 - (a) Aluminum panel (25.4 x 25.4 mm) with a glossy topcoat containing Deft® X. (b-c) Central and lower portions of panel (9 mm vertical scale) showing close-up view of fungi growing on the hydraulic fluid and lanolin treated portions, respectively. (d-f) ESEM micrographs showing fungal growth on all three surfaces (untreated, hydraulic fluid treated, and lanolin treated) of the Deft® X containing panel.

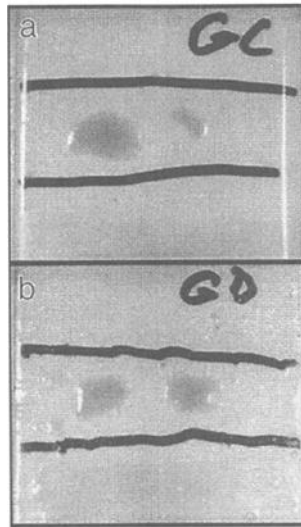


Figure 11 - (a,b) Aluminum panels (25.4 x 25.4 mm) with glossy topcoats containing omacide and zinc omadine, respectively. No growth was evident on any of the surfaces after 110 days.

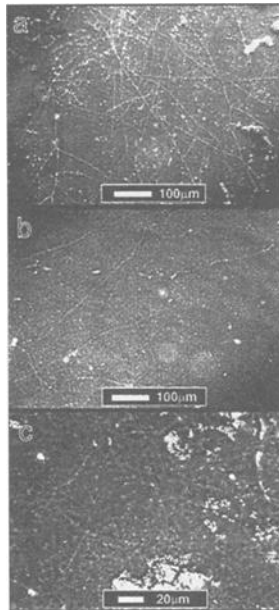


Figure 12 - Cleaning experiment with the Deft[®] X containing panel from Fig. 10. (a) ESEM micrograph of the upper portion of the panel prior to cleaning. (b) Same section after cleaning with detergent and water followed by 100% isopropanol. (c) Same section after 45 days showing fungal hyphae and spores

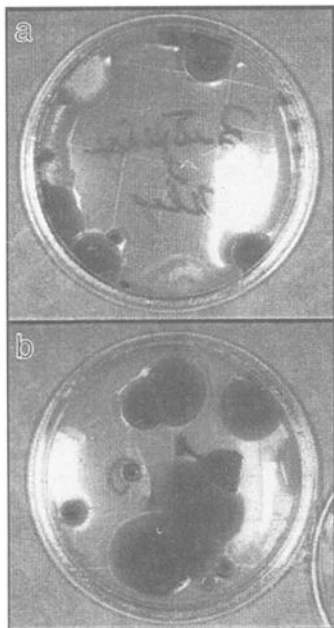


Figure 13 - Contact plates made from surfaces of a freshly cleaned aircraft. (a) Contact plate from cleaned panel treated with Biofinish®. (b) Contact plate from cleaned panel treated with 100% isopropanol and subsequently after drying with Biofinish. Plates show growth from spores or hyphae left on the surfaces after cleaning.

before and after cleaning it was possible to demonstrate that only spores were removed or in some cases relocated by the cleaning procedures so that immediately hyphae continued to grow in the presence of water and nutrients. In-situ cleaning was equally ineffective, as demonstrated by contact plates made after cleaning surfaces with MIL-C-85570 detergent and a MIL-A-9962 pad, and subsequent treatments with either Biofinish® alone (Fig. 13a), 100% isopropanol and subsequently after drying with Biofinish®, (Fig. 13b), or with 100% isopropanol and coated twice with So-Sure® per MIL-C-81309E, Type III (data not shown). However, the numbers and types of fungi cultured from the surfaces were altered by the cleaning techniques.

Conclusions

Fungi appear to be able to use (MIL-H-83282) hydraulic fluid and lanolin as nutrients. Hydraulic fluid does not appear to be the source of the fungi. Instead, spores of the contaminants are ubiquitous in their distribution, and growth depends on availability of water and nutrients. The approved military cleaning procedure using 100% isopropanol is ineffective in removing fungal hyphae, often embedded in the polyurethane coating. Alternative cleaning procedures using either Biofinish® or So-Sure® corrosion preventative compound were equally ineffective. ESEM micrographs indicate that surface cleaning removed spores from hyphae and often the discoloration

associated with the fungi, but fragments of the hyphae remained and grew as soon as conditions were favorable. Glossy polyurethane fouled more readily than did the same formulation with a flat finish. Aged paint (flat gray, color 36231) fouled more rapidly than new coatings. Fungicides and fungistats incorporated in the polyurethane topcoates produced mixed results. Fungi caused localized corrosion of uncoated aluminum specimens.

Acknowledgments

This work was performed under Program Element 0601153N, NRL Contribution Number NRL/PP/7303--00-0006. Robert K. Pope was supported by a CORE/NRL postdoctoral research fellowship. Fungi were identified by Dr. Raymond W. Scheetz, University of Southern Mississippi, Hattiesburg, MS.

References

- [1] Lavoie, D. M. and Little, B. J., "Fungal Contamination of H-53 Aircraft," *NRL Memorandum Report NRL/MR/7333--96-7725*, Naval Research Laboratory, Stennis Space Center, MS, 1996.
- [2] Zabel, R. A. and Terracina, F., "The Role of *Aureobasidium pullulans* in the Disfigurement of Latex Paints," *Developments in Industrial Microbiology*, 1980, Vol. 21, pp. 179-190.
- [3] Cook, W. J., Cameron, J. A., Bell, J. P., and Huang, S. J., "Scanning Electron Microscopic Visualization of Biodegradation of Polycaprolactones by Fungi," *Journal of Polymer Science, Polymer Letters Edition*, 1981, Vol. 19, pp. 159-165.
- [4] Wales, D. S. and Sager, B. F., "The Mechanism of Polyurethane Biodeterioration," *Biodeterioration and Biodegradation of Plastics and Polymers*, K. J. Seal Ed., Biodeterioration Society, Kew, UK, 1985, pp. 56-59.
- [5] Collins, S. P., Pope, R. K., Scheetz, R. W., Ray, R. I., Wagner, P. A., and Little, B. J., "Advantages of Environmental Scanning Electron Microscopy in Studies of Microorganisms," *Microscopy Research and Technique*, 1993, Vol. 25, pp. 398-405.
- [6] Videla, H., "The Action of *Cladosporium resinae* Growth on the Electrochemical Behavior of Aluminum," *Biologically Induced Corrosion*, S. C. Dexter, Ed., NACE, Houston, TX, 1986, pp. 215-222.

Héctor A. Videla,¹ Carolyn Swords,² and Robert G. J. Edyvean³

Features of SRB-Induced Corrosion of Carbon Steel in Marine Environments

Reference: Videla, H. A., Swords, C., and Edyvean, R. G. J., “Features of SRB-Induced Corrosion of Carbon Steel in Marine Environments,” *Marine Corrosion in Tropical Environments*, ASTM STP 1399, S. W. Dean, G. Hernandez-Duque Delgadillo, and J. B. Bushman, Eds., American Society for Testing and Materials, West Conshohocken, PA, 2000.

Abstract: Sulfate reducing bacteria (SRB) growth induces several important features in the steel/seawater interface such as changes in pH, redox potential, ion concentrations and structure and composition of corrosion product films. These features, absent in abiotic media, produce drastic changes in the corrosion behavior of the metal. In addition to pitting and crevice corrosion, conditions conducive to the enhancement of corrosion-fatigue crack growth and of hydrogen embrittlement can be generated by the metabolic production of hydrogen sulfide by SRB. While SRB produces more hydrogen entry into susceptible metals when compared with similar levels of abiotic sulfides, corrosion fatigue crack growth rates are slower in biological environments than in similar abiotic conditions. Moreover, bacteria also decrease the performance of cathodic protection of steel and protective coatings in marine environments. A review of the literature and recent results from our laboratories involving the use of electrochemical techniques for corrosion assessment, surface analyses and different types of microscopy also are briefly described.

Keywords: sulfate-reducing bacteria, SRB, carbon steel, cathodic protection, hydrogen embrittlement, localized corrosion, sulfides, hydrogen sulfide, biofilms, extracellular polymeric substances, corrosion fatigue, protective coatings

Introduction

SRB-induced corrosion of steel in marine environments has received significant attention in the specialized literature [1-4] owing to the wide variety of industrial activities affected (offshore oil extraction, coastal power plants, harbor and fishing activities, etc.).

The action of SRB on corrosion can be notoriously enhanced by microbial

¹Department of Chemistry, College of Pure Sciences, University of La Plata, Av. 51-337. 1900. La Plata, Argentina.

²Department of Materials and Department of Chemical Engineering, University of Leeds, LS2 9 JT, Leeds, U.K.

³Department of Chemical & Process Engineering, The University of Sheffield, S1 3 JD, Sheffield, U.K.

consortia with other bacteria within biofilms formed at the seawater/steel interface [5, 6]. Biofilms and biofouling deposits are the result of an accumulation process not necessarily uniform in time or space [7] that leads to a “biologically conditioned” metal/solution interface involving a reciprocal action between inorganic corrosion products and biofilms. Thus, electrochemical concepts and measurements used for assessing abiotic corrosion in seawater must be revised and adapted to correspond to the characteristics of the biofilmed metal surface [8].

One of the distinctive features of SRB-induced corrosion in marine environments is that in an aggressive medium like seawater, metal dissolution takes place simultaneously with biofilm formation. Thus, a very active interaction between the corrosion process and biofouling settlement can be expected [9] and the consequent corrosion behavior of the steel will vary according to the intensity and nature of this reciprocal interaction. Biofilms are influenced by both the substratum and the bulk phase [10]. Consequently, on an active metal like carbon steel, the gelatinous matrix of the biofilm, essentially formed by extracellular polymeric substances (EPS), bacterial cells and water [11] is mixed with corrosion products formed within the same time scale and complex corrosion products/biofilm interactions develop.

Biofilms can either slow or accelerate metal dissolution. Retardation or inhibition of the corrosion reaction at the metal surface may be due to a “barrier effect” of the biofilm, as it has been reported in the literature [12]. Conversely, as biofilms are rarely uniform, the opposite effect of enhanced metal dissolution may be prevalent owing to the permanent separation of anodic and cathodic sites at the steel surface, to the breakdown of inorganic passive films, or to the stimulation of either the anodic or cathodic reactions [13].

Until recently, several review papers discussing the influence of SRB on corrosion in natural and industrial waters were limited to consideration of planktonic organisms. Nevertheless, it should be recognized that the complex mechanisms of chemical and biological processes contributing to the biocorrosion of carbon steel in natural waters can be adequately described only under simplified laboratory conditions [14]. SRB influence corrosion of steel in seawater occurs through a combination of biological and chemical factors. In corroded pipelines and other industrial structures, SRB activity involves a number of chemical entities like the sulfur anions derived from the dissimilatory reduction of sulfate anions (sulfides, bisulfides and hydrogen sulfide) as well as metastable sulfur compounds such as thiosulfate and polythionate [15, 16]. All these sulfur compounds are well recognized in the literature for their deleterious effects on ferrous metals [17].

When exposed to SRB-related sulfur compounds, carbon steel first develops a film of mackinawite (an iron rich sulfide) of poor protective characteristics [18] that later changes through different chemical and biological paths to more stable iron sulfides [19].

Iron sulfides enhance the cathodic hydrogen reduction reaction which indirectly causes an increase in the corrosion rate while SRB consume the adsorbed hydrogen produced in the cathodic areas by their hydrogenase enzyme. Thus, the recombination step of hydrogen atoms that requires high activation energies is bypassed. In this way SRB would provide an alternative “depolarization pathway” to the corrosion reaction, although the term “depolarization” is not conceived here in a strict electrochemical sense [20]. Another important feature of SRB-induced corrosion of carbon steel in

seawater is that due to its active corrosion behavior, the carbon steel surface is covered by corrosion products of different nature (iron sulfides, iron oxides or iron hydroxides) and also by biofilms. Consequently, biocorrosion process should be related to the breakdown of the passive behavior of carbon steel by SRB corrosive metabolic products assisted by the chloride anions present in marine media [21]. Localized corrosion and breakdown processes are markedly dependent on the protective characteristics of the corrosion products films on the carbon steel surface. Several aspects of the corrosion of steel in chloride containing media have been clarified through a series of electrochemical experiments using alkaline [22] and neutral [23] buffered solutions as well as SRB cultures in artificial seawater [21] under well controlled laboratory conditions.

The main conclusions of these studies can be summarized in this way: (i) biotic and abiotic sulfides induce the breakdown of passivity on carbon steel through a similar mechanism; (ii) the type and intensity of sulfide effects on passivity breakdown is strongly dependent on the nature and characteristics of the protective film present on the steel surface; (iii) the anodic process would be the first step in the corrosion reaction whereas cathodic effects would be developed later when metal dissolution is in progress; (iv) physicochemical parameters of seawater like pH, ionic composition and oxygen levels change the type of protective film on the steel surface and consequently the SRB influence on corrosion that would be turned from aggressive to passivating; (v) a distinctive feature of SRB-induced corrosion of carbon steel in seawater is that there are two synergistic effects on the corrosive action of sulfides: one related to the presence of chlorides and another related to the biofilms at the metal/seawater interface [24, 25].

Influence of Physicochemical Characteristics of Seawater on SRB-Induced Corrosion of Carbon Steel

Influence of pH, Oxygen Concentration, SRB Intermediate Metabolites

Local acidification is characteristic of pitting corrosion. Therefore, the capacity of SRB to regulate local pH to a neutral value, as it has been claimed recently [26], would have marked effects on the biocorrosion process. Traces of oxygen oxidize sulfides and decrease the local pH. If SRB intermediate metabolites like thiosulfates are present and recycled by the bacteria, the pH could reach values as low as 5.4. Conversely, the cathodic reaction may decrease the oxygen and thiosulfate concentrations leading to neutral pH values in the order of 6.7 [26]. The final result of combined SRB metabolism and oxygen concentrations gradients is the creation of galvanic cells with acidic anodes and nearly neutral cathodes. Supporting this assumption it was found [27] that the current of such galvanic cells could be correlated with the SRB populations at the anode.

Recent studies on non SRB sulfidogenic bacteria [28] showed that these bacteria were able to reduce thiosulfate to hydrogen sulfide inducing pitting of carbon steel at unusually high corrosion rates similar to those frequently found in the field. Thiosulfate would therefore, be a more effective pitting agent than sulfides in certain marine environments as it has been reported for stainless steel [29, 30].

The role of oxygen concentration in SRB-induced corrosion of carbon steel has

been highlighted in several publications [14, 31-33]. The most severe corrosion attack on steel due to SRB is generally found when oxygen is allowed to enter the system as it occurs in marine sediments in the offshore oil production where high rates of pitting are always associated with aerobic environments.

The multiple effects of oxygen in SRB-induced corrosion of carbon steel can be summarized as follows [14]: (i) microbial activity within the growing biofilm decreases oxygen concentration and cathodic current; (ii) at long periods of time (e.g. one month) very low concentrations of oxygen in the bulk correspond to a complete absence of oxygen at the base of the biofilm; (iii) a close correlation between sulfur and oxygen is observed, the former is found within pitting areas whereas oxygen is found in the surroundings; (iv) the biocorrosion process in anoxic/oxic biofilms involves more chemical and microbiological processes than in a strict anoxic environment; (v) only reduced iron sulfides (i.e., mackinawite and greigite) are found in anoxic environments whereas more oxidized iron sulfides (i.e., pyrite) and elemental sulfur are usually detected in an aerobic system.

Elemental sulfur is very corrosive to steel. Two mechanisms have been proposed: the formation of sulfur concentration cells [34] or the action of sulfur as cathodic depolarizer [35]. In both mechanisms sulfur acts as the electron acceptor in an electrochemical cell. Electron transfer requires electron-conductive iron sulfides at the steel surface.

The Role of Iron and Corrosion Products Films on SRB-Induced Corrosion of Carbon Steel

Soluble iron is important in SRB-induced corrosion of carbon steel because it influences the whole corrosion process. When continuous culture techniques were used over extended time periods [36], low corrosion rates were obtained whenever thin adherent ferrous sulfide films covered the metal surface. Conversely, film breakdown after longer periods of exposure, drastically increased the corrosion rate. Similar effects could be reproduced in laboratory experiments in the presence of high soluble iron concentrations which allowed bulky precipitates to form, rather than adherent sulfide films. The high corrosion rates measured in the presence of high iron levels and bulky precipitates at the metal surface were in good correlation with corrosion rates measured in natural environments, like waterlogged soils. Further studies [37, 38] on sulfidation of the primary iron sulfide mackinawite to greigite in environments with low iron concentrations showed similar trends in the corrosion rate.

A series of studies, using a continuous flow biofilm reactor [39, 40], showed that in iron-free media there was no noticeable corrosion as well as no traces of iron in the biofilm. When the steel surface was previously coated with an iron sulfide film before bacterial adhesion and biofilm formation, localized corrosion was observed at defect sites of the film or at inclusions or grain boundaries in the metal matrix. Usually, soluble iron concentration above a threshold value of 60 mg/l of ferrous iron caused a significant increase in the corrosion rate, and established a close physical contact between sulfide deposits in the biofilm and the plain metal. Recent experimental work [41] in our laboratory, using electrochemical techniques and electron probe micro-analysis (EPMA) to study iron sulfide layers, support the relevant role of soluble iron in the biocorrosion process. Some of the main conclusions of this work are: (i) in chloride

media like seawater, the thickness and protective characteristics of ferrous hydroxide layer on carbon steel depends on the concentration of ferrous ion in solution; (ii) pH dependant competitive adsorption between different anions occurs at the metal/solution interface, favoring or inhibiting the corrosion process; (iii) the characteristics of the iron sulfide, whether a compact film, a loosely adherent film, or solid particles in suspension affects corrosion; (iv) scenarios developed in abiotic solutions become more complex in the presence of microorganisms and their biofilms because dissimilar areas are formed as a consequence of the biofilm heterogeneity.

SRB-influenced corrosion of carbon steel strongly depends on the nature and structure of sulfide films produced during the corrosion process. The environmental characteristics of the metal/biofilm/solution interface and its surroundings (pH, ionic composition, oxygen levels) influence the chemical and physical nature of sulfide films and may change their effects from corrosive to protective. Whereas thin adherent films of iron sulfide are protective, bulky and loosely adherent precipitates enhance corrosion rates [42].

Several surface analysis techniques (energy dispersion X-ray analysis (EDXA); X-ray photoelectron spectroscopy (XPS); X-ray diffraction (XRD) and EPMA, were recently used [43] in combination with scanning electron microscopy (SEM) and atomic force microscopy (AFM) to elucidate the role of biotic and abiotic corrosion products in the corrosion behavior of steel. Microbiological experiments were made under well controlled laboratory conditions using a strain of SRB (*Desulfovibrio alaskensis*) isolated from a soured oil reservoir [44]. AFM was used to image the SRB biofilms and the related EPS. Electrochemical techniques were used to assess the corrosion behavior of carbon steel, and SEM coupled with surface analysis techniques were employed to examine the structure and composition of biotic and abiotic sulfide films at the surface of the steel specimens. It was concluded that the composition and structure of sulfide films formed in the presence of SRB and in abiotic sulfide media are different. In biotic solutions the corroded metal surface contains both iron and sulfur in agreement with previous work [38] where it was reported the formation of an initial thin tarnished layer of mackinawite (FeS) in the presence of bacteria. Moreover, when this layer grows in thickness it becomes less adherent. Depending on the ferrous iron concentration mackinawite can turn into greigite (Fe₃S₄), smythite (Fe_(3+x)S₄) or pyrrhotite (Fe_(3-x)S). Thermodynamic analysis indicate that pyrite (FeS₂) is the most stable compound. Our XPS results [43] show that FeS is the most abundant iron sulfide although FeS₂ is present in few layers at the upper part of the film. In abiotic media, EPMA revealed the absence of sulfur and the presence of iron oxides or hydroxides, in accordance with other publications [45, 46]. To preserve a FeS film on the steel surface, a continuous supply of hydrogen sulfide is needed; whereas in the absence of hydrogen sulfide, the film will convert into iron oxides and hydroxides. XRD spectra of both a biogenic and an abiotic sulfide film revealed two distinct differences (Fig. 1): the intensity of the iron peaks in the biogenic film are almost double than those in the abiotic film and the ratio of the iron peaks 110 and 211 is different for both films [47].

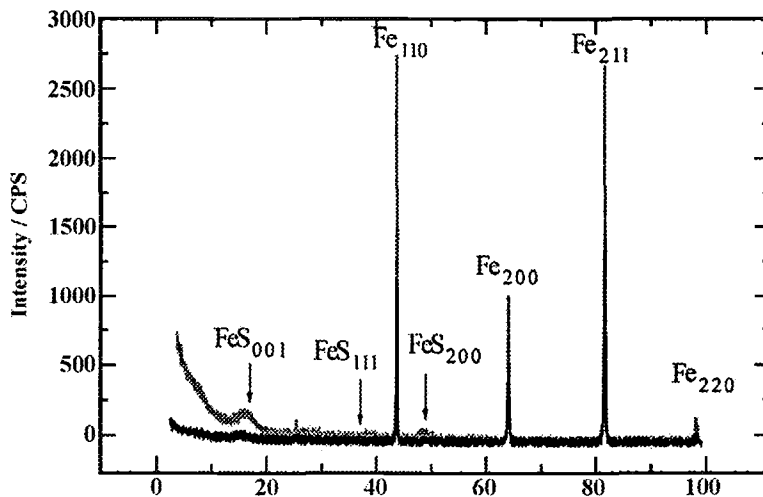


Figure 1 - XRD spectra of an abiotic and biogenic sulfide film (from Ref. 47).

In conclusion, the chemical and structural characteristics of sulfide films formed under abiotic and biotic conditions present common and distinctive features: (i) in both conditions the outer layer is formed by FeS and FeS₂. However, in biogenic sulfide solutions FeS is the major specie, whereas in abiotic solutions FeS₂ is predominant; (ii) the corroded steel surface underneath a biogenic film is covered with iron sulfide whereas in a non-biogenic film it is covered with an iron hydroxyde or oxide. Generally, biogenic films are more adherent to the surface than those formed in abiotic media which are flaky and loosely adherent.

Cathodic Protection of Carbon Steel and Biofilm Interactions in Marine Environments

Cathodic protection using sacrificial anodes or impressed current is widely used to prevent corrosion of carbon steel structures exposed to seawater. Cathodic protection alters the local chemistry at the metal surface, inducing an increase of pH due to electrolytic production of hydroxyl anions. The alkalinity reduces the solubility of calcium and magnesium compounds in the medium, and precipitates calcareous scales. These inorganic deposits reduce the required current for maintaining a selected potential and decrease the protection costs.

According to recent publications [48, 49], cathodic protection seems to control the growth of anaerobic bacteria, whereas under marine sediments or anaerobic biofilms, cathodically produced hydrogen can encourage the growth of SRB. Organic material in seawater affects both the current requirement and the nature of the calcareous deposits formed at the steel surface. A pre-existing biofilm makes the calcareous deposit more uniform at all current densities [50]. At high current densities the mixed bacterial/calcareous film acts as a beneficial diffusion barrier but as a detrimental cathodic depolarizer at low current densities. The last effect increases the current level

needed for protection and consequently the cathodic protection costs.

For aerobic bacteria, cathodic protection reduces bacterial adhesion and growth during the early stages of biofouling settlement [51]. However, when a steady state of biofilm growth is reached, the effect of cathodic protection on microbial biofilms is less relevant. At low seawater temperatures, microbial growth is low and the effect of cathodic protection is more noticeable because the biofilm needs longer time to reach steady state [52].

It is widely accepted that a cathodic potential of -0.88 V (vs. SCE) is enough to protect steel structures from marine corrosion [53]. However, in anaerobic media like marine sediments or biofouling deposits this potential requirement must be increased in the negative direction due to the possible presence of SRB and acid-producing bacteria [49]. The increase in negative potential is not applied to prevent bacterial growth but to assure the passive behavior of steel. Even at potential levels so low as -1.13 V (vs. SCE) SRB growth has been reported [54]. It can be inferred then, that an insufficient polarization level of cathodic protection for extended periods of time could lead to severe corrosion of the steel surface [55]. Moreover, cathodic protection seems to be unable to avoid localized corrosion initiation even at high cathodic potentials when stable SRB biofilms were formed on carbon steel surfaces in marine environments.

SRB-Induced Corrosion of Carbon Steel and Hydrogen Effects in Marine Environments

In seawater, hydrogen is available at the surface of cathodically protected carbon steel structures, particularly in anaerobic environments, due to the cathodic electrochemical proton reduction. Usually only a small amount of this hydrogen is able to enter the metal, the rest moving from the surface in the molecular form or taking part in other reactions at the metal surface. Biological activity, specially SRB growth, enhances the entrance of hydrogen into the metal lattice, causing hydrogen embrittlement, which is well known in the corrosion literature [56] and could be a major cause of failure of components, structures, pipelines and vessels.

SRB will be active in just the areas where hydrogen will be generated under cathodic protection. These areas are particularly important as pipelines and the bottoms of legs of offshore structures can be buried in marine muds, and both the metal and welds will be exposed to anaerobic conditions and SRB activity. A biologically active environment involves not only the presence of SRB and their metabolites (i.e., sulfides) but also the effect of all the activities of the bacteria in relation to the environment like the microbial degradation of fouling deposits, production of EPS, interactions of bacteria and the metal. Such a biologically active environment is able to induce conditions conducive to hydrogen embrittlement and corrosion-fatigue crack growth [57-59].

To illustrate the hydrogen permeation through steel in open seawater, hydrogen probes attached to the back of 50D type of steel were installed on a floating pontoon and the hydrogen flux through the plates were monitored over a period of 12 months. After that time elapsed, the plates were brought to the shore and buried in marine mud for a further six months. The plates were cathodically protected by zinc sacrificial anodes throughout the experiments [60]. It can be seen in Fig. 2 (curve 1) that for the non-coated, cathodically protected plate, hydrogen levels gradually rise as the steel fills

up with hydrogen and the flux remains relatively constant until the plate is placed in

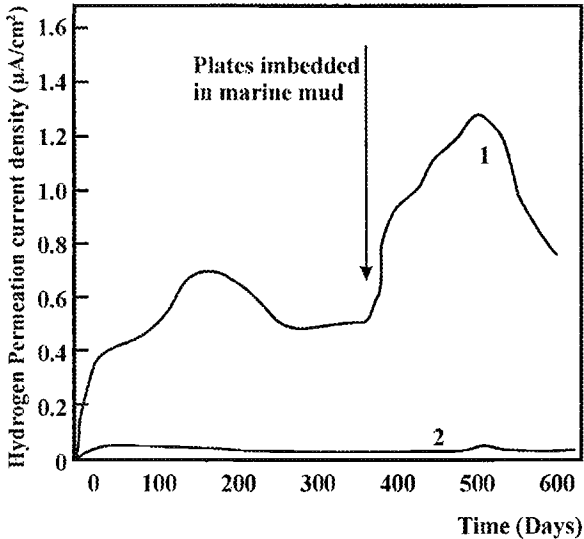


Figure 2 - Hydrogen permeation through 50 D type steel. Curve 1: Grit blasted and cathodically protected; Curve 2: protected with anti-fouling paint.

marine mud. This results in a step rise in hydrogen flux followed by a steady climb and then a steady fall. The rise in hydrogen flux when the plate is embedded in marine mud indicates the beginning of the decay of the marine fouling on the plate and the concomitant increase in SRB activity. Once the nutrient source is used the bacteria become less active with the result that hydrogen flux decreases. Curve 2 shows that an anti-fouling coating remained intact and the hydrogen permeation was almost nil.

Environmental effects on corrosion-fatigue are usually assessed in the laboratory by measuring crack growth rates under different conditions using pre-cracked specimens. The specimen is then placed under a cyclic load, (designed for example to reproduce seawave loading) in a chamber containing the seawater, and the growth of the crack is measured. As the crack grows the cyclic load per unit across sectional area increases until the load exceeds the ultimate tensile strength of the material and catastrophic failure occurs [57]. Figure 3 shows results from such experiments and indicates that biologically active environments have much less effect on corrosion fatigue than do sterile environments at similar levels of sulfide.

SRB not only can interact directly with the metal surface but can change the chemistry at that surface. In addition, bacteria can produce copious amounts of EPS which can have different effects in different situations like in hydrogen embrittlement or in corrosion fatigue crack growth.

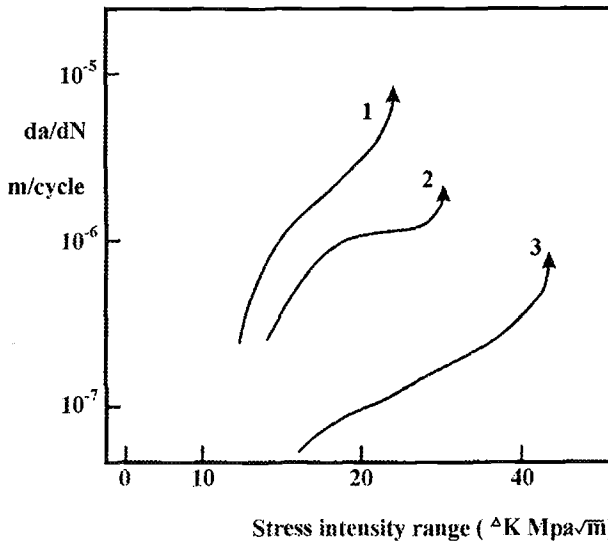


Figure 3 - Crack growth rates of RQT 701 steel in biologically active and abiological sulfide seawater ($R = 0.7$; $f = 0.167$ Hz). Curve 1: 589 ppm abiotic sulfide; Curve 2: 500 ppm biogenic sulfide; Curve 3: crack grow rates in seawater without sulfide.

Sour acidic environments such as those frequently found in oil production activities are held to be particularly aggressive due to the high levels of hydrogen available at the steel surface or in a crack and as a consequence of sulfide poisoning of the hydrogen recombination reaction at the cathodic surface [61]. The effects of such environments can be drastically altered by the presence of organic molecules on the steel surface. Thus the presence of a biofilm and its EPS may modify hydrogen effects considerably. Although the hydrogen sulfide would become toxic to the SRB they are protected by EPS to a considerable extent.

Conclusions

SRB activity in seawater introduces several corrosive sulfur compounds in the environment either as final metabolites (sulfides, hydrogen sulfide) or metastable intermediate compounds (thiosulfates). All of these compounds are corrosive to carbon steel and their result is localized corrosion.

SRB biofilms induce several important alterations in the steel/seawater interface such as changes in pH, ions concentrations and a modification of the structure and composition of the protective layers of corrosion products. Whereas corrosion products films formed in biotic seawater are more adherent to the steel surface, films formed in abiotic seawater are flaky and loosely adherent.

Some physicochemical characteristics of seawater may play a relevant role in the SRB-induced corrosion of carbon steel like pH, oxygen levels and soluble iron concentration. Mixed oxic/anoxic biofilms are generally more corrosive than totally

anoxic biofilms. In chloride environments the thickness and protective characteristics of the ferrous hydroxide layer depend on the concentration of ferrous iron.

The interaction between biofilms and calcareous deposits can affect the performance and cost of cathodic protection of carbon steel in seawater. Whereas SRB growth is enhanced by cathodic protection, anaerobic bacterial growth is inhibited at the early stages of the biofilm formation.

In addition to pitting, SRB growth induces conditions conducive to the enhancement of hydrogen permeation through the steel, facilitating hydrogen embrittlement, whereas corrosion fatigue crack growth rates are slower in the presence of SRB biofilms than in similar abiotic media.

Acknowledgment

The first author acknowledges the University of La Plata and all the authors acknowledge the British Council-Antorchas Foundation (Contract BNS/992/38) and the Commission of the European Communities (Contract C11*-CT94-0025) for financial support.

References

- [1] Sanders, P. F., and Hamilton, W. A. "Biological and Corrosion Activities of Sulfate-Reducing Bacteria in Industrial Process Plant," *Biologically Induced Corrosion*, S. C. Dexter, Ed., NACE International, Houston, TX, 1986, pp. 47-68.
- [2] Hamilton, W. A., and Maxwell, S. "Biological and Corrosion Activities of Sulfate-Reducing Bacteria within Natural Biofilms," *Biologically Induced Corrosion*, S. C. Dexter, Ed., NACE International, Houston, TX, 1986, pp. 131-136.
- [3] Videla, H. A., de Mele, M. F. L., and Brankevich, G. "Assessment of Corrosion and Microfouling of Several Metals in Polluted Seawater," *Corrosion*, Vol. 44, 1988, pp. 423-426.
- [4] Salvarezza, R. C., and Videla, H. A. "The Influence of Sulfate-Reducing Bacteria on the Electrochemical Behavior of Steel in Seawater," *Marine Biology*, Proceedings 5th International Congress on Marine Corrosion and Fouling, Barcelona, Spain, 1980, pp. 7-12.
- [5] Costerton, J. W., and Geesey, G. G. "The Microbial Ecology of Surface Colonization and of Consequent Corrosion," *Biologically Induced Corrosion*, S. C. Dexter, Ed., NACE International, Houston, TX, 1986, pp. 223-232.
- [6] Hamilton, W. A. "Sulfate-Reducing Bacteria and Anaerobic Corrosion," *Annual Reviews of Microbiology*, 1985, Vol. 39, pp. 195-217.
- [7] Characklis, W. G., and Marshall, K. C. "Biofilms: A Basis for an Interdisciplinary Approach," *Biofilms*, W. G. Characklis, K. C. Marshall, Eds., John Wiley & Sons, Inc., New York, 1990, pp.3-15.
- [8] Videla, H. A. "Electrochemical Aspects of Biocorrosion," *Bioextraction and Biodeterioration of Metals*, C. C. Gaylarde, H. A. Videla, Eds., Cambridge University Press, Cambridge, UK, 1995, pp. 85-127.
- [9] Videla, H. A. "Biofilms and Biofouling," *Manual of Biocorrosion*, CRC-Lewis

- Publishers, Boca Raton, FL, 1996, pp.47-71.
- [10] Videla, H. A. "Biocorrosion Problems in the Marine Environment: New Perspectives," *Developments in Marine Corrosion*, S. A. Campbell, N. Campbell, F. C. Walsh, Eds., Royal Society of Chemistry, Cambridge, UK, 1998, pp. 1-25.
- [11] Geesey, G. G., "Microbial Exopolymers; Ecological and Economic Considerations," *Am. Soc. Microbiol. News*, 1982, Vol.48, pp. 9-14.
- [12] Videla, H. A., "Corrosion Inhibition in the Presence of Microbial Corrosion," *CORROSION/96*, Paper 223, NACE International, Houston, TX, 1996.
- [13] Videla, H. A., "An Overview of Mechanisms by Which Sulfate-Reducing Bacteria Influence Corrosion of Steel in Marine Environments," *Biofouling* (in press).
- [14] Lee, W., Lewandowski, Z., Nielsen, P. H., and Hamilton, W. A., *Biofouling*, Vol. 8, 1995, pp. 165-194.
- [15] Cragolino, G., and Tuovinen, O. H. "The Role of Sulfate-Reducing Bacteria and Sulfur-Oxidizing Bacteria in the Localized Corrosion of Iron-Base Alloys- A Review," *International Biodeterioration*, Vol. 20, 1984, pp. 9-26.
- [16] Videla, H. A. "Microbially Induced Corrosion : An Updated Overview," *Biodeterioration and Biodegradation* 8, H.W.Rossmoore, Ed., Elsevier Applied Science, London, UK, 1991, pp. 63-88.
- [17] Szklarska-Smialowska, Z. "Effects of Environmental Factors in Pitting. Composition of the Electrolyte," *Pitting Corrosion of Metals*, NACE International, Houston, TX, 1986, pp. 201-219.
- [18] Shoesmith, D. W., Taylor, P., Bailey, M. G., and Owen, D. G. "The Formation of Ferrous Monosulfide Polymorphs During the Corrosion of Iron by Aqueous Hydrogen Sulfide at 21 C," *J. Electrochem. Soc.*, Vol.127, 1980, pp. 1007-1019.
- [19] Rickard, D. T. "The Chemistry of Iron Sulfide Formation at Low Temperature," *Stockh. Contr. Geol.*, Vol. 20, 1969, pp. 67-95.
- [20] Duquette, D. J., and Ricker, R. E. "Electrochemical Aspects of Microbially Induced Corrosion," *Biologically Induced Corrosion*, S. C. Dexter, Ed., NACE International, Houston, TX, 1986, pp. 121-130.
- [21] Videla, H. A. "Corrosion of Mild Steel Induced by Sulfate-Reducing Bacteria. A Study of the Passivity Breakdown by Biogenic Sulfides," *Biologically Induced Corrosion*, S. C. Dexter, Ed., NACE International, Houston, TX, 1986, pp. 162-171.
- [22] Salvarezza, R. C., Videla, H. A., and Arvía, A. J. "The Electrodeposition and Passivation of Mild Steel in Alkaline Sulphide Solutions," *Corrosion Science*, Vol. 22, 1982, pp. 815-829.
- [23] Salvarezza, R. C., Videla, H. A., and Arvía, A. J. "The Electrochemical Behavior of Mild Steel in Phosphate-borate-sulfide Solutions," *Corrosion Science*, Vol. 23, 1983, pp. 717-732.
- [24] Hamilton, W. A. "Sulfate-Reducing Bacteria and their Role in Biocorrosion" *Biofouling and Biocorrosion in Industrial Water Systems*, H. C. Flemming, G. G. Geesey, Eds., Springer-Verlag, Berlin, 1991, pp 187-193.
- [25] Videla, H. A. "Electrochemical Interpretation of the Role of Microorganisms in Corrosion," *Biodeterioration* 7, D. R. Houghton, R. N. Smith and H. O. W.

- Rossmore, Eds., Elsevier Applied Science, London, UK, 1988, pp. 359-371.
- [26] Crolet, J. L., Dumas, S., and Magot, M. "pH Regulation by Sulfate-Reducing Bacteria," CORROSION/93, Paper 303, NACE International, Houston, TX, 1993.
- [27] Campaignolle, X., Luo, J. S., Bullen, J., White, D. C., Guezennec, J., and Crolet, J. L., "Stabilization of Localized Corrosion of Carbon Steel by Sulfate-Reducing Bacteria," CORROSION/93, Paper 302, NACE International, Houston, TX, 1993.
- [28] Crolet, J. L., and Magot, M. "Observations of Non-SRB Sulfidogenic Bacteria from Oilfield Production Facilities," CORROSION/95, Paper 188, NACE International, Houston, TX, 1995.
- [29] De Cristofaro, N. B., Acosta, C. A., Salvarezza, R. C., and Videla, H. A. "The Effect of Sulfides on the Electrochemical Behaviour of AISI 304 Stainless Steel in Neutral Buffered Solutions," Corrosion, Vol 42, 1984, pp. 240-242.
- [30] Newman, R. C., Webster, B. J., and Kelly, R. G. "The Electrochemistry of SRB Corrosion and Related Inorganic Phenomena," ISIJ International, Vol. 31, 1991, pp. 201-209.
- [31] Hardy, J. A., and Bown, J. L. "The Corrosion of Mild Steel by Biogenic Sulfide Films Exposed to Air," Corrosion, Vol. 40, 1984, pp. 650-654.
- [32] Lee, W. C., Lewandowski, Z., Okabe, S., Characklis, W. G., and Avci, R. "Corrosion of Mild Steel underneath Aerobic Biofilms Containing Sulfate-Reducing Bacteria, Part I: At Low Dissolved Oxygen Concentration," Biofouling, Vol. 7, 1993, pp. 197-216.
- [33] Lee, W. C., Lewandowski, Z., Nielsen, P. H., Morrison, M., Characklis, W. G., and Avci, R. "Corrosion of Mild Steel Underneath Aerobic Biofilms Containing Sulfate-Reducing Bacteria, Part II: At High Dissolved Oxygen Concentration," Biofouling Vol. 7, 1993, pp. 217-239.
- [34] Schaschl, E. "Elemental Sulfur as a Corrodent in Deaerated, Neutral Aqueous Solutions," Materials Performance, Vol. 19, 1980, pp. 9-12.
- [35] Schmitt, G. "Effect of Elemental Sulfur on Corrosion in Sour Gas Systems," Corrosion Vol. 47, 1991, pp. 285-291.
- [36] Tiller, A. K., "Aspects of Microbial Corrosion," Corrosion Processes, R. N. Parkins, (Ed.), Appl. Sci. Publ., London, UK, Chapter 3, 1982, pp 115-125.
- [37] Mara, D. D., and Williams, D. J. "The Mechanisms of Sulfide Corrosion by Sulfate-Reducing Bacteria," Biodeterioration Materials, Vol. 2, 1982, pp. 103-113.
- [38] McNeil, M. B., Jones, J., and Little, B. J. "Mineralogical Fingerprints for Corrosion Processes Induced by Sulfate-Reducing Bacteria," CORROSION/91, Paper 580, NACE International, Houston, TX, 1991.
- [39] Lee, W. C., and Characklis, W. G. "Anaerobic Corrosion Processes of Mild Steel in the Presence and Absence of Anaerobic Biofilms," Biodeterioration and Biodegradation 8, H. W. Rossmore (Ed.), Elsevier Applied Science, London, UK, 1991, pp 89-111.
- [40] Lee, W. C. and Characklis, W. G., "Corrosion of Mild Steel under Anaerobic Biofilm," Corrosion, Vol. 49, 1993, pp. 186-198.
- [41] Videla, H. A., Swords, C. L., de Mele, M. F. L., Edyvean, R. G., Watkins, P., and Beech, I. B. "The Role of Iron in SRB Influenced Corrosion of Mild Steel,"

- CORROSION/98, Paper 289, NACE International, Houston, TX, 1998.
- [42] Videla, H. A., "Practical Cases: Biocorrosion of Carbon steel in Anaerobic Environments", *Manual of Biocorrosion*, CRC-Lewis Publishers, Boca Raton, FL, 1996, pp. 179-187.
- [43] Videla H. A., Edyvean, R. G., Swords, C. L., de Mele, M. F. L., and Beech, I. B. "Comparative Study of the Corrosion Product Films Formed in Biotic and Abiotic Sulfide Media," CORROSION/99, Paper 163, NACE International, Houston, TX, 1999.
- [44] Beech, I. B., Zinkevich, V., Tapper, R., and Avci, R. "Study of the Interaction of Exopolymers Produced by Sulphate-Reducing Bacteria with Iron Using X-ray Photoelectron Spectroscopy and Time-of-Flight Secondary Ionisation Mass Spectrometry," *Journal of Microbiological Methods*, Vol. 36, 1999, pp. 3-10.
- [45] Herro, H. M. "Tubercle Formation on Ferrous Alloys in Low-flow Systems", CORROSION/93, Paper 261, NACE International, Houston, TX, 1993.
- [46] Misawa, K., Hashimoto, K., and Shimodaira, S. "The Mechanism of Formation of Iron Oxide and Oxyhydroxides in Aqueous Solutions at Room Temperature", *Corrosion Science*, Vol. 14, 197, pp. 131-149.
- [47] Swords, C. L. "The Corrosion of Steels in Microbial and Non-Microbial Hydrogen Sulfide Environments," Ph.D. Thesis, The University of Leeds, Leeds, UK, 1998, pp. 161-222.
- [48] Edyvean, R. G. J., Maines, A. D., Hutchinson, C. J., Silk, N. J., and Evans, L. V. "Interactions between Cathodic Protection and Bacterial Settlement on Steel in Seawater," *Int. Biodet. & Biodegrad.*, Vol. 29, 1992, pp. 251-271.
- [49] Guezennec, J. G. "Cathodic Protection and Microbially Induced Corrosion," *International Biodeterioration & Biodegradation*, Vol. 34, 1994, pp. 275-288.
- [50] Dexter, S. C., and Lin, S. H. "Effect of Marine Biofilms on Cathodic Protection", *International Biodeterioration & Biodegradation*, Vol. 29, 1992, pp. 231-249.
- [51] Gomez de Saravia, S. G., de Mele, M. F. L., Videla, H. A., and Edyvean, R. G. J. "Bacterial Biofilms on Cathodically Protected Stainless Steel", *Biofouling*, Vol. 11, 1997, pp. 1-17.
- [52] Videla, H. A., Gomez de Saravia, S. G., de Mele, M. F. L., Hernandez, G., and Hartt, W. "The Influence of Microbial Biofilms on Cathodic Protection at Different Temperatures", CORROSION/93, Paper 298, NACE International, Houston, TX, 1993.
- [53] Edyvean, R. G. J. "Interactions between Biofouling and the Deposit Formed on Cathodically Protected Steel in Seawater", *Marine Biology*, Proceedings 6th International Congress on Marine Corrosion and Fouling, Athens, Greece, 1984, pp. 469-483.
- [54] de Mele, M. F. L., Gomez de Saravia, S. G. and Videla, H. A. "An Overview on Biofilms and Calcareous Deposits Interrelationships on Cathodically Protected Steel Surfaces," Proceedings of 1995 International Conference on MIC", P. Angell, S. W. Borenstein, R. A. Buchanan, S. C. Dexter, N. J. E, Dowling, B. J. Little, C. D. Lundin, M. B. MacNeil, D. H. Pope, R. E. Tatnall, D. C. White, and H. G. Ziegenfuss, Eds., NACE International, Houston, TX, 1995, pp. 50/1-50/8.
- [55] Little, B. J. and Wagner, P. A. "Interrelationship between Marine Biofouling and Cathodic Protection," *Materials Performance*, Vol. 32, 1993, pp. 17-20.

- [56] Jones, D. A. "Environmentally Induced Cracking", Principles and Prevention of Corrosion, 2nd Edition, Prentice Hall, Upper Saddle River, NJ, 1996, pp. 235-290.
- [57] Thomas, C. J., Edyvean, R. G. J., and Brook, R. "Biologically Enhanced Corrosion Fatigue," Biofouling, Vol. 1, 1988, pp. 65-77.
- [58] Edyvean, R. G. J., Benson, J., Thomas, C. J., Beech, I. B., and Videla, H. A. "Biological Influences on Hydrogen Effects in Steel in Seawater," CORROSION/97, Paper 206, NACE International, Houston, TX, 1997.
- [59] Edyvean, R. G. J., Benson, J., Beech, I. B., and Videla, H. A. "Microbiological Influences on Hydrogen Effects on Steels," J. C. Bolcich, and T. N. Veziroglu, Eds., Hydrogen Energy Progress XII, Vol. 3, 1998, pp. 1755-1762.
- [60] Edyvean, R. G. J., Benson, J., Thomas, C. J., Beech, I. B. and Videla, H. A. "Biological Influences on Hydrogen Effects in Steel in Seawater," *Materials Performance*, Vol. 37, 1998, pp. 40-44.
- [61] Edyvean, R. G. J., "Biodeterioration Problems of North Sea Oil and Gas Production," *International Biodeterioration*, Vol. 23, 1987, pp. 199-231.

Robert M. Kain¹

Use of Coatings to Assess the Crevice Corrosion Resistance of Stainless Steels in Warm Seawater

Reference: Kain, R. M., "Use of Coatings to Assess the Crevice Corrosion Resistance of Stainless Steels in Warm Seawater," *Marine Corrosion in Tropical Environments, ASTM STP 1399*, S. W. Dean, G. Hernandez-Duque Delgadillo, and J. B. Bushman, Eds., American Society for Testing and Materials, West Conshohocken, PA, 2000.

Abstract: This paper focuses on the utility of epoxy-type coatings for testing the crevice corrosion resistance of a variety of stainless type alloys in warm, natural seawater. Details of surface preparation, coating application and exposure to 30°C seawater for periods of up to six months are provided. Testing comprised exposure of UNS S31603, UNS N08367 and UNS S20910 in one or more of the following forms: pipe, sheet, welded plate. Results are discussed in terms of alloy resistance to crevice corrosion initiation and propagation. The attributes of coatings as a crevice former are reviewed. While alloy N08367 was clearly the most resistant to crevice corrosion initiation at coating sites, it suffered intense attack in some cases.

Keywords: warm seawater, crevice corrosion, coatings, austenitic stainless steel

Introduction

In the absence of cathodic protection, crevice corrosion is the most problematic issue affecting stainless steel utilization in seawater [1]. The problem is particularly acute in warm natural seawater where the cathodic process is enhanced by the ennobling effects of biological films which form on stainless steel surfaces [2]. Although crevice corrosion can occur in cold seawater, propagation of attack is generally greater in warm seawater. Susceptibility is not limited just to the common "300 series" grades (e.g., UNS S30400/ S30403 and UNS S31600/ S31603). Under certain conditions, higher alloyed duplex and austenitic stainless steels, including "super" varieties are also susceptible [3-9]. Even 9 to 15 percent molybdenum containing nickel-base alloys (e.g., UNS N06625 and UNS N01276) are not completely immune [5, 7, 9]. Testing and modeling based research has shown that crevice corrosion is more likely to occur when crevices are deep and tight [10-12]. Crevices may be of the metal-to-metal or metal-

¹ Senior Corrosion Scientist, LaQue Center for Corrosion Technology, Inc.,
P. O. Box 656, Wrightsville Beach, NC 28480.

to-nonmetal type. Variations in alloy behavior can result from differences in crevice geometry, and due to other environmental and metallurgical factors described elsewhere [11,12].

ASTM Standard Guide for Crevice Corrosion Testing of Iron-base and Nickel-base Stainless Alloys in Seawater and Other Chloride-Containing Aqueous Environments (G78-95) describes a number of different types of non-metallic crevice devices which have been used to investigate crevice corrosion. Presently, G78 does not address the use of coatings as crevice formers.

Coatings have been implicated with the failure of "20Cr-6Mo" alloy condenser tubes [6]. While not intentionally coated, overspray from a condenser tube sheet coating operation produced crevices which led to the tube failures. Problems with crevice corrosion affecting partially coated stainless steel and nickel alloy electrochemical test specimens have been reported by several researchers [13,14]. The use of "coatings" to investigate crevice corrosion resistance has been proposed previously. Celis et al. [14], for example, proposed testing of crevice corrosion susceptibility by a photomasking technique capable of producing various size crevice-forming dots on the stainless steel test surfaces. The technique, however, relied on "potentio-staircase polarization" in a simple 0.1 M KCl solution.

Earlier, Degerbeck and Gille [16] described simple immersion trials conducted with a crevice former of dried plastic from a felt tip pen. Some of the attributes described for this technique included:

- a constant critical geometry
- no need for a fixture
- applicable to convex, concave and uneven surfaces (e.g., weldments)
- crevice area can be varied
- simple to make specimens

Besides the inadvertent coating issue described previously, there are occasions where stainless steel might be intentionally coated. Coating of stainless steel has been suggested, for example, as one way to mitigate galvanic corrosion when stainless steel is the cathodic member of a couple [17]. In some applications, there may be need to coat stainless steel with an antifouling type paint, to minimize fouling in general and to preclude barnacle-related crevice corrosion. The behavior of three different grades of stainless steel when fully and partially coated with epoxy barrier paints and antifouling type paints, in a recent test program, are reported elsewhere [8].

This paper discusses three series of tests that were either directly and indirectly related to reference [8]. Results of two of these have not been published previously. Tests were performed on three diverse grades of austenitic stainless steel: Type 316L (UNS S31603), AL6XN^{TM1} (N08367) and a Cr-Ni-Mn-Mo alloy (UNS S20910). N08367 is the nitrogen-containing version of the "20Cr-6Mo" alloy (UNS N08366) which had suffered crevice corrosion under the epoxy paint over-spray mentioned earlier.

¹ AL6XNTM is a registered trademark of Allegheny Ludlum Corporation, Brackenridge, PA.

Experimental

Materials and Specimens

Table 1 gives the nominal compositions for the three alloys tested. As will be described later, different product forms from different heats of material were tested.

Testing included exposure of 2-inch (50.8 mm) diameter pipe specimens of S31603, 1/8-inch (~3 mm) sheet specimens of all three alloys, and 1/2-inch (12.7 mm) plate specimens of S20910 and N08367. Surface preparation and coating details are described in the specific test series sections.

Table 1 - *Nominal Composition of Test Materials*

UNS Designation	Weight Percent							
	Fe	Cr	Ni	Mo	Mn	S*	N	
S31603 ¹	0.030	Base	16.0-18.0	10.0-14.0	2.0-3.0	2.0*	0.03	--
S20910 ²	0.06	Base	20.5-23.5	11.5-13.5	1.5-3.0	4.0-6.0	0.03	0.22-0.4
N08367 ³	0.03	Base	20.0-22.0	23.5-25.5	6.0-7.0	2.0*	0.03	0.18-0.25
N06625 ⁴	0.10	5.0*	20.0-23.0	Base	8.0-10.0	0.5*	0.015	--

* denotes maximum allowed

¹ Type 316L, ² 22-13-5 alloy, ³ AL6XN

⁴ alloy 625 filler metal was used to weld N08367 specimens in Series 2 and Series 3

Environments

All three test series described below were conducted in constantly refreshed, recirculated, filtered (5-10 μm), natural seawater at an average temperature of $30^\circ\text{C} \pm 2^\circ\text{C}$. Table 2 provides weekly hydrology data. Series 1 and Series 2 ran concurrently for 60 days. Subsequent Series 3 tests also ran up to 60 days, but with interim removal of some specimens.

Table 2 - *Weekly Source Seawater Hydrology*

	Series 1 and 2	Series 3
Temperature $^\circ\text{C}$ ¹	25.4 - 7.6	29.4 - 14.9
Dissolved O ₂ (mg/L)	5.6 - 9.8	4.7 - 8.0
Percent Saturation	81 - 100	72 - 90
pH	7.8 - 8.1	7.7 - 8.0
Salinity (g/L)	26.2 - 36.1	25.8 - 35.6
Chlorinity (g/L)	14.5 - 19.8	14.5 - 20.4

¹ temperature at sampling time

Series 1 — Pipe Tests

As noted elsewhere [9], crevice corrosion of alloy 625 (UNS N06625) was found beneath epoxy paint which had been applied to the OD of 3-inch (76.2 mm) schedule 40 pipe. The coated areas had been inserted into sections of clear vinyl tubing and clamped in place to form a “piping system” handling natural seawater. A series of tests was subsequently performed to assess if epoxy paint, without the overlaying vinyl tubing would promote crevice corrosion. As described in the following, several test variables were considered.

Procedure

Type 316L (UNS S31603) was selected as the crevice-corrosion-susceptible control material. A total of twenty-four 12-inch (305 mm) long sections of 2-inch (50.8 mm) schedule 40 pipe were prepared. Twelve of the specimens were blasted with clean, 80-mesh aluminum oxide to prepare the surface for coating application. The other 12 were left in the as-produced mill finish. Subsequently, the outside diameter (OD) of the pipe specimens was partially coated with epoxy paint, leaving either 20% or 80% of OD surface uncoated. The bare inside diameter (ID) surfaces were included in determining the cathode to crevice area ratios. The interface between the epoxy and the bare metal section was considered to be the crevice mouth. An equal number of pipes were coated with two different epoxy paint systems. One system (Coating I) comprised a dual-layer coating of conventionally sprayed epoxy (gray over red) identical to that used in another study [8]. The total dry film thickness was about 10 mils (250 μm). The second system (Coating II) comprised a one-coat brush applied (~20 mils or 500 μm) layer of a two-part epoxy paint of the type used in the earlier testing of the alloy N06625 pipe. Both coating systems were produced by the same company. Specimens were tested in triplicate. A typical pre-test view of the coated pipes is shown in Figure 1. The specimens were exposed to warm, filtered seawater for six months in the same large test tank containing a number of other coated specimens reported in reference [8].

Results and Observations

While the depth of the seawater test tank precluded a thorough in-situ inspection of all specimens, it was apparent from the easily visible specimens that crevice corrosion had initiated on some within a few days. Post-test inspection revealed that 18 specimens had incurred extensive crevice corrosion at the primary site, i.e., where the paint created an interface with the bare OD, and also at the edge of the paint at the other end. For the remaining six specimens, the attack was confined at the latter sites. In one case, the attack too close to the pipe end precluded accurate measurements.

Figure 2 provides a representative view of the specimens after cleaning. The poor paint adhesion on the mill surface may have influenced the crevice corrosion process for some specimens. The paint was much more adherent to the grit blasted surfaces. For these, coating disbondment was observed only at areas affected by crevice corrosion.

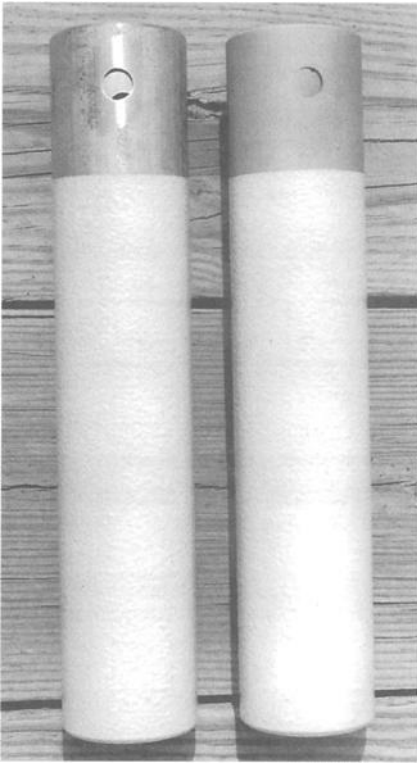


Figure 1 - Pre-test view of coated S31603 pipe. Shown (left) as-produced and (right) grit blasted pipe specimens with 80% of OD surfaces coated with spray applied epoxy.

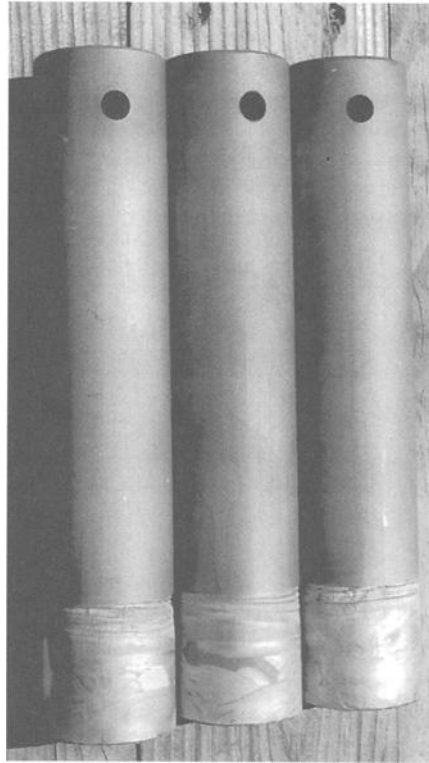


Figure 2 - Examples of crevice corrosion which developed on partially coated S31603 pipe exposed to warm seawater for 6 months. Shown triplicates of grit blasted pipe specimens with brush-applied epoxy paint on 20% of OD surface.

In addition to visual appearance, the quantitative extent of lateral and maximum depth of attack are commonly used to characterize crevice corrosion resistance. Differences in initiation times, as well as other factors, can influence crevice corrosion propagation results. Table 3 gives the maximum depth of penetration results for 23 specimens. It is evident that values ranged from 0.53 mm to 3.85 mm. The minimum and maximum values were measured for two specimens of the triplicate specimens sprayed with two coats of epoxy on 20 percent of the original mill surface. The third specimen was resistant to attack at the primary crevice site, but did crevice corrode at the painted end. The results in Table 3 also illustrate that there was greater variability in the specimen-to-specimen maximum depths of attack for those specimens with either coating system applied to 20 percent of the pipe OD surface. Conversely, those with the smallest cathodic surfaces, i.e., 80 percent paint covered, exhibited the least variability.

Table 4 gives average and standard deviation data for all 23 specimens, and for subsets of 11 or 12 specimens grouped according to surface preparation, paint application and area coverage. The overall average and standard deviation values were 1.73 mm and 0.88 mm, respectively. While the differences in the average value is greatest for the grit blasted versus mill-finish surfaces, the greatest difference in standard deviation is observed for the two coating types. Considering that the maximum depths of attack (Table 3) differed by an order of magnitude, the average values shown in Table 4 indicate a fair degree of reproducibility. Somewhat surprisingly, the set with the brush applied coating exhibited the lowest standard deviation value, while that with the spray applied coating exhibited the greatest. Again, the latter data were influenced by the "rogue" behavior of some specimens with 80 percent of the bare mill-produced surface exposed to seawater.

Table 3 - *Maximum Depth of Penetration Incurred by Partially Coated UNS S31603 Stainless Steel Pipe Specimens in Six-Month Filtered Seawater Test at 30°C*

Coating System	Maximum Depth (mm)							
	20% Paint Coverage*				80% Paint Coverage*			
	Pipe No.	Grit Blasted	Pipe No.	Mill Finish	Pipe No.	Grit Blasted	Pipe No.	Mill Finish
Coating I (Sprayed)	1	1.05	1	**	1	1.27 ¹	1	2.85 ¹
	2	0.95	2	0.53	2	0.57	2	2.75 ¹
	3	2.45 ¹	3	3.85 ¹	3	0.82	3	2.35 ¹
Coating II (Brushed)	1	1.68 ¹	1	1.35 ¹	1	2.30 ¹	1	1.51 ¹
	2	2.42 ¹	2	2.40 ¹	2	2.15 ¹	2	1.45 ¹
	3	2.05 ¹	3	1.76 ¹	3	1.82 ¹	3	1.13 ¹

* Based on OD surface area

** Attacked but not measurable

¹ Denotes deepest attack at primary interface site

Table 4 - *Summary of UNS S31603 Pipe Specimen Test Results*

Total Conditions Considered	Total Number of Specimens	Maximum Depth of Attack (mm)	
		Average Value	Standard Deviation
All	23	1.73	0.88
Coating I	11	1.77	1.12
Coating II	12	1.84	0.43
Grit Blasted	12	1.63	0.67
Mill Finish	11	1.99	0.95
20% OD Coverage	11	1.86	0.92
80% OD Coverage	12	1.75	0.74

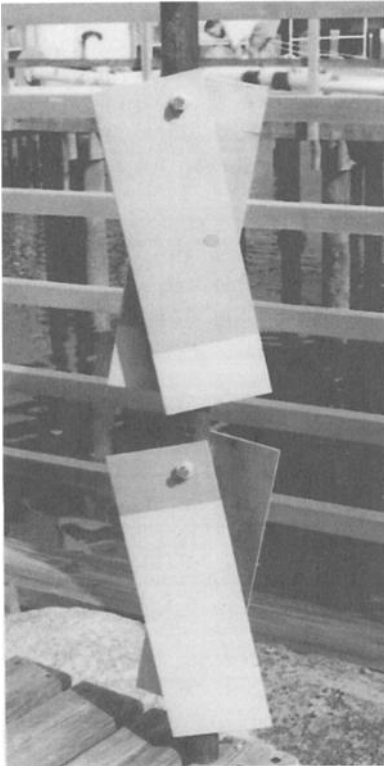


Figure 3 - Pre-test view of partially coated stainless steel sheet specimens (same coating system as in Figure 1).



Figure 4 - Examples of crevice corrosion which developed under coating on sheet specimens. Shown N08367 with 20% of original mill surface coated

Series 2 — Flat Plate Tests

Results of a much larger test program comprising 180 fully and partially coated flat stainless steel specimens have been reported elsewhere [8]. Again, those tests comprised the three alloys (S31603, S20910 and N08367) listed in Table 1, and three types of coatings (epoxy-barrier paint, ablative copper and elastomeric); the latter two are antifouling coatings. In each case, the flat panels were coated with two layers of spray applied epoxy (gray over red). Other test variables included weldments, surface condition, coating defects and the effects of sacrificial protection with zinc anodes. Because of the relationship between the previously described pipe test, and other tests described later in this paper, only the results for the referenced tests comprising panels partially coated with two layers of sprayed-applied epoxy are reviewed in detail.

Figure 3 shows the typical pre-test appearance of the 4-inch x 12-inch (100 x 300 mm) test panels with 20% and 80% paint coverage, or conversely 80% and 20% bare metal, respectively. As reported previously, one surface of each panel was grit blasted

with 80-mesh aluminum oxide while the other was left in its mill finish condition. For S31603 and S20910, the mill finish was a standard 2B. In the case of N08367, the mill finish was much coarser and approached the surface roughness achieved by the grit blasting. Triplicate specimens were exposed for each alloy-paint coverage combination. Testing was performed concurrently with the previously described pipe test specimens in 30°C seawater for six months.

Results and Observations

Tables 5 and 6 summarize the results from the referenced testing of stainless steel panels with 20% and 80% epoxy barrier paint coverage. In Table 5, material performance is compared in terms of crevice corrosion initiation and lateral propagation (affected area). For each stainless steel tested, the data base comprises a total of 12 crevice sites, i.e., two per specimen. That data shows that all available sites on the two lower molybdenum-containing alloys, S31603 and S20910, were attacked. In contrast, only 50 percent of the primary interface sites on the “6Mo” alloy (N08367) panels were attacked. Figure 4 shows the post-test condition of N08367 panels tested with 20% paint coverage. No significant difference in the affected areas was observed between S31603 and S20910. Both alloys consistently exhibited larger affected areas at sites associated with grit blasted surfaces versus those with the original 2B finish. This was most apparent for those panels with the least cathodic surface area, i.e., 80% paint coverage. In addition to enhanced resistance to initiation, N08367 exhibited greater resistance to lateral propagation, particularly when the cathode surface area was relatively small (i.e., 20% of total).

Table 5 - Crevice Corrosion Resistance of Three Stainless Steels Partially Coated with an Epoxy Type Barrier Paint and Exposed to Warm Seawater for Six Months

Material	Affected Crevice Area (cm ²)					
	20% Paint Coverage			80% Paint Coverage		
	Panel Code	Grit Blasted Surface	Mill Surface	Panel Code	Grit Blasted Surface	Mill Surface
S31603	04	36.0	33.5	04	29.5	5.8
	05	35.0	29.5	05	26.8	15.0
	06	53.5	52.5	06	26.0	2.8
	avg.	41.5	38.5	avg.	27.4	7.8
S20910	04	22.5	37.5	04	20.5	15.5
	05	54.5	20.0	05	38.0	4.5
	06	45.0	37.5	06	25.5	19.5
	avg.	40.7	31.9	avg.	28.0	13.2
N08367	04	6.8	52.0	04	0.0	0.0
	05	15.0	0.0	05	0.0	0.0
	06	1.0	25.3	06	0.6	0.0
	avg.	7.6	27.2 ¹	avg.	0.6	0.00

¹ Average of #04 and #06

Table 6 provides additional propagation results comparing the maximum depths of penetration. Because of the possible influence of edge effects, penetrations within 1/2-inch (13 mm) of the edges are not included. As indicated by (E), through-plate penetrations were found within this zone on two of the S31603 specimens. Considerable variations in the maximum depth values for some sets of specimens are apparent. The reduction in the affected area and maximum depth of attack for S31603 and S20910 specimens with 80% paint coverage in the 2B surface is likely attributed to the combination of smaller cathodic surface area and poor adhesion of the coating. Overall, S31603 exhibited the greatest average depth of attack (0.92 mm) and the most variability (std. dev. 0.82 mm) among the three alloys tested. Average depths of attack for S20910 and N08367 were nominally 40 to 50 percent less than those for S31603.

Table 6 - *Maximum Depth of Crevice Corrosion Incurred by Three Stainless Steels Partially Coated with an Epoxy Type Barrier Paint and Exposed to Warm Seawater for Six Months*

Material	Maximum Depth (mm)					
	20% Paint Coverage			80% Paint Coverage		
	Panel Code	Grit Blasted Surface	Mill Surface	Panel Code	Grit Blasted Surface	Mill Surface
S31603	04	1.58 (E)	1.71	04	0.43	0.10
	05	1.72 (E)	0.30	05	1.83	0.01
	06	1.61	0.53	06	2.13	0.02
	avg.	1.64	0.85	avg.	1.46	0.04
S20910	04	0.15	1.05	04	1.07	0.26
	05	1.15	0.50	05	0.59	0.00*
	06	0.24	0.73	06	0.16	0.13
	avg.	0.51	0.76	avg.	0.61	0.20
N08367	04	0.05	0.96	04	0.00	0.00
	05	0.93	0.00	05	0.00	0.00
	06	0.00*	0.75	06	0.20	0.00
	avg.	0.49	0.86	avg.	0.20	0.00

* Measurable attack within 1/2-inch (13 mm) of panel edge

The testing mentioned previously clearly demonstrates the susceptibility of a range of stainless steel compositions to crevice corrosion when partially coated and exposed to natural seawater. The reference document [8] has shown that the same materials were fully resistant if they were coated in total, and exposed without defects. Specimens exposed with intentional and inadvertent defects, but protected with zinc anodes were also fully resistant in a one-year test. However, the degree of cathodic protection imposed caused paint blisters to form and promoted coating disbondment, particularly on 2B mill surfaces.

Series 3 — Cruciform Specimens

Procedure

The effects of coating on the crevice corrosion resistance of N08367 and S20910 were also investigated in a third series of seawater tests. In this case, 35 specimens of each material were exposed. Testing was performed on cruciform shaped welded specimens as depicted in Figure 5. The nominal cross arm dimensions were 4-inches x 4-inches x 1/2-inch (100 mm x 100 mm x 12.7 mm) and 4-inches x 8-inches x 1/2-inch (100 mm x 200 mm x 12.7 mm). While the S20910 cruciforms were welded with like metal filler; alloy N06625 filler was used to weld the N08367 cruciforms. The specimens had been prepared for a mechanical test, but were utilized as a convenient “multi-crevice” type specimen to incorporate the effects of crevice corrosion.

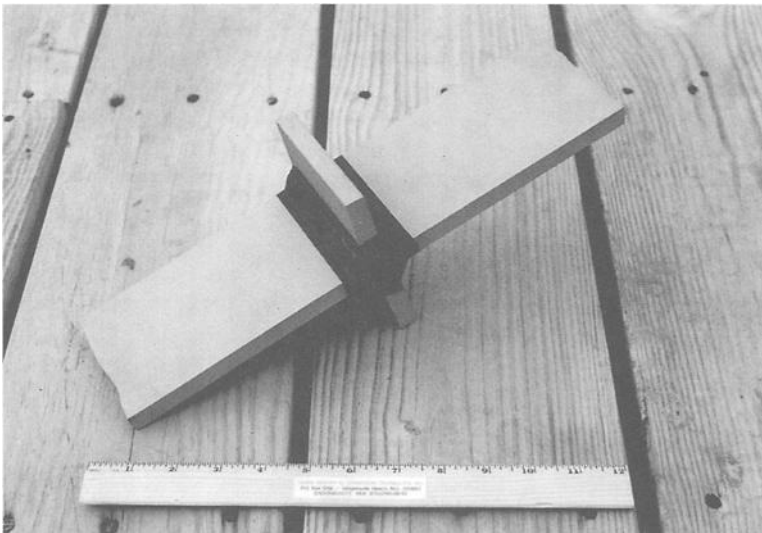


Figure 5 - *Pre-test view of partially coated welded cruciform specimen with multiple crevice sites.*

Prior to coating, all surfaces were blasted with clean, 80-mesh aluminum oxide. The coating was the same as the first coat in the previous pipe and panel tests, but brush-applied. For this series, it was the intent to provide a large boldly exposed surface area of stainless steel. Accordingly, only the weldment and a small overlap area on the base metal shown in Figure 5 was coated. As discussed later, the overlap area on the N08367 specimens was intentionally varied. When completed, each specimen had two potential crevice sites in each quadrant of the cruciform, or eight all together. The full complement of 35 specimens, therefore, had a total of 280 crevice sites per alloy. As

discussed later, a number of N08367 specimens were reblasted, recoated and re-exposed, thus providing even more data. The short length crevices produced on the edges of the specimens were not included in the subsequent evaluation. It is noted, however, that some attack did occur at these sites.

UNS S20910 Testing and Results

All 35 of S20910 cruciform specimens were prepared with the epoxy coating covering the weldment and 1/16 - 1/8 inch (~1.6 mm - 3.2 mm) of the base metal from the weld toe. The specimens were divided for exposure in two shallow seawater test troughs approximately 10 inches (250 mm) deep. These exposure conditions provided an opportunity for in-situ inspection of the upward-facing surface crevice sites. Within three days, attack was detected at 31 visible sites on 25 of the specimens. By day seven, attack was detected at 50 visible sites on 30 of the specimens. Five affected specimens were removed for evaluation after 10 days, 12 more after 30 days and another 6 after 45 days. The remaining 12 were tested for a full 60 days. At each interim removal, there was a conscious attempt to select specimens exhibiting varying degrees of propagation. Test duration notwithstanding, all 35 specimens crevice corroded within 60 days. Moreover, 76 percent of the primary interface sites were affected. Table 7 includes a summary of the incidence of attack. Had all 35 specimens been exposed for the full 60 days, the total number of affected sites may have been greater. It is perhaps a more significant observation to note the substantial number of sites which did initiate in the relatively brief exposure time.

Figure 6 shows a representative view of an attacked S20910 cruciform specimen after only 10 days' exposure. Subsequent propagation beneath the coating affected the base-metal heat affected zone, and, in most cases, a significant portion of the weld metal. Albeit varying in length, the attack was continuous along the interface on most surfaces. In a few cases, however, two or three discrete sites had propagated. As shown in Table 7, the average length of the attacked sites increased somewhat with test duration.

Table 7 - Summary of Results for UNS S20910 Welded Cruciform Specimens

Test Duration (days)	Number of Specimens Exposed	Percent of Sites Attacked	Average Length of Attacked Sites (mm)	Maximum Depth of Attack (mm)*			Percent of All Sites ≥ 0.50 mm
				Overall Range	Average Value	Std. Dev.	
10	5	58	32	0.48 to 1.61	0.90	0.27	96
30	12	77	44	0.09 to 1.65	0.84	0.34	85
45	6	85	42	0.17 to 1.84	0.73	0.37	78
60	12	77	48	<0.01 to 2.21	0.76	0.41	78

* Base metal-heat affected zone measurements

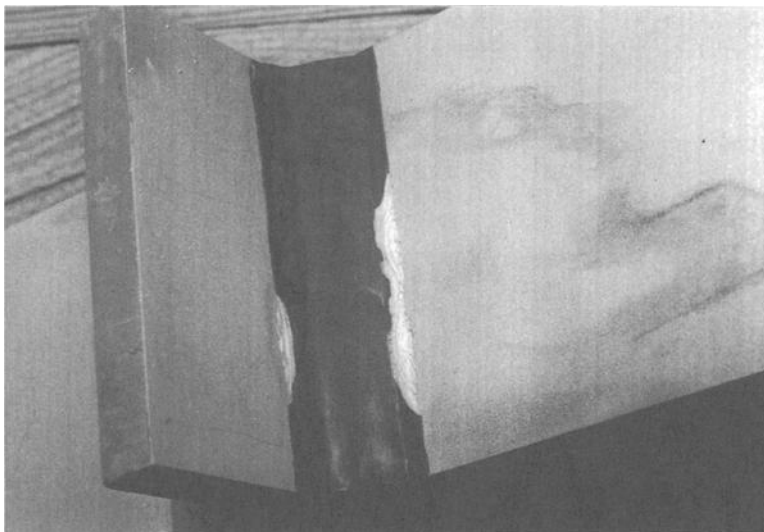


Figure 6 - Example of crevice corrosion affecting welded S20910 cruciform specimen after only 10 days exposure to warm seawater.

Table 7 also provides depth of penetration data for the S20910 cruciform specimens. Because of the geometry of the specimens, accurate measurements were limited to the base metal-heat affected zone regions within the crevice site. Again, there were considerable site-to-site differences in the maximum depths of attack incurred. Those specimens exposed for 60 days exhibited the broadest range of attack values (std. dev. 0.41 mm). Conversely, those exposed for only 10 days exhibited the least degree of variability (std. dev. 0.27 mm). It is observed from the overall depth of attack range data in Table 7 that the absolute values for maximum depth increase (exponentially) with exposure time. On the other hand, the average value of the maximum depth determinations, and the percent of all sites with attack depths ≥ 0.50 mm decreased with exposure time.

N08367 Testing and Results

A total of 27 welded N08367 cruciform specimens were prepared and exposed in the same manner described above for S20910. In contrast to the behavior described for S20910, only two specimens (two sites) exhibited attack within the first three days of exposure. After seven days, only one site on each of five N08367 specimens was found to be corroding. By the end of 30 days, the total had increased to nine specimens with one affected site each. These were allowed to continue in test for another 30 days (total 60 days), while the 18 resistant ones were removed for subsequent re-exposure.

At the conclusion of the 60-day test, a total of 20 affected sites were found on the nine specimens. This constitutes 28 percent of the 72 potential sites for initiation. The average length of the attack across the width of the specimen was 54 mm; slightly more

than that found at the S20910 sites. In each case, the alloy N06625 weldment was also attacked. While not quantified by depth measurement, the weld attack shown, for example, in Figure 7 was significant. For the above nine specimens, base metal-heat affected zone depth of attack near the weld toe ranged from 0.12 mm to 2.77 mm (max.). Eighty percent of the sites measured ≥ 0.50 mm. The average maximum value and standard deviation value for the preceding were 1.37 mm and 0.82 mm, respectively.

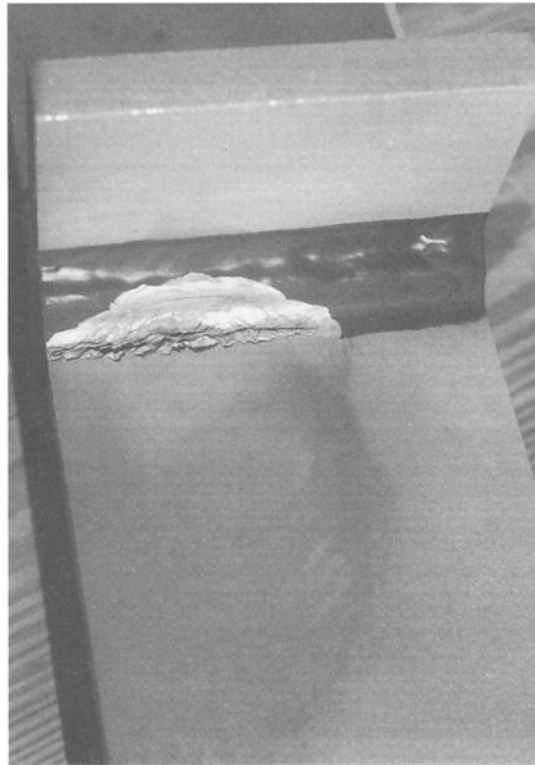


Figure 7 - *Example of crevice corrosion affecting weld metal (N06625) used for joining N08367 cruciform specimen and exposed to warm seawater for 60 days.*

The previously mentioned 18 resistant specimens were reblasted and re-coated; this time with a paint overlap of 1/8-inch to 3/16-inch (3.2 mm - 4.8 mm) from the weld toe. In-situ inspection revealed attack at one site after 19 days. With the one exception, no other evidence of attack was found during or after the course of a 54-day exposure to warm seawater. The length and maximum depth of attack at the sole affected site was 40 mm and 1.55 mm, respectively; not far from the average values for the nine sites attacked in the preceding test.

Eight other N08367 cruciform specimens were also tested for periods ranging from 30 to 52 days. Four each were coated with 1/4-inch (~6.4 mm) to 1/2-inch (~12.7 mm) overlaps from the weld toe. Some attack was again observed within the first three days of exposure. Notwithstanding the differences in coating overlap and exposure time, 52 percent of the 64 crevice sites on these eight specimens initiated. The overall penetration range was 0.07 mm to 1.73 mm. The absolute maximum was associated with a specimen prepared with 1/2-inch overlaps and exposed for 30 days. The average and standard deviation values for the 33 affected sites were 0.60 mm and 0.41 mm, respectively.

Summary and Conclusions

The propensity for stainless steels to suffer crevice corrosion in warm seawater has been reviewed. Particular attention has been given to crevice conditions associated with epoxy type coatings applied to different grades of stainless steel in several product forms. Based on the testing and evaluation of 124 test specimens with a combined total of 752 crevice sites, a number of conclusions can be drawn. These are expressed below as they relate to crevice corrosion testing and to the performance of stainless steels in warm seawater.

- Epoxy coating can be used as a crevice former for the purpose of testing the crevice corrosion resistance of different grades of stainless steel. While both coating systems utilized were produced by the same manufacturer, there is no reason to suspect that similar coatings produced by other manufacturers would affect stainless steel any differently.
- This type of crevice former can be applied to flat as well as curved and irregular surfaces and requires no fixturing or standard torquing.
- Epoxy coatings are suitable for testing the crevice corrosion resistance of as-deposited weldments, mill-produced and surface treated (for example, grit blasted) material.
- Consideration for including epoxy coating as another type of crevice former in ASTM G-78 is recommended.
- The effects of cathodic surface area can be investigated by varying the amount of coverage by the coating.
- Unlike some other types of crevice-forming devices having fixed dimensions, the true depth of a crevice formed by a coating is not readily apparent. Moreover, as crevice corrosion propagates, the crevice gap may change, for example, due to coating disbondment.
- Epoxy coating is suitable for long-term exposure to seawater within the normal ambient temperature range. Present research has not evaluated its performance above 30°C.
- It has been demonstrated that austenitic stainless steels such as S31603 and the manganese-containing grade S20910 are highly susceptible to crevice corrosion when partially coated with epoxy.
- While the "26Cr-6Mo" grade tested (N08367) was also found to be susceptible, its overall resistance to crevice corrosion initiation was substantially greater. However, once initiated, significant propagation occurred even for this alloy.

- As might be expected, the N08367 was more sensitive to area ratio effects than the more susceptible grades. Test results for N08367 appear to complement field experience with a related alloy, for example, when inadvertently oversprayed with epoxy.
- Related work reported elsewhere [8] demonstrated the resistance of fully coated stainless steel, while at the same time noting that small defects in the coating provided sites for initiation. Present test results demonstrated that crevice corrosion susceptibility and the extent of attack increased with increased bare metal (i.e., cathodic) surface.
- If coatings are to be used on large stainless steel structures, e.g., ship hulls, exposure of bare metal due to coating damage could result in attack at the interface between the coating and any exposed metal.
- Attack of alloy 625 (N06625) weldments, associated with N08367 cruciform specimens, confirmed the susceptibility of this Ni-base alloy to attack beneath epoxy coatings. Moreover, it has been demonstrated that the coating need not be "held" in place, e.g., by a vinyl sleeve or other mechanism, in order for crevice corrosion to initiate.

Acknowledgment

The author expresses his appreciation for assistance provided by co-workers at the LaQue Center for Corrosion Technology, Inc. Also recognized are Mr. Chip Becker and Mr. Dave Kihl of the Carderock Division - Naval Surface Warfare Center for providing the cruciform test specimens. Portions of the testing described were funded by the Office of Naval Research under Contract N00014-97-C-0216.

References

- [1] Sedriks, A. J., *Corrosion of Stainless Steels, 2nd edition*, Chapter 5- Crevice Corrosion, Wiley-Interscience Publication, John Wiley & Sons, Inc., 1996.
- [2] Mollica, A., et al., *Corrosion*, Vol. 45, No. 1, 1989, p. 48-56.
- [3] Aylor, D. M., Hays, R. A., Kain, R. M., and Ferrara, R. J. "Crevice Corrosion Performance of Candidate Naval Ship Seawater Valve Materials in Quiescent and Flowing Natural Seawater," Paper No. 99329, CORROSION/99, NACE International, Houston, TX, 1999.
- [4] Zeuthen, A. W. and Kain, R. M., "Crevice Corrosion Testing of Austenitic, Superaustenitic, Superferritic and Superduplex Stainless Type Alloys in Seawater," *Corrosion Testing in Natural Waters, ASTM STP 1300*, R. M. Kain and W. T. Young, Eds., American Society for Testing and Materials, West Conshohocken, PA, 1997, pp. 91-108.
- [5] Kain, R. M., "Evaluation of Crevice Corrosion Susceptibility," Research

Symposium, CORROSION/96, NACE International, Houston, TX, 1996.

- [6] Klein, P. A., Krause, C. D., Friant, C. L., and Kain, R. M., "A Localized Corrosion Assessment of 6% Molybdenum Stainless Steel Condenser Tubing at the Calvert Cliffs Nuclear Power Plant," Paper No. 490, CORROSION/94, NACE International, Houston, TX, 1994.
- [7] Kroughman, J. M. and Ijjeseling, F. P., *Proceedings of 5th International Congress on Marine Corrosion and Fouling*, Barcelona, Spain, May 1980, p. 214.
- [8] Kain, R. M., "Crevice Corrosion Behavior of Coated Stainless Steel in Natural Seawater," Paper No. 00827, CORROSION/2000, NACE International, Houston, TX, 2000.
- [9] Hays, R. A., "Alloy 625 Crevice Corrosion Countermeasures Program: Evaluation of Concentric Pipe and Metal-to-Metal Gap Specimens," Report No. CDNSWC-SME-92/53, Carderock Division - Naval Surface Warfare Center, West Bethesda, MD, January 1993.
- [10] Sedriks, A. J., *International Metals Review*, Vol. 27, 1982, p. 321.
- [11] Oldfield, J. W. and Sutton, W. H., *British Corrosion Journal*, Vol. 13, 1978, p 104.
- [12] Kain, R. M., *ASM Metals Handbook*, 9th ed., Vol. 13, ASM International, Metals Park, OH, 1987, pp. 109-112.
- [13] Lee, T. S., "A Method of Quantifying the Initiation and Propagation Stages of Crevice Corrosion," *Electrochemical Corrosion Testing, ASTM STP 727*, F. Mansfeld and U. Bertocci, Eds., American Society for Testing and Materials, West Conshohocken, PA, 1979, pp. 43-68.
- [14] Kain, R. M., *Materials Performance*, Vol. 23, No. 2, 1983, p. 24.
- [15] Celis, J. P., Roos, J. R., Kinawy, N. and Ruelle, C. Della, *Corrosion Science*, Vol. 26, 1986, pp. 237-254.
- [16] Degerbeck, J. and Gille, I., *Corrosion Science*, Vol. 19, 1979, pp. 1113-1114.
- [17] LaQue, F. L., *Marine Corrosion - Causes and Prevention*, Chapter 6 - Galvanic Corrosion, Wiley-Interscience, John Wiley & Sons, New York, 1975, p. 185.

Author Index

- | | |
|----------------------------|------------------------------|
| A | K |
| Almeida, E., 3 | Kain, R. M., 60, 284 |
| B | King, G. A., 114 |
| Balasubramanian, R., 75 | Klassen, R., 48 |
| C | Kucera, V., 18 |
| Cabezas, A., 3 | L |
| Calderón, L. A., 197 | Little, B. J., 257 |
| Carpio, J. J., 75 | M |
| Castro, P., 159 | Maldonado, L., 150 |
| Cebada, M. C., 170 | Mariaca-Rodriguez, L., 3, 98 |
| Chaudhary, Z., 218 | Marrocos, M., 3 |
| Cole, I. S., 33 | Micat, G., 98 |
| Cook, D. C., 75 | Mikhailov, A. A., 18 |
| D | Morcillo, M., 3 |
| De Bósquez, A., 3 | N |
| De Gutiérrez, R., 190, 197 | Norberg, P., 114 |
| Delvasto, S., 190 | O |
| Dreyman, E. W., 247 | Oh, S. J., 75 |
| E | P |
| Edyvean, R. G. J., 270 | Peña, J., 3 |
| F | Phull, B. S., 60 |
| Fernando-Alvarez, J., 3 | Piazza II, J. L., 207 |
| G | Pikul, S. J., 60 |
| Guimaraes, A. T. C., 135 | Pope, R. K., 257 |
| H | Prato, M. R., 3 |
| Helene, P. R. L., 135, 231 | R |
| Hinton, B., 48 | Ray, R. I., 257 |
| J | Reyes, J., 75 |
| Joseph, G., 3 | Rivero, S., 3 |
| | Roberge, P., 48 |
| | Rosales, B., 3 |

S

Salas, G., 3
Swords, C., 270

T

Talero, R., 190
Tidblad, J., 18
Townsend, H. E., 75
Tula, L., 231

U

Uruchurtu-Chavarin, J., 3, 98

V

Valencia, A., 3
Van Orden, A. C., 75
Véleva, L. P., 159, 170
Videla, H. A., 270

Subject Index

- A**
- Absorption
 - gaseous, 33
 - water, 135, 190
 - Aerosol transport and deposition, 48
 - Aircraft, 48, 257
 - Akaganeite, 75
 - Aluminum, 3, 75, 114, 247, 257
 - Ammonia, 33
 - ASTM subcommittees, 60
 - Australia, 33, 48, 114
- B**
- Bacteria, sulfate-reducing, 270
 - Biofilms, 270
 - Biological films, 284
 - Blast furnace slag, 190
 - Bond strength losses, 231
 - Brazilian standards
 - water absorption, hardened mortars and concretes, 135
- C**
- Calcareous aggregates, 150
 - Calcium hydroxide, 170
 - Carbonation, 207
 - Caribbean Islands, 247
 - Cathodic protection, 207, 218, 247, 270
 - Cement, 170
 - blended, 190
 - mortars, 190
 - paste, 135
 - Chloride, 3, 190, 197, 207
 - airborne, 60
 - concentration, 75
 - contamination, 231
 - deposition, 18
 - diffusion, moisture effect on, 135
 - effect on electrochemical corrosion behavior, 170
 - localized corrosion promotion, 98
 - Cleaning, surface, 257
 - CLIMAT, 48
 - Coatings and finishes, 114, 270, 284
 - polyurethane, 257
 - Coconut, 197
 - Coil coating, 114
 - Compressive strength, 190, 197
 - Concrete, 150, 170, 231
 - blocks, 159
 - reinforced, 135, 207
 - Conductivity, 150
 - Copper, 3, 75
 - Coral sands, 247
 - CORRAG model, 18
 - Crack stabilization, 197
 - Crevice corrosion, 284
 - Curing time, 150
- D**
- Decay criterion, 218
 - Durability, 135, 190, 231
 - assessment, 114
 - fiber reinforced mortar, 197
 - stainless steel reinforced concrete, 231
 - structure, 159
- E**
- EDAX, 170
 - Electrical conductivity, 150
 - Electrochemical behavior, 231
 - Electrochemical impedance spectroscopy, 170
 - Electrochemical measurement evaluation, 98
 - Embrittlement, hydrogen, 270
 - Epoxy coatings, 284

- F**
- Fiber, natural and synthetic, 197
 - Fique, 197
 - Fly ash, 190
 - Fungal hyphae, 257
- G**
- Gaseous absorption, 33
 - Glass, 197
 - Gulf of Mexico, 75, 150
- H**
- Humidity, relative, interior, 159
 - Hydrated cement paste, 135
 - Hydrogen embrittlement, 270
 - Hyphae, 257
- I**
- Ibero-American Map of Atmospheric Corrosiveness (MICAT), 3, 98
 - Impressed current cathodic protection, 218
 - Indonesia, 33
 - International Organization for Standardization (ISO) CORRAG, 18
 - Iron, 75
- K**
- Kure Beach, North Carolina, 60
- L**
- Latin-American test sites, 3
 - Limestone, 150
 - Linear polarization resistance, 98
- M**
- Mercury intrusion porosimetry, 190
 - Metals (See also specific types), 10, 33, 114, 270
 - Mexico
 - Gulf of, 75, 150
 - Yucatan Peninsula, 150, 159
 - MICAT, 3, 98
 - Microscopy, 270
 - Models and modeling
 - aerosol, 48
 - chemical reaction simulator, 33
 - corrosion prediction, 18
 - Moisture effects on chloride diffusion, 135
 - Monitoring, sea spray airborne chlorides, 60
 - Mortars, 150
 - cement, 190
 - fiber reinforced, 197
 - Mössbauer spectroscopy, 75
 - Muds, saline, 247
- N**
- North Carolina, 60
- O**
- Oxidation, 33
 - Oxide protective properties, 98
- P**
- Performance indices, 114
 - Petrochemical plants, 218
 - Philippines, 33
 - Piping, 247
 - Polarization curves, 170
 - Polymeric substances, extracellular, 270
 - Polypropylene, 197
 - Pore structure, 190
 - Porosity, 150
 - Portland cement mortars, 190, 197
 - Portugal, 3, 98
 - Precipitation, 3, 33, 60
 - frequency, 75
- R**
- Rainwater, 33
 - Rebars, 170, 231
 - deterioration, 159

S

Sacrificial anode cathodic protection, 218
 Salt candles, 48
 Sands, coral, 247
 Saturation degree, 135
 Scanning electron microscopy, 170
 Sea spray corrosion monitoring, chlorides in, 60
 Seawater intake structures, 218
 Service life prediction, 135, 231
 Silica fume, 190, 197
 Slag, blast furnace, 190
 Sodium sulfate, 98
 Spain, 3, 98
 Spectroscopy
 electrochemical impedance, 170
 Mossbauer, 75
 Stabilization, crack, 197
 Steel, 114, 197, 247
 bars, 159
 carbon, 60, 75, 270
 design steel current density, 218
 mild, 3, 33, 98
 mild, reinforcing, 170
 prestressed structures, 207
 reinforced, 207
 stainless, 231
 stainless, austenitic, 284
 Sulfate-reducing bacteria, 270
 Sulfides, 270
 Sulfur dioxide pollutants, 3, 18, 33, 75
 Superplasticizer, 197
 Surface preparation, 284

T

Temperature effects, 18
 Temperature, corrosion risk tool, 159
 Tensile strength losses, 231
 Thailand, 33
 Time of wetness, 18, 60, 159

U

UN ECE, 18

W

Washing, surface coatings, 257
 Water-to-cement ratio, 150
 Wind flow pattern, 48

X

X-ray diffraction, 190

Y

Yucatan Peninsula, 150

Z

Zinc, 3, 33, 60, 75
 zinc-hydrogel, 207

ISBN 0-8031-2873-8